NRL REVIEW

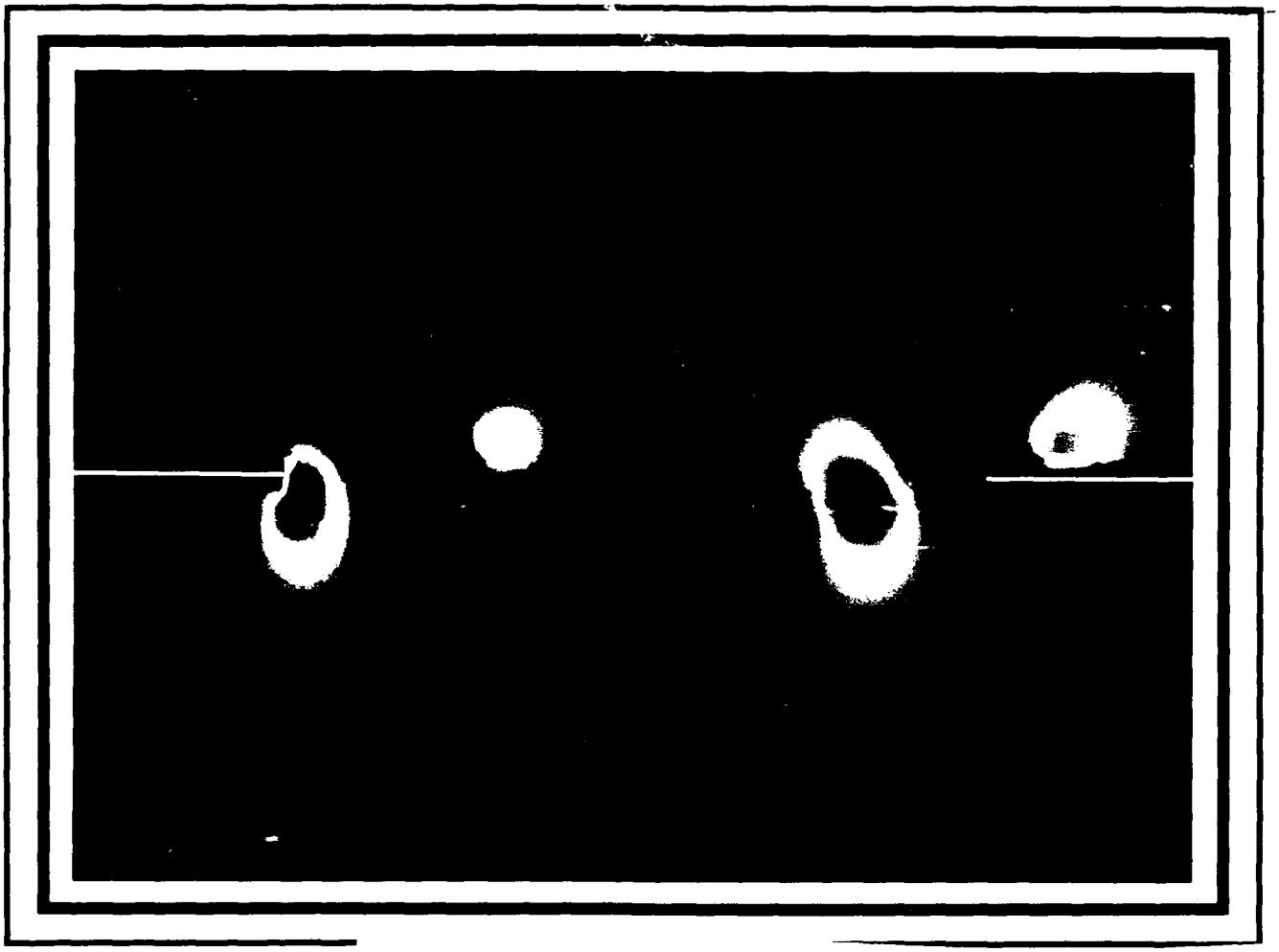

"Original contains color plates: All DTIC reproductions will be in black and white"

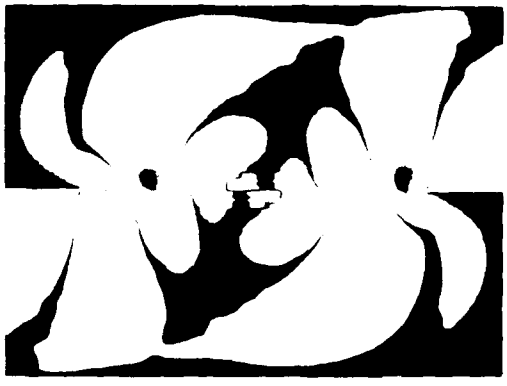

Naval Research Laboratory

NRL REVIEW

In this Review, NRL presents highlights of the unclassified research and development programs for fiscal year 1988. This book fulfills a dual purpose: it provides an exchange of information among scientists, engineerings, scholars, and managers; and it is used in recruiting science and engineering professionals. As you read this Review, *you will become even more aware that the Laboratory is a dynamic team working together to promote the programs, progress, and innovations that will continue to foster discoveries, inventiveness, and scientific advances for the Navy of the future.*

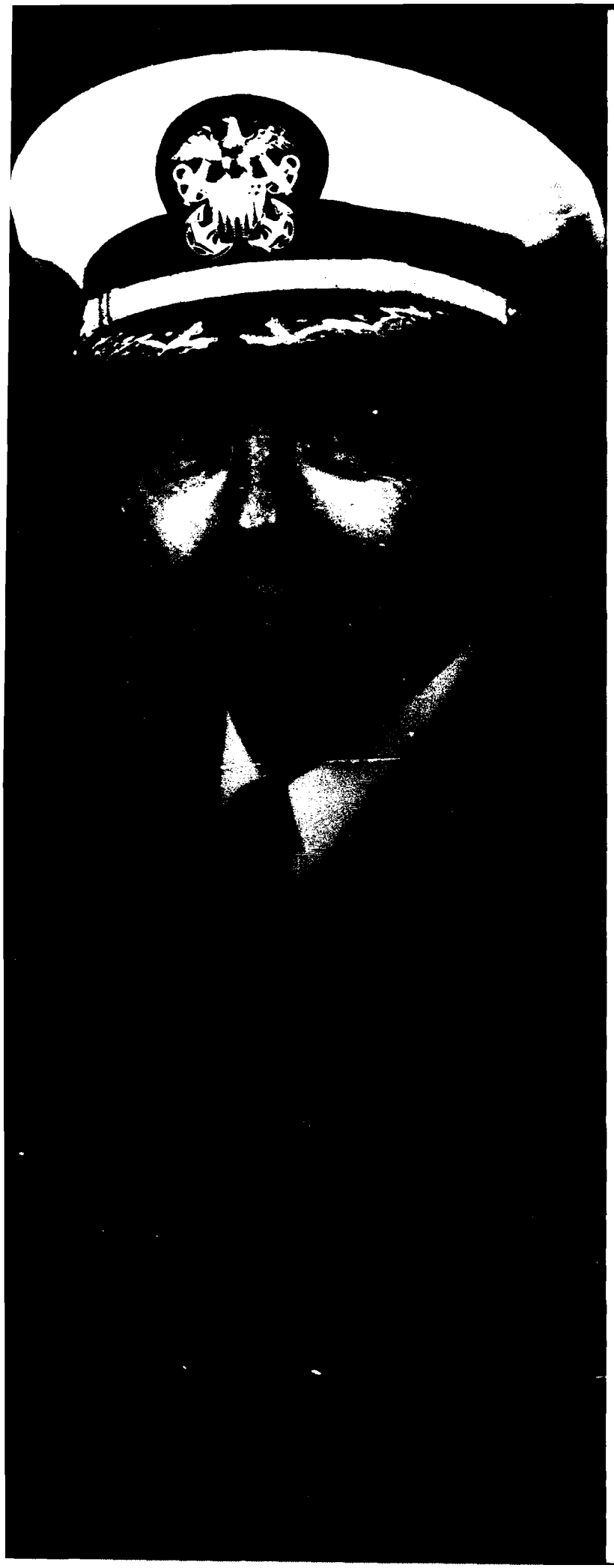

EXECUTIVE

Q: *What are some of your parting thoughts about NRL?*

I have been most fortunate to spend 8 of the last 10 years as commander of three superb organizations. As my picture shifts once again to the gallery of "Past C.O.s," it is a joy to reflect on NRL and my final 2 years (of 30) in the world's finest Navy.

The Laboratory is indeed a "national trust" because of the outstanding scientists, engineers, and support personnel with whom I have been associated. I am proud and honored to have been a member of the NRL "family."

When I think about what makes NRL tick, I wonder what are the incentives that have resulted in the myriad of NRL's accomplishments. Certainly, for the researchers, it is the freedom to think. I am convinced that there are few breakthroughs—just a constant chipping away at understanding why something appears or behaves the way it does. I envy the scientist who, for that moment, understands something that no one else in the world understands. I envy the engineer who experiences the joy of using that understanding to make something work for the first time.

Let's not forget what else makes NRL tick—the dedication and expertise of our support personnel. I salute each of you, and I would encourage our scientists and engineers to pause and say "thanks" when a job is well done. That is an important incentive we sometimes forget.

I wish there were some way that the scientists, engineers, and support personnel at NRL could see the fruits of their labor as it finds its way into the ships and aircraft of the "service of choice," the Navy we sometimes take for granted—a Navy that will always be there, with your help, to defend our freedom to think and preserve the quality of life we so enjoy.

Command of NRL is a real crown jewel and my last thought is simply, what a pleasure it has been to serve!

Captain William G. Clautice
Commanding Officer

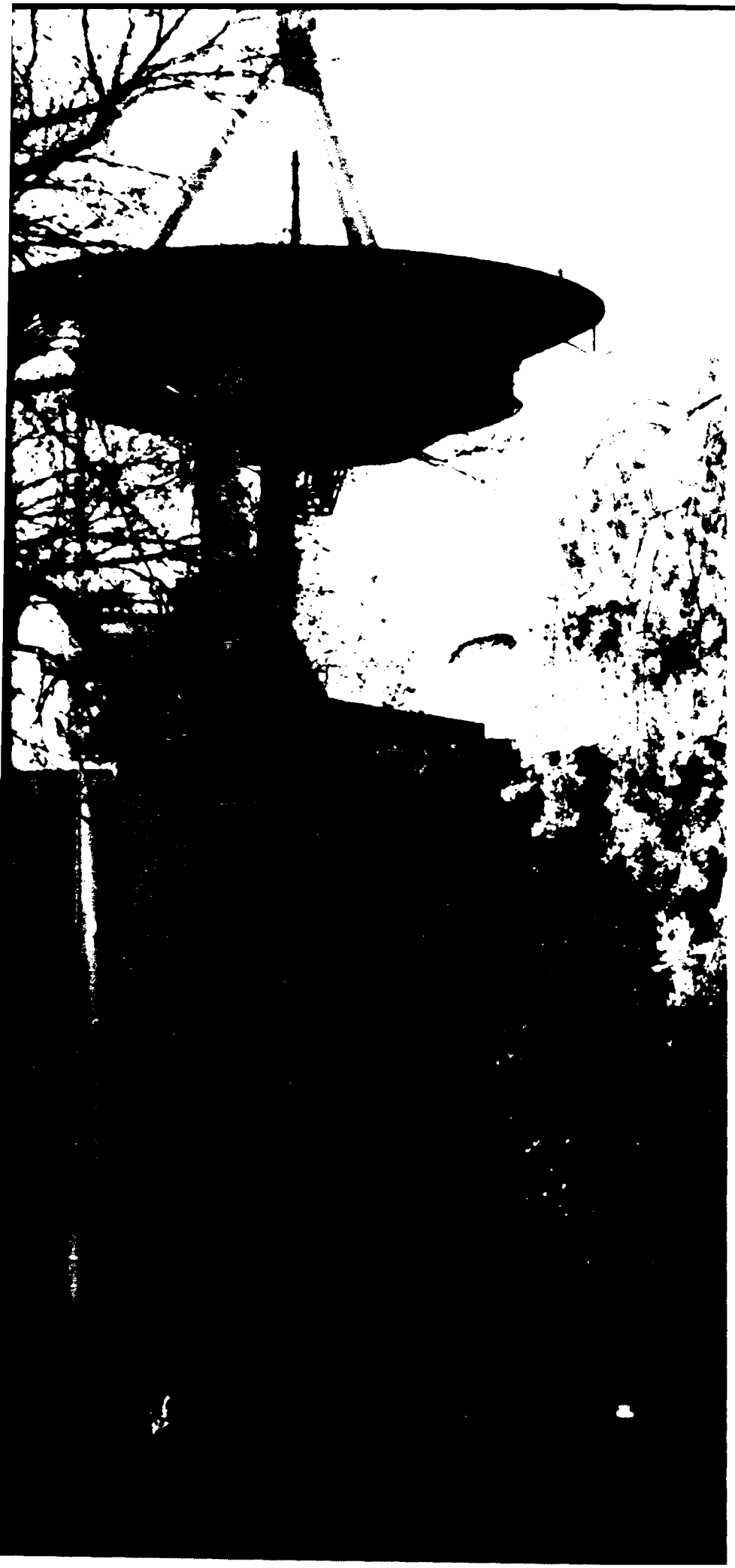

MISSION

To conduct a broadly based multidisciplinary program of scientific research and advanced technological development directed toward new and improved materials, equipment, techniques, systems, and related operational procedures for the Navy.

RESPONSIBLE FOR NAVY-WIDE LEADERSHIP IN:

- **The performance of primary in-house research for the physical, engineering, and environmental sciences;**
- **The conduct of a broadly based exploratory and advanced development program in response to identified and anticipated Navy needs;**
- **The development of space systems for the Navy.**

CONTENTS

THE NAVAL RESEARCH LABORATORY

"I believe [that] the Government should maintain a great research laboratory, jointly under military and naval and civilian control. In this could be developed the continually increasing possibilities of . . . all the technique of naval progression ... .

"When the time came, if if ever did, we could take advantage of the knowledge gained through this research work and quickly produce the very latest and most efficient instruments ...."

Thomas A. Edison
The New York Times Magazine
May 30, 1915

THE NAVAL RESEARCH LABORATORY

Our Heritage

Today, when government and science seem inextricably linked, when virtually no one questions the dependence of national defense on the excellence of national technical capabilities, it is noteworthy that in-house defense research is relatively new in our Nation's history. The Naval Research Laboratory (NRL), the first modern research institution created within the United States Navy, began operations in 1923.

Thomas Edison's Vision—The first step came in May 1915, a time when Americans were deeply worried about the great European war. Thomas Edison, asked by a *New York Times* correspondent to comment on the conflict, argued that the Nation should look to science. "The Government," he proposed in a published interview, "should maintain a great research laboratory.... In this could be developed... all the technique of military and naval progression without any vast expense." Secretary of the Navy Josephus Daniels seized the opportunity created by Edison's public comments to enlist Edison's support. He agreed to serve as the head of a new body of civilian experts—the Naval Consulting Board—to advise the Navy on science and technology. The Board's most ambitious plan was the creation of a modern research facility for the Navy. Congress allocated $1.5 million for the institution in 1916, but wartime delays and disagreements within the Naval Consulting Board postponed construction until 1920.

The Laboratory's two original divisions, Radio and Sound, pioneered in the fields of high-frequency radio and underwater sound propagation. They produced communications equipment, direction-finding devices, sonar sets, and, perhaps most significant of all, the first practical radar equipment built in this country. They also performed basic research, participating, for example, in the discovery and early exploration of the ionosphere. Moreover, the Laboratory was able to work gradually toward its goal of becoming a broad-based research facility. By the beginning of World War II, five new divisions had been added: Physical Optics, Chemistry, Metallurgy, Mechanics and Electricity, and Internal Communications.

The War Years and Growth—Total employment at the Laboratory jumped from 396 in 1941 to 4400 in 1946, expenditures from $1.7 million to $13.7 million, the number of buildings from 23 to 67, and the number of projects from 200 to about 900. During the war, scientific activities necessarily were concentrated almost entirely on applied research. New electronics equipment—radio, radar, sonar—was developed. Countermeasures were devised. New lubricants were produced, as were antifouling paints, luminous identification tapes, and a sea marker to help save survivors of disasters at sea. A thermal diffusion process was conceived and used to supply some of the ^{235}U isotope needed for one of the first atomic

bombs. Also, many new devices that developed from booming wartime industry were type-tested and then certified as reliable for the Fleet.

NRL Reorganizes for Peace—Because of the major scientific accomplishments of the war years, the United States emerged into the postwar era determined to consolidate its wartime gains in science and technology and to preserve the working relationship between its armed forces and the scientific community. While the Navy was establishing its Office of Naval Research (ONR) as a liaison with and supporter of basic and applied scientific research, it was also encouraging NRL to broaden its scope and become, in effect, its corporate research laboratory. There was a transfer of NRL to the administrative oversight of ONR and a parallel shift of the Laboratory's research emphasis to one of long-range basic and applied investigation in a broad range of the physical sciences.

However, rapid expansion during the war had left NRL improperly structured to address long-term Navy requirements. One major task—neither easily nor rapidly accomplished—was that of reshaping and coordinating research. This was achieved by transforming a group of largely autonomous scientific divisions into a unified institution with a clear mission and a fully coordinated research program. The first attempt at reorganization vested power in an executive committee composed of all the division superintendents. This committee was impracticably large, so in 1949 a civilian director of research was named and given full authority over the program. Positions for associate directors were added in 1954.

The Breadth of NRL—During the years since the war, the areas of study at the Laboratory have included basic research concerning the Navy's environment of sea, sky, and space. Investigations have ranged widely from monitoring the sun's behavior, to analyzing marine atmospheric conditions, to measuring parameters of the deep oceans. Detection and communication capabilities have benefited by research that has exploited new portions of the electromagnetic spectrum, extended ranges to outer space, and provided means of transferring information reliably and securely, even through massive jamming. Submarine habitability, lubricants, shipbuilding materials, fire fighting, along with the study of sound in the sea, have also been steadfast concerns.

The Laboratory has pioneered naval research into space, from atmospheric probes with captured V-2 rockets, through direction of the Vanguard project—America's first satellite program—up to involvement in such projects as the Navy Global Positioning System. Today, NRL is the Navy's lead laboratory in space systems research, fire research, tactical electronic warfare, microelectronic devices, and artificial intelligence. NRL has also evaluated new issues, such as the effects of intense radiation and various forms of shock and vibration on aircraft, ships, and satellites.

Many significant accomplishments occurred in 1988, and a few are recorded here. Researchers at NRL demonstrated lasing at soft X-ray wavelenghs in copper and germanium plasmas that were heated by a high-power infrared laser. A broadly tunable, infrared color-center laser was also developed that shows promise for a wide range of military, industrial, and scientific applications. A team of scientists developed a photolithographic method that improves the quality of metallic meshes used in far infrared spectrometers and reflectors. The presence of radioactive cobalt in the massive cloud surrounding the recent supernova (1987A) in the Large Magellanic Cloud was detected by NRL scientists who were working with scientists at the University of New Hampshire and the Max Plank Institute for Extraterrestrial Physics in West Germany. New fluorinated polymers were developed at NRL that have unique and advantageous properties to fulfill many Navy needs both on land and at sea. As part of the NRL's long-term interest in space research, scientists and

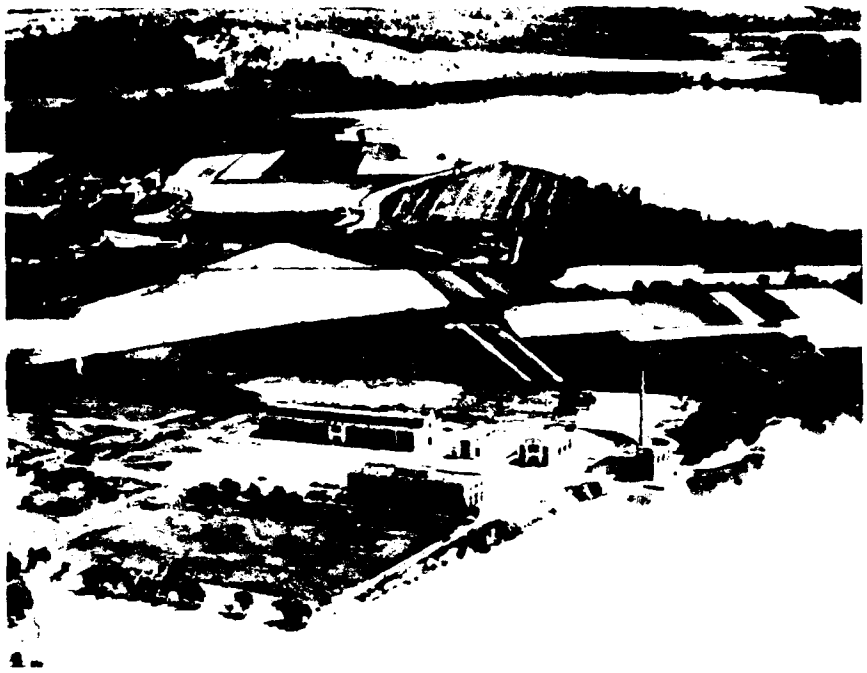

The original Naval Research Laboratory in 1923 as viewed from the Potomac River among the farmlands of Blue Plains

NRL today as viewed from the east

engineers have completed development of a second, more advanced Solar UV Spectral Irradiance Monitor (SUSIM) to further study solar ultraviolet (UV) radiation. Also completed was the development of the Oriented Scintillation Spectrometer Experiment (OSSE), which is part of NASA's Gamma Ray Observatory (GRO) mission.

One goal, however, has guided NRL's diverse activities through the years—to conduct pioneering scientific research and development that will provide improved materials, equipment, techniques, systems, and operations for the Navy, for the Department of Defense (DoD), and for the U.S. Government.

NRL Today

ORGANIZATION AND ADMINISTRATION

The position of NRL within the Navy is that of a field command under the Chief of Naval Research.

Heading the Laboratory with joint responsibilities are the naval commanding officer, Capt. William G. Clautice, and the civilian director of research, Dr. Timothy Coffey. Line authority passes from the commanding officer and the director of research to five associate directors of research and the director of one technology center. Research is performed in the following areas:

- Technical Services
- Business Operations
- General Science and Technology
- Warfare Systems and Sensors Research
- Materials Science and Component Technology
- Naval Center for Space Technology.

The first two directorates provide centralized technical support; the other four are responsible for executing NRL's research and development programs. Further details of the Laboratory's organization are given on the organizational chart appearing in the "General Information" Section.

NRL operates as a Navy Industrial Fund (NIF) activity. As a NIF activity, all costs, including overhead, must be charged to various research projects. Funding in 1988 came from the Chief of Naval Research, the Naval Systems Commands, and other government agencies, such as the Defense Advanced Research Projects Agency, the Department of Energy, and the National Aeronautics and Space Administration as well as several nongovernment activities. NRL's relationship to its sponsoring agencies, both inside and outside DoD, is defined by a comprehensive policy on interagency support agreements.

Besides funding for scientific work, NRL receives Navy monies for general construction, maintenance, and operations.

PERSONNEL DEVELOPMENT

At the end of 1988, NRL employed 3864 personnel—34 military officers, 8 enlisted men and women, and 3822 civilians. In the research staff, there are 791 employees with doctorate degrees, 340 with masters degrees, and 488 with bachelors degrees. The support staff provides administrative, computer-aided designing, machining, fabrication, electronic construction, publication, personnel development, information retrieval, large mainframe computer services, and contracting and supply management services to the research staff.

Opportunities for higher education and other professional training for NRL employees are available through several programs offered by the Employee Development Branch. These programs provide for graduate work leading to advanced degrees, advanced training, college course work, short courses, continuing education, and career counseling. Graduate students, in certain cases, may use their NRL research for thesis material.

For non-NRL employees, several post-doctoral research programs exist. There are also cooperative education agreements with several universities, summer and part-time employment

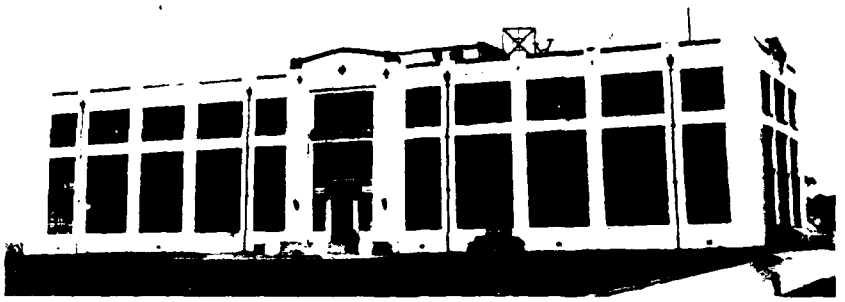

Building 1, circa 1923

The staff of NRL, circa 1935

programs, and various summer and interchange programs for college faculty members, professional consultants, and employees of other government agencies.

NRL has active chapters of Women In Science and Engineering, Sigma Xi, Toastmaster's International, and the Federal Executive and Professional Association. Three personal computer clubs meet regularly—Edison Atari, NRL IBM-PC, and Edison Commodore. An amateur radio club, a wives' club, a drama group—the Showboaters, and several sports clubs are also active. NRL has a recreation club that provides swimming, sauna, whirlpool bath, gymnasium, and weight-room facilities. The recreation club also offers classes in karate, aerobics, swimming, and cardiopulmonary resuscitation.

A community outreach program at NRL provides tutoring for local students, science fair judging, participation in high school and college career day programs, an art and essay contest during Black History Month, and a Christmas

party with donated gifts for disadvantaged children.

NRL has an active, growing Credit Union with assets of $116.5 million and a membership numbering 14,200. Public transportation to NRL is provided by Metrobus.

More information on these programs can be found in the *Review* chapter entitled "Programs for Professional Development."

SCIENTIFIC FACILITIES

In addition to its main campus of about 130 acres and 152 buildings, NRL maintains 12 other research sites and a Flight Support Detachment. The many diverse scientific and technological research and support facilities are described in the following paragraphs.

Research Facilities

- Space Science

NRL is the Navy's main laboratory for conducting basic research and development in the space sciences. The Space Science Division has a number of commitments for space experiments in the areas of upper atmospheric, solar, and astronomical research aboard NASA, DoD, and other space projects. Division scientists are involved in major research thrusts that include remote sensing of the upper atmosphere by using ultraviolet sensing, studies of the solar atmosphere by using spectrographic techniques, and studies of astronomical radiation ranging from the ultraviolet through the cosmic rays. The division maintains facilities to construct, assemble, and calibrate space experiments. A network of VAX computers, an array processor, image processing hardware, a PDS microdensitometer, and CRAY access are used to analyze and interpret space data. The division also includes the Radio Astronomy Branch, which uses its radio telescope at the Laboratory's Maryland Point site and its computational capability as represented by the Washington, DC Correlator Facility, and by the national radio astronomy facilities to conduct a broad program of radio astronomy.

Dr. David Mozurkewich of the Space Science Division is making delicate adjustments to an ultrahigh precision siderostat used for astrometric measurements with the Mt. Wilson Optical Interferometer. This instrument has led directly to a new project to build a similar interferometer that will become a mainstay of the Navy's astrometric program.

- Computational Physics and Fluid Dynamics

The Laboratory for Compuational Physics and Fluid Dynamics (LCP&FD) has developed a Graphical and Array Processing System (GAPS). The system provides communications and common memory for large simulations on parallel array processors and immediate displays of results from other sources on high-resolution, high-speed graphics monitors. The system is front ended by two VAX 11/780s that provide control and communication to other sites at NRL and outside laboratories. A 1.4-gigabyte high-speed disk is incorporated for simulations storage and replay. The computational engines are six 30-megaflop array processors supported by a vectorizing Fortran compiler. The current graphics devices are a Tektronix and a Metheus with 1024 × 1280 color raster resolution and high-speed block data transfer capability, and an IRIS 4D vector display.

The LCP&FD also maintains fluid dynamic laboratory facilities that include a 30-m wind/wave tank to study nonlinear ocean wave processes and fluid/structure interactions; a 20-m stratified tow channel to study geophysical flows, jets, and wakes; and blow-down water tunnels to study hydroacoustics, turbulent boundary layers, and non-Newtonion flows. Experimental efforts using these facilities are supported by flow measurement systems including multicomponent laser

velocimeters and anemometers; digital image processing of flow visualization; hydrophones; imaging infrared radiometers; and a variety of microwave radar measurement systems for remote sensing studies of hydrodynamic processes. On-line experiment control, data acquisition, and processing are achieved with a central HP1000 system or one of a number of smaller, portable units.

• Condensed Matter and Radiation Sciences

Ion Implantation Facility—The facility consists of a 200-keV ion implanter with specialized ultrahigh vacuum chambers and associated *in situ* specimen analysis instrumentation. The facility is used to develop advanced surface treatments of materials to modify their properties and improve corrosion and wear resistance.

3-MeV Tandem Van de Graaff—This facility is used to study charged particle radiation damage effects such as occur in space, to perform Rutherford backscattering spectroscopy and nuclear reaction analysis to provide high-sensitivity composition depth profiles, and to perform MeV energy implants in materials.

65-MeV Electron Linear Accelerator (LINAC)—The LINAC produces intense electron beams with 10 to 65 MeV energies. Pulse rates from 1 to 360 s and widths from 50 ns to 1.4 μs are selectable. This facility is widely used to study radiation effects on microelectronics and materials for both NRL and other important DoD satellite and missile programs. It is also used to study radiation effects on the new high critical temperature superconductors. Single beam pulses can be analyzed and stored in a fast multichannel digitizer system. Plans for the future also include making available a narrow, 3-ns pulse and increasing the beam current on all pulse widths. The goal is to obtain a dose rate of 10^{12} rads (Si)/s.

Hypervelocity Impact Facilities—Three facilities are used for ballistics research at speeds exceeding 6 km/s with toxic or explosive targets. The projectile velocity, orientation, and dynamic projectile-target interaction can be measured.

Building 60 houses a portion of the Condensed Matter and Radiation Sciences Division

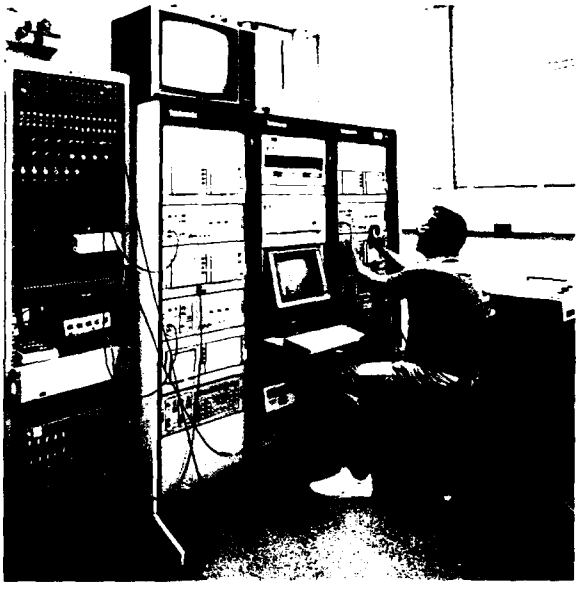

Bob Farr of the Condensed Matter and Radiation Sciences Division sets up the digitizer system for user data collection

Synchrotron Radiation Facility—An intense monochromatic X-ray photon source, tunable from 4 to 12 keV, is available on the NRL-developed beam line at the National Synchrotron Light Source at Brookhaven National Laboratory. Environmental target chambers can span a pressure range from ambient to several hundred kbar and temperatures from 10 to 1500 K. A six-circle computer controlled goniometer is used to control and position targets.

• Plasma Physics

The Plasma Physics Division is the major center for in-house Navy and DoD plasma physics research. The division is involved in theoretical space plasma studies related to communications' effectiveness and in programs with experimental counterparts. These experimental programs include development of pulsed sources to generate electron and ion beams, powerful discharges, and various types of radiation. The largest of these pulsers, GAMBLE II, is used to study the production of megampere electron beams and for producing very hot, high-density plasmas. Other generators are used to produce particle beams that are injected into magnetic fields and/or cavities to generate intense microwave pulses. A charged particle beam (CPB) propagation facility exists for testing advanced, CPB propagation (both endo- and exoatmospheric) concepts. A 5-MW generator injects pulses of electron current into preheated ionization channels to study the effectiveness of propagation under various conditions. An extremely high power laser, PHAROS III, is used in inertial fusion research and in high-altitude nuclear explosion effects studies. This divison also operates a modified betatron facility for the study of methods to accelerate high-current electron beams to energies in the 25 to 50 MeV range.

• Acoustics

NRL's facilities in support of acoustical investigations are located at the main Laboratory site and in Orlando, Florida at the Underwater Sound Reference Detachment (USRD). At the main Laboratory site, there are two research tanks instrumented to study echo characteristics of targets and to develop devices. There is also an underwater acoustic holography facility for research in acoustic fields and a water tunnel having a large blow-down channel with a 15-m test section used for acoustic and flow-induced vibration studies of towed line arrays and flexible cables. For acoustic surveillance array processing and acoustic data processing, researchers have access to the multichannel, programmable, digital data processing system—a system of DEC computers, high-speed array processors, and peripherals for up to 256 channels. The Connection Machine, an experimental facility that exploits the natural computational parallelism inherent in data-intensive research problems, has been established for use by researchers both within and outside the Laboratory. The USRD facilities are described with NRL's field stations.

This radar display facility is for testing, demonstrating, and improving the engineering of non-NTDS shipboard radar displays

• Radar

NRL has gained worldwide renown as the "Birthplace of Radar" and has maintained its reputation as a leading center for radar-related research and development for a half century. An impressive array of facilities managed by NRL's Radar Division continues to contribute to this reputation. These include land-based, airborne, and laboratory radar cross section measurement systems; an airborne APS-116 radar with ISAR image processing; and an airborne adaptive array laboratory. Also, the division manages and maintains a radar display test bed, an IFF ground station, a digital signal processing facility, a digital image processing laboratory, and a radar cross section prediction facility. A radar research and

development activity is located at the Chesapeake Bay Detachment (CBD), Randle Cliff, Maryland. It has separate facilities for specific types of systems that range from high-frequency, over-the-horizon systems to millimeter wave radars. The SENRAD radar test bed, a flexible and versatile system for demonstrating new developments in radar, is also located at CBD.

• Information Technology

The Information Technology Division, which includes the Navy Center for Applied Research in Artificial Intelligence, is at the forefront of DoD research and development in telecommunication, computer science, and artificial intelligence. The division maintains a local area computer network to support its research.

The network comprises VAX 11/750s, 780s, a Gould 9005 UNIX machine, Symbolics, LMI and Xerox Dolphin LISP machines, SUN and ISI work stations, laser printers, network gateways, and terminal servers. A Butterfly 128-node parallel processor is also part of the division's computer resources. The network is connected to NRL's Central Computing Facility and to the MILNET, ARPANET, and other university networks. The network will become part of the Strategic Defense Initiative (SDI) Battle Management Technology validation facility.

• Electronic Warfare

The scope of research and development at NRL in the field of electronic warfare covers the entire electromagnetic spectrum, from basic technology research to component and subsystem development to system design and effectiveness evaluation. Major emphasis is placed on providing the method and means to counter enemy's hostile actions in all phases of battle, from the beginning when enemy forces are mobilized for an attack to the final stages of the engagement. For this purpose, NRL has extensive research and development laboratories, anechoic chambers, and modeling and simulation facilities. NRL is also in the process of adding extensive new facilities where scientists can focus on the coordinated use of all organic defensive and offensive resources now present in the Fleet.

Ed Claybaugh, Peggy Toot, and Alvin Cross, of the Tactical Electronic Warfare Division (left to right), work to design, test, and fabricate decoy vehicles

Building 210 houses the Tactical Electronic Warfare Division

• Laboratory for the Structure of Matter

The Laboratory investigates the atomic arrangement of matter to improve old materials or to invent new materials. Various diffraction methodologies are used to make these investigations. Subjects of interest include the structural and functional aspects of energy conversion, ion transport, device materials, and physiologically active substances such as drugs, antibiotics, and antiviral agents. Theoretical chemistry calculations are used to complement the structural research. A real-time graphics system aids in modeling and molecular dynamics studies.

Dr. Nagarajan Pattabiraman of the Laboratory for Structure of Matter uses high-resolution graphics computers to model biomolecules such as proteins, nucleic acids, and lipids

• Chemistry

NRL has been a major center for chemical research in support of Navy operational requirements since the late 1920s. The Chemistry Division continues its tradition with a broad spectrum of basic and applied research programs concerned with fuels and combustion, corrosion, advanced polymeric materials, ultrasensitive detection methods for chemical agents, special materials for electronic warfare applications, and biomolecular engineering research. Modern facilities for research include a wide range of the most modern optical, magnetic, and ion-based spectroscopic devices, a 325 m^3 (11,400 ft^3) fire research chamber (Fire I), multiple facilities for materials synthesis and physical/chemical characterization, high- and low-temperature equipment, and extensive surface-analytical instrumentation. The division has recently developed the 475-ft ex-*Shadwell* (LSD-15) into an advanced fire research ship.

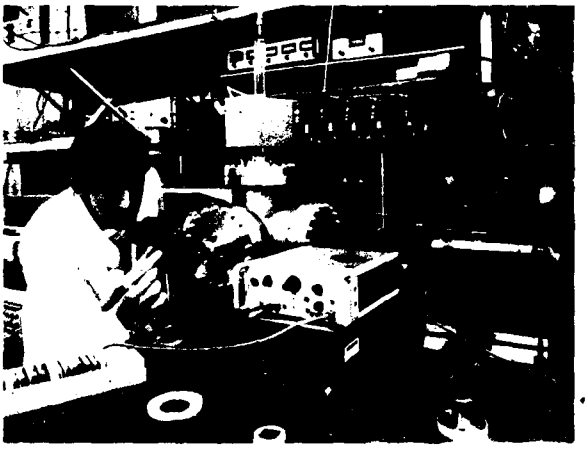

Dr. Francis Celii, an NRL/NRC postdoctoral student working in the Chemistry Division, is using laser diagnostics to study the chemistry of diamond growth from gases.

• Materials

NRL has capabilites for X-ray and electron diffraction analysis and for electron and Auger spectroscopy. It has a high-performance, secondary ion mass spectrometer for surface analysis and significantly extends the diagnostic capability of the technique. A high-resolution, high-performance, reverse-geometry mass spectrometer is used to probe reactions between ions and molecules. The Laboratory has fracture and fatigue testing machines with capacities to

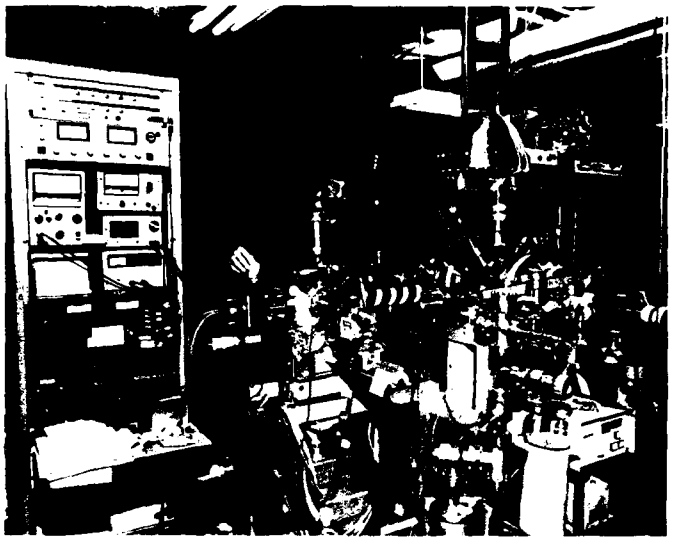

Dr. Berend Jonker, Materials Science and Technology Division, observes growth of single crystal magnetic films on semiconductor substrates for electronic applications.

272,000 kg, an ultrasonic gas atomization system that has a molten alloy capacity up to 5 kg with a gas inlet pressure capacity of up to 27.6 MPa, and hot isostatic press facilities. The Laboratory's cryogenic facilities include dilution refrigeration equipment and superconducting magnetic sensors for measuring ultrasmall magnetic fields.

• Optics

Ultralow-Loss, Fiber-Optic Waveguides—NRL has developed record-setting ultrahigh transparency infrared waveguides. These fluoride glass materials offer the promise of long-distance communications without the need of signal amplification or repeaters.

Focal Plane Evaluation Facility—This facility has extensive capabilities to measure the optical and electrical characteristics of infrared focal plane arrays being developed for advanced Navy sensors.

IR Missile-Seeker Evaluation Facility—This facility performs open-loop measurements of the susceptibilities of infrared tracking sensors to optical countermeasures.

Large Optic, High-Precision Tracker—NRL has developed a tracker system with an 80-cm primary mirror for atmospheric transmission and target signature measurements. By using a quadrant detector, the servo system has demonstrated a 12-μrad tracking accuracy. An optical correlation tracker system tracks objects without a beacon.

High-Energy Pulsed Hydrogen Fluoride, Deuterium Fluoride Laser—NRL has constructed a pair of pulsed chemical lasers each capable of producing up to 30 J of laser energy at 2.7 to 3.2 μm and 3.8 to 4.5 μm in a 2-μs pulse. This facility is used to investigate a variety of research areas including stimulated Brillouin scattering, optical phase conjugation, pulsed laser amplification, propagation, and beam combining.

Fiber-Optics Sensors—The development and fabrication of fiber-optic sensor concepts, including acoustic, magnetic, and rate-of-rotation sensors, are conducted in several facilities within the Laboratory's Optical Sciences and Acoustics Divisions. Equipment includes facilities for evaluating optical fiber coatings, fiber splicers, an acoustic test cell, a three-axis magnetic sensor test cell, a rate table, and various computers for concept analysis.

Dr. Gerald M. Borsuk, Superintendent of the Electronics Science and Technology Division, spearheads the research on basic physical phenomena related to solid-state and vacuum electronics. He also serves as ONR subelement monitor for electronics, is the NRL block manager for electronics and electro-optics, and is the Navy's deputy program manager and technical director for the DARPA/Tri-Service MIMIC Program.

Dr. Joseph E. Blue is the superintendent and civilian officer in charge of the Underwater Sound Reference Detachment in Orlando, FL. Dr. Blue is a Fellow of the Acoustical Society of America and a member of the Society of Exploration Geophysicists where he served on a working group that wrote the Marine Geoacoustic Standards.

Dr. Barry Feldman, head of the Laser Physics Branch, operates an NRL-designed Nd:YALO laser that has been frequency converted to exactly match the cesium atomic resonance filter in the blue-green. The Nd:YALO laser represents the only solid-state laser compatible with diode pumping that accesses the cesium filter resonance and as such is a leading candidate for underwater laser communications.

Dr. Robert R. Meier is the head of the Upper Atmospheric Physics Branch. His research experience encompasses numerous topics in upper atmospheric physics such as auroras, comets (Kohoutek, West, and Halley), the ionosphere and magnetosphere, radiative transfer theory, and remote sensing. He is currently co-investigator on the RAIDS, HIRAAS, UVLIM, and MAHRS missions.

Digital Processing Facility—This facility is used to collect, process, analyze, and manipulate infrared data and imagery from several sources.

Emittance Measurements Facility—NRL routinely performs measurements of directional hemispherical reflectance from 2 to 16 μm in the infrared by using a diffuse gold integrating sphere and a Fourier Transform Spectrophotometer (FTS). Sample temperatures can be varied from room temperature to 250°C and incidence angles from 0° to 60°.

• Electronics Science

In addition to specific equipment and facilities to support individual scientific and technology programs in electronics and electronic-materials growth and analysis, NRL operates two major central facilities that provide services to electronics programs throughout the Laboratory and to external organizations. The latter two facilities are the nanoelectronics processing facility and the high magnetic field facility.

Nanoelectronics Processing Facility—This facility provides support for NRL programs that require microelectronics processing skills and equipment. The facility recently acquired a nanowriter that fabricates nanoscale (80 Å) structures and, in general, supplies NRL programs with a range of items from discrete structures and devices to complete integrated circuits with very large scale integration (VLSI) complexity based on silicon metal oxide semiconductors (MOS) submicrometer technology.

High Magnetic Field Facility—This facility is used to support research projects throughout NRL, DoD, and, to a limited extent, the local scientific community. The facility provides the capability to determine the response of materials and devices to high magnetic fields up to 17 T with a variety of electrical, optical, and magnetic probes.

• Naval Center for Space Technology

In its role as a center of excellence for space systems research, NRL establishes and supports the development of spacecraft, systems that use these spacecraft, and their ground command and control stations. The Naval Center for Space Technology (NCST) designs, builds, analyzes, tests, and operates spacecraft, as well as identifies and conducts promising research to improve spacecraft and their support systems. NCST facilities that support this work include large and small anechoic radio frequency chambers, clean rooms, shock and vibration facilities, an acoustic reverberation chamber, large and small thermal/vacuum test chambers, and modal analysis test facilities. NCST has a 31-m, computer-controlled wind and wave tank and special airborne instrumentation for developing electromagnetic remote sensing systems; a facility for long-term testing of satellite clock time/frequency standards under thermal/vacuum conditions linked to the Naval Observatory; a 5-m optical bench laser laboratory; and a hologram research laboratory to conduct research in support of the development of space systems.

Research Support Facilities

• Engineering Services

The Engineering Services Division (ESD) provides NRL and other Navy laboratories with engineers/technicians and highly skilled mechanics to support research projects.

Joel Golden and Sungjoo Park design and test circuits in one of the Engineering Services Division's laboratories by using microprocessor development systems

ESD personnel work with the researchers on freehand sketches or detailed drawings according to MILSTD requirements and NASA standards. ESD's personnel perform a broad spectrum of tasks such as engineering analysis; fabrication of heavy structures; design and fabrication of original electronic devices and instruments; the computerized production of dense, printed circuit boards; and conventional/numerically controlled machining.

ESD has extensive shop capabilities for sheet metal fabrication, machining, and electroplating. It has a plastics shop where devices and forms are fabricated or molded from laminates, polymers, fiberglass, and plastics. ESD also operates a foundry where heat treating of metals, castings, and sand-blasting jobs are performed.

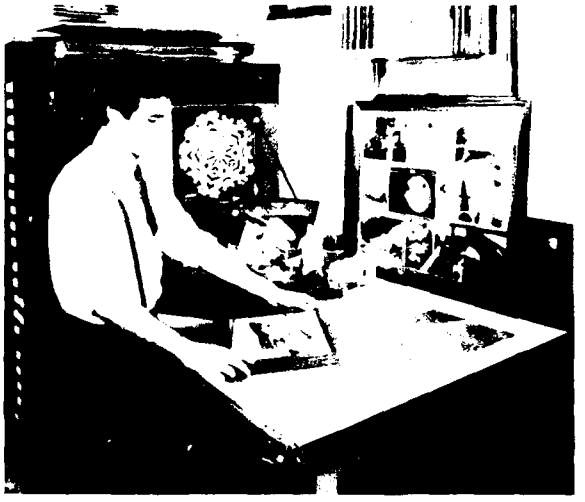

Micheal McMullin, Technical Information Division, evaluates a photograph for a composite

• Technical Information Services

The Technical Library contains more than one million items including 2000 current journals. The collection can be accessed by computer-based catalogs. The Library also provides interlibrary loans, on-line literature searches, loans of microcomputer software, and a variety of reference services.

Publication services include writing, editing, composition, phototypesetting, and publications consultation. The primary focus is on using computer-assisted publication techniques to produce scientific and technical information containing complex artwork and equations.

Graphic services include presentation and publications artwork.

Photography services include motion picture, video, and still-camera coverage for data documentation both at NRL and in the field.

Information specialists prepare written and visual materials for dissemination to the public, for use at exhibitions, professional meetings and seminars, and for internal information.

The DICOMED computer graphics system produces high-resolution, high-quality color images on 35-mm slides, 8 × 10 in. viewgraphs, 16-mm movies, or microfiche. It is driven by tapes generated on many different computer systems.

• Central Computing Facility

The Central Computing Facility (CCF) consists of a Cray X-MP/24 Class 6.5 supercomputer supported by five DEC/VAX 700/8000 front-end processors. The Class 6.5 supercomputer is a balanced vector and a very high-speed scalar processor. The peak processing speed of the two processor Class 6.5 supercomputer is 488 million floating point operations per second (MFLOPS) with a sustainable speed of 105 MFLOPS per processor. It has four million (64-bit) words of static MOS memory in sixteen interleaved banks, and three interconnected I/O processors with four million words of shared buffer memory.

The Class 6.5 system is accessed by VAX minicomputers at the central computing site, by local area networks, by the Defense Data Network (MILNET/ARPANET), and by SURANET/NSFNET at remote sites. The front-end systems recognize and exploit the features of typical modern terminals whether they are connected by dial-up, direct line, local area networks, or DDN/MILNET. It also provides data base management, document processing, and graphics support. FORTRAN, PASCAL, C, and ADA are

the primary programming languages for the Class 6.5 system. A wide range of scientific, statistical, and mathematical software is also available. MAC NASTRAN and ABAQUS are available on the Cray. PATRAN and ABAQUS are available on the front ends.

A high-quality, high-performance pen plotter and a high-speed electrostatic plotter/printer are available. Plots can also be previewed on graphics terminals. Plotting software can generate tapes for the DICOMED system, located in the Technical Information Division.

FIELD STATIONS

NRL has acquired or made arrangements over the years to use a number of field sites or auxiliary facilities for research that cannot be conducted in Washington, DC. They are located in Maryland, Virginia, California, and Florida. The two largest facilities are the Chesapeake Bay Detachment (CBD) and the Underwater Sound Reference Detachment (USRD).

• Chesapeake Bay Detachment (CBD)

CBD occupies a 168-acre site near Chesapeake Beach, Maryland, and provides facilities and services for research in radar, electronic warfare, fire research, optical devices, materials, com- munications, and other subjects. Because of its location on the west shore of the Chesapeake Bay, unique experiments can be performed. Radar antennas 50 to 60 m above the water overlook the bay. Another site, Tilghman Island, is 16 km across the bay from CBD and in a direct line of sight from CBD. This creates a unique environment for low clutter and generally low background radar measurements. Experiments involving dispensing chaff over water and radar target characterizations of aircraft and ships are examples of military-oriented research. Basic research is also conducted in radar antenna properties, testing of radar remote sensing concepts, use of radar to sense ocean waves, and laser propagation.

• Underwater Sound Reference Detachment (USRD)

Located at Orlando, Florida, USRD functions in many ways like a standards bureau of underwater sound and also performs R&D for sonar transducers and related acoustic materials. Its semitropical climate and two clear, quiet lakes (the larger 11-m deep and nearly circular) are distinct assets to its research and development on sonar transducers and underwater reference standards and to its improvement of techniques to calibrate, test, and evaluate underwater acoustic devices. USRD has an anechoic tank for simulating ocean depths to 700 m and smaller pressure tanks for simulating depths to 7000 m. A spring-fed lake located in a remote area about 40 miles north of USRD, (the Leesburg Facility) provides a natural tank for water depths to 52 m with an ambient noise level 10 dB below that for sea state zero; larger objects can be calibrated here. The detachment has provided acoustic equipment and calibration services not only to hundreds of Navy activities and their contractors but also to private firms and universities not engaged in DoD contracts.

• Marine Corrosion Test Facility

Located on Fleming Key at Key West, Florida, this facility offers an ocean air environment and clear, unpolluted, flowing seawater for studies of environmental effects on materials. Equipment is available for experiments involving weathering, general corrosion, fouling, and electrochemical phenomena, as well as coatings, cathodic protection devices, and other means to combat environmental degradation.

• Other Sites

Some field sites have been chosen primarily because they provide favorable conditions to operate specific antennas and electronic subsystems and are close to NRL's main site. Maryland Point, south of NRL, operates two radio

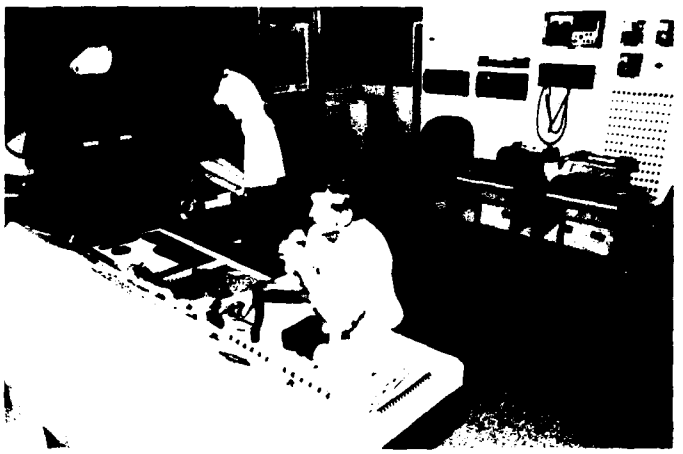

Commander S. Kummer and Mr. B. Bratschi in the control room in Building 1 at the Chesapeake Bay Detachment (CBD). The control room is used to communicate with ships and airplanes operating near CBD.

Aerial view of Pomonkey, Maryland. At the site, a free space antenna range exists to develop and test a variety of antennas

Two of the uniquely configured P-3 aircraft used in airborne research at NRL's Flight Support Detachment located at the Naval Air Station, Patuxent River, Maryland

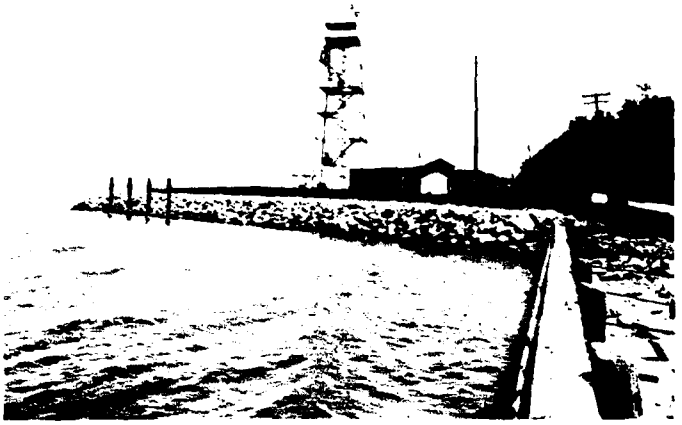

The Tilghman Island site is 16 km across the bay from CBD and in a direct line of sight from it, thus creating a unique environment for low clutter and generally low background radar measurements

This radio telescope, located at Maryland Point, Maryland, is one of two used for high-precision radio astronomy research

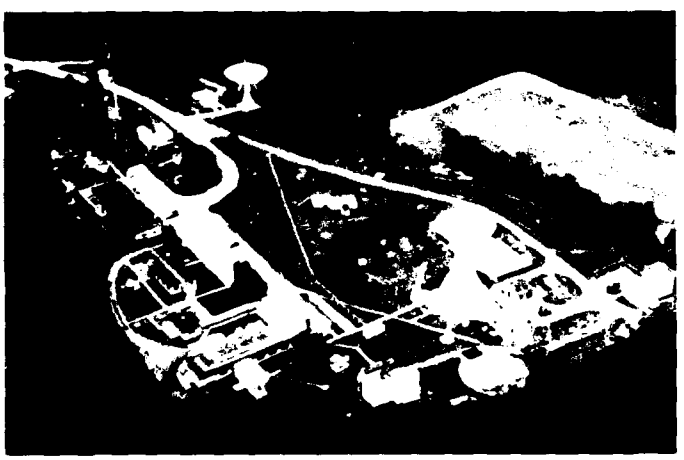

NRL's Waldorf, Maryland facility operates X-band and S-band Antennas for space and communications research

telescopes (25.6 and 26 m in diameter) for radio astronomy research. NRL's Waldorf Facility, south of NRL, operates 18.3-m, X-band and S-band antennas for space and communications research. Pomonkey, a field site south of NRL, has a free-space antenna range to develop and test a variety of antennas. The antenna model measurement range in Brandywine, Maryland, has a 4.6-m diameter turntable in the center of a 305-m diameter ground plane for conducting measurements on scale-model shipboard and other antenna designs.

• Research Platforms

NRL uses ships and aircraft to conduct some of its research. For airborne research, NRL uses four four-engine turboprop P-3 Orion aircraft. These airplanes annually log over 2300 hours of flying time on a wide variety of projects ranging from bathymetry and electronic countermeasure research to studies of radar signal reflections. Oceangoing research ships are obtained from a pool of vessels maintained by the Naval Oceanographic Office, Bay St. Louis, Mississippi.

NRL in the Future

To continue its growth and provide preeminent research for tomorrow's Navy, NRL must maintain and upgrade its scientific and technological facilities at the forefront. Its physical plant to house these facilities must also be adequate. NRL recently embarked on a Corporate Facilities Investment Plan (CFIP) to renew its physical plant. This plan and future facility plans are described below.

THE CORPORATE FACILITIES INVESTMENT PLAN (CFIP)

The CFIP is a financial spending plan to provide modern research facilities at NRL by the year 2000. The plan calls for both Congressional and Laboratory investment and is updated and altered as changes occur in scientific emphasis and congressional attitude. Over the past several years, congressionally approved military construction (MILCON) funds were used to construct the new Electro-Optics laboratory and to complete the final phase of the Tactical Electronic Warfare facility. At this time, funds are being requested to build a second wing to the Electro-Optics building and a facility to house the Naval Center for Space Technology.

In the past years, NRL general and administrative (G&A) funds were used to renovate Buildings 16, 32, 34, 35, 46, 47, 56, 58, and major portions of several other buildings. Approximately $4 million of Laboratory funding is budgeted for modernization each year.

• Electro-Optics Laboratory

Construction of a new electro-optics laboratory building (Phase I), has recently been completed. The new building provides 3359 m^2 (37,000 ft^2) of prime space for NRL. It includes structurally isolated, vibration-free, electro-optics laboratory rooms; class 100 clean suites; a 7.32-m fiber draw tower; electromagnetic shielding; vaults and computational facilities; and 24-h temperature, humidity, and pressure control. Completion of the second phase (Phase II) of construction is slated for 1990.

• Plasma Physics Facilities

A major, 2-kJ krF-laser facility will be established in the Plasma Physics Division by the end of FY 92. This facility is being initiated to provide intense radiation for studying inertial confinement fusion target heating at short wavelenghts.

• General-Purpose Laboratory

The Department of the Navy will be asked to program construction of a general-purpose laboratory in the future. This environmentally controlled facility will provide stringently clean

laboratories with carefully controllable temperature, humidity, ambient dust, and power for investigations in the rapidly evolving fields of electronic technology and composite materials synthesis and exploitation.

• EW Optical Integration Laboratory

An optical integration laboratory facility will be incorporated into expanded Tactical Electronic Warfare Division spaces. This facility will accommodate experimental optical and electronic capabilities that will enable the integration of critical technologies essential to enhanced electronic warfare capability. These spaces and the specialized optical assembly and electronic warfare evaluation equipment will be used as a staging facility providing for effective realistic evaluation early in the development cycle.

• Coordinated EW Simulation (CEWS) Laboratory

The CEWS Laboratory construction project (MILCON P-380) began in FY-1986. It will provide the Navy with significant new force level simulation capabilities to assess and optimize the coordinated use of distributed U.S. EW systems in battle group engagement situations to oppose threat activities coupled across all combat stages, i.e., force coordination, surveillance, targeting, and terminal homing of missiles. EW decision nodes and EW system operators will be key elements in real-time closed loop simulations. The new R&D complex will permit simulated operational evaluation of new cooperative EW concepts, techniques, tactics, strategies, and the quantitative assessment of the contributions of individual EW systems' upgrades and improvement programs.

This new facility, scheduled for completion in April 1989, will also eliminate the need for much of the very expensive at-sea and in-air EW system tests and evaluations and will provide better focus and understanding for those that are conducted. It will support and expedite R&D by permitting evaluation of system concepts and techniques before actual hardware R&D is begun; it will also optimize performance during development.

• Midway Research Center

NRL's newest field site, the Midway Research Center (MRC), is located on a 158-acre site in Stafford County, Virginia. Located adjacent to the Quantico Marine Corps Base, the MRC consists of a 5000 ft^2 operations/ administration building and two of three programmed 60-ft diameter parabolic antennas housed in 100-ft radomes. The third MRC antenna is scheduled for construction in the 1990-91 timeframe. When completed, the MRC, under NRL Code 8000, will provide NRL with a state-of-the-art facility dedicated solely to space communications and research.

• Electronics Science and Technology

An enhanced effort in narrow energy gap semiconductors has been initiated, and a new molecular beam epitaxy (MBE) machine is on order for this program. Continued improvement of the Nanoelectronics Processing Facility will include greater capability in the processing of GaAs and development of techniques to fabricate nanoscale (80 Å) structures with the recently acquired nanowriter.

• Fire Research Facility

Construction is under way at the Fire Research Facility at CBD to expand the current facilities. Once completed the facility will have a 50 × 50 × 50-ft burn building with an attached control center, three lab/office complexes of about 2500 ft^2 each, and a new, large, concrete minideck (to simulate air-capable ship decks) for expanded large-scale firefighting studies. FIRE-I, NRL's 325-m^3 (11,400-ft^3) pressurizable fire research chamber, is being relocated to this site.

• Radar Mode Test System

The Radar Division has acquired the Radar Mode Test System to evaluate the performance of NATO compliant Mark XI IFF radar mode (RM)

equipment. It has been used to test equipment from the United Kingdom and will have application to the evaluation of NRL and contractor developed RM equipment

• Fourier Transform Spectroscopy Facility

This facility in the Condensed Matter and Radiation Sciences Division consists of a dynamically aligned Michelson Fourier transform spectrometer with sources, beam splitters, and detectors capable of covering the range 5 to 50,000 cm^{-1} (2000 to 0.2 μm). A cryostat, cryostat manipulator, and reflectance accessory—all of special design—enable serial transmission and reflectance studies to be carried out on the same sample between 4 and 400 K without breaking the vacuum. The facility is currently used for studies of the electromagnetic properties of solid materials.

REHABILITATION OF SCIENTIFIC FACILITIES

Specialized facilities are being installed or upgraded in several of the research and support divisions.

• Information Technology

An expanded computer network is being planned to provide access to a computer from the office to each researcher in the division. Special test facilities are also being planned along with test-beds in support of specific R&D tasks. Facilities to support human-computer interaction research will include an eye monitoring system, touch screens and tablets, speech I/O hardware, high-resolution graphic displays, a 6-D tracker, and a wall-size display.

• Plasma Physics

An inductive energy storage facility, PAWN, is being upgraded to increase the output power from 0.1 up to as much as 1.0 terawatt. This facility will be more than an order of magnitude more compact than similar generators when final development stages are completed. PAWN will be used for intense electron and ion beam generation research and in X-ray laser development. A low-frequency (300 MHz to 10 GHz), high-power microwave facility, which uses a relativistic klystron concept, is being upgraded to produce multigigawatt coherent radiation pulses. A new laser facility is also planned. It will use a powerful KrF laser and a target chamber to conduct inertial confinement fusion research.

• Engineering Services

An advanced technology and fabrication facility is being planned. It will be used to study fabrication methods by using new and/or unusual materials, processes, and techniques (such as powdered-metal mixtures, ion implantations, various composites, and laser machining of composites) developed by NRL research divisions or other Navy laboratories. Longer range plans call for new machines: both computer-controlled drives by our new computer-aided device/computer-aided manufacture (CAD/CAM) system, and human-controlled drives with enhanced precision capability using new and unusual material fabrication.

• Radar

The Radar Division has installed a Computer-Aided Engineering (CAE) facility to aid in digital system design. The system has seven full-color graphics workstations to provide capabilities for circuit design and simulation and printed circuit board layout. The facility has been used to design systems based on commercially available components as well as advanced systems incorporating VHSIC and gate array technologies. It has proven to be a valuable tool in evaluating new technologies for radar signal-processing requirements.

The facility is currently being expanded to include three Sun workstations and ADAS software, which will allow designs to be modeled

and simulated at the system level. Future plans call for acquiring VHDL (VHSIC Hardware Description Language) software for the workstations, which is supported by ADAS. This would provide designers with an integrated toolset to model and simulate their designs from the system level down to the device level.

- Acoustics–Target Research Tank

Tank facilities for acoustic target research in the Acoustics Division will be significantly expanded to extend the range of target sizes. The expanded model tank is planned to contain a water volume of approximately 30,000 m^3.

- High–Pressure Acoustic Test Facility

A new tank facility at NRL's Underwater Sound Reference Detachment (USRD) in Orlando, Florida, will be used for underwater acoustic–materials research, development, test, and evaluation of much larger objects at significantly increased pressures and lower frequencies. This new tank is patterned after the smaller, lower pressure anechoic tank that has been used to develop virtually every submarine and torpedo transducer in the Fleet today. It will be operational in 1990 and will simulate ocean depths to 2100 m.

- Explosive Shock Test Facility for Sonar Transducers

Currently, some sonar transducers undergo explosive shock testing in open–water facilities and are often calibrated in USRD's Anechoic Tank Facility before and after undergoing shock tests. These will reduce the development time of transducers up to 12 months, substantially reduce the cost of shock tests, and provide basic research tools. This new facility will become operational in 1989.

Further Information: The NRL Fact Book gives more details about the Laboratory and its operations. It lists major equipment, current fields of research, field sites, and outlying facilities, and it also presents information about the responsibilities, organization, key personnel, and funding of the divisions, detachments, and other major organizational units.

Information on the research described in this *Review* may be obtained by contacting Dr. George Abraham, Head, Technology Transfer and Special Programs, Code 1003.2, (202) 767–3744. General information about NRL may be obtained from Information Services, Code 2610, (202) 767–2541. The sources of information on the various nonresearch programs at NRL are listed in the *Review* chapter entitled "Programs for Professional Development."

HIGHLIGHTS OF NRL RESEARCH IN 1988

Ocean Acoustics and System Performance

A nonredundant, high-speed technique for generating acoustic wave equation solutions for changing, complex ocean environments was developed to aid in predicting sonar performance. This approach takes advantage of precalculation of stable ocean acoustic quantities that reduces the final wave equation solution procedure to one of rejuggling partial wave equation solutions.

***

Suppressing Electromagnetic Interference

An additive for Navy haze gray paint markedly decreases the intermodulation interference caused by the nonlinear "mixing" of two or more radio frequency signals, a phenomenon most acute in the high-frequency communications bands. Considerable improvements in maintenance costs and performance are expected from increased use of this coating.

***

Magnetic Metal Superlattices

Synthetic ferromagnetic/silver crystals in thin film form prepared on a GaAs substrate have potential application to nonvolatile, radiation-hard memory devices because of the changed magnetic properties of the very thin iron layers as compared to bulk crystals.

***

Modeling of Ambient and Ship-Generated Waves

A model for ocean and ship wake/wave hydrodynamics has been developed that includes the prediction of ship wake modifications, ambient wave modifications, wave-breaking, and ship-generated Kelvin waves. This development enhances the Navy's capability to predict the disturbance signature of transiting surface ships.

***

Brillouin Scattering of a Pulsed Hydrogen Flouride Laser

Demonstration of the multiline simulated Brillouin scattering and phase conjugation of the entire spectral output of pulsed hydrogen fluoride laser radiation is a major development in the SDI effort to coherently beam combine the output of multiaperture HF laser amplifiers.

***

Relativistic Klystron Amplifier

New, high-power RF klystron-like amplifiers have been developed that use modulated intense relativistic electron beams exceeding 10 gigawatts of power. One application is to coherently combine RF pulses from many high-power RF amplifiers.

***

Macromolecular Structure Determination

An exact linear system of simultaneous equations for the analysis of macromolecular structures is being used to increase the range, speed, and ease of performing structure determinations. The system is being expanded for use in industrial and biomedical research and in protein and genetic engineering.

***

Nearfield Holography for Studying Modal Vibration in Underwater Structures

A generalized nearfield holography technique has been developed for the noncontact measurement of the vibration of cylindrical underwater structures. This technique provides accurate, high-spatial-resolution mapping of the normal velocity of the surface of a vibrating structure. This technique enables better understanding of how complex underwater targets produce detectable echoes and noise.

***

HF Heating of the Auroral Ionosphere

Modification of the auroral ionosphere was observed during HF heating experiments, and it was demonstrated that even very small ionospheric changes can be monitored satisfactorily with a relatively small, transportable measuring device.

***

Radioactive Cobalt in a Supernova in the Large Magellanic Cloud

Gamma-ray lines at 847 and 1238 keV from radioactive cobalt have been detected in a recent Magellanic supernova explosion (1987), thus confirming that supernovae are the source of heavy elements. This detection indicates that the cobalt is dispersed throughout the supernova envelope and has led to the detection of other radioactive elements.

The color photographs on these four pages represent some of NRL's scientific and engineering results and state-of-the-art equipment.

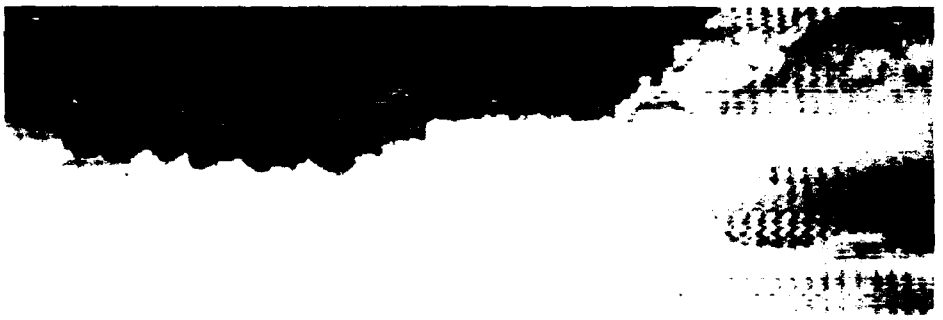

Pseudocolored image of clouds obtained with the NRL IRAMMP infrared sensor aboard a P–3 aircraft. The wavelength region is 8 to 12 μm. (E. Stone, Code 6521)

Computer–generated synthetic cloud images projected on the continent of Europe are used in a study of the effectiveness of infrared surveillance from space against aircraft flying at varying altitudes. Pie graphs indicate the percentages of high, medium, and low clouds. (E. Stone, Code 6521)

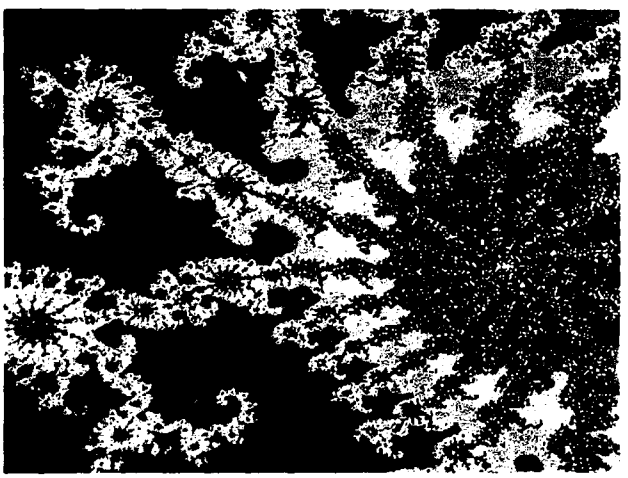

Mandelbot set, a chaotic fractal image. The different colors represent the rate of divergence of the mapping $z_{n+1} = z_n^2 + z_0$ in the complex $z = x + iy$ plane. It is interesting that such a simple mapping can give rise to chaotic behavior. This image was calculated on an HP 9816S computer and displayed on the NRL Dicomed system. (W.H. Carter, Code 8304)

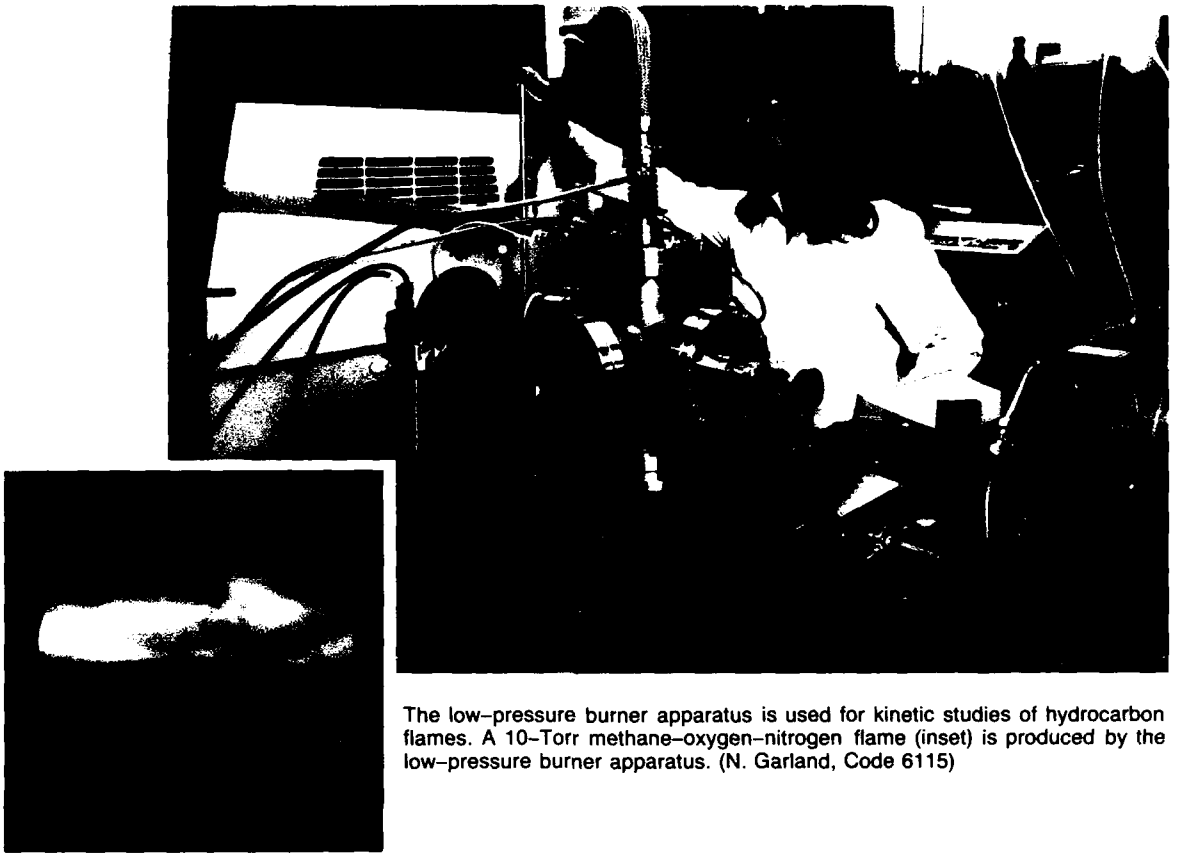

The low-pressure burner apparatus is used for kinetic studies of hydrocarbon flames. A 10-Torr methane-oxygen-nitrogen flame (inset) is produced by the low-pressure burner apparatus. (N. Garland, Code 6115)

Length of time particles spend in the Earth's magnetotail. A trilinear magnetic field model is used that is representative of the Earth's magnetic field in the magnetotail. (J. Chen and H.G. Mitchell, Code 4780)

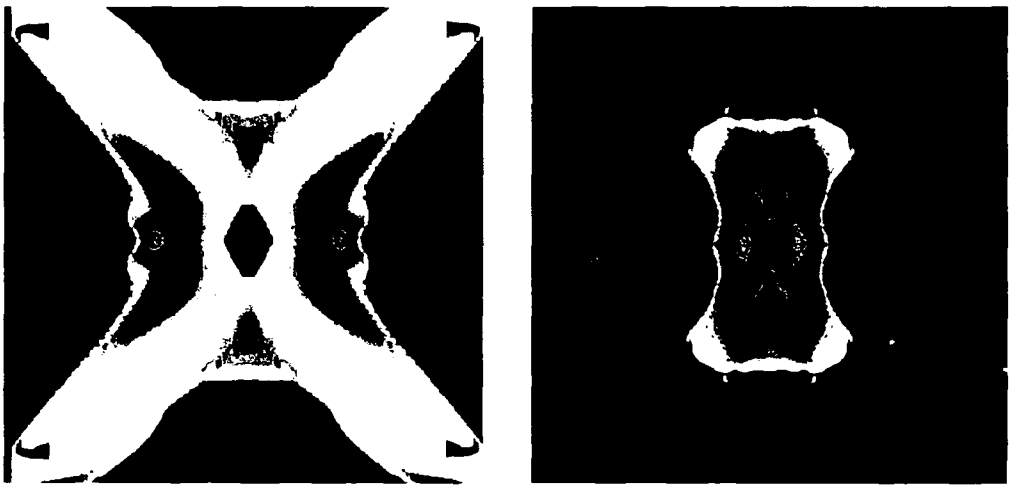

Copper wire X-pinch disassembly at 20 ns. The peak current reached during this simulation was 2 MA. The configuration modeled here is made by twisting multiple wires strung between the anode and cathode of a pulse power generator. The color spectrum at the top goes from left to right with the minimum values shown in cyan and the maximum values shown in yellow. (J. Davis, Code 4720)

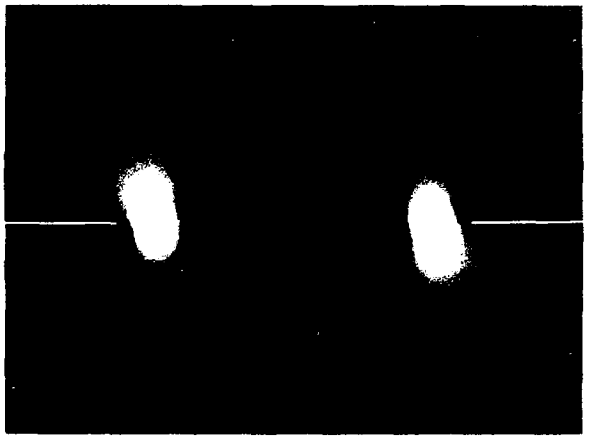

A color contour plot of the fluid density for the same calculation and time as shown in the cover figure. Here the purple-blue coloring indicates lower density than average in the flow, and green-yellow colors indicate higher density. The low densities occur at the center of the vortices as centrifugal force whirls the compressible gas out of these regions. The high densities occur between the vortices, providing the pressure needed to deflect the onrushing streams of fluid past each other. At very low speed and at high speed, the two opposed streams mix very little. In intermediate velocity regimes however, such as shown in this and the cover figure, there is appreciable turbulent mixing. (J. Boris, Code 4400)

A time history plot of the vertical velocity between and along the plate surfaces in a horizontal slice through the center of the cover illustration. Here the flow is fast enough for some of the vorticity generated at the plate edges to get into the central region without necessarily turning around the plate. This vorticity results in the red-orange tiger-stripe effect in the central band. The flow is also slow enough that the two shocks, clearly seen as the wavy boundary between the central red-orange band and the green-yellow region above and the purple-blue region below, are too weak to iron out the shear layer completely, as they do in high-velocity cases. (J. Boris, Code 4400)

The pressure variations for a shock wave in an accretion flow onto a white dwarf compact star. Such shock waves are believed to occur in AM Herculis type cataclysmic binaries where a low mass normal star is losing mass to its white dwarf companion. The horizontal axis represents time, and the vertical axis represents height away from the dwarf surface, with red indicating high pressure and green indicating low pressure. The shock-front position varies with time in a manner that can be observed with X-ray telescopes. These simulations were performed on the NRL Cray X-MP computer under the Modeling of Stellar Transients (MOST) program in the Space Science Division. (M. Wolff, Code 4121)

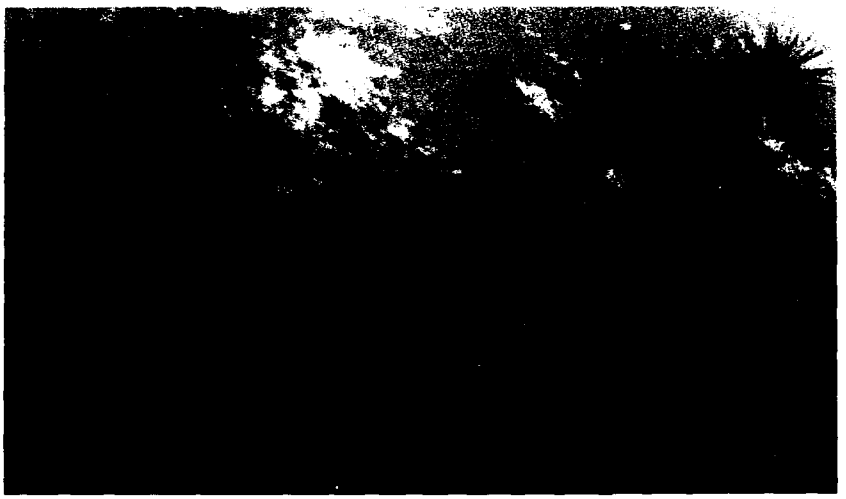

Color visualization of a tactical missile/EW engagement simulation featuring a realistic view of the ship, antiship missile, and chaff. The natural scene of the ocean and clouds is formed by using fractal geometry. An Evans and Sutherland PS 330 graphics system is used to display the scenario. (A. Di Mattesa, Code 5706)

Yorke set, an example of chaotic behavior. The different colors represent the final, normal mode reached by $\theta(t)$ in the nonlinear equation $\ddot{\theta}\ (t) + 0.1\ \dot{\theta}\ (t) + \sin\theta\ (t) = 1.75 \cos t$ plotted as a function of the two initial conditions $\theta\ (t)$, $\dot{\theta}\ (t)$. This chaotic phenomenon was discovered by Prof. James Yorke, at the University of Maryland. The data in the figure were generated on an HP 9816S computer and displayed on the NRL Dicomed system. (W.H. Carter, Code 8304)

FEATURED RESEARCH AT NRL

NRL, the Navy's corporate laboratory, has a tradition of national and international leadership in several areas of research and development important to the Navy. These areas include radar, artificial intelligence, numerical simulation, and many facets of materials, microelectronics, fire, tactical electronic warfare, acoustics, and space research and systems development. In this chapter, in-depth articles describe the recent work in the dynamic areas of pulsed-power research, radiation effects in space systems, ceramic composites, and biomolecular engineering.

Biologically Based Self-Assembly: Bio/Molecular Engineering

Bio/Molecular Engineering Branch

Introduction

Spurred by the rapid rate of advance of the biosciences, the Naval Research Laboratory (NRL) elected to invest its resources in research at the interface of biology, physics, chemistry, and engineering for solving problems of interest to the Navy and the Department of Defense (DoD). The Bio/Molecular Engineering Branch was established in October 1984 to assess the potential of nonmedical applications in this developing area. This article highlights some of the research areas currently under study and the potential technological impact of the work.

The long-term direction of the research focuses on the way in which biological molecules self-assemble into microstructures. These microstructures, both naturally occurring and synthetic, are studied for their possible utility. The staff of the Bio/Molecular Engineering Branch, supported by visiting research associates, is an interdisciplinary team performing basic and applied research in a number of diverse areas including immunology, biochemistry, biophysics, synthesis, thin-film fabrication, and advanced diagnostics.

Much of this work deals with some aspect of membrane biochemistry—the activity of lipids and the proteins associated with lipids. Lipids are the molecular building blocks for biological membranes. They are surfactant materials with *water-loving* (hydrophillic) and *water-avoiding* (hydrophobic) areas and, when mixed with water, they self-organize to minimize exposure of the hydrophobic regions. The result of such self-assembly is a bilayer membrane, which in its simplest form is a closed spheroid filled with water. The spheroids are called liposomes or vesicles, the latter name indicating the use to which they are put, both naturally and in technological applications. These uses include encapsulation and concentration of contents, control of the chemistry within, and the delivery or storage of the contents held there. In their most elaborate form, mixtures of lipids make up cell membranes and are thus one of the fundamental bases of life, permitting the flux of food, water, oxygen, and wastes necessary to maintain cell metabolism. Such activities are governed by the proteins that are attached to the membrane. These proteins catalyze chemical reactions, control membrane permeability, and serve as a sensing and identification system. These complex, exquisitely specific and sensitive processes have been studied intensively for many decades with the goal of using them in technological applications. As a result, in recent years, simpler versions of vesicles have been designed for use in drug delivery, blood surrogates, and sensors.

Research Programs

Red Blood Cell Surrogate—Liposome-Encapsulated Hemoglobin

The study of blood substitutes is one of the founding programs of the Bio/Molecular Engineering Branch. Almost a decade ago it was recognized that one promising application of liposomes would be the development of liposome-based blood substitutes, or liposome-encapsulated hemoglobin (LEH) (Fig. 1). This blood substitute is based on the encapsulation of hemoglobin (the naturally occurring protein responsible for oxygen transport) inside the aqueous compartment created by the self-assembly of phospholipids during the formation of liposomes. Currently, we are embarking on the development of a final product that we hope to bring to the Food and Drug Administration (FDA)

Fig. 1 —Lipsome encapsulated homoglobin total exchange transfusion in small animal rodent models is currently being studied. This rat received a 95% blood replacement with LEH and was photographed 28 h postexchange.

for clinical trials within the next 5 years. As part of this goal, the program is focusing on quality control issues, large-scale production improvements, stability and shelf life, and second generation development.

The issue of quality control is of paramount importance to the successful development of LEH. All of the ingredients of the liposome formulation as well as the hemoglobin used in the production of LEH must be defined for their purity and stability during processing. We are currently developing high-pressure liquid chromatography methods to address these questions. Based on the results of these experiments, the final formulation of LEH will be made and clinical trials can begin.

We are continually improving the methods used in the large-scale production of LEH. We have developed methods to improve the yield of LEH during the critical steps of LEH production. These methods have focused on improved hydration of the lipids with hemoglobin, which results in an increased encapsulation efficiency. Also, we have improved the centrifugation procedures used to concentrate and collect LEH.

A major goal of the LEH program is to define better ways to increase the shelf life and improve the stability of LEH. One of the principal methods we are investigating is the lyophilization (freeze-drying) of LEH. We have successfully demonstrated oxygen carrying capacity after the lyophilization process. We are also examining the stabilization of LEH during cold storage by the addition of antioxidants. These efforts will ensure that once the optimal LEH is attained we will have methods to guarantee its long shelf life and stability.

The development of second generation LEH is one of the most exciting areas of the LEH program. The next generation of LEH will be more biocompatible, that is, more compatible with the immune system (the natural defense system). We are developing ways to incorporate gangliosides into the liposome. Gangliosides are the naturally occurring glycolipids found on cellular membranes and are thought to be responsible for the masking of these membranes from removal by the immune system.

Anhydrobiosis

This new program (founded in fiscal year 1988 (FY88)) examines the stability of biomolecular self-assemblies in the absence of water. The application of many of the biomolecular assemblies developed by the Bio/Molecular Engineering Branch depends on their ability to survive harsh environmental conditions, in some cases with little or no water present. The program was initiated as part of the red blood cell surrogate program where the need to store LEH in the dry state was defined and accomplished [1]. Subsequently, the ability to preserve other microstructures of interest, such as the monomeric tubules formed from diacetylenic lecithins, was developed [2].

Currently, one of the goals of this program is to examine the stabilization of erythrocytes in the freeze-dried state. This effort concentrates on the modification of existing methods that we have developed in stabilizing liposomes and other lipid microstructures. In addition, we have begun to design and create amphiphiles with protective

chemical groups covalently bound to the molecule. Incorporation of these amphiphiles into the microstructure of choice (a living cell or liposome) could result in inherent stabilization as a result of self-assembly.

Biosensors

Sensitive detection systems capable of distinguishing a wide range of substances are required by the Navy and the DoD for a number of applications. The Bio/Molecular Engineering Branch is attempting to address this requirement with the development of fiber optic-based and electronic biosensors. These systems have the potential not only to meet various Navy needs, but also to be used for medical, environmental, and process-control monitors. Medical applications include early diagnosis of infectious disease, drugs of abuse, and drug monitors. Chemical/biological warfare (CBW) defense applications include monitoring decontamination and personnel protection. Pollution control applications include explosive manufacture regulation and harbor monitors.

As the name implies, biosensors rely on biologically derived molecules (biomolecules) for detection. The success of the detection scheme depends on effectively coupling the specificity and sensitivity characteristic of certain biomolecules (most often antibodies, enzymes, or receptor proteins) with fiber optics and microelectronics technologies. When the biomolecule binds the substance of interest, an optical or electronic signal is generated that can be measured by the hardware if the system is appropriately configured. At NRL, a team of biochemists, chemists, immunologists, and engineers is addressing these challenges.

Fiber Optic Biosensor. Several reasons exist for incorporating antibodies into fiber optic sensors. Such biosensors can monitor the presence or amount of the chemical of interest on a continuous basis, like a thermometer or a pH electrode. Also, they can remotely monitor the chemical. This is important deep in the ocean where a delicate instrument cannot withstand the high pressures but the optical fiber can. The optical fiber's immunity from electrical interference is important on ships and aircraft, which present a noisy environment because of the radars, generators, and motors present. Also, optical fibers are much smaller, much lighter, and can carry more information than equivalent electrical cables. Finally, the existing technology bases both in fiber optics and in antibody-based detection are useful in developing fiber optic sensors (Fig. 2).

To make the sensor work, we must transduce the antibody's recognition of the target molecule into an optical signal. That is, when the target molecule sticks to the antibody molecule, it must cause an optical change that can be sensed through the optical fiber. To do this, we take advantage of a peculiar property of light in optical fibers. Although optical fibers act like light pipes, the light is not totally confined within them. Rather, a weak optical field lies very close to the surface of the optical fiber and is called the evanescent wave. Thus if a fluorescent molecule comes close to or is attached to the surface, its fluorescence may be excited by the evanescent wave and be coupled back into the optical fiber. Essentially, the evanescent wave enables us to see only the fluoresence of molecules stuck to the optical fiber, which is, in turn, based on whether the antibodies attached to the surface recognize the target molecules.

The presence of the target molecule is detected as an increase in fluorescence. It is important to design the optics of the instrument to excite the fluorescence and collect it as efficiently as possible. To use the evanescent wave strategy, antibodies or other biomolecules must be attached to the glass surface of the fiber. Also, they must be attached so that the selectivity and strength with which the antibody binds its target are unimpaired. Moreover, the antibodies must be attached to the optical fiber surface in numbers sufficient to assure sensitivity. Finally, the portion of the surface not covered with antibodies must not significantly bind the target molecule on its own; this is called

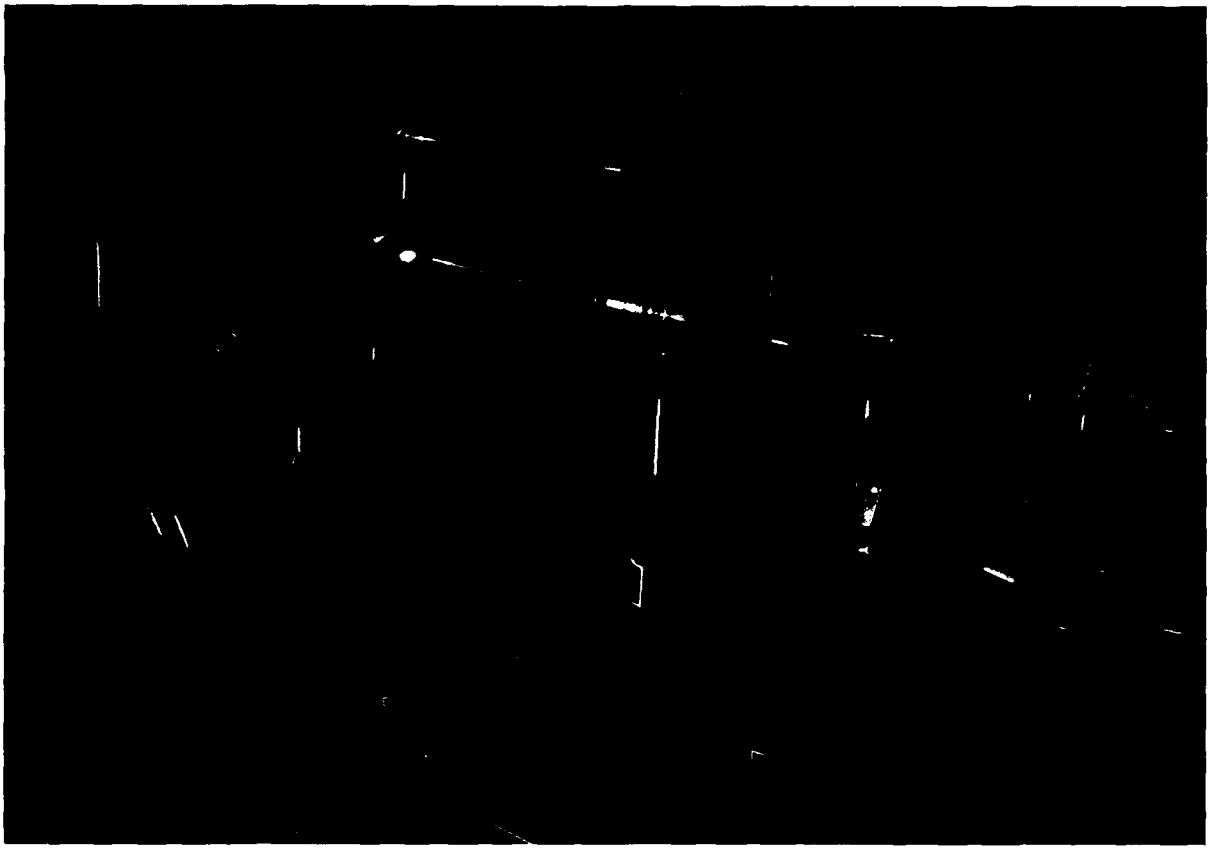

Fig. 2 — Fiber-optic sensor concept: the green laser beam is launched into the fiber through the silvery microscope objective, through a short loop of fiber and exits into the solution, where it excites the red fluorescence of a dye therein. The red fluorescence reenters the fiber and passes back through the microscope objective, which spreads it out; the perforated mirror then reflects it into the blue detector through the filter.

nonspecific binding and can increase background noise. The chemical methods for doing all this take advantage of unique chemical moieties on the antibody molecules and the silica surface to attach the antibodies under very gentle conditions. The novel NRL method for attaching antibodies to surfaces has demonstrated excellent coverage and sensitivity, as well as the lowest nonspecific binding reported to date.

Electronic Biosensor. The use of ion channel receptors in biosensors is promising for several reasons. These receptors have a broader range of reactivity than antibodies have. They recognize classes of compounds that may or may not have similar chemical structures but that have the same physiological consequences. For instance, such receptors control neuromuscular activity, and a variety of toxic chemicals that interfere with neuromuscular function do so by blocking the receptors. The ion channel receptors can be used to detect toxic chemicals whose structures are unknown but that interfere with physiological function. The ion channel receptors have a built-in mechanism for signal amplification. When the ion channel receptor binds the compound of interest and opens, thousands of ions flow through. Thus one binding event results in many ions interacting with the underlying electronic components.

Key issues involved in the development of an ion channel-based electronic biosensor include the integration of the ion channel receptor into a stabilized membrane on the chip and signal transduction of the functioning channel by the electrode. NRL has shown that functional ion channel proteins can be inserted into polymerized lipid membranes. The procedures for depositing

Fig. 3 — Porous silicon electrodes have been fabricated and are being used to develop membrane deposition techniques

the membranes on the silicon surface are currently under development. At NRL, the silicon surface itself has been modified to make it porous, providing an aqueous space below the membrane to receive the ions when the channel opens (Fig. 3). When the channel opens, the ion flow into the pore can be measured as a displacement current in the silicon. In subsequent devices, the ions will flow into the base of bipolar junction transistors. Difference amplification techniques can be incorporated to further discriminate signal from noise.

Tubule Microstructures

As a result of their biological and technological importance, liposomes have been the subject of intensive research for over 30 years [3]. One of the first efforts of the branch in this field was to try to improve liposome performance by making them stronger and more stable [4], so that they would be less likely to break open or leak their contents when sheared, heated, or subjected to other forms of stress. The approach taken was to design lipids that could be cross-linked by including polymerizable diacetylenic units in their hydrocarbon chain regions. Exposure of the lipid to ultraviolet radiation would cause neighboring diacetylenes to join to form a strong network reinforcing the liposomal structure.

To a certain extent this intent was realized, but the diacetylenic lipids also revealed a more interesting property: they undergo a phase transformation from the spheroidal liposomal structure to a hollow cylindrical structure. The new *tubules*, [5] as they are called, are about 0.5 μm in diameter, tens to hundreds of micrometers in length, hollow, open ended, extremely thin walled (approximately 100 Å), crystalline in molecular structure, rigid, and straight. They self-assemble into a hollow, high-aspect-ratio microstructure that would be very difficult to manufacture by any other means (Fig. 4).

The exposed lipid headgroups on the tubule surface proved to be susceptible to the attachment of catalysts, which allowed the microstructures to be electrolessly coated with metal. Thus, the tubules serve as templates for the manufacture of copper, nickel, and permalloy cylinders [6] with

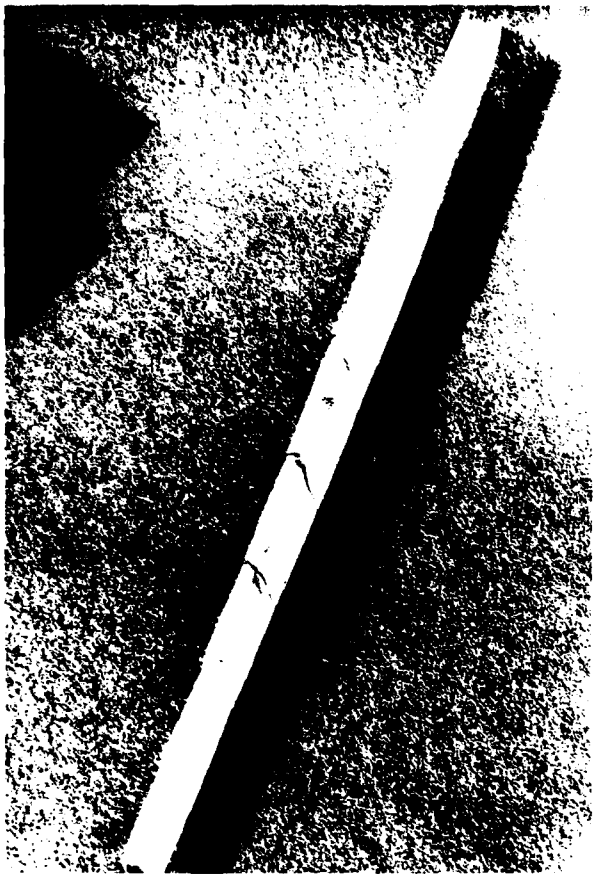

Fig. 4 — Scanning electron micrograph (SEM) of one tubule; diameter 0.5 μm; length 50 μm; wall thickness approximately 200 Å

submicron diameters. These metal tubules are strong, electrically conductive, highly magnetic (and magnetically alignable [7]), resistant to high temperatures, chemically reactive, and capable of storing material in their hollow cores.

Once the lipid structures have been metallized the resulting microstructures are quite robust, and compatible with most material environments. They have been suspended in liquids and gels, and are oriented by flow, electric fields, and magnetic fields in polymer and metal matrices. Composites with novel electrical and dielectric properties [8] have been fabricated.

The technological implications of tubules, both lipid tubules themselves as well as metallized, appear to be very promising [9]. Identified applications include composites, electro-optics, novel liquid media, microelectronic elements, reagent delivery vehicles, and microsurgery materials.

The purely scientific aspects of tubule formation are also quite fascinating. The branch is devoting substantial effort, by using synthesis, microscopy, spectroscopy, X-ray and neutron scattering, and calorimetry [10–16], to the investigation of why the structures form and into methods of controlling and modifying this behavior. A fundamental understanding of these processes could lead to the *molecular engineering* of a molecule for specific device applications.

Molecular Design Of Microstructures

The pharmaceutical industry has pioneered what is called *rational drug design*. The premise is that a detailed understanding of the underlying rules by which molecules interact can lead to rational (rather than random) choices for the synthesis of therapeutic compounds. We have adopted this approach to the *bottom-up* design of lipid microstructures. Thus our fundamental goal is to understand why lipid microstructures form. With that information we have the possibility of controlling the process and rationally preparing microstructures for specific purposes.

Our approach is threefold, consisting of characterization, theory, and synthesis. Characterization involves the use of a variety of biophysical probes to describe the chemical and physical properties of our lipid microstructures. These techniques include electronic and vibrational spectroscopy, calorimetry, microscopy, magnetic resonance, and X-ray and neutron diffraction. Theory seeks to describe experimental observations both mathematically and visually. Our theoretical work includes the traditional pencil and paper approach of the chemical physicist as well as the modern computational chemistry techniques of molecular graphics, mechanics, and dynamics. The insights of biophysical characterization and theoretical studies are then used to guide the synthesis of candidate compounds.

A clear understanding of the structure of the molecular building blocks that form our

microstructures is absolutely essential to our rational design approach (Fig. 5). For this reason NRL has pioneered the use of computer graphics for the depiction of lipid molecules. We have also developed a powerful molecular graphics program for the Macintosh personal computer. Using this program, which we call Nano Vision™, we can quickly depict many essential aspects of lipid structure.

The basic building block is the individual phospholipid. The molecule is amphiphilic (literally "loving both ends") as a consequence of its polar (hence water-loving) headgroup and its nonpolar (oily) hydrocarbon chain. Individual phospholipid molecules interact to form structures such as the bilayer, the major structural element of the cell membrane. Longer range interactions result in lipid microstructures such as the closed, spherical liposome that has been used at NRL as the basis of a red blood cell surrogate.

Unique lipids, unknown in nature but with very useful properties, have been designed, synthesized, and characterized at NRL. An example is the lipid that contains diacetylenic moieties in the hydrocarbon chain. The diacetylenes may be polymerized to form unusually stable bilayers. Self-assembly of this lipid to microstructures results in long, thin tubules. Computer graphics are an important link in NRL's rational design cycle and provide a tool for the biophysical chemist to display and analyze the results of experiments and for the organic chemist to design novel lipid molecules.

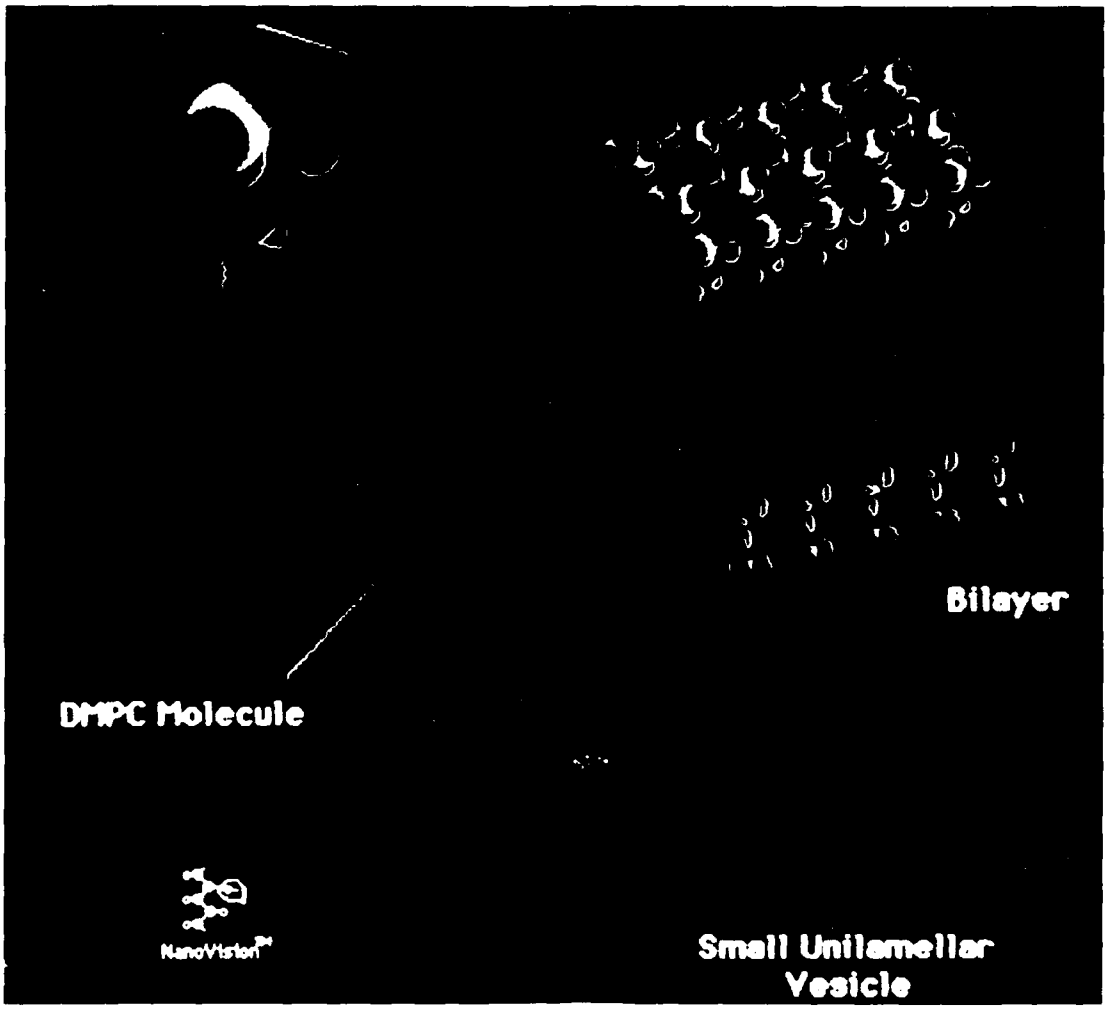

Fig. 5 — Relationship between a single lipid molecule, lipid bilayer, and lipid microstructure

Molecular Dynamics Of Lipids

One of the major goals of research in the Bio/Molecular Engineering Branch is to understand lipid bilayer properties such as stability, transport, and fusion. Biological membranes are composed of tightly packed lipids and proteins. They provide sites for important enzyme systems involved in intercellular communication and recognition, adhesion, and energy transduction. Diffusion in the plane of the membrane occurs readily for both lipids and proteins. The transport of materials within and across a biomembrane is strongly modulated by the fluidity of its component lipids, as are the functions of some of the membrane proteins. Therefore, to understand the functioning of biological membranes one must study the molecular motions of the fluid bilayer. Only then can the interaction of membranes with water, detergents, drugs, proteins, and other membranes be understood on a detailed molecular basis.

The objective of this project is to create and study the molecular dynamics of models of lipid bilayers by using new, fast algorithms developed at NRL. The information obtained from the simulations will help evaluate the importance of various structures and mechanisms in bilayers.

The Bio/Molecular Engineering Branch, in collaboration with the Laboratory for Computational Physics and Fluid Dynamics (LCP&FD), is developing and applying fast, efficient algorithms for membrane analysis [17-19] based on a novel, near-neighbors algorithm developed in LCP&FD [20]. One of the most important procedures we have developed, MSHAKE [17], holds bond lengths constant. This enables us to use a longer time step than if we allow the bonds to vibrate, and we can therefore simulate longer intervals. Figure 6 shows the improved performance of MSHAKE vs traditional methods and shows the convergence of the constraint force as calculated by the program. The curve labeled $m = 0$ is equivalent to the traditional method of constraining bonds, whereas $m = 1$ and $m = 2$ label the results of applying MSHAKE. The advantage of using MSHAKE is clear. We have also developed algorithms to calculate angle bending and torsion [1] and a procedure to handle multiple force fields [19]. We anticipate that these algorithms will enable us to simulate more realistic bilayers within the allotted computer time. The information obtained from these simulations will help resolve questions concerning conformations associated with the chain melting transition, intermolecular conformational correlations, and the transport of small molecules in membranes. The simulation of more realistic double-tail lipid membranes will provide more detailed models for comparison with experimental studies of the static structure and dynamic behavior of biological membranes.

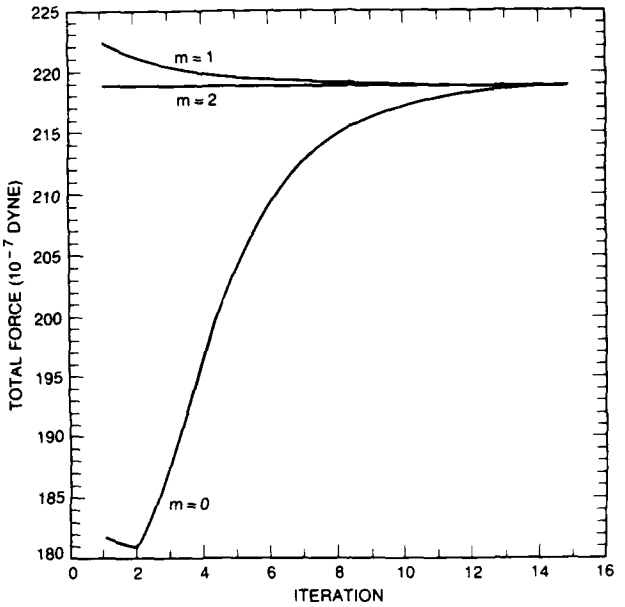

Fig. 6 — Convergence of the MSHAKE algorithm as a function of iteration and estimation: the sum of the external forces and the constraint forces are plotted against the number of passes through the constraint force procedure. The forces are not actually applied to the particles until the total force has converged. $m = 0$ — no estimate of constraint force provided; $m = 1$ — magnitude of constraint force from the previous time step used as an initial estimate; $m = 2$ — linear extrapolation of the magnitude of the constraint forces at the preceding two time steps used as an initial estimate.

Stabilized Microstructures

Biotechnology is on the verge of growth in applications such as sensors and new materials.

These applications depend, in large part, on exploiting the unique properties of biological systems. A common weakness to all biologically-based technologies is the inherent instability of biosystems. For membrane-associated applications such as liposomal-based assays, artificial red blood cells (RBCs), or membrane-based biosensors, the inherent instability of the lipid membrane with respect to thermal, chemical, and humidity conditions is a central concern (Fig. 7). We have focused on two systems: the extraordinary archaebacterial membranes and the role of sugar in anhydrobiotic survival.

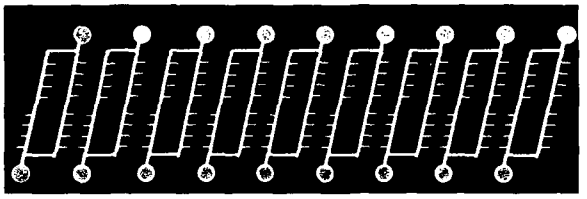

Fig. 7 — A possible monolayer membrane structure: the side chains denote methyl groups; red = polar headgroup; yellow = hydrocarbon interior

Archaebacteria (*archaios* = ancient) are most interesting for their ability to thrive in extremely hostile environments. Certain archaebacterial thermophiles can live at temperatures up to 105°C (1 atm), while other archaebacterial thermo-acidophiles live at somewhat lower temperatures (~85°C) but at pH 1.0 to 2.0 (Fig. 8). These conditions, normally considered sterilizing, represent optimal growth conditions for the archaebacteria. In the last few years we have learned that the lipids of the archaebacteria are based on a branched C_{20} hydrocarbon chain. In some of the most hardy species, the bilayer structure itself may have been replaced by a monolayer with long dimers of the C_{20} alkyl chain spanning the membrane. These tetraether-lipid molecules are unique to archaebacteria, and the membranes of these microorganisms have been found to remain intact even in boiling water.

Although the length of the tetraether lipid suggests that the molecule can span the membrane

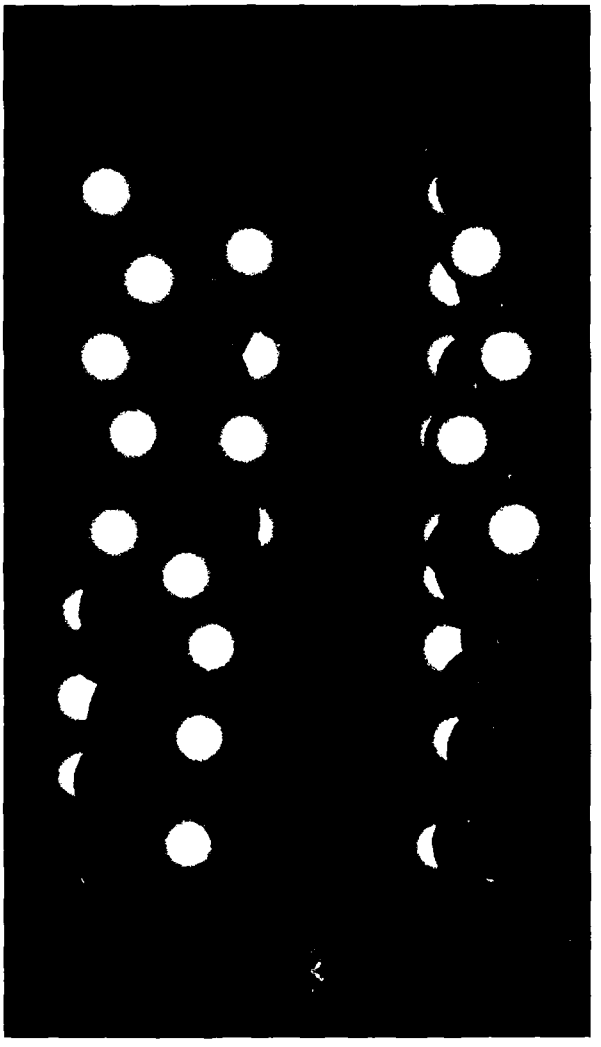

Fig. 8 — Depiction of a symmetric, hydrolyzed, archaebacterial lipid, glycerol dialkyl glycerol tetraether (GDGT) with half-sized Van der Waal radii: green = carbon; yellow = methyl carbon; red = oxygen

to form a monomolecular layer, no definitive data exist to prove this hypothesis. Freeze-fracture work at NRL shows that the tetraether membrane does not fracture along midplanes of bilayers, and, therefore, tetraether membranes are not likely to possess the classic bilayer structure of other lipid membranes [21]. In fact, although the chemical structure of the lipid strongly suggests correlations between structure (e.g., ether bonds, saturated hydrocarbons) and stability, how the unique chemical structure of the tetraethers contributes to the stability of archaebacterial membranes remains

largely unknown [22]. Until recently, it was not certain whether the tetraethers can spontaneously form membranes by themselves or whether other components are needed.

We have performed molecular mechanical calculations to determine conformational energy minima for the simplest tetratethers [23]. The results point to a highly disordered conformation for these molecules with many *gauche* bonds along the alkyl chains—expecially toward the center of the chains. This prediction is consistent with a priori considerations of relative conformational energies of *trans* and *gauche* conformations, which show that the *trans* conformation is degenerate in energy with one of the *gauche* conformations. That is, there should be as many *gauche* bonds as *trans* bonds at any temperature.

More recently, we have developed a procedure for obtaining highly pure tetraether lipids from *Sulfolobus acidocaldarius*, a thermoacidophilic archaebacteria [24]. These lipids do not spontaneously form vesicles in aqueous buffer, but we find that they will suspend in hot water when injected from an acetone solution [25]. The suspension appears to be liposomal (vesicular), and we are in the process of ascertaining the nature of the suspension. Surface film studies (Langmuir-Blodgett (L-B)) have also begun as a prelude to transferring the films onto solid substrates. Future work will focus on the permeability, as well as stability, properties of these tetraether lipid membranes. Eventually, efforts will be made to incorporate proteins into the membranes.

The technological potential of lipid membranes based on the tetraether structure is only beginning to be explored. Once we understand their structure and stability relationships and how to manipulate them, applications may be found in such diverse areas as resist materials for microelectronic fabrication, membrane-ion filters, or boundary-layer lubrication.

Optical Nanolithography

A new process has been developed at NRL to fabricate high-resolution microstructures of metal and other materials on a variety of substrates. The process has applications in numerous areas of microcircuit lithography (Fig. 9).

Microcircuit lithography is the patterning of materials with near-micrometer features. A patternable, etch-resistant material (called a *resist*) serves as a mask to transfer the features to the underlying semiconductor substrate, which is then used as a circuit element. Optical lithography currently offers the best combination of throughput, low cost, and adequate resolution for rapid throughput production of high-speed devices at resolutions of < 1 μm. For numerous other applications such as the fabrication of microwave circuits or masks, the selectively deposited metal serves as the conductive path or optically opaque region.

A major potential use of this process is in the area of microcircuit fabrication. The new process has numerous advantages over conventional photoresist technology. The availability of a deep UV-sensitive, ultrathin film in combination with the protective metal layer is unique and will allow definition of features (transistors, wires, capacitors) in the semiconductor substrate of < 250 nm because of the lowering of the diffraction limit and elimination of other optical limitations such as standing waves. Working transistor test structures have been fabricated by using the new process to 500-nm gate length. Step coverage over 400-nm high polysilicon lines has been demonstrated. Pinhole-free capacitors with areas of several centimeters [2] have been made.

The process involves an ultrathin imaging layer that is quickly and easily deposited on a substrate, exposed to masked deep-UV radiation, then selectively metallized such that a thin metal layer is deposited only in the reactive areas. In the area of semiconductor microcircuit lithography, the ultrathin film/metal assembly serves as a plasma-impervious barrier to reactive ion etching that can be stripped from the substrate after feature definition.

The process is sufficiently general and has been used to define high-resolution features on all

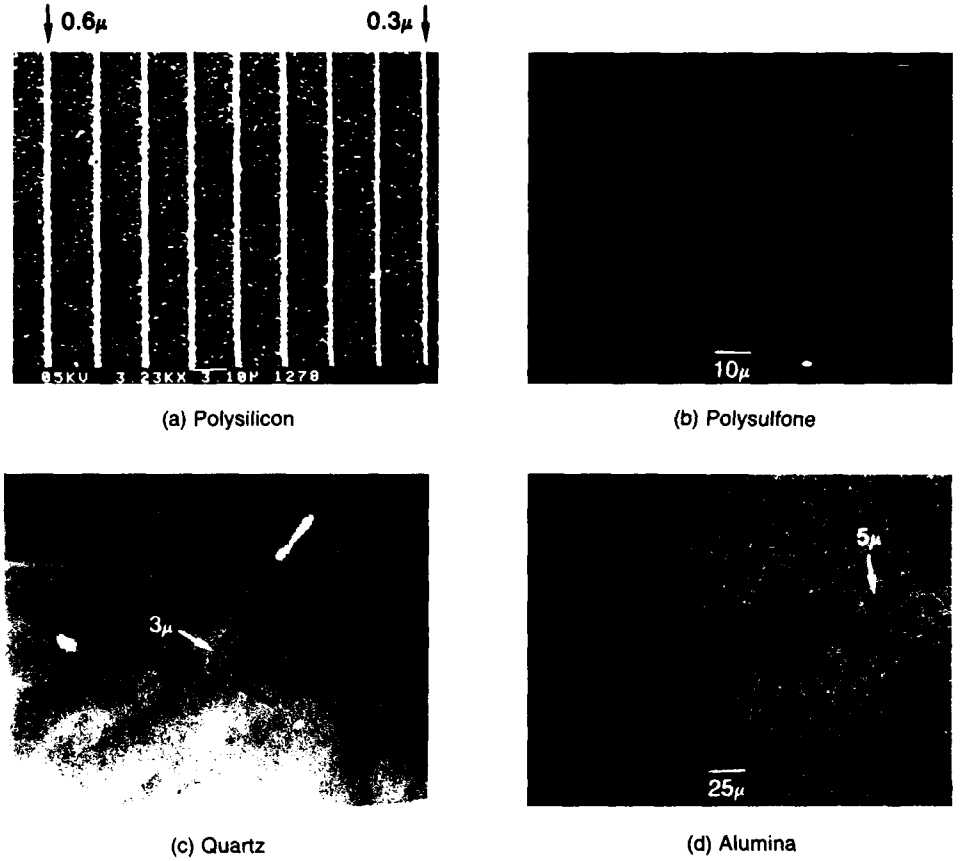

(a) Polysilicon (b) Polysulfone

(c) Quartz (d) Alumina

Fig. 9 — (a) Sub–0.5 μm metal lines, deposited on polycrystalline silicon, protect the underlying substrate against reactive ion etching. (b) Copper pattern (upper half of photo) deposited on polysulfone, an important plastic for molded printed circuit boards. (c) Copper pattern on quartz, a typical substrate for optical lithography masks. (d) Copper patterns on alumina, a substrate used for microwave communication circuitry.

of the commonly used substrates required for microcircuit fabrication, such as p-type or n-type silicon, polycrystalline silicon, thermally grown or chemical-vapor-deposited silicon dioxide, and silicon nitride. Deposition of metal at high resolution only in the desired regions of the substrate eliminates the need for etching or removal of metal from unwanted areas. Preliminary results have shown that this process can be modified to employ an electron beam as the irradiation source, to produce metal patterns with feature resolution of 100 nm. Further reductions in feature size are anticipated, particularly through the use of a scanning tunneling microscope as the exposure tool.

Acknowledgments: Work in the Bio/Molecular Engineering Branch is funded by the Defense Advanced Research Projects Agency, the Department of the Treasury-U.S. Customs Service, the Federal Aviation Administration, the Naval Medical Research and Development Command, the Office of Naval Research, and the Office of Naval Technology. The National Science Foundation is also acknowledged for their support of collaborative university research with NRL.

References

1. A.S. Rudolph, *Cryobiology* **25**, 942 (1988).
2. A.S. Rudolph, A. Singh, and J.M. Schnur *Biophys. J.* **53**, 120a (1988).
3. See for example: D. Chapman, *Biological Membranes* (Academic Press, London, 1968).

4. A. Singh and J.M. Schnur, *Synth. Commun.* **16**(7), 847 (1986). Also U.S Patent Application Number 946,440, allowed Jan. 1989.

5. P. Yager and P.E. Schoen, *Mol. Cryst. Liq. Cryst.* **106,** 371 (1984).

6. J.M. Schnur et al., *Thin Solid Films*, **152,** 181-206 (1987).

7. C. Rosenblatt, P. Yager, and P.E. Schoen, *Biophys. J.* **51**(2 part 2), 185A (1987).

8. M. Orman and P.E. Schoen, unpublished data.

9. Patent Applications:

   P.E. Schoen, P. Yager, J.M. Schnur, and T.G. Burke, "Method for the Production of Lipid Based Tubules by Double Thermal Cycle," U.S. Patent Application Number pending, filed Sept. 1988.

   J.M. Schnur, P.E. Schoen, P. Yager, R. Price, J.M. Calvert, and J.H. Georger, "Fabrication of Metallic Microstructures," U.S. Patent Application Number 07/063,029, filed June 1987.

   P.E. Schoen, J.M. Schnur, P. Yager, R. Price, A. Singh, and J.H. Georger, "Direct Fabrication of Lipid Microstructures from Solvent/Nonsolvent Solutions," U.S. Patent Application Number 07/011,838, filed Feb. 1987.

   P.E. Schoen, P. Yager, and J.M. Schnur, "Method of Making Lipid Tubules by a Cooling Process," U.S. Patent Application Number 07/852,596, filed Apr. 1986.

10. J.H. Georger et al., *J. Am. Chem. Soc.* **109,** 6169 (1987).

11. P. Yager et al., *Biophys. J.* **48,** 899 (1987).

12. A. Singh et al., *Chem. Phys. Lipids* **47,** 135 (1988).

13. P. Schoen and P. Yager, *J. Pol. Sci.* **23,** 2203 (1985).

14. T.G. Burke et al., *Chem. Phys. Lipids*, in press.

15. A.S. Rudolph and T.G. Burke, Biochimica et Biophysica Acta **902,** 349 (1987).

16. J.P. Sheridan, NRL Memorandum Report 5975, 1988.

17. S.G. Lambrakos, J.P. Boris, E.S. Oran, I. Chandrasekhar, and M. Nagumo, *J. Comput. Phys.*, in press.

18. M. Nagumo, S.G. Lambrakos, and J.H. Dunn, personnel communication.

19. S.G. Lambrakos, M. Nagumo, and E. Oran, personnel communication.

20. S.G. Lambrakos and J.P. Boris, *J. Comput. Phys.* **73**, 183-202 (1987).

21. C. Montague, E.L. Chang, A. Singh, and R. Price, *Biophys. J.* **51**, 254a (1987).

22. E.L. Chang and C. Montague, *Biophys. J.* **53**, 502a (1988).

23. E.L. Chang, C. Montague, and A.H. Lowrey, *Biophys. J.* **49**, 322a (1986).

24. S.L. Lo, C. Montague, and E.L. Chang, *J. Lipids Res.*, in press.

25. C. Montague, S.L. Lo, and E.L. Chang, *Biophys. J.* **55**, 26a (1989).

Authors: Row 1 (left to right): Alan S. Rudolph, Joel M. Schnur, Bruce P. Gaber, Frances S. Ligler, Paul E. Schoen. Row 2 (left to right): Alok Singh, Thomas L. Fare, Sharon W. Menton, Anne Kusterbeck, Warren Schultz. Row 3 (left to right): Beth A. Goins, W. Richard Light, Lisa Shriver-Lake, Jeffrey M. Calvert. Row 4 (left to right): Gregory Wemhoff, Richard B. Thompson, Eddie Chang.

New Horizons in Pulsed-Power Research

Gerald Cooperstein
Plasma Physics Division

Introduction

The Naval Research Laboratory (NRL) has established a history of leadership in high-power (10^{12} W), low-impedance ($\sim 1\ \Omega$), pulsed-power research during the past 20 years. Until recently, the technology has involved primarily capacitive-energy-storage techniques that used closing switches with water as the dielectric-energy-storage medium. In the early 1980s, the development of fast-opening plasma switches at NRL had a dramatic influence on this *conventional* pulsed-power technology. These switches were first used to improve existing generator performance by the addition of a final stage of inductive pulse compression. More recently, they have been used in conjunction with other technologies to develop a new class of pulsed-power generators based on inductive-energy storage techniques that use opening switches and vacuum-insulated inductors. This development has led to a reduction in size over previous generators of one to two orders of magnitude. Based on these results, the Plasma Physics Division, with joint funding from NRL and the Defense Nuclear Agency (DNA), is presently undertaking a major multimegajoule upgrade of its pulsed-power, inductive-storage facilities.

History: The NRL Gamble I facility (750 kV, 250 kA, 50 ns), completed in 1968, was called Gamble because it was the first high-power, low-impedance facility to use demineralized water as a dielectric-energy-storage medium at high voltage [1]. The main advantages of water as a capacitive-energy-storage medium are that it has a high dielectric constant, is self-healing to electrical breakdowns, and acts as a good insulator for high-voltage pulses of 10-μs duration or less. This technology was pioneered by J.C. Martin of the Atomic Weapons Research Establishment in Aldermaston, England. The initial success of Gamble I led to DNA funding for Gamble II.

The Gamble II generator (Fig. 1) was, when completed in 1970, the largest pulsed-power facility of its kind in the world; it was capable of delivering 1 MV across a 1-Ω load for 50 ns (5×10^{-8} s) [2]. The 1-TW output power was more than the combined electrical power capacity of the United States. At that time, the primary purpose for this newly developed pulsed-power capability was to provide an intense radiation source for simulating nuclear-weapon effects in the laboratory to supplement DNA's (formerly the Defense Atomic Support Agency (DASA)) underground simulation testing program. The intense X-ray bremsstrahlung radiation was produced by generating a 1-MV, 1-MA electron beam in a vacuum diode placed across the generator's output and allowing the beam to hit a high-atomic-number target in a manner similar to a medical X-ray tube. Military electronics were exposed to this radiation to assess their survivability in a real nuclear environment.

Gamble II was the prototype for all modern high-power, low-impedance generators now in existence at private industry laboratories and at both Department of Defense (DoD) and Department of Energy (DoE) laboratories. At present, the largest DoD facility is the Maxwell Laboratory, Inc. (MLI) Blackjack V (2 MV, 5 MA, 80 ns), and the largest DoE facility is the Sandia National Laboratory, Albuquerque (SNLA) Particle Beam

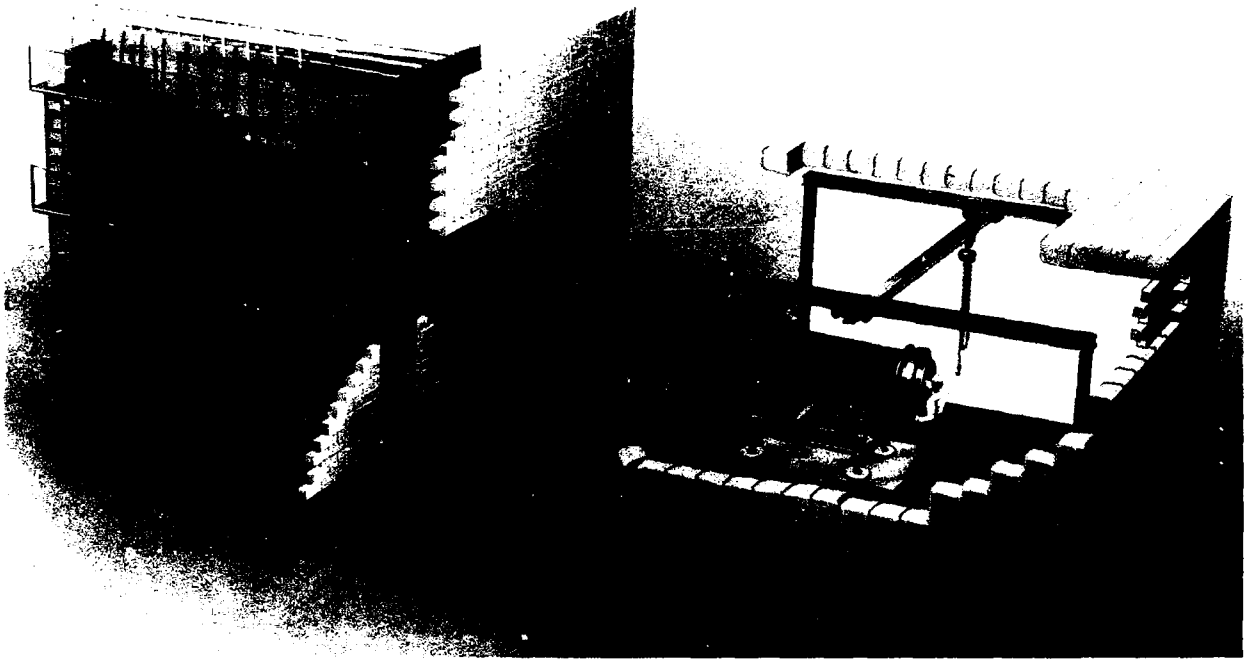

Fig. 1 — Gamble II is a high-power (>1 TW) pulse generator that uses water-dielectric, capacitive-energy-storage techniques

Fusion Accelerator (PBFA) II (15 MV, 6 MA, 40 ns).

Since the completion of Gamble II, NRL has continued to play a pioneering role in the development of the state-of-the-art pulsed-power technology based on capacitive energy storage. Major contributions include the development of:

- electrostatic field plotting and transmission line computer codes for the design of more efficient pulsed-power devices;
- advanced, single surface, plastic insulators to separate the water dielectric from the vacuum diode loads;
- more reliable water switching techniques; and
- triggered oil output switches to replace the final stage untriggered water output switch.

These and other advances led to an NRL-funded upgrade of Gamble II in 1978 that increased the output power to over 2 TW [3]. The upgrade also allowed the facility to operate in positive as well as negative polarity so that intense beams of light ions (such as protons and deuterons) could be produced. These ion beams were used for research into inertial confinement fusion (ICF) in a manner similar to the way intense laser beams were being developed to create fusion from small pellets of deuterium and tritium. Today, Gamble II is still one of the world's largest positive-polarity facilities.

Applications: Besides the important nuclear-weapon-effects simulation (NWES) and light-ion-beam ICF research mentioned above, pulsed-power technology based on water-dielectric capacitive energy storage has generated other new areas of research. These types of facilities are now used in industry, universities,

NRL, and government laboratories both here and abroad to produce high-power electron and ion beams and soft X rays from z-pinch plasmas, for the general study of matter at high-energy densities, for the development of directed-energy weapons, for the generation of high-power microwaves, for flash X-ray radiography, and for X-ray laser development.

The NRL Gamble research program has trained many leaders in pulsed power who have left the laboratory to assume major positions in private industry, at universities, and other government laboratories. Other scientists have stayed on at NRL to assume leadership roles elsewhere in the Plasma Physics Division in areas of research involving applications of this pulsed-power technology. At present, five Plasma Physics Division branches—Advanced Beam Technologies, High Power Electromagnetic Radiation, Charged Particle Physics, Experimental Plasma Physics, and my own Plasma Technology Branch—are all engaged in experimental research involving various applications of this pulsed-power technology. Twenty years ago, no sessions of an American Physical Society or an Institute of Electrical and Electronics Engineers (IEEE) meeting were devoted to this technology or its applications. Today, numerous sessions at professional meetings and several regularly scheduled international meetings are devoted to these subjects. NRL is presently considering hosting in 1992 the Ninth International Conference on High-Power Particle Beams.

The Growing Importance of Inductive Storage Techniques

The successful technology of the Gamble devices and their descendents is based on water-dielectric, capacitive-energy-storage techniques. The cost and size advantages of inductive-energy-storage techniques for pulsed power over conventional capacitive techniques have long been recognized. The key to the development of inductive systems is the advancement of opening-switch technology that, at the terawatt level, invariably involves plasma physics. Research efforts in this area have recently provided new and exciting results. The most important results involve very fast opening (~ 10 to 100 ns) plasma switches, because they can be used immediately to upgrade existing pulsed-power generators by adding a vacuum-inductive-storage, pulse-compression stage for power and voltage multiplication. In the longer term, these new switches, when used in parallel with an additional slower stage of plasma switching (~ 0.1 to 1 μs opening time), form the basis for a new generation of inexpensive, compact, single-shot or repetitively-pulsed, high-power devices.

Role of Plasma Physics: Although the operation of most opening switches involves complex plasma-physics phenomena, earlier research usually considered the opening switch to be an engineering problem. For this reason, little progress was made in the development of high-power inductive storage until recently, even though inductive storage was first considered 30 or 40 years ago. Examples of the plasma-physics phenomena, which can occur at different stages of operation in such systems, include plasma-wall interactions, electrode sheaths, energetic-particle emission from electrodes, complex mechanisms for electron current conduction across strong magnetic fields, magnetic insulation of electron flows, plasma microinstabilities and associated anomalous resistivity, and plasma hydrodynamics. Plasma physics theoretical tools that can be applied to these problems include kinetic (Vlasov) and fluid analytic treatments, 2.5-dimensional electromagnetic particle-in-cell (PIC) codes, and various fluid and hybrid codes. During the past few years, these sophisticated theoretical tools and understanding have been successfully applied to the opening switch operation problem. The detailed understanding arising from the theoretical research, together with recent plasma diagnostic measurements, has provided many of the breakthroughs in opening switch operation and will

provide many more breakthroughs. Much of the remainder of this paper discusses this new plasma opening switch technology with emphasis on NRL's pioneering contributions and the way the technology has reshaped, and continues to reshape, pulsed-power research.

Previous NRL Research: Even before these recent breakthroughs in plasma opening switches, NRL was a leader in inductive-storage technology. In 1975, NRL operated a state-of-the-art homopolar generator capable of delivering 3 MJ of pulsed energy to a 1.4-mH inductor and driving pulsed-power loads, by use of opening switches, at peak powers up to 1.6×10^{10} W. This facility was used in conjunction with experimental research involving high-current capacitor banks, water capacitors, large copper-coil inductors, explosively driven opening switches, and copper-wire and aluminum-foil fuses (used as opening switches) to achieve the first demonstration (TRIDENT I and II) of inductive energy storage at high power [4]. The explosively driven opening switches are now being used by many laboratories in connection with the development of rapid-fire as well as single-shot rail-gun technology. The fuses are an important component of our Pawn facility to be described later. NRL has also made significant contributions to repetitive opening-switch technology by researching electron-beam-controlled switches and phase-transition, solid-state switches. These and other contributions were highlighted when I.M. Vitkovitsky, formerly Head of the Plasma Technology Branch and then Associate Superintendent of the Plasma Physics Division (now retired), was awarded the prestigious international Erwin Marx Award at the Sixth IEEE Pulsed Power Conference in 1987 for his many contributions to pulsed power research.

A Comparison of Capacitive and Inductive Storage Techniques

A simple comparison of capacitive and inductive energy storage systems is now presented to identify the advantages of inductive systems and clarify the key role played by fast-opening plasma switches in inductive systems.

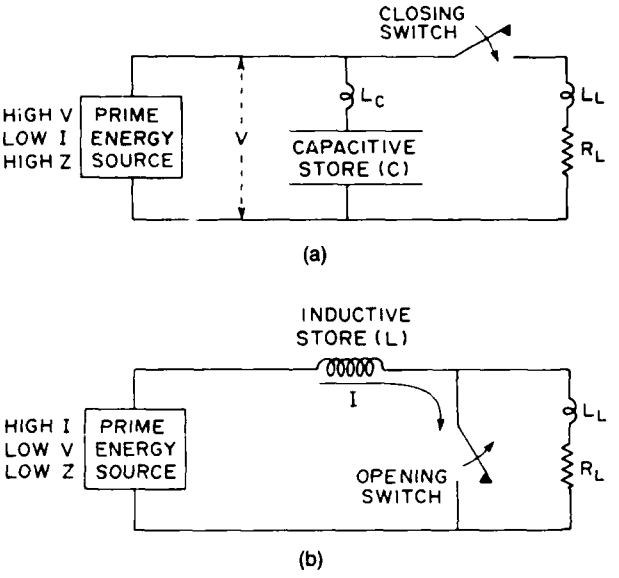

Fig. 2 — (a) Simple capacitive energy storage system with a closing switch. (b) Simple inductive energy storage system with an opening switch.

Simple Circuits: Figure 2(a) shows a simple capacitive-energy-storage system where a high-voltage, low-current primary energy source charges a capacitance C. When the peak voltage V is reached, a closing switch connects the capacitor to the resistive load R_L. The characteristic output duration is $R_L C$, and the peak current is about V/R_L. The prime energy source is high impedance and can be treated as an open circuit after the switch is closed. For such a system, the primary charging voltage is transferred to the load and the current is multiplied by the ratio of the charging time to the output pulse duration. It appears that a high-power, short-duration output pulse could be obtained simply by using a low-resistance output load. Unfortunately, parasitic inductance limits the output pulse rise time to L/R_L for small R_L, where L is the total parasitic inductance, $L_C + L_L$, of the capacitive energy store, the output closing switch, and the load.

For the simple inductive store system shown in Fig. 2(b), a high-current, low-voltage primary energy source *current charges* an inductor (i.e., drives the current through an inductor that stores

magnetic field energy). When the peak current I is reached an opening switch opens, connecting the inductor to the resistive load R_L. If the load inductance L_L is very much smaller than the storage inductance L, then the characteristic output-pulse duration is L/R_L and the peak voltage is about IR_L. Here, the primary energy source is low impedance and can be treated as a short circuit after the switch is opened. For such a system, the primary charging current is transferred to the load and the voltage is multiplied by the ratio of the charging time to the output-pulse duration. It appears in this case that a high-power, short-duration output pulse could be obtained simply by using a high-resistance output load. Unfortunately, the output-pulse rise time and voltage are limited by the opening time and the voltage hold-off capability of the opening switch. Generally, all that can be expected for a single opening switch is about a factor of 10 for the ratio of switch conduction time (charging time) to opening time (output-pulse duration).

One of the major advantages of inductive systems over capacitive systems is the very high energy densities obtainable with inductors. Capacitive energy densities are limited by the voltage breakdown of materials, whereas inductive energy densities are limited by the mechanical strengths of materials. The energy density in an inductor can be several orders of magnitude larger than the energy density in a capacitor, though present research on advanced capacitors is narrowing this difference. When a vacuum inductor is used, the size of the system can be further reduced because electron flow generated from the cathode surfaces is at low voltage and can be self-magnetically insulated during both charging and discharging. Other advantages of vacuum inductive systems are presented below when staging is discussed.

Staged Systems: Capacitive and inductive systems, which are more realistic than the simple systems shown in Fig. 2, use the staging concept to achieve high-power, short-duration pulses. The rise-time limiting problem of finite parasitic inductance in capacitive systems is solved by using several successive stages of lower inductance connected in series by closing switches to multiply current and power. Figure 3(a) illustrates a typical capacitive system conceptually. A large, high-voltage, low-current, oil-insulated Marx generator, consisting of many capacitors charged in parallel and discharged in series, charges a water capacitor in several microseconds, typically through a triggered gas closing switch. The water capacitor, which has much lower inductance than the Marx generator, then charges an even lower inductance, water-dielectric pulse-forming line (PFL) section in a few hundred nanoseconds through a closing switch. This section acts like a simple capacitor during the charging time but acts like a low-impedance PFL while discharging in less than 100 ns through a low-inductance, multichannel closing switch. Ideally, voltage into a matched load is a square wave with an amplitude of one half the PFL voltage. Voltage (with the exception of the last stage) and energy are preserved, and current and power are multiplied by the successive stages of pulse shortening. Gamble II is good example of a typical, staged, high-power capacitive system.

The finite switch-opening-time problem in inductive systems is solved by using several successive stages of opening switches in parallel. Each stage is capable of conducting current during the longer opening time of the previous stage and then opening in a shorter time to multiply voltage and power. Figure 3(b) shows an ideal, staged, inductive system conceptually. A high-current (>1 MA), low-voltage (<100 kV) source, such as a compact, air-insulated, low-voltage capacitor bank, current charges a vacuum inductor through the first-stage, long-conduction-time switch. A shorter conduction time, faster opening switch is used to provide the final stage of pulse compression and voltage multiplication. The inductance between the two opening switches and the inductance between the final opening switch and the load should be minimized to maximize the energy delivered to the load. Sometimes, as in our

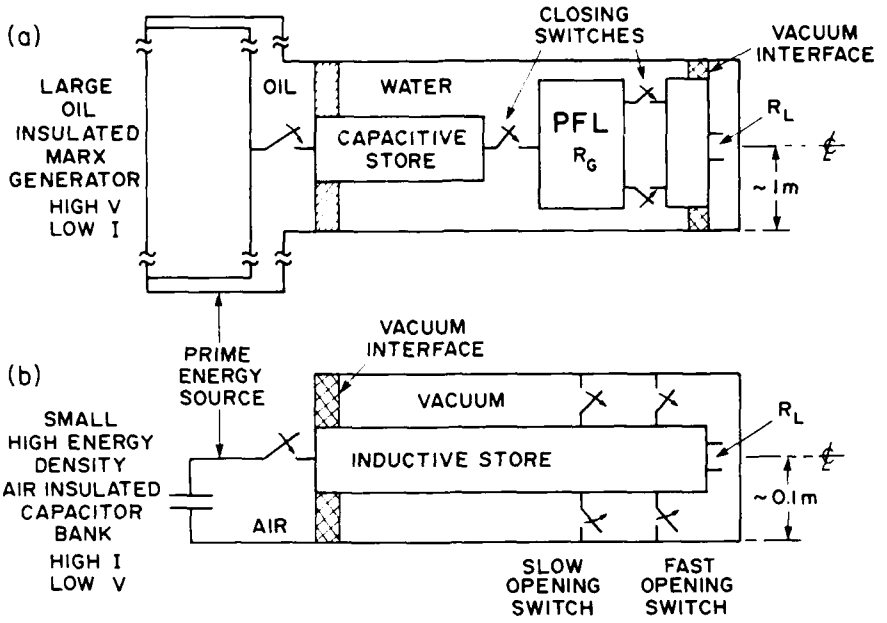

Fig. 3 — (a) Typical staged capacitive system with successive lower inductance stages in series with closing switches. (b) An ideal staged inductive system with two successive stages of faster opening switches in parallel.

Pawn facility to be described later, a closing switch is used to provide isolation between the two opening switches. In the ideal case, the inductor acts like a simple, lumped-circuit element during the long charging time, but acts like a short, current-charged PFL during discharge into the load. The current into a load whose resistance is matched to the vacuum impedance of the inductor is a square wave with amplitude of one half the charging current. Current (with the exception of the last stage) and energy are preserved, and voltage and power are multiplied by the successive stages of faster opening switches.

Advantages of Inductive Systems: Several potential advantages of an inductive system over a capacitive system exist. Both typically have first-stage capacitive storage, but the lower voltage capacitive store of the inductive system is inherently more compact, lighter, and less expensive. The vacuum inductive store has similar size, weight, and cost advantages over the dielectric capacitive store. These advantages increase with the elimination of the storage tanks and associated hardware required for water and oil maintenance in the capacitive system. Also, the voltage across the most critical component in these systems, the vacuum interface, is significantly reduced in an inductive system. In the capacitive system, the full output voltage appears across the vacuum interface. In an inductive system, the vacuum interface sees only the low charging voltage, not the high output voltage. The vacuum interface is physically removed from the load in an inductive system and thus is less affected by ultraviolet radiation and load debris. Even if the vacuum insulator were to flash over when the final switch opens in an inductive system, most of the energy would have already been transferred to the vacuum inductor and thus would be available to drive the load. The staged-vacuum-inductive system concept, shown in Fig. 3(b), has not yet been attempted; however, recent advances in opening switch technology may make this possible in the near future. The NRL Pawn generator, to be described later, is a major step in the direction of this ideal system.

Capacitive Generator With Final Stage Opening Switch: Up to the present, much of the

opening switch research at NRL has involved the addition of a final vacuum-inductive pulse-compression stage to the output of a conventional, 100-ns, capacitive generator to achieve voltage and power multiplication. In most of the capacitive pulsed-power generators in use today (such as Gamble II), voltage hold-off limitations across the vacuum interface dictate large spacings that, in turn, create large inductances between the coaxial-water-line output and the vacuum-diode load. This inductance is usually the limiting factor in obtaining short output-pulse rise times (< 10 ns) at high output powers. By employing this parasitic inductance and an additional vacuum inductance terminated with a fast-opening plasma switch in parallel with the load, it has been possible to obtain short duration, fast rise-time output pulses with substantial power and voltage multiplication. Because the vacuum inductor at the opening switch location can have a small radius compared to that of the water line and vacuum interface but comparable to that of a typical load, the parasitic inductance between the switch and the load can be very much smaller than the equivalent parasitic inductance in the unmodified capacitive system. Thus the output-pulse rise time is primarily limited by the switch opening time. For most plasma opening switches this opening time can be very fast, and the voltage hold-off can be very high because both involve self-magnetic insulation of the electron flow in the switch region.

Figure 4 illustrates the electrical circuit for such a hybrid system. A capacitive generator, with open-circuit voltage V_G and characteristic output impedance R_G, current charges an inductor through a fast-opening plasma switch operating in the closed state. The peak electrical energy stored in the inductor can be greater than 80% of the energy available in the output pulse of the generator. When the current in the inductor reaches its peak, the switch opens and discharges the inductor current through the load impedance R_L. Assuming no energy loss, $R_L > R_G$, and $L >> L_L$, the power and voltage are multiplied by R_L/R_G

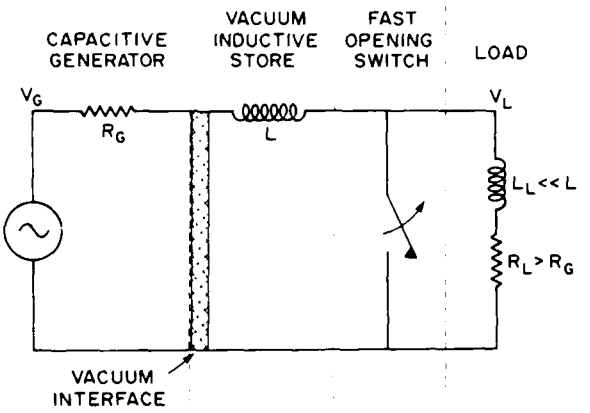

Fig. 4 — Conceptual circuit diagram of conventional capacitive generator with an inductive-store, pulse-compression final stage

over the matched load values. This results because the characteristic charging time is L/R_G while the discharge time is L/R_L. Even if the vacuum interface flashes over and becomes a short circuit, the energy already stored in the inductor will be delivered to the load.

Plasma Erosion Opening Switch Research at NRL

As seen from the above discussion, opening switches are the critical elements in inductive-energy-storage systems. For terawatt systems, opening switches must conduct megampere currents, then rapidly switch these currents to loads on timescales short compared with conduction times under megavolt stresses. One opening switch that has these properties is the plasma erosion opening switch (PEOS). NRL pioneered the development of the PEOS as a final-stage, fast-opening plasma switch to enhance the outputs of conventional pulsed-power generators.

A PEOS consists of plasma sources that inject flowing plasmas into the region between the output conductors of a generator. Figure 5 shows a PEOS used on the Gamble I generator. This PEOS configuration is typical of all NRL experiments that use different generators as the current source. A coaxial inductive-energy-storage section is added at the generator output where magnetic energy accumulates while the PEOS is *closed*. The outer

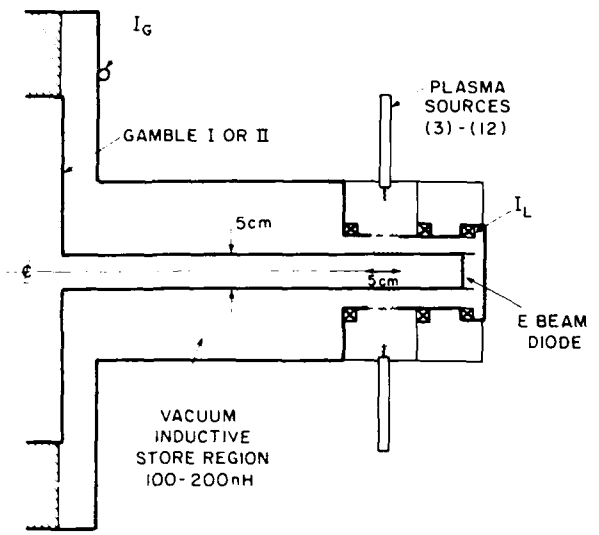

Fig. 5 — PEOS setup on the Gamble I and II generators at NRL

conductor in the PEOS region is made of a metal screen or an array of rods. Plasma flows through this outer conductor toward the center conductor, filling the annular region over a limited axial length, typically 5 to 10 cm. A load is located downstream of the PEOS; in Fig. 5, an electron-beam (e-beam) diode is shown. The plasma sources are fired 1 to 3 μs before firing the generator so that the plasma bridges the gap between the inner and outer conductors before the generator pulse arrives at the switch. For optimum conditions, the PEOS conducts the generator current as a short circuit, completely isolates the load, and opens when a current threshold is exceeded. The switch opening generates a large voltage at the load, and the current is transferred from the PEOS to the load. The PEOS is capable of opening in 10 ns or less and so is able to produce an electrical pulse at the load with short rise time and high voltage and power.

Experiments: In 1977, Mendel et al. [5] reported the first demonstration of opening switch behavior that used an injected plasma on a pulsed-power generator. In this experiment, the plasma served to short out the prepulse on the Proto I generator at SNLA. The prepulse reduction improved the performance of the diode load by preventing premature plasma formation and impedance collapse. The research effort at NRL and other laboratories followed from this work.

The NRL research effort changed the role of the PEOS from prepulse suppression and rise-time sharpening to power multiplication and inductive energy storage. The ability of the PEOS to enhance the output of conventional generators led to their incorporation in experiments on electron and ion beam diodes and imploding z-pinch loads. PEOS research is continuing in laboratories in the United States, France, Japan, West Germany, and the Soviet Union [6].

The first results demonstrating inductive energy storage, pulse compression, and power multiplication by use of a plasma opening switch were published by Meger et al. in 1983 [7]. These experiments were performed on Gamble I. Figure 6 shows typical data from Gamble I for short circuit and diode loads. The plasma conducts the generator current I_G, rising to 200 kA in 50 ns, then opens and transfers current to the load I_L in less than 10 ns. With an 11-Ω diode load, 1.4 MV is generated, over a factor of two greater than the matched load (2 Ω) voltage, and the peak load power exceeds the matched load value.

The Gamble I results motivated a concentrated research effort to improve the understanding of the physics of the PEOS and to perform scaling experiments at higher current on the 1-MA Gamble II generator. This work was carried out in support of light-ion ICF for DoE and advanced inductive-storage generator development for DNA and the Office of Naval Research (ONR). PEOS experiments on the Gamble II generator demonstrated power multiplication factors of 1.8 at power levels in excess of 2.5 TW [8]. More recent data are shown in the left-hand side of Fig. 7. The measured currents, I_G and I_L, are shown in Fig. 7(a). The PEOS conducts for 60 ns then opens in less than 10 ns, transferring 770 kA to the load. The output voltage calculated from

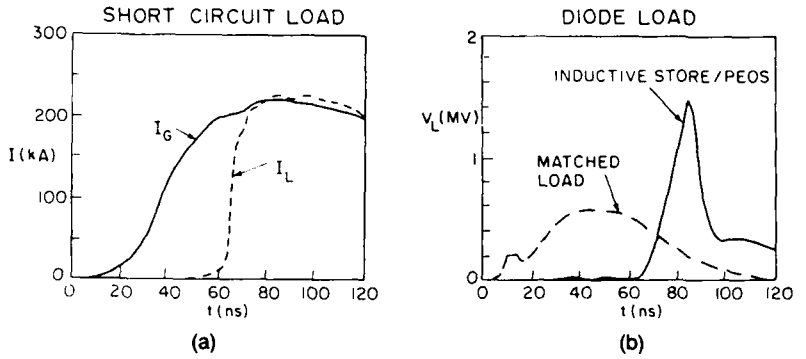

Fig. 6 — Gamble I PEOS data: (a) measured currents with short circuit load, (b) load voltage and matched load voltage with diode load

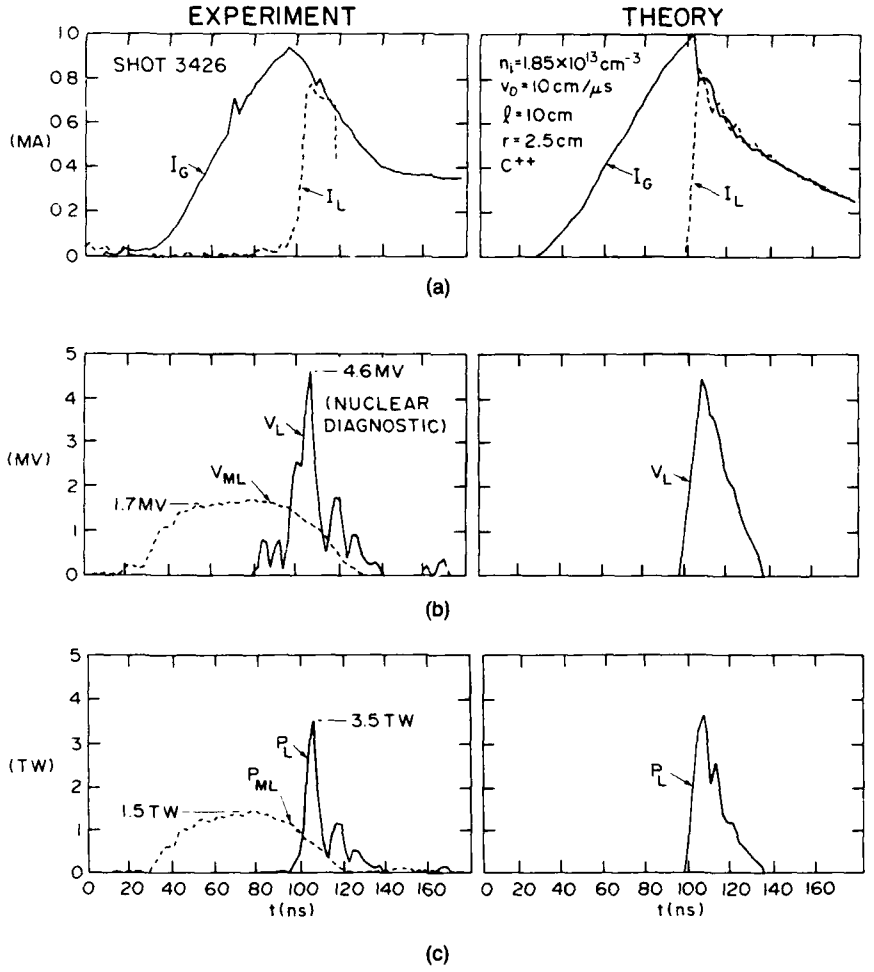

Fig. 7 — Gamble II PEOS data: (a) generator and load currents, (b) load voltage compared with matched load voltage, (c) load power compared with matched load power

electrical monitors is noisy (Fig. 7(b)) but agrees with the 4.6 MV peak load voltage from a nuclear diagnostic. The matched load voltage in Fig. 7(b) shows pulse compression and a voltage multiplication of 2.7. The peak power (3.5 TW) obtained on this shot (Fig. 7(c)) is 2.4 times the ideal (zero inductance) matched load value with less than 10-ns rise time. These results demonstrate the ability of the PEOS to dramatically enhance the performance of terawatt-level generators. These data are compared to PEOS model predictions (described below) on the right-hand side of Fig. 7.

PEOS experiments at other laboratories began after the successful Gamble results [6]. NRL was given the responsibility of developing the PEOS for the DoE Light Ion Fusion Program at SNLA with an eventual goal of halving the pulse width (40 to 20 ns) and doubling the voltage (15 to 30 MV) of PBFA II, the world's most powerful (~ 100 TW) pulsed-power generator. Experiments up to 3 MA have so far been performed at reduced power levels on PBFA II [9] and PEOS experiments at the 2-MA level were also performed on the 10-TW DNA Blackjack V generator at MLI with NRL collaboration [10].

Theory: The theoretical analysis of PEOS operation is a particularly difficult problem because it involves the multidimensional dynamics of low-density plasmas, space-charge sheaths, high-energy electron flows, and excitation of microinstabilities. The large, rapidly increasing electric and magnetic fields combined with these instabilities determine the electron current flow pattern in the plasma during the conduction phase. Complex sheath dynamics with magnetically insulated electron flow controls the opening phase and subsequent switching of current to the load.

A simple theory developed at NRL [11] explains the observed properties of the PEOS as a sequence of four phases. During the conduction phase, plasma ions drift toward the cathode (inner conductor) and electrons are emitted from the cathode and cross a small space-charge sheath to enter the plasma. The electron and ion current across the sheath are related by the space-charge-limited flow conditions across the sheath that dictates that the current densities are inversely proportional to the square root of their masses. For C^{++} ions, the dominant species, this ratio is 0.01 and the small ion current controls the much larger electron current. As the generator current through the switch increases, the electron emitting area increases since the electron current density is held constant by the constant plasma ion flux. The conduction phase ends when the total cathode area covered by plasma is emitting. This threshold, or conduction current, is determined by plasma density, drift speed, and switch area. The erosion phase begins when the generator current exceeds the conduction current. Ions are collected at the cathode faster than they are replaced by the plasma so the cathode sheath gap widens to uncover more ions. The enhanced erosion phase begins when the sheath gap becomes comparable to the average electron Larmor radius. Under these conditions, the space-charge condition is modified in such a way that the erosion rate is greatly increased. A high voltage is generated across the gap, and a substantial fraction of the current is diverted to the load. The switch is totally open when the magnetic insulation phase is reached. This occurs at a value of current for which the average Larmor radius is less than the gap size so that electrons cannot cross the sheath into the plasma and all the total electron current reaches the load.

The above theory leads to a simple set of equations that form a zero dimensional (0-D) model that has successfully reproduced experimental results under a large variety of conditions. An experiment is simulated by including the PEOS in a transmission-line code as a nonlinear circuit element whose impedance is determined by the equations governing the four phases. This procedure can be used to estimate the effects of parameter changes on PEOS performance and to scale the PEOS to higher current and voltage. Examples of this modeling are shown on the right-hand side of Fig. 7.

Although the theory described above explains the global electrical properties of the PEOS, it does not treat the physics of electron conduction inside the plasma. The spatial distribution of plasma and fields during conduction is strongly related to the opening properties of the switch. These processes are beginning to be understood by using the theoretical tools mentioned above. Understanding how the phenomena treated by these analyses affect operation of long-conduction switches is an important ongoing research effort.

Long-Conduction PEOS: The conduction time in the experiments described above is typically less than 100 ns because of the fast-pulsed-power generators used as drivers. The PEOS is capable, in principle, of much longer conduction times. Conduction time approaching 1 μs or longer would be useful for inductive generator systems that use capacitor bank drivers without water-line compression stages. PEOS experiments reported in 1986 from the Soviet Union [12] and NRL [13] demonstrated opening in less than 100 ns, after conduction times approaching 1 μs. The PEOS used in the Pawn experiment described below is based on these results.

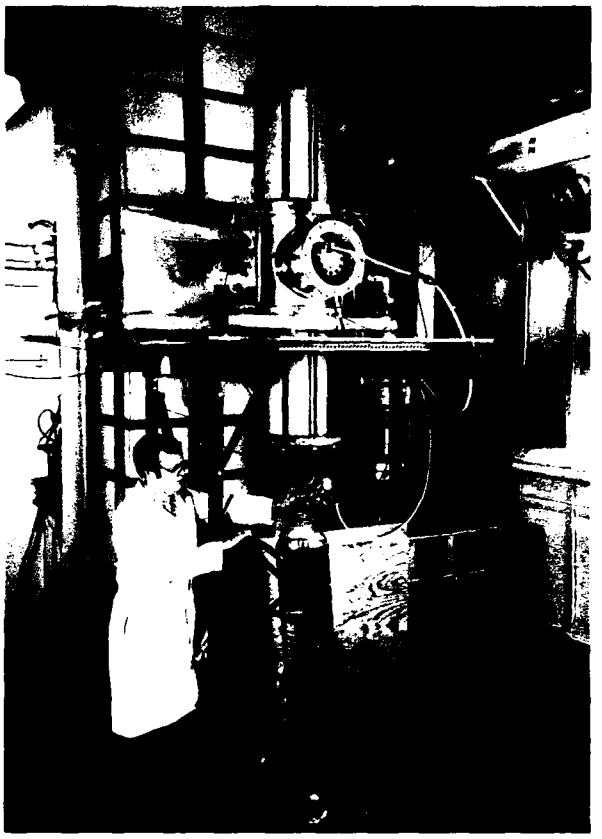

Fig. 8 — Pawn is a compact 1-MJ high-power pulse generator that uses vacuum-inductive-storage techniques with two stages of opening switches having fuses and plasmas, respectively

The NRL Pawn Generator

Figure 8 shows a prototype, compact, pulsed-power generator called Pawn under development at NRL [14]. It uses a high-energy-density capacitor bank (1 MJ, 3 MA, and 20 μs at 44 kV) as the prime energy store combined with staged inductive energy storage similar to Fig 3(b): a fuse and a PEOS are used as the first and second stage opening switches, respectively. The capacitors are discharged into an inductor by using *rail gap* closing switches. The circuit is closed with a fuse, consisting of an array of copper wires in a high-pressure gas, designed to explode when an appropriate current level is reached in the inductor. A triggered flashover switch (not shown in Fig. 3(b)), between the fuse and the PEOS, is closed during the rapid rise of the fuse voltage. Current then flows through the PEOS, rising to about 1 MA in under 1 μs. The PEOS is designed to open in less than 100 ns and divert the current into a load. The objective is to generate a 1-MV, 1-MA, 100-ns output pulse with Pawn.

Figure 9 illustrates Pawn performance. The capacitor bank current, the current transferred by the fuse into the PEOS, and the current transferred by the PEOS to the electron-beam diode load are plotted together as a function of time. The capacitor bank voltage, the voltage generated at the fuse, and the voltage of the load are shown on the same time scale. At each stage of switching, the current rate of rise increases (0.1 to 1.3 TA/s, 1.3 to 6.5 TA/s) as does the voltage (39 to 250 kV, 250 to 410 kV). The PEOS conducts the fuse output current for

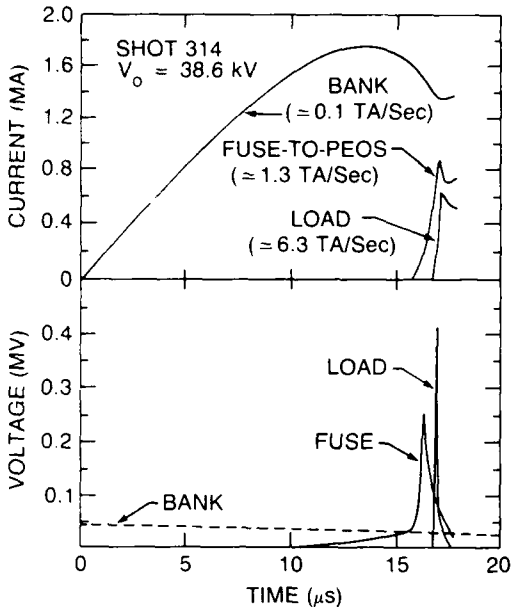

Fig. 9 — Pawn PEOS data showing current and voltage on the capacitor bank, the fuse, and the load

0.7 μs to a level of almost 1 MA before opening and transferring 0.7 MA in about 0.09 μs to the load. The 400-kV load voltage is more than a factor of 10 higher than the initial capacitor voltage. This 1/4-TW output power is higher than that of Gamble I, which occupies 20 times the volume of Pawn.

With Pawn, we have demonstrated that low-voltage inductive energy storage and sequential opening switches for power conditioning can economically generate high-power electrical pulses from compact generators. Optimizing this system should produce about a twofold increase in the current and voltage delivered to the load. Another area of research consists of developing a very long conduction time (10 to 20 μs) plasma opening switch to replace the present inefficient and cumbersome fuse stage. This would also remove the high-pressure gas insulators surrounding the present fuse that, in turn, would lead to the ideal, all-vacuum-inductive system illustrated in Fig. 3(b). If we are successful, Pawn will provide an electrical power pulse comparable to Gamble II from 1/100 of its volume.

Future Facility Upgrade

The success of Pawn has led us to undertake a major upgrade of our inductive storage facilities. The project, jointly funded by NRL and DNA, will consist of two new inductive facilities—a versatile 3-MJ slow bank called Rook and a lower energy companion device called Hawk. Part of this upgrade also involves the purchase of new data acquisition equipment and diagnostics. With the present Pawn device and the requisite diagnostic capability, Rook and Hawk will give NRL a uniquely flexible, highly instrumented facility. They will be primarily used to support DNA's advanced simulator development program over the next decade by continuing research on both short- and long-conduction-time plasma opening switches and the advanced bremsstrahlung and imploding plasma radiation sources to be driven by this new class of inductive generators.

Hawk: The smaller facility, Hawk, will replace most of the present Gamble I facility while using its Marx tank and oil storage facilities. Physics International Co., Inc. will supply a compact, 300-kJ, high-voltage (700 kV) oil-insulated Marx generator that will be used to *current* charge a vacuum inductor to 1 MA in 1 μs. This facility will allow a high data rate of 10 to 20 shots per day compared to 2 to 4 for Gamble II and 1 to 2 for Pawn (limited by fuse replacement).

Rook: The larger facility, Rook, will consist of three 1-MJ, 40-kV Pawn banks supplied by MLI, which will be connected together to charge a common vacuum inductor. With a scaled-up Pawn fuse, it will supply 3 MA in 1 μs at more than 250 kV into a PEOS. More important, without the fuse stage, it will supply over 10 MA in 8 μs at its output for research on very long- conduction-time plasma opening switches to replace the present first-stage fuse opening switch. The development of such long-conduction-time plasma opening switches would allow this new inductive-energy-storage technology to be scaled up to even higher power and energy levels.

Conclusion

The newly emerging plasma opening switches being developed at NRL and elsewhere are already being used to significantly upgrade existing pulsed-power facilities. With further development, these new switches, used in conjunction with recent advances in high-energy-density capacitors, could lead to a new generation of inexpensive, compact, single-shot or repetitively pulsed, high-power accelerators that use inductive-energy-storage techniques. Many applications of this new pulsed-power technology are envisioned in areas such as nuclear-weapon-effects simulation, inertial-confinement fusion, X-ray lasers and lithography, neutron radiography, and directed energy weapons.

Acknowledgments: The author acknowledges the many pioneering contributions to pulsed-power technology by his colleagues at NRL over the years, only some of which are noted in the references. The author also specifically thanks Drs. P.F. Ottinger, R.J. Commisso, and B.V. Weber for contributing material for this manuscript and, in particular, Dr. D. Mosher for valuable advice during its preparation. Finally, this research effort is particularly indebted to both Dr. S.L. Ossakow, Superintendent, Plasma Physics Division and Dr. T. Coffey, Director of Research at NRL, for their continued support and encouragement.

References

1. A. Kolb and I.M. Vitkovitsky, private communication. For information about a later upgrade to Gamble I, see G. Cooperstein, J.J. Condon, and J.R. Boller, "The Gamble I Pulsed Electron Beam Generator," *J. Vac. Sci. Technol.* **10,** 961-964 (1973).

2. J.D. Shipman, Jr., "Final Electrical Design Report of the Gamble II Pulse Generator," NRL Memorandum Report 2212, 1971.

3. J.R. Boller, J.K. Burton, and J.D. Shipman, Jr., "Status of the Upgraded Version of the NRL Gamble II Pulse Power Generator," Proceedings of the 2nd IEEE International Pulsed Power Conference, Lubbock, Texas, 1979, p. 205.

4. D. Conte, R.D. Ford, W.H. Lupton, and I.M. Vitkovitsky, "Trident—A Megavolt Pulse Generator Using Inductive Energy Storage," Proceedings of the 2nd IEEE International Pulsed Power Conference, Lubbock, Texas, 1979, p. 276.

5. C.W. Mendel, Jr. and S.A. Goldstein, "A Fast-Opening Switch For Use in REB Diode Experiments," *J. Appl. Phys.* **48,** 1004-1006 (1977).

6. See papers in the Special Issue on Fast-Opening Vacuum Switches, G. Cooperstein and P.F. Ottinger, eds., *IEEE Trans. Plasma Sci.* **PS-15**(6) (1987).

7. R.A. Meger, R.J. Commisso, G. Cooperstein, and S.A. Goldstein, "Vacuum Inductive Store/Puise Compression Experiments on a High Power Accelerator Using Plasma Opening Switches," *Appl. Phys. Lett.* **42,** 943-945 (1983).

8. J.M. Neri et al., "High-voltage, High-power Operation of the Plasma Erosion Opening Switch," *Appl. Phys. Lett.* **50,** 1331-1333 (1987).

9. R.W. Stinnett et al., "Plasma Opening Switch Development for Particle Beam Fusion Accelerator II (PBFA II)," *IEEE Trans. Plasma Sci.*, **PS-15**(5), 557-563 (1987).

10. B.V. Weber et al., "Plasma Erosion Opening Switch Research at NRL," *IEEE Trans. Plasma Sci.* **PS-15**(6), 635-648 (1987).

11. P.F. Ottinger, S.A. Goldstein, and R.A. Meger, "Theoretical Modeling of the Plasma Erosion Opening Switch for Inductive Storage Applications," *J. Appl. Phys.* **56,** 774-784 (1984).

12. S.P. Bugaev et al., "High-Power Nanosecond Pulse Generator with a Vacuum Line

and a Plasma Interrupter," Proceedings of the 6th International Conference on High-Power Particle Beams, Kobe, Japan, 1986, pp. 878-881.

13. D.D. Hinshelwood et. al., "Long Conduction Time Plasma Erosion Opening Switch Experiment," *Appl. Phys. Lett.* **49,** 1635-1637 (1986).

14. R.J. Commisso, "A Compact Pulsed-Power Generator," 1987 NRL Review, pp. 69; and G. Cooperstein et al., "Inductive Energy Storage Research at NRL," Proceedings of the 6th International Conference on High-Power Particle Beams, Kobe, Japan, 1986, pp. 843-846.

THE AUTHOR

Dr. COOPERSTEIN received a B.S. in physics in 1963 and a PhD in experimental, high-energy physics in 1968, both from MIT. His first two positions were with EG&G in Bedford Mass. and Ion Physics Corp. in Burlington, Mass. where he worked on generating intense electron beams for simulating nuclear weapon effects. He joined NRL as a section head in the Plasma Physics Division in 1971, where he was responsible for performing similar research on the newly developed Gamble high-voltage, pulsed-power generators (1 MA, 1 MV, 50 ns). Over the years, he has co-authored over 100 publications and professional society presentations on the subjects of high-voltage, pulsed power and intense electron and ion beam generation. In 1987, he was elected to Fellowship in the American Physics Society "for pioneering work in the production and focusing of intense electron and ion beams, and for contributions to and leadership in applying inductive storage techniques to pulsed power accelerators." He is presently head of the Plasma Technology Branch, which is responsible for research into the technology and applications of pulsed-power science.

Research in Ceramic Composites at NRL

David Lewis III
Materials Science and Technology Division

Introduction

The U.S. Navy has long supported fundamental and applied research directed toward its present and future needs. In recent years, the perceived need for improved high-temperature structural materials, as well as the need for higher performance materials for specialty applications such as radomes and IRdomes, has led to substantial efforts in ceramic matrix composite materials. These efforts were initially conducted in the Ceramics Branch and now are carried on in the Composites and Ceramics Branch, which consists of approximately 40 professionals and 10 contract employees covering a wide range of disciplines and expertise in ceramics, ceramic composites, and metal matrix composites. Much of the work of this group is directed toward present or perceived future Navy needs, but a substantial portion is also devoted to other Department of Defense (DoD) and government activities, including the Strategic Defense Initiative (SDI), the National Aerospace Plane (NASP), materials for stealth applications, and ceramics for advanced heat engines. Some of these outside research activities relate very directly to the programs in ceramic matrix composites, e.g., the NASP and materials for advanced gas turbine engines.

The research efforts in ceramics at Naval Research Laboratory (NRL), both those internally funded and those supported by outside funding, have historically been divided into three major subject areas: electronic ceramics, structural ceramics, and fundamental studies in the physical behavior of ceramics. Each of these subject areas has typically included some efforts involving ceramic matrix composites. The research efforts have addressed needs for ceramic materials in applications including: advanced heat engines, e.g., adiabatic diesels and advanced gas turbines; armor; bearing and seals; electronic packaging and substrates; IR windows (IRdomes); laser hardening; radar windows (radomes), radar absorbing materials and structures, and sonar. In many of these cases the needs suggested or required the use of composite material approaches, and thus a large part of the research in ceramics at NRL has, in fact, been devoted to the development and understanding of the behavior of ceramic matrix composites of various types and for a variety of applications.

The efforts at NRL in ceramic matrix composites are currently supported in part by indirect funding from the Office of Naval Research (ONR) through NRL core funds and by funds from the Naval Air Systems Command (NAVAIR). In the past, the ceramic composites program at NRL has been supported extensively by direct funding from ONR, NAVAIR, the Defense Advanced Research Projects Agency (DARPA), and to a lesser extent by monies from the other Navy System Commands and the Department of Energy. Historically, the efforts in ceramic composites at NRL have been funded at the level of $100,000 to $500,000 a year. Table 1 shows a partial listing of past and present NRL ceramic composites research programs and related efforts roughly in chronological order.

Specific Research Programs

Electronic Ceramics: In research on electronic ceramics, the Ceramics Branch has historically worked in several areas directly related to specific Navy needs. Some programs have addressed the needs of high-speed circuitry for

Table 1 — Research Programs in Ceramic Composites and Related Programs at NRL

Title	Funding Source
Laser Hardening and Effects in Ceramics	DARPA
Processing of Ceramic Turbine Materials	DARPA, ONR
Processing of Particulate Ceramic Composites	NAVAIR, ONR
Mechanical Properties of IR and Radar Ceramics	NAVAIR
Thermal and Corrosion Barrier Coatings for Marine Gas Turbines	NAVSEA[(a)]
Low-Radar Cross Section Materials	NAVAIR
Composite Tranducer Ceramics	ONR (NRL)
Ceramic Fiber Composit s	NAVAIR
Precipitation Toughening of Ceramics	ONR
Rapid Solidification Processing of Ceramics	ONR (NRL)
Self-Propagating Synthesis Processing of Ceramics	DARPA
Oxidation-Resistant Carbon-Carbon Composites	DARPA
Fracture Toughening and Tribology of Ceramics	ONR (NRL)
Evaluation of BN-Producing Polymers	ONR
Ceramics with Ordered Voids	ONR, NAVAIR
Ordered Void Materials for Towed Sonar Arrays	NUSC[(b)]
Substrates for High Speed, High Density Circuitry	ONR
Strengthening of Ceramics with Ordered Voids	NAVAIR
High-Temperature Structural Composites	NASPO[(c)]
Evaluation of Fibers for Ceramic Matrix Composites	NAVAIR

[(a)] Naval Sea Systems Command
[(b)] Naval Undersea Systems Command
[(c)] National Aerospace Plane Office

packaging and substrates and various other electronic ceramic applications. The largest of these programs has sought the improvement of existing ceramic piezoelectric materials and the development of new materials. The piezoelectric ceramic materials, barium titanate and lead zirconate titanate (PZT), are incorporated into the many active and passive sonar systems that consume a significant amount of the Navy budget. The Ceramics Branch initially worked primarily in the area of failure analysis and the development of appropriate test procedures, but subsequently has become involved in the development of new sonar transducer materials.

Recently, the group has worked extensively on the design, fabrication, and testing of sonar transducer materials incorporating arrays of ordered voids. These materials are effectively composite materials, in this case an atypical composite consisting of a ceramic material (PZT) and air. These materials, produced by combinations of tape casting and silk screen printing techniques, convert an isotropic polycrystalline (monolithic) material into a highly anisotropic composite body with significantly different piezoelectric properties, see Figs. 1 and 2. The most impressive gains have been in the area of hydrostatic sensitivity, but the same technique can be used for precise control of local dielectric properties (e.g., in substrates) to provide cooling passages in packaging and has been shown to increase the strength and toughness of the PZT [1-3] (see Figs. 3 and 4). The latter effect, where the addition of 10 to 20 volume percent (v/o) porosity increases both the flexural strength and toughness (work-of-fracture) of a material is rather unexpected. However, it may have application to other materials if the scale of the ordered void pattern and the tape thickness can be reduced to dimensions on the order of 10 to 20 μm (this is close to the limit of current tape casting and fugitive ink patterning technology).

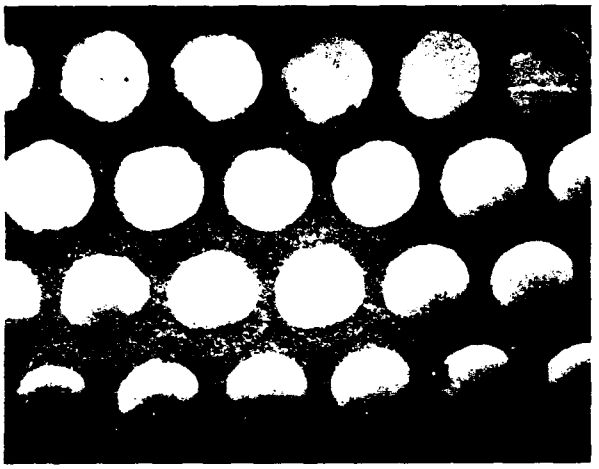

(a)

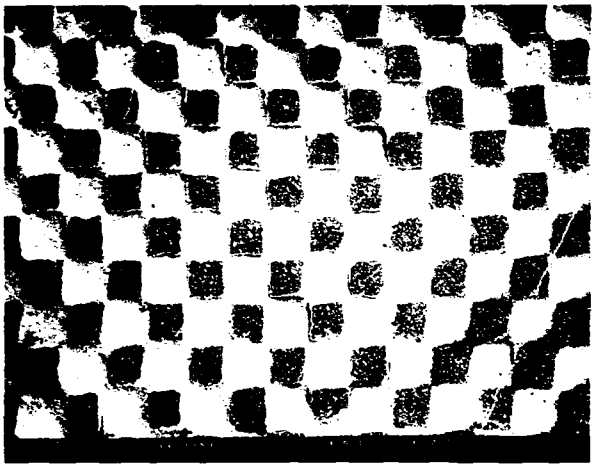

(b)

Fig. 1 – Ordered voids in PZT ceramic produced by silk screen/tape casting process: (a) top view of material with lenticular voids, approximately 0.7–mm diameter by 0.06–mm thickness; (b) top view of square void array pattern

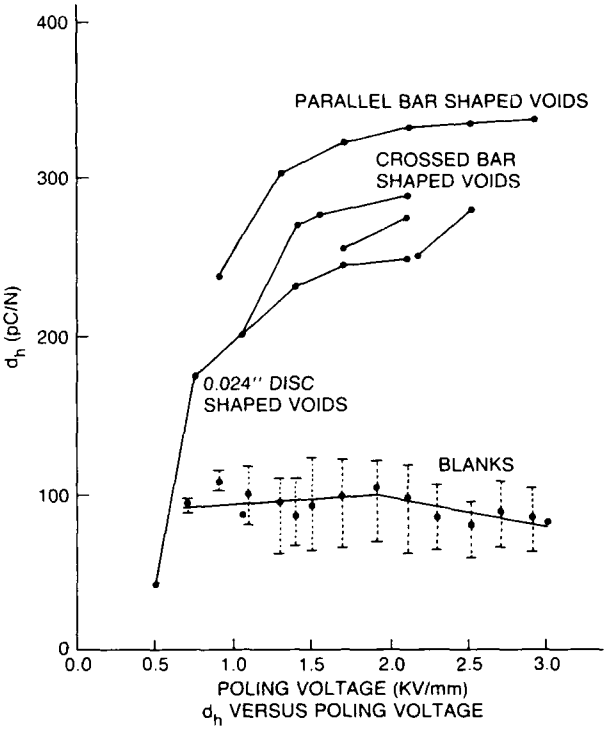

Fig. 2 – Hydrostatic sensitivity d_h vs poling voltage for various ordered void materials and control material (blanks) showing increase of 300% to 400% in hydrostatic sensitivity

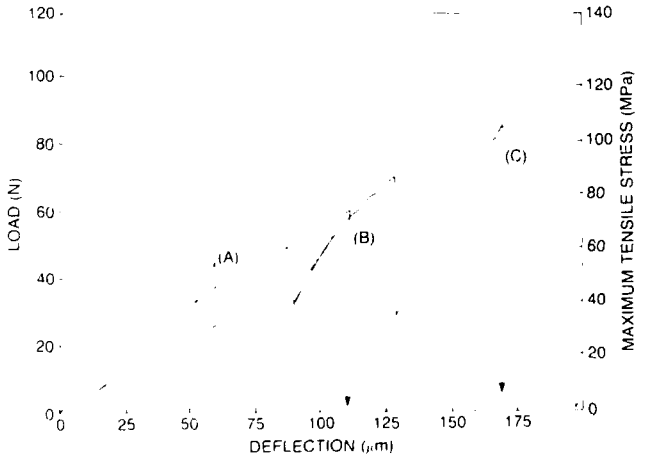

Fig. 3 – Load deflection (stress–strain curves) for monolithic PZT and PZT–containing ordered void arrays showing an increase in load or stress at failure and an increased work–of–fracture (area under curve) associated with introduction of ordered voids

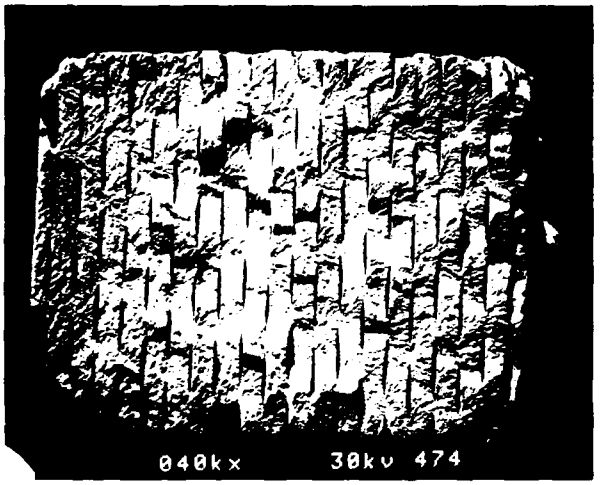

Fig. 4 – Fracture surface in PZT ceramic with an array of lenticular voids, showing the complex fracture interaction with void arrays associated with an increase in strength and work-of-fracture over dense PZT. The fracture direction is left to right, and void plane spacing is approximately 0.12 mm.

Current work on these materials stresses the use of combinations of experimental development and three-dimensional (3D) finite difference analyses to optimize the ordered void materials for various piezoelectric properties, to explain the effects on strength and crack propagation, and to explore other possible uses of this unusual type of composite technology.

Basic Fracture Studies: Recent efforts at NRL in basic fracture mechanics research have focused on three areas: the details of fracture in ceramic single crystals, improving and measuring the fracture toughness of ceramic matrix-ceramic fiber composites, and tribology and wear in ceramics. As part of the long-term efforts to provide reliable fracture mechanics data for ceramics, the applied moment double cantilever beam (AMDCB) fracture toughness specimen was developed at NRL [4,5]. This specimen has been applied to a great variety of materials, ranging from alkali halides (detector crystals for the Gamma Ray Observatory) with K_{Ic} (fracture toughness) values less than 0.1 MPa-$m^{1/2}$, to highly anisotropic ceramic composites with toughnesses in excess of 50 MPa-$m^{1/2}$ and on samples ranging in size from less than 1 cm to greater than 20 cm in length. This test has the great advantage (for opaque materials) of neither requiring measurement of crack length during testing, nor for any compliance calibrations, all of which are problems for typical ceramic composite materials.

The modification of this test and its successful adaptation for high-toughness, highly anisotropic ceramic matrix-ceramic fiber composites has been a significant accomplishment and permitted, for the first time, an accurate determination of the true toughness of these materials. Recently, this modified AMDCB test has been successfully applied to ceramic fiber composite materials such as United Technology Research Center's (UTRC's) Compglas™ and to natural fiber composites such as jade [6], see Figs. 5 and 6. The difficulty here is in testing highly anisotropic materials, where the fracture toughness may vary by more than an order of magnitude for different directions, e.g., from 2 to 50 MPa-$m^{1/2}$ for the weak and strong directions in Compglas™ unidirectional ceramic fiber-ceramic composite materials. The previous design for the AMDCB apparatus was modified to constrain the crack propagation to the desired direction, and this modification, with the necessary corrections to the K_{Ic} calculations has been tested successfully on a wide range of materials.

The wear efforts initially focused on *conventional* ceramics, such as alumina, silicon nitride, and silicon carbide, using the pin-on-disc (POD) test, and the POD test has now been applied to the study of the wear behavior of some natural fiber composites, jadeite and hornblende [7], with very interesting results in one case. These natural materials are interesting model materials in this regard (wear) and in relation to mechanical properties such as fracture toughness, since they represent a wide variety of microstructures, ranging from randomly oriented, elongated grains to highly oriented, fibrous grains (Fig. 6). In the last case, the material consists of essentially 100% unidirectional fibers (highly acicular grains), bonded together by a minimal amount of matrix phase. The wear results here suggest that a suitable

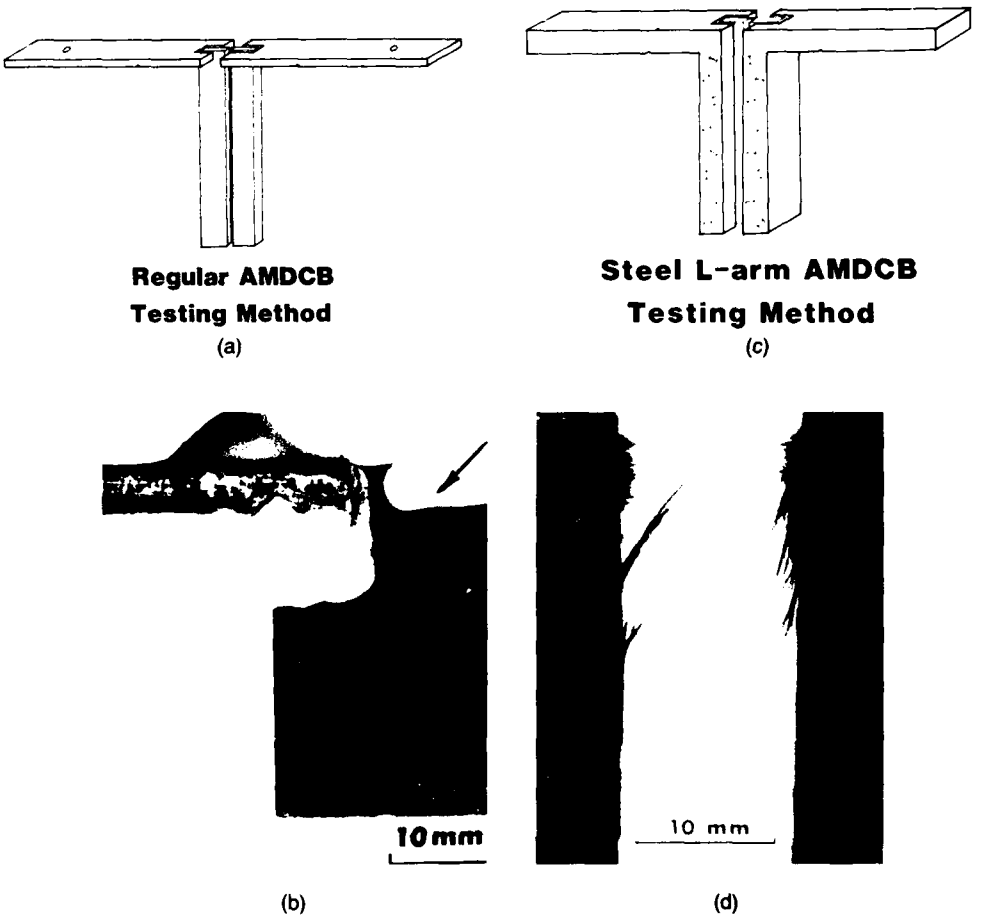

Fig. 5 – Modification of AMDCB fracture toughness test (L-arm method) permitting successful testing of tough, anisotropic fiber composite (sample on right)

Fig. 6 – Fracture surface topography in an AMDCB specimen of commercial Lou Bon hornblende (one of the *jade* family of minerals, showing fibrous structures associated with high-fracture toughness. Fracture surfaces are from a fracture toughness test specimen performed with the L-arm AMDCB technique.

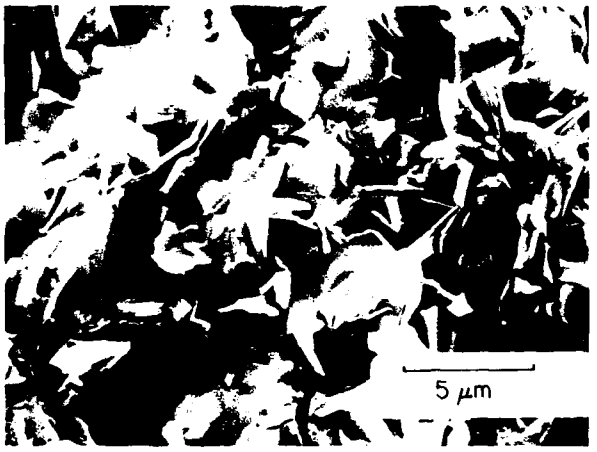

Fig. 7 – Fracture surface in mullite (aluminum silicate)–30 v/o BN particulate composite showing flaky BN grains embedded in mullite matrix

composite (i.e., one with hard fibers and matrix) with the bulk of the fibers oriented normal to the wear surface should have exceptional resistance to sliding wear.

Structural Ceramics: NRL has long had a strong program in structural ceramics and ceramic composites, initially focusing on such materials as silicon nitride and silicon carbide. This work evolved into a program studying particulate and fiber composites as well, producing significant results on alumina–BN and mullite–BN particulate composites, as shown in Fig. 7, which exhibit favorable combinations of erosion resistance, thermal-shock resistance, dielectric properties, toughness, and machinability. This work, which was reported extensively in the past [8–10], produced composites with the combination of moderately high strength (400 to 500 MPa), high toughness (8 to 10 MPa-$m^{1/2}$), excellent machinability (similar to Macor™), and good dielectric properties. This work was also directed toward production of better material for supersonic radomes. More recently, the focus of the work in structural ceramics and composites has fallen on fiber-reinforced ceramic matrix composites, and, in particular, on interface control in these materials [11–15]. The group at NRL was one of the pioneers in the use of fiber coatings for interface control in ceramic matrix composites (CMCs), obtaining a patent on the use of borazine-derived BN for this purpose. Figure 8 shows an example of the beneficial effects of the BN coatings. The use of borazine and low-pressure chemical vapor deposition (CVD) allowed the reasonably uniform coating of unspread fiber tows at a deposition temperature low enough (900°C) to minimize fiber degradation. This process also involved the evolution of no aggressive species such as HCl gas, with similar benefits. Subsequent work explored the use of various multilayer coatings to overcome some of the limitations of the single-layer BN coatings. Two-layer BN/BN coatings were produced, with the lower layer derived from borazine, deposited at a low temperature to protect the fiber, and the upper layer derived from BCl_3 at higher temperature to obtain a more chemically stable hex-BN coating. Various other materials and combinations of materials were tested as coatings, including carbon and combinations of BN and SiC, the latter derived from trichlor-methylsilane.

For these fiber composites, using two-layer, BN/SiC coatings on Nicalon fibers in a $ZrTiO_4$ matrix, Fig. 9 shows that the most successful results have been tensile strengths of approximately 1000 MPa and fracture toughnesses of about 50 MPa-$m^{1/2}$. Figure 5 shows an example of a fiber-matrix interface for a BN/SiC-coated Nicalon fiber in a $ZrTiO_4$ matrix. These mechanical properties for ceramic matrix composites are sufficient to make them strong candidates for high-temperature structural materials, replacing superalloys if the problems of high-temperature oxidative degradation of the interface can be overcome (Fig. 10). Research is currently in progress at NRL on several problems related to this oxidative degradation: fiber degradation at high temperature in various environments, the effects of fiber coatings on this problem, and the effects of fiber coatings on the degradation of the mechanical properties of ceramic matrix composites at high temperatures in oxidizing environments [16–17]. This research is

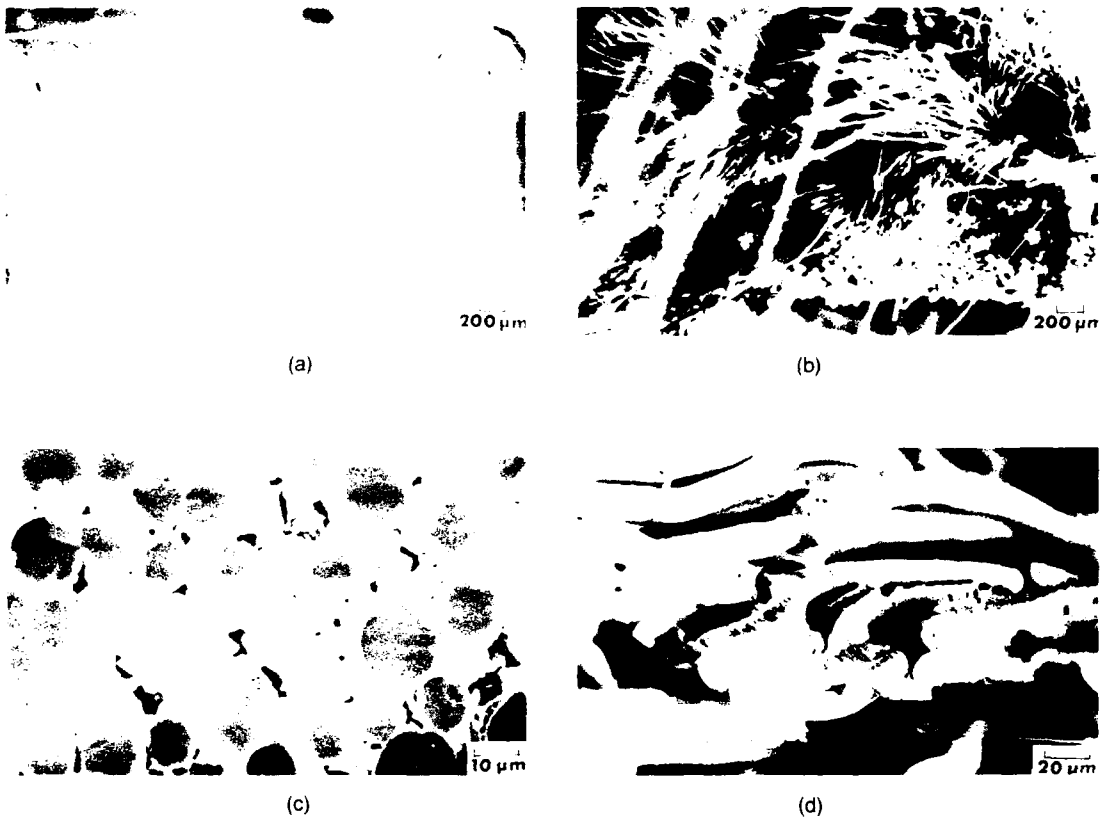

Fig. 8 – Effects of BN coatings on fracture behavior of $ZrTiO_4$ matrix–Nicalon SiC fiber composites: (a) and (c) composite without fiber coating exhibits low fracture toughness and relatively planar fracture; (b) and (d) composite with coated fibers exhibits extensive fiber pullout and fracture toughness approximately 25 times higher.

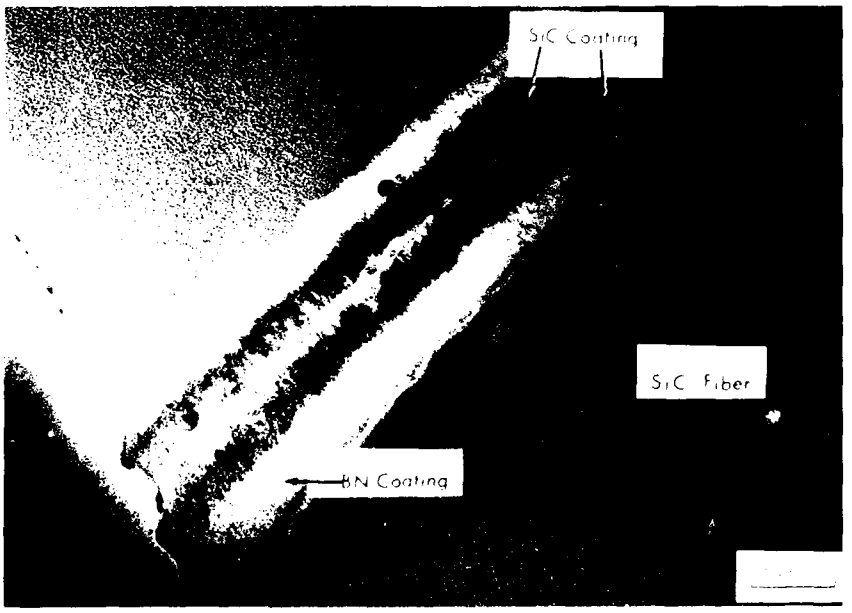

Fig. 9 – Bilayer SiC/BN coating on Nicalon SiC fibers in composite; micrograph shows the region where the two fibers touch.

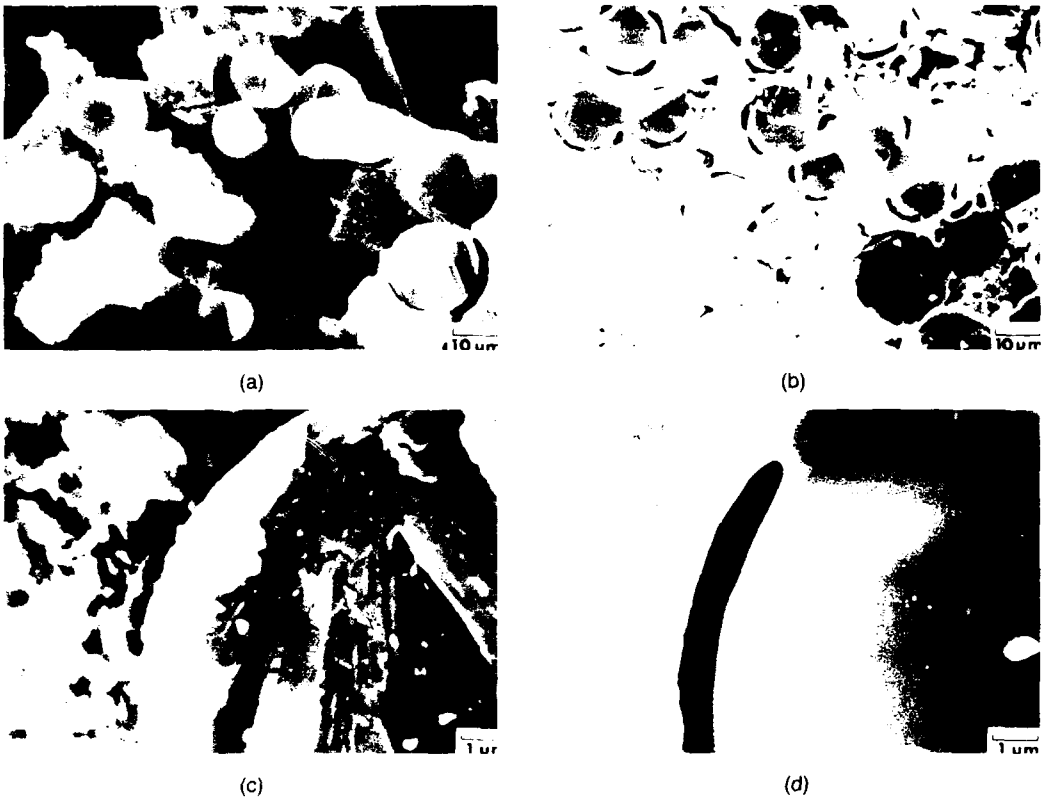

Fig. 10 – Effect of oxidation at 1000°C on $ZrTiO_4$ matrix–SiC/BN–coated Nicalon fiber composite: (a) and (c) as–prepared composite shows high toughness, rough fracture surface, and extensive fiber pull–out associated with low bonding; (b) and (d) oxidized composite shows low toughness, smooth fracture surface, and strong matrix–fiber bonding

also exploring further developments in the coating areas, including the use of three–layer coatings designed to minimize the interaction of the fiber *and* the matrix with the BN layer.

The part of this current research program that may have the most significant implications for ceramic matrix composites is the study of the dependence of fiber degradation on environment. While it is well known that fibers such as Nicalon degrade significantly in air at high temperatures, because of oxidation of the free carbon in the fibers and the loss of CO and SiO from the fibers, this is not the environment typical of either processing or service for these fibers. Where composites are prepared by hot pressing, the processing environment is likely to be reducing, and a high overpressure of CO may be present. The environment within a composite in service at high temperature is more difficult to define, but is certainly not equivalent to free air at 1 atm. The study [16,17] noted has sought to characterize the changes and degradation in fibers such as Nicalon SiC and other polymer–derived fibers in various atmospheres, such as air, argon, nitrogen, oxygen, and carbon monoxide over a wide range of temperatures and times. Figure 11 shows the changes in the fiber chemistry occurring with heat treatment of a ceramic fiber in CO, where the surface chemistry of the fiber is significantly modified.

One of the results of this study was an indication that very large differences exist in the extent of fiber property degradation for various atmospheres, the degradation here characterized primarily by the tensile strength measured on individual fibers for various atmospheres. Another result indicated that some atmospheres, e.g., nitrogen with a carbon source present to provide

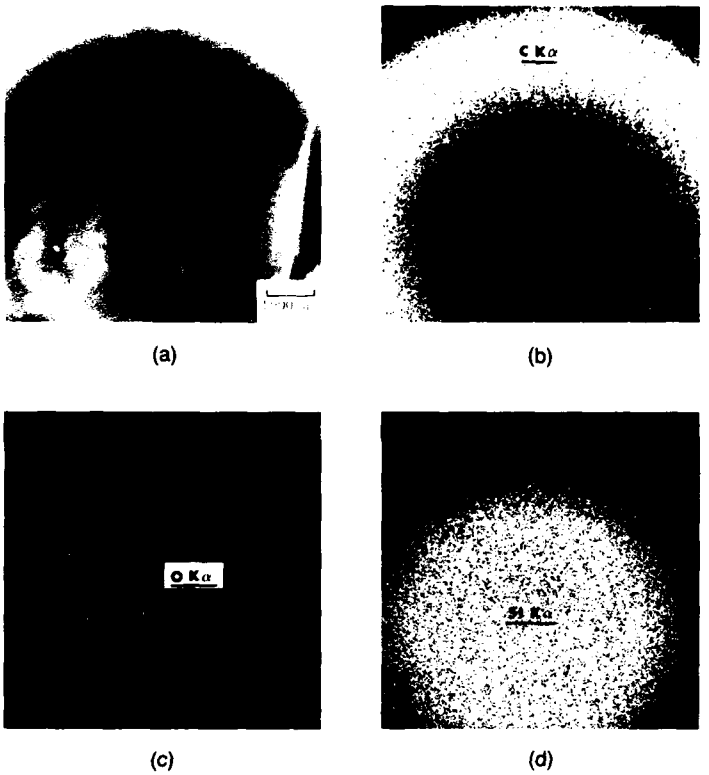

Fig. 11 – Elemental maps for polymer-derived SiC fiber after heat treatment in CO, showing surface depletion of Si (removed as SiO vapor) leaving a C-rich surface layer

reducing conditions, have very little effect on fiber properties. In addition to the effects on fiber strength, many visible and very interesting changes in the fiber morphology exist with these heat treatments, as shown in Fig. 12. This shows in-situ formation of silicon nitride whiskers on a polymer-derived SiC fiber associated with one particular treatment. Although significant fiber degradation is associated with this whisker growth there is also potential here, especially with carbon-carbon or metal matrix composites, for providing significantly increased transverse shear and tensile properties in these composites. Currently, these properties, not the greatly higher longitudinal tensile strength, are design-limiting, and a tradeoff of longitudinal tensile strength for increased transverse tensile strength and shear strength may well be worthwhile. Other effects noted here include the formation of a dense SiC layer on these fibers; this coating may serve a useful protective function on these relatively unstable and reactive fibers.

Another current project (in the Composites and Ceramics Branch), which is interesting from a basic scientific standpoint, is the incorporation of metal particles into a glass or glass-ceramic matrix to form a model particulate composite [18-19]. This type of particulate composite, which has been widely used in the past for various studies regarding composite properties, has the advantage of great flexibility in a number of composite parameters, such as volume fraction, particle size, particle shape and orientation, and residual stress state. Figure 13 shows fracture surfaces in such a glass matrix-metal particle composite for unbonded and bonded particles, showing the effect of such differences on the fracture mode. Here the experimental analysis is coupled with a theoretical analysis based on that of Eshelby for arrays of ellipsoidal particles in a matrix. With some

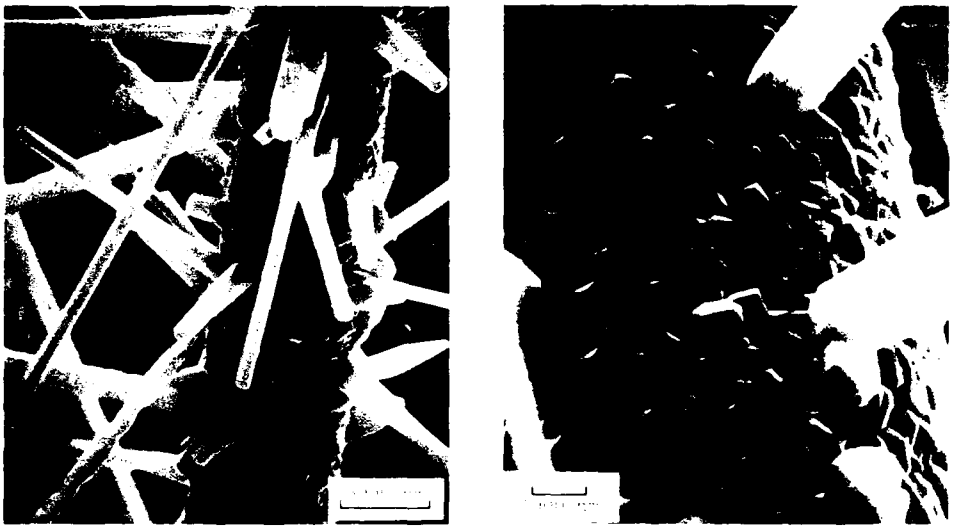

Fig. 12 – Effect of heat treatment in nitrogen on polymer-d[illegible]C fibers, resulting in extensive growth of silicon nitride whiskers from su[illegible]e of fibers

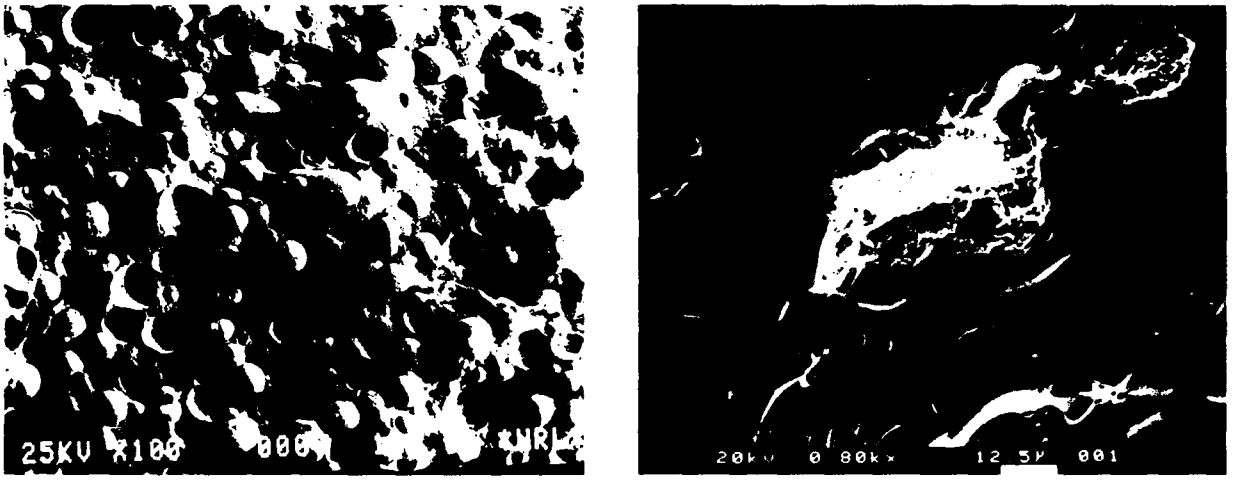

(a) (b)

Fig. 13 – Fracture surfaces in model particulate composites: (a) Si_3N_4–coated iron alloy particles in Macor™ glass–ceramic matrix, with minimal particle–matrix bonding and matched thermal expansion coefficients resulting in particle debonding during fracture; and (b) oxidized Kovar particles in Corning 7052 glass matrix with matched expansion coefficients but strong particle–matrix bonding, resulting in particle fracture and higher fracture toughness

processing techniques such as uniaxial hot-pressing, it is possible to produce particle alignment of nonspherical particles, or to distort spherical particles into oblate spheroids. Theoretical calculations of various properties, e.g., strength, modulus, fracture toughness, optical properties, electromagnetic properties, of these materials can here be compared directly with experimental measurements.

Current efforts on these model particulate systems address the details of the interactions of a crack front with the dispersed phase, and the effects of crack size and crack velocity on the effectiveness of the dispersed phase in making the composite tougher. One interesting result of this research program is the finding that the major effect of the dispersed metal particles is on the initiation of crack propagation, not on its

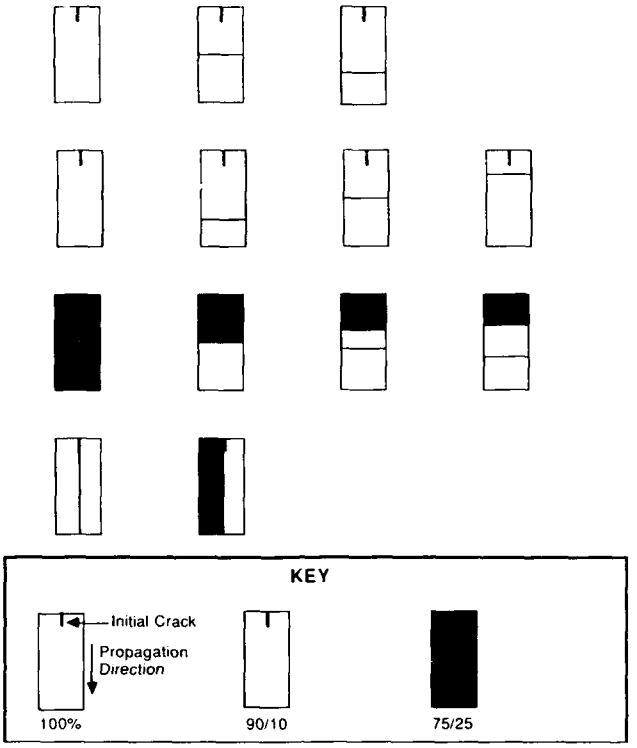

Fig. 14 – Schematic of various possible graded composite structures to assess effects of crack velocity and other factors on toughening effects of particulate dispersions. Fracture proceeds downward from starter crack at top of specimen.

subsequent propagation. Experimental measurements on composites with graded structures (see Fig. 14) have shown that a layer of composite material with a high volume fraction of particulate phase, overlying a material with a lower or zero volume fraction of particulates, is as tough (resistant to fracture) as a monolithic material with the high volume fraction of particulates (see Fig. 7). This implies that it is only necessary to toughen the surface or near-surface region of a material, thus achieving large savings in both weight and cost, since the reinforcing particulate phases are typically both more dense and more costly than the matrix materials.

Another interesting area of research at NRL, which includes a significant ceramic composite effort, is that of rapid solidification processing (RSP) of materials. This effort has included work to produce fine Si_3N_4-coated iron particles, which have been used as one of the particulate phases in the model particulate system noted earlier. Another effort in this regard has been the production of alumina-zirconia and zirconia alloys of unique phase structure and with extremely good chemical homogeneity [20]. The alumina-zirconia materials can be prepared by several techniques from melts of the eutectic composition and have potential as a hard, tough, refractory, insulating material. The reduction in scale of the eutectic structure associated with RSP should permit fabrication of alumina-zirconia eutectic materials with high strength values as well. A result with more technological importance has been obtained with yttria-partially stabilized zirconia materials produced by rapid solidification from the melt (at about 2800° to 3000°C). Here unique phase structures are obtained, e.g., t′-ZrO_2 in a nominally two-phase, tetragonal-cubic region, and the material shows very great chemical homogeneity. One particular process has been used to produce spherical particles intended as a plasma spray feed powder (see Fig. 15). It has already

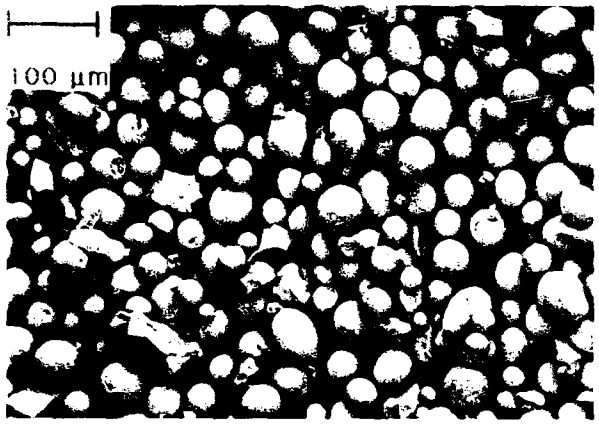

Fig. 15 – Hollow, fine-grain, spherical particles of t'-ZrO_2, intended for use as a plasma spraying feed material, single phase and with chemical homogeneity, obtained by rapid solidification processing of zirconia from a melt

been demonstrated, in a joint project with the Chemistry Division [21], that the RSP zirconia is significantly more resistant to molten salt corrosion than the conventionally prepared zirconia turbine coating materials. This presumably results from the chemical and phase homogeneity and the high purity of the powder. These same features are also expected to result in greater thermal stability as well; thus these materials may also function better as turbine coatings where thermal rather than chemical stability is the issue.

Summary

This article is intended as a broad overview of past and present research programs in ceramic composites at NRL, and we hope that it will give the reader an idea of the breadth of the efforts here as well as some details of some of the more interesting research projects and developments. Those interested in further details should contact the author.

Acknowledgments: The author gratefully acknowledges the extensive assistance of the many individuals at NRL, especially those in the Composites and Ceramics Branch, in the preparation of the manuscript, and the continuing financial support of the Office of Naval Research and the Naval Air Systems Command for the ceramic composites program at NRL.

References

1. M. Kahn, R. W. Rice, and D. Shadwell, "Preparation and Piezoelectric Response of PZT Ceramics with Anisotropic Pores," *Adv. Ceram. Mater.* **1**(1), 55-60 (1986).

2. M. Kahn, "Acoustic and Elastic Properties of PZT Ceramics with Anisotropic Pores," *J. Am. Ceram. Soc.* **68**(11), 623-628 (1985).

3. M. S. Duesbery, M. Kahn, B. A. Kovel, and D. Lewis, "Fracture in PZT Ceramics Containing Arrays of Flat Voids," submitted to *Am. Ceram. Soc.* (1988).

4. S. W. Freiman, D. R. Mulville, and P. W. Mast, "Crack Propagation Studies in Brittle Materials," *J. Mater. Sci.* **8**(11), 1527-1533 (1973).

5. C. Cm. Wu, K. R. McKinney, and D. Lewis, "Grooving and Off-Center Crack Effects on Applied Moment Double Cantilever Beam Tests," *J. Am. Ceram. Soc.* **67**(8), C166-C168 (1984).

6. C. Cm. Wu, K. R. McKinney, and J. Cunniff, "Modified DCB Method for Measurement of High Toughness Ceramic Composites," *Ceram. Eng. Sci. Proc.* **6**(7-8), 550-557 (1985). Also see C. Cm. Wu, D. Lewis, and K. R. McKinney, "Strength and Toughness Measurements of Ceramic Fiber Composites," in *Fracture Mechanics of Ceramics*, R. C. Bradt et al., eds. (Plenum Publishing Corp., New York, 1986), pp. 53-60.

7. C. Cm. Wu, "Wear of Ceramic Natural Fiber Composites," in *Engineered Materials for Advanced Friction and Wear Applications*, F. A. Smidt and P. J. Blau, eds. (ASM International, 1988), pp. 79-84.

8. D. Lewis, R. P. Ingel, W. J. McDonough, and R. W. Rice, "Microstructure and Thermomechanical Properties in Alumina- and Mullite-Boron Nitride Particulate Ceramic-Ceramic Composites," *Ceram. Eng. Sci. Proc.* **2**(7- 8) (1981).

9. R. W. Rice, P. F. Becher, S. W. Freiman, and W. J. McDonough, "Thermal-Structural Ceramic Composites," *Ceram. Eng. Sci. Proc.* **1**(7-8(A)), 424-443 (1980).

10. D. Lewis and R. W. Rice, "Thermal Shock Fatigue of Monolithic Ceramics and Ceramic-Ceramic Composites," *Ceram. Eng. Sci. Proc.* **2**(7- 8), 712-718 (1981).

11. B. Bender, D. Shadwell, C. Bulik, L. Incorvati, and D. Lewis III, "Effect of Fiber Coatings and Composite Processing on Properties of Zirconia-Based Matrix SiC Fiber Composites," *Am. Ceram. Soc. Bull.* **65**(2), 363-369 (1986).

12. D. Lewis and R. W. Rice, "Further Assessment of Ceramic Fiber Coating Effects on Ceramic Fiber Composites," J. D. Buckley, ed., NASA Conference Publications No. 2406, 13-26 (1985).

13. W. S. Coblenz et al., "Progress in Ceramic Refractory Fiber Composites," J. D. Buckley, ed., NASA Conference Publication No. 2357, 191-216 (1984).

14. D. Lewis, C. Bulik, and D. Shadwell, "Standardized Testing of Refractory Matrix/ Ceramic Fiber Composites," *Ceram. Eng. Sci. Proc.* **6**(7- 8), 507-523 (1985).

15. D. Lewis III, "Strength and Toughness of Fiber-Reinforced Ceramics and Related Interface Behavior," in *Whisker and Fiber Toughened Ceramics* (ASM International, 1988), pp. 265-274.

16. J. S. Wallace, B. A. Bender, and D. Schrodt, "Thermochemical Treatment of Tyranno Fibers," J. D. Buckley, ed., NASA Conference Publications No. 2482, 201- 212 (1987).

17. B. A. Bender, J. S. Wallace, and D. J. Schrodt, "Effect of Thermochemical Treatments on the Strength and Microstructure of SiC Fibers," Proceedings NASA/DoD Conference on Metal Matrix, Carbon and Ceramic Matrix Composites, Cocoa Beach, FL. January 1988, publication pending.

18. T. L. Jessen, "Examination of the Slow Fracture Characteristics of a Metal Particulate Glass Composite," Master of Science thesis, Pennsylvania State University, August 1987.

19. T. L. Jessen, "Fracture Toughness Testing of Graded Particulate Composites," *Ceram. Eng. Sci. Proc.*, publication pending.

20. B. A. Bender, R. P. Ingel, W. J. McDonough and J. R. Spann, "Novel Ceramic Microstructures and Nanostructures from Advanced Processing," *Adv. Ceram. Mater.* **2**(2), 137-144 (1986).

21. R. L. Jones and C. E. Williams, "Hot Corrosion Studies of Zirconia Ceramics," *Surf. Coatings Tech.* **32**, 349-358 (1987).

THE AUTHOR

DAVID LEWIS III graduated from the University of Colorado with a B.S. in mechanical engineering in 1965. He received an M.S. and Ph.D. in mechanics from the Illinois Institute of Technology in 1967 and 1970, respectively. From 1968 to 1979 he was a professor of engineering mechanics at the New York State College of Ceramics, where he received extensive on-the-job training in ceramics. As a participant in the Intergovernmental Personnel Act, Dr. Lewis worked at NRL from 1977 to 1978.

Dr. Lewis joined NRL as a research ceramic engineer in 1979. He is currently the associate branch head of the Composites Branch and is the head of the Structural Ceramics Section. His areas of expertise include processing and characterization of ceramics and ceramic composites, fracture mechanics, mechanical properties of ceramic and ceramic composites, theoretical modeling of the fracture and toughening processes in ceramics and ceramic composites, and the statistical analyses of mechanical properties of ceramics. He has authored approximately 75 publications and made over 200 technical presentations.

Radiation Effects in Space Systems

James C. Ritter
Condensed Matter and Radiation Sciences Division

Background

The Navy is critically dependent on space systems for communication, navigation, surveillance, and weather information. The Joint Chiefs of Staff have required that U.S. military spacecraft be hardened to the effects of nuclear weapons if their missions require it. Also, spacecraft must operate in their natural environment; without sustaining frequent upsets in their electronics that might compromise their reliability. To meet these needs, it is necessary to understand how space systems are affected by radiation and how they can be hardened to survive its effects.

The Naval Research Laboratory (NRL) has an active research program, briefly reviewed here, in radiation effects in space systems. The program spans the range from basic research on charge collection in microelectronic structures and damage in semiconductor and superconductor materials to exploratory development in single-event upset (SEU) effects and radiation damage in solar cells and finally to advanced development in radiation hardening of Navy space systems and development of space experiments.

History of the Problem

The history of the observation of radiation effects in space systems began shortly after SPUTNIK I was launched on October 4, 1957. The first successful U.S. spacecraft was Explorer I, launched on January 31, 1958. A geiger counter experiment put on board by J.A. Van Allen discovered a high count rate region that was caused by charged particles trapped in Earth's radiation belts (now called the Van Allen belts). Early space experiments mapped the radiation belts and measured the population of trapped particles.

Nuclear weapon experiments conducted from 1958 to 1962 demonstrated that electrons from beta decay of fission fragments could also be trapped by Earth's magnetic field to form artificial radiation belts. The Starfish test (July 9, 1962) produced an intense, artificial belt. Starfish electrons and redistributed protons produced premature degradation and failure in the solar arrays of several satellites in low-altitude orbits at the time (Table 1). In all, Starfish caused serious problems or failure in up to seven spacecraft and dramatically pointed out the need to study and understand radiation effects in solid-state devices used in satellites such as solar cells and microelectronic devices.

Solar cells, simple semiconductor devices, have been used for reliable space power. These cells degrade rapidly in space radiaiton environments because they are on the outside of the spacecraft. Electronic devices were introduced into spacecraft as transistors and later as simple integrated cirucits. As the solid-state devices used in space systems became more complex, they also became more sensitive to the effects of radiation. Even after the artificial radiation belts decayed, the natural belts were sufficiently intense to produce damage in sensitive devices.

In the 1960s, Harold Hughes, Electronics Science and Technology Division, started programs in radiation hardening of complementary metal oxide semiconductor (CMOS) integrated circuits. These programs have continued successfully and a new program has recently been started with the Defense Nuclear Agency (DNA) in submicron devices. Both the complexity and the

Table 1 — Solar Cell Degradation and Failure in Satellites Caused by Starfish

Spacecraft/Orbit		Time Period	Power Degradation of Solar Cells	Spacecraft Active Life
TRANSIT 4B				
Apogee:	1100 km	Before Starfish	17% (as expected)	Nov. 15, 1961 to
Perigee:	950 km	(236 days)		Aug. 2, 1962
Inclination:	32.4°	After Starfish (24 days)	22% (additional)	(failed 24 days after Starfish)
TRAAC				
Apogee:	1120 km	Before Starfish	17% (as expected)	Nov. 15, 1961 to
Perigee:	950 km	(236 days)		Aug. 14, 1962
Inclination:	32.4°	After Starfish (36 days)	22% (additional)	(failed 36 days after Starfish)
ARIEL				
Apogee:	1210 km	Before Starfish	Unknown	Apr. 26, 1961 to
Perigee:	390 km	(78 days)		Nov. 1962
Inclination:	54°	After Starfish (4 days)	Total Degradation of 25%	(protective undervoltage power relay cutoff occurred 104 h after Starfish)

hardening levels of the devices have grown steadily.

As device feature sizes decreased, a new effect, SEU began to be observed. The history of SEUs is interesting. The possibility that a single, heavy ionizing particle such as a cosmic ray could upset a small microcircuit was first published in 1962, was mentioned again in 1975 in connection with anomalous upsets observed in a satellite system, but by 1978 it had been observed in the laboratory. Alpha-particle-induced upsets had also been observed by then, and the potential impact of this new effect was becoming clearer.

Eligius Wolicki and Charles Guenzer, Condensed Matter and Radiation Sciences Division (CMRSD), realized that if cosmic-ray ionization could upset a microcircuit, then, possibly, nuclear reactions induced by energetic neutrons and protons could also produce SEUs. They performed experiments at the NRL cyclotron in which they discovered that high-energy neutrons and protons could, indeed, produce upsets in dynamic RAMs. These results were presented at the 1979 IEEE Annual Conference on Nuclear and Space Radiation Effects. The name introduced by that paper, "single event upset," is now given to the active field that has developed since that time. NRL continues to play a lead role in the SEU area. CMRSD helped to develop a cooperative DNA/DARPA (the Defense Advanced Research Projects Agency) SEU program and has been the program area reviewer since that time. It chaired a national symposium on single event effects held annually in Los Angeles between 1983 and 1988.

In the early 1970s, the Navy became concerned about the vulnerability of its planned fleet satellite communications system satellite (FLTSATCOM). In 1971 NRL began construction of the FLTSATCOM processor under contract with TRW. The author, James Butler, CMRSD, and Harold Hughes, Electronics Science and Technology Division, participated in and monitored the radiation hardening and testing of

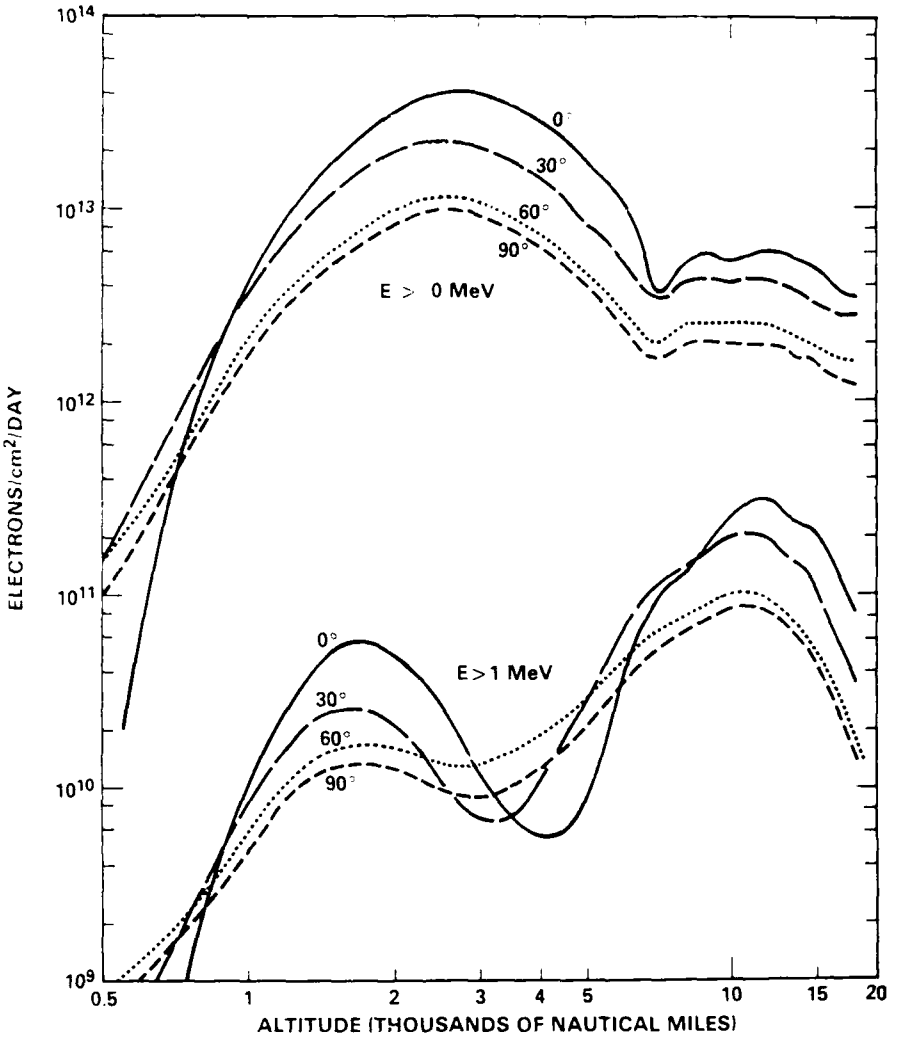

Fig. 1 — Electron integral fluences in electrons/cm^2/day averaged over circular Earth orbits of various inclinations (based on NASA AE4 and AE6 radiation belt models). The electron threshold was 40 keV for the measurements.

the FLTSATCOM processor and later the entire satellite system. FLTSATCOM was the first satellite system to be hardened to all the effects of both natural and nuclear radiation. The first FLTSATCOM satelite was launched in 1976. NRL is now participating in the radiation hardening of the ultrahigh frequency (UHF) follow-on to FLTSATCOM.

The Navy has a strong and continuing commitment to space as witnessed by the formation of the Navy Center for Space Technology at NRL in October 1986. Knowledge of the effects of radiation on space systems and hardening against those effects is important to the proper operation of Navy spacecraft in peacetime and their survivability in wartime.

Natural Space Environment

Earth's radiation belts constitute a significant hazard to the operation and survivability of Navy space systems. These belts are made up primarily of electrons and protons and extend from low-altitude satellite orbits of several hundred kilometers to beyond geosynchronous-altitude orbits. Figure 1 shows the electron integral fluences in electrons/cm^2/day for electron energies greater than 0 MeV (the actual lower limit is 40 keV) and 1 MeV as a function of satellite altitude

and orbital inclination [1,2]. The curves marked E > 0 MeV are the fluence incident upon the outer skin of the satellite. A typical spacecraft has about a 30-mil skin, and electronic circuits are usually placed inside of boxes made of about 50 mils of aluminum (Al) making a total of about 80-mils Al shielding between the outside surface and the closest electronics device. 1-MeV electrons are absorbed by approximately 80 mils of Al so the curves marked E > 1 MeV may be thought of as the fluence incident on the inside of the spacecraft where the electronic boxes are located. It is clear that the skin and the electronic boxes provide substantial protection for the electronics from the natural environment at all altitudes.

Figure 2 shows similar curves for natural radiation-belt protons [3]. Eighty mils of Al is about the range of a 20-MeV proton, so the curves marked E > 0 MeV represent the fluence incident on the outer surface of the spacecraft and the curves marked E > 20 MeV represent the fluence just inside the electronics boxes. The skin and electronic boxes provide a great deal of protection for electronics from protons at high altitudes but less at low altitudes.

Two more natural space environments of importance exist, solar flares and cosmic rays. The total dose deposited by these two environments is not significant compared to the electron and proton environments, but they can both produce significant effects in spacecraft electronics through SEUs. The solar flare protons can also cause serious damage to solar cells particularly during anomalously large events, which can occur up to three or four times per 11-yr solar cycle. James Adams has written an NRL report [4] that is considered the standard reference in the field for the cosmic-ray environments of interest to spacecraft. Solar-flare environments are generally determined from the National Space Sciences Data Center publications [5,6].

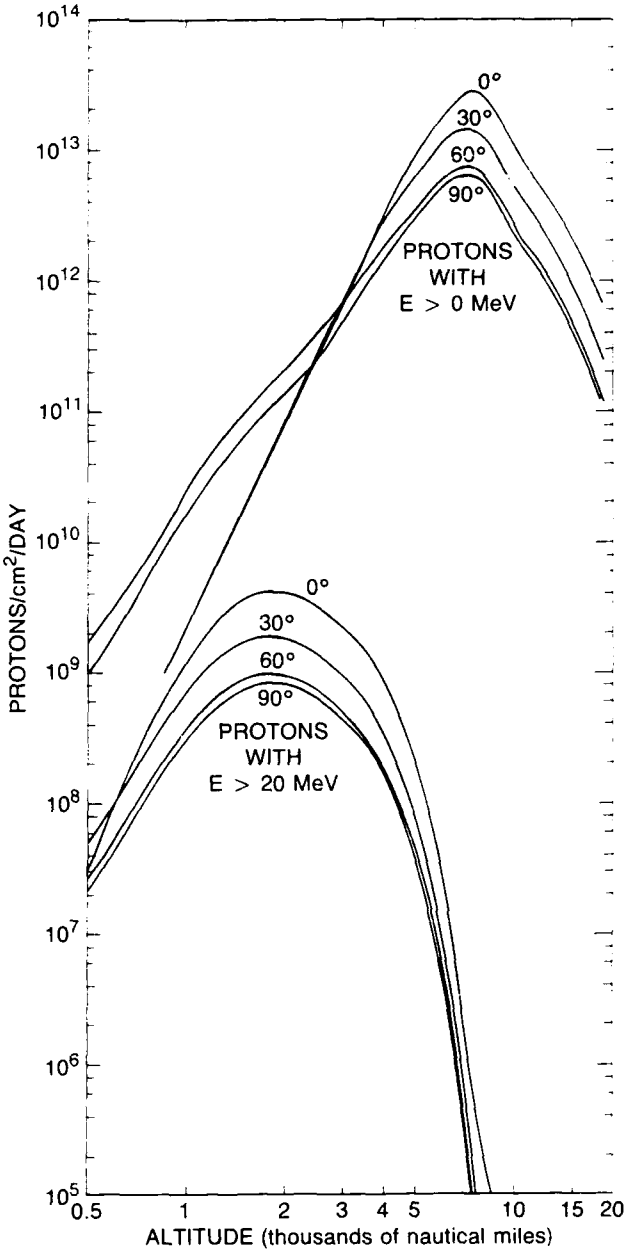

Fig. 2 — Proton integral fluences in protons/cm²/day averaged over circular Earth orbits of various inclinations (based on NASA AP8 min model)

Nuclear Space Environment

An exoatmospheric nuclear burst produces copious amounts of radiation that can damage spacecraft. The primary environments are prompt X rays, gamma rays, neutrons, and electrons from subsequent fission decay. The most severe environments are X rays and weapon-injected electrons. The electrons are injected into Earth's radiation belts where they are trapped by Earth's field. As spacecraft pass through the belts they are exposed to this environment.

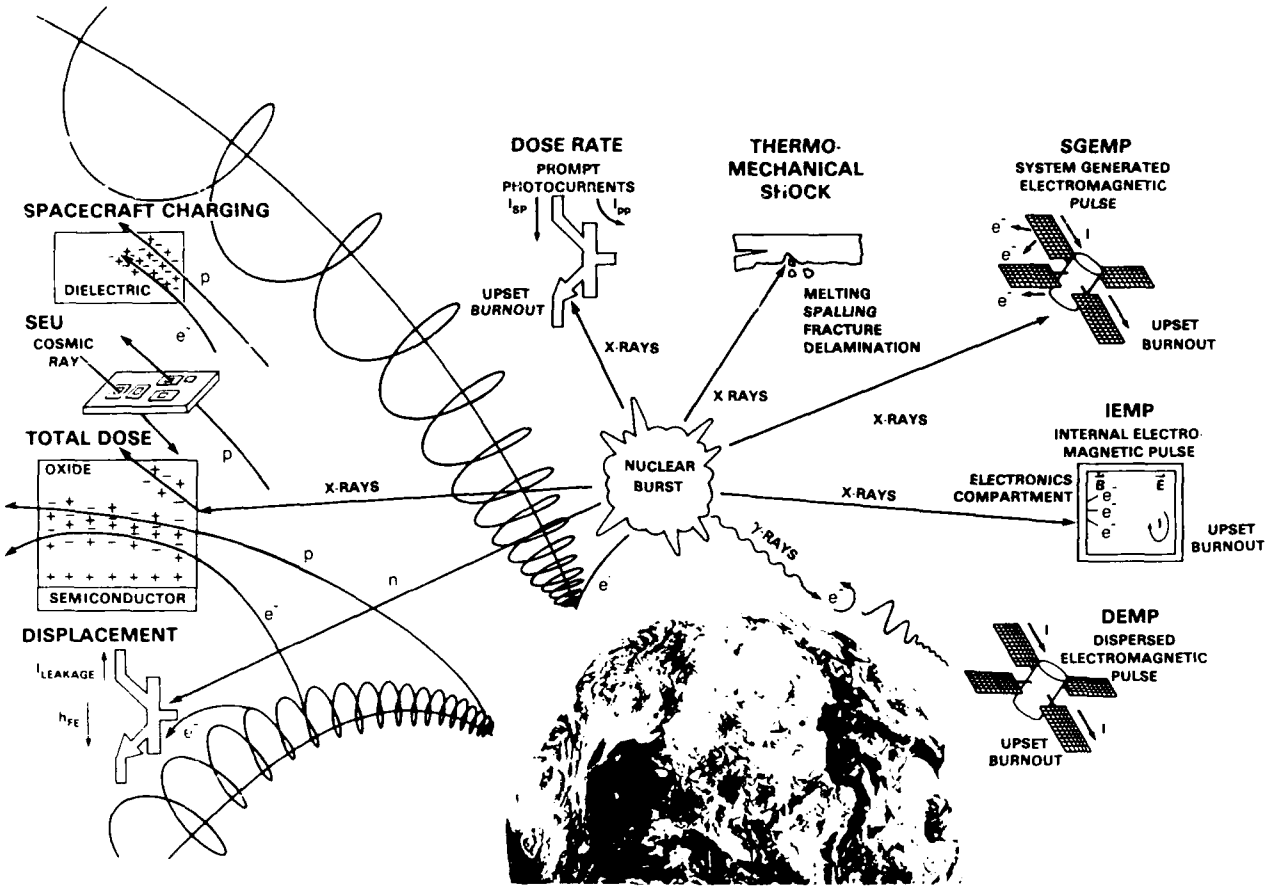

Fig. 3 — Effects produced in spacecraft by the natural (left) and the nuclear (top and right) space environments. The damage mechanisms are illustrated pictorially and show the relevant radiations or particles producing the damage.

Two secondary or indirect environments also exist, the dispersed electromagnetic pulse (DEMP) and the system-generated electromagnetic pulse (SGEMP). DEMP is produced by gamma rays interacting with the upper atmosphere, producing Compton electrons. These electrons are deflected by Earth's field, radiating an electromagnetic pulse. The high-altitude waveform is spread or dispersed as it passes through the ionosphere. SGEMP arises from the production of Compton electrons and photoelectrons from spacecraft surfaces by the X rays incident upon the spacecraft. These emitted electrons produce electric and magnetic fields and deposit charge and energy or dose within various materials. The resulting fields and currents can couple to electronic circuits, producing permanent damage in electronics.

Reference 7 provides a thorough discussion on the nuclear environments of interest to spacecraft and their effects on satellites.

Radiation Effects in Devices and Materials

A variety of radiation effects or damage mechanisms in semiconductor materials and devices are produced by the natural space and nuclear environments described above. Figure 3 shows both the damage mechanisms and the causes. The effects of the natural environment are shown on the left-hand side of the figure, and the effects of the nuclear environment are shown on the top and right-hand side. Some of the effects, mainly nuclear, are described briefly for completeness (DEMP, internal electromagnetic pulse (IEMP), SGEMP, thermomechanical shock,

dose rate, and spacecraft charging), but this article concentrates on radiation effects in semiconductor devices and materials with an emphasis on the natural environment effects on which work has been done at NRL, namely SEU, displacement damage, and total ionizing dose.

Before describing each effect, it is useful to differentiate between the environment itself and the effects or damage it produces. The total spacecraft threat environment is determined by specifying the intensity for each of the primary and secondary threat environments. When the vulnerability or hardness of a device or material is discussed, it is not useful to state it in terms of individual threat environments. Several different environments may be present and they must be combined; they may also affect the device in different ways. Effects or damage in devices or materials are given in terms of the damage mechanisms as shown in Fig. 4. For example, trapped protons, solar flares, and cosmic rays all contribute to single-event phenomena, and all of the primary environments contribute, to some extent, to the total ionizing dose received. The device hardness and damage or upset parameters are therefore specified in terms of the total ionizing dose, dose rate, or upset rate the device can withstand without permanent damage or temporary memory errors.

The nuclear effects in Fig. 3 will now be described. Some ambiguity exists in the use of the terms DEMP and SGEMP. They are often used as environments, but they can also be used to describe the effects produced by those environments. Another term that is sometimes used to describe an effect that is a part of the overall SGEMP effect is the term IEMP. IEMP however, is never used as an environment. SGEMP describes the effect produced by X rays interacting with the whole spacecraft system. A pulse of X rays produces Compton electrons and photoelectrons from spacecraft surfaces. This electron pulse produces electric and magnetic fields within the spacecraft and deposits charge and dose in materials. IEMP describes the effect within an individual electronic box. DEMP also induces electromagnetic fields within the spacecraft. The resulting fields and currents from both DEMP and SGEMP can couple to electronic circuits, damaging them.

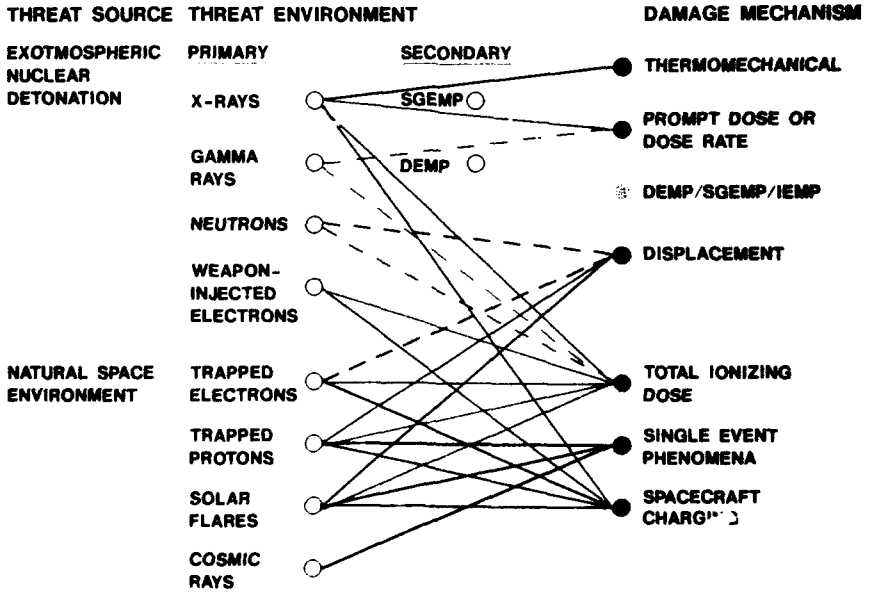

Fig. 4 — Radiation effects or damage mechanisms to electronic devices produced by nuclear and natural space environments. This figure provides a translation between various threat environments and the damage mechanisms that they produce in devices. The effects of combined environments are shown.

Thermomechanical damage is caused when surface materials exposed to X-ray pulses absorb energy rapidly and then undergo melting, spallation, or thermomechanical shock.

Dose-rate or prompt-dose effects occur when a pulse of photons or charged particles ionizes a device, producing primary and secondary photocurrents. The photocurrents can cause circuit upset or latchup (transient) or device burnout (permanent). Latchup can also result in permanent damage if the latching current is sufficiently high to burn the device out. The NRL linear accelerator (LINAC) is often used by NRL, industrial, and university personnel to study dose-rate effects.

Spacecraft charging is caused when electrons and protons in the space environment stop in a spacecraft material and deposit charge. This buildup of charge can cause destructive discharges within the spacecraft.

The radiation effects in semiconductor devices and materials can be broadly classified as producing either permanent damage (displacement and total ionizing dose) or transient effects (SEU and dose rate). Permanent radiation effects will be discussed first, then SEU. A brief discussion of damage in solar cells will follow because of their special importance to spacecraft.

Displacement Damage: Permanent damage in microelectronics can be caused when the incident radiation displaces atoms from their locations in the crystalline lattice of the semiconductor material. Displacement damage generally results in gain degradation of a transistor and can cause failure if the gain degradation goes beyond the permitted operating range for the device as used in the circuit.

For many years it was believed that displacement damage would depend strongly on the particle producing the damage. That is, the damage was expected to be determined by the way in which defects clustered along the particle path, which depends on the particle type. Clusters of defects near the end of the path were supposed to behave differently from isolated defects along the path. Recent NRL research [8-11] has shown, however, that displacement damage depends linearly on a simple parameter called the nonionizing energy loss of the particle (see Fig. 5) and is independent of cluster effects. This is a surprising result. It is true for nearly six orders of magnitude in nonionizing energy deposition and has been observed for particles as heavy as copper ions and as light as electrons. Copper ions and electrons differ by nearly six orders of magnitude in the total rate of energy loss. This linear dependence has been shown for many semiconductor materials, viz., silicon (Si), germanium, and gallium arsenide (GaAs) and appears to be quite general. This important conclusion enables one to predict displacement damage for any particle by use of inexpensive neutron damage measurements and simple, accurate calculations of the nonionizing energy loss of the particle. This advance has already benefitted strategic defense initiative (SDI) neutral-particle-beam effects research because it has substantially reduced the amount of data needed.

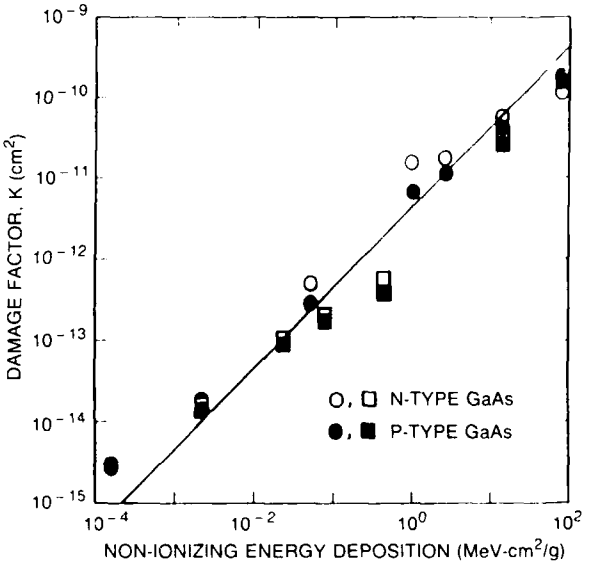

Fig. 5 — Change in damage factor (decrease in carrier concentration and mobility) for GaAs devices as a function of the calculated energy producing displacement damage

Total Ionizing Dose: Ionizing radiation causes the accumulation of trapped charge in the insulators that all electronic devices contain. In metal oxide semiconductor (MOS) devices, the most serious problems are associated with the gate oxide and the shifts in threshold voltage that the trapped charge causes. If the threshold voltage (the voltage needed to switch a transistor) shifts beyond the range of operation of the device, permanent failure can occur. In bipolar devices, the problem is likely to be an increase in leakage current caused by trapped charge in the field oxide used to passivate the surface. Increased leakage currents can cause the device to fail.

The effects described above are often permanent, but time-dependent effects, such as annealing of trapped holes and generation of interface states, are also common. Dennis Brown and Charles Dozier, CMRSD, have published many significant papers on this subject. Brown and Dozier have also been part of a collaborative effort involving NRL, Harry Diamond Laboratories, and Sandia Laboratories, to develop accurate dosimetry procedures for comparing 10-keV irradiations of microcircuits with Co-60. Harold Hughes, Nelson Saks, and Joseph Killiany, Electronics Science and Technology Division, have measured total ionizing dose effects on a variety of devices and have developed methods for hardening CMOS and charge-coupled devices. CMRSD is developing a test plan for measuring ionizing radiation dose effects in devices for the Navy's UHF Follow-on Satellite.

Single-Event Upset: In 1979, the extent and potential impact of SEUs on Department of Defense (DoD) spacecraft was not known. As a first priority, SEU experiments were performed at NRL on a large variety of devices and under experimental conditions designed to reveal the mechanisms responsible for SEUs and how they depend on such quantities as track ionization density, particle type, and device feature size. The ultimate goal was to understand the upset mechanisms so that hardening solutions could be found and harder devices could be developed for Navy space systems.

A variety of devices was studied to assess the causes and importance of SEUs. NRL observed the first proton and neutron upsets in devices (dRAMS); the first upsets in microprocessors, in GaAs devices, and in superconducting Josephson junctions; the first temperature and dose dependence of SEU sensitivity; and the first upsets in error detection and correction (EDC) circuits [12-18]. Observing an upset in an EDC circuit is both significant and worrisome because EDC circuits are used to protect systems from SEUs!

A variety of new SEU mechanisms was discovered at NRL [19-21], and three are summarized here. The existence of the *funnel effect* was predicted at IBM and was experimentally verified at NRL by Knudson and Campbell [19] using the newly developed microbeam. When a charged particle passes through a microelectronic device, it leaves a highly ionized track. The track penetrates deeply into the substrate beyond the sensitive region of the device and shorts out the fields that define the sensitive region. The extended field then assists in collecting charge produced outside of the sensitive volume. More charge is therefore collected than expected, sometimes by as much as a factor of five. This makes it easier than expected to exceed the critical charge and produce upset. It also suggests a hardening mechanism, namely inserting an insulating layer just under the sensitive area to cut off the funnel. This may be done by ion implantation.

Knudson et al. [20] also discovered an unexpected second SEU mechanism. It is called the *ion-shunt effect*. They noticed in layered structures that sometimes much more charge was collected than was deposited by the particle. It was realized that the tracks were shorting two terminals of the device, say the emitter and the collector, for a brief period of time, and this was allowing the power supply to drive a large current through the device. Of course, this effect would also raise the upset rate of the device.

Another new mechanism discovered by the NRL group [21] was *edge effects*. When large test structures were irradiated with the microbeam (a beam of particles about 2 μm in diameter), much more charge is collected near the edges than near the center, as much as a factor of two or three. The enhanced charge collection region was over 10-μm wide. Since modern devices typically have dimensions of only about 1 μm, almost all regions would show enhanced collection making it hard to calculate the expected collected charge. It is believed that the enhanced collection is due to fringing fields.

Recently, NRL succeeded in making the fastest reported charge collection measurements. By using a superconducting delay line and sampling system as a transient digitizer, measurements have been made with resolutions of about 10 ps [22]. As devices become smaller and faster, it will become necessary to know the shape of the charge collection pulse with a resolution exceeding the device speed to develop SEU hardening techniques.

Because of the Navy's interest in space, NRL has pursued a long-term effort to develop methods of predicting upset rates in all orbits. Bendel and Petersen [23] have devised a method for calculating SEU rates owing to protons anywhere in the radiation belts based on only a few upset cross sections at different energies. Petersen et al. [24] also calculated the effects of device scaling on SEU sensitivity. The figure from this paper showing critical charge for upset vs device feature size is widely referenced (Fig. 6). This figure shows almost no dependence on whether the device is made with CMOS, silicon on sapphire (SOS), bipolar silicon on insulator (SOI), or even GaAs technology. The lack of dependence of upset rate on device technology is startling.

Petersen et al. [25] also developed an approximate method for calculating cosmic-ray-induced SEU rates from the dimensions of the sensitive region of the device and the critical charge. This method enables a figure of merit for SEU sensitivity to be assigned to each device. The

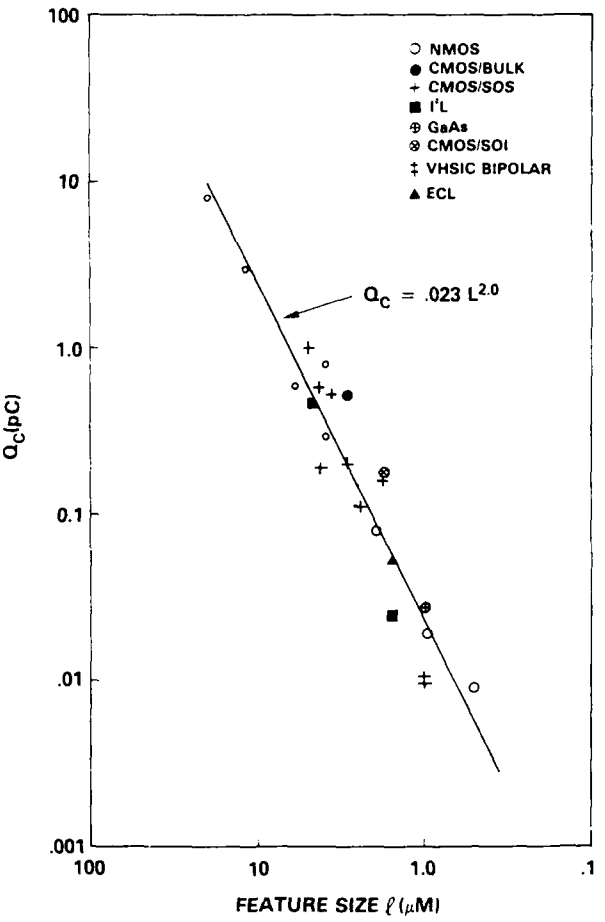

Fig. 6 — The critical charge in pico Coulombs (pC) required for an SEU in a microcircuit as a function of the device feature size in microns

equation for calculating the figure of merit (now called the Petersen equation) is used almost universally. Shapiro [26] developed a computer code called Cosmic Ray Upset Program (CRUP) for calculating upset rates in space applications, and Adams [27] has developed a related one called CREME. Recently, Stapor developed an analytic code for calculating the energy density in individual charged particle paths, called TRKRAD [28]. This code produces results equivalent to time consuming, expensive Monte Carlo codes. NRL's combination of calculational techniques is now used routinely for predicting upset rates in DoD satellites.

Damage in Solar Cells: Solar cells are very important for spacecraft since they are used in

essentially all space power systems for Earth-orbiting satellites. As mentioned above, the satellites affected by Starfish were damaged by degradation of the solar cells. It happened that, at the time, the United States was using *p* on *n* solar cells on all spacecraft in orbit. Laboratory experiments in late 1960, however, had shown that *n* on *p* cells were much more radiation resistant. Accordingly, space-quality cells were developed for the Telstar I satellite. Telstar I was launched on July 10, 1962, one day after Starfish, with *n* on *p* cells aboard. Telstar demonstrated the superior hardness of the new cells.

Most solar cells used in the current generation of satellites are made of Si. Several years ago GaAs cells were introduced. Such cells are more efficient and degrade less than Si cells in a radiation environment. Recently, an even more radiation resistant indium phosphide (InP) solar cell, of approximately the same efficiency as GaAs was developed. Figure 7 shows that InP can absorb 30 to 50 times more fluence for the same damage. Richard Statler, CMRSD, is now managing a program to demonstrate the manufacturability of InP solar cells. An interesting research question is why the observed radiation damage in InP solar cells anneals in sunlight. No other solar cell material has this property. Photon annealing of InP is currently being studied at NRL.

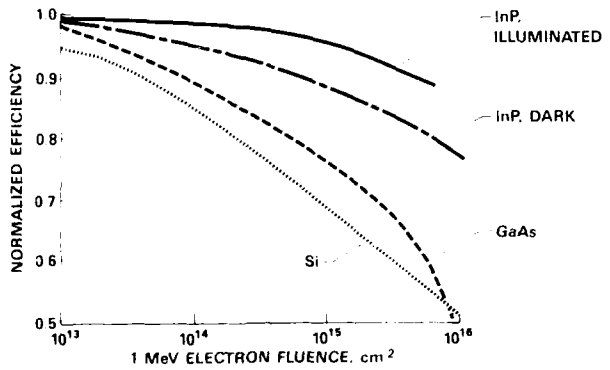

Fig. 7 — Energy conversion efficiencies for various types of solar cell as a function of 1-MeV electron fluence in electrons per cm^2. The curves have been normalized to the pre-irradiation values. This figure shows that illuminated InP is 30 to 50 times harder than GaAs.

Space Experiments

Combined Release and Radiation Effects Satellite (CRRES): Most single-event data from spacecraft are obtained by accident. Typically the spacecraft is designed and built without knowledge that a device has been included that is susceptible to, say, proton-induced SEU. When the spacecraft reaches orbit it is quickly discovered that the device upsets and that the spacecraft now has a serious problem. In this case it is often not easy to evaluate the extent of the problem. It may be that the device is not very sensitive but that the spacecraft has encountered an unusually large proton flux for this period of time. But it could equally well be true that the device is extremely sensitive but the proton fluence for that orbit is unusually low for this period. The extent of the problem only becomes clear later. Obviously, this is not the way to design and deploy spacecraft. It is for this reason, among others, that space experiments are done.

CRRES is the first experimental satellite built to measure simultaneously all the major components of the space-radiation environment as well as SEU rates and total dose damage in space for a wide variety of microelectronic devices. CRRES is a complete program, including space measurements, ground tests, modeling, and prediction.

The ground-test program measures the upset-cross section by using particle accelerators and the modeling program predicts upset-cross sections from basic principles. From the models and accelerator measurements upset rates can be predicted by using NASA particle environments. These predictions will be compared to the space measurements after correcting for the actual space environments encountered. This will enable us to refine our SEU predictive capabilities for the first time.

Figure 8 shows an artist's conception of the CRRES satellite in orbit. The planned elliptical orbit is 400 by 35,786 km with an 18° inclination. When the spacecraft is far from Earth, it will

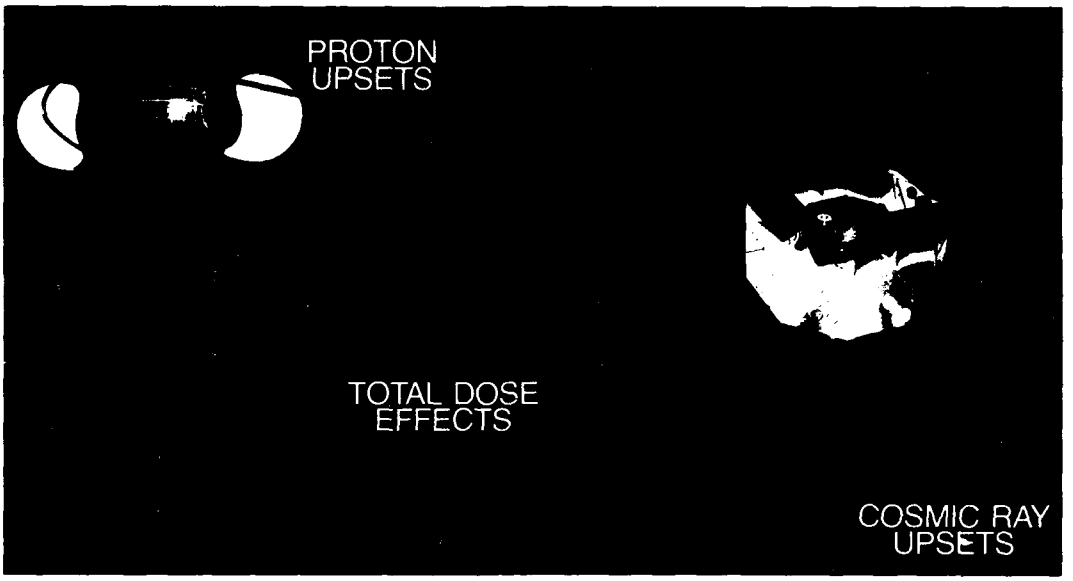

Fig. 8 — Artist's conception of the CRRES satellite in its elliptical orbit illustrating that it is expected to experience cosmic-ray upsets at apogee and proton upsets at perigee and will accumulate total dose over the entire orbit

experience primarily cosmic-ray-produced SEUs. When it is near Earth, passing through the belts, it will suffer primarily proton-produced upsets. Total dose effects will be seen throughout the orbit.

CRRES is a space experiment that has been jointly sponsored by the Air Force, the Navy, DNA, DARPA, and NASA and is planned for a June 1990 launch on an expendable launch vehicle. The Air Force Geophysics Laboratory (AFGL) is responsible for the space-environment measurements and the overall SPACERAD program. The author conceived the idea for the microelectronics experiments, convinced AFGL to include it in their space experiment, and obtained major support for it. Andrew Fox, Spacecraft Engineering Department, directed the design and construction of the microelectronics experiment package (MEP) by the Assurance Technology Co. under contract to NRL. The MEP contains SEU and total-dose experiments and is one of the most complicated space experiments ever built. Figure 9 shows the MEP with the cover removed, showing the outside circuit boards. It weights over 100 lb and requires 75 to 100 W to operate. The MEP contains over 400 devices of more than 60 different device types. The devices were the latest state-of-the-art GaAs, Si very high speed integrated circuit (VHSIC), and advanced memories and microprocessors when the MEP was completed in 1987. Its launch was delayed by the loss of the shuttle resulting from the Challenger accident, but it has now acquired a new launch vehicle. Some devices will be updated in the MEP before launch. Fortunately, the experiment was designed with devices with several different feature sizes and various technologies so that extrapolations can be made to future smaller devices. Better SEU and total dose prediction capabilities and better, time-dependent models of Earth's radiation belts are expected to result from CRRES.

Living Plume Shield (LIPS) III: The LIPS III is a space experiment launched in the spring of 1987 into a 1100 km, 60° inclination orbit by the Naval Center for Space Technology. It was built under the direction of James Severns, Space Systems Development Department. LIPS III contains 140 separate experiments on Si, GaAs, and InP solar cells. The solar cells were supplied by 18 different groups, including universities, industrial manufacturers, and by NRL and other government agencies. From conception to

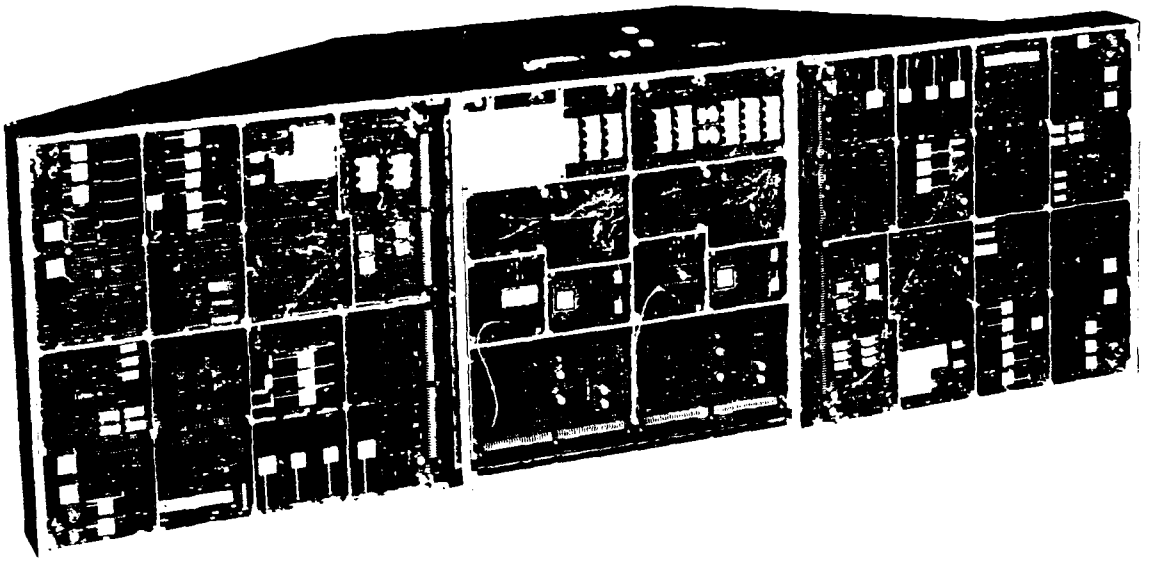

Fig. 9 — The CRRES MEP with the outside cover removed to show the outside layer of circuit boards. The front surface of the MEP has dimensions of 45 × 15 in.

completion, the LIPS III spacecraft took less than one year. Space data on solar cell degradation are being obtained now and many papers have been presented at scientific conferences on the results of the LIPS III experiments. LIPS III is providing much-needed data on solar cell performance in the radiation belts for future Navy spacecraft.

High-Temperature Superconductivity Space Experiment (HTSSE): Last year's NRL Review contained a feature article on high-temperature superconductivity that discussed the breakthroughs that have recently occurred in this area. NRL recently began the HTSSE under sponsorship of CDR William J. Meyers, Space and Naval Warfare Systems Command (SPAWAR). The overall goal of the HTSSE is to demonstrate the feasibility of incorporating the revolutionary technology of high-temperature superconductivity into space systems. It is expected that use of superconductivity will make possible breakthroughs in spacecraft operational capability. Initial experiments will be ready for space tests within 2 to 3 years. The results of the space experiment will enable operational systems designers to evaluate the benefits of using superconducting components in their systems.

The HTSSE is a multidivision effort within NRL involving CMRSD, the Materials Science and Technology Division, the Electronics Science and Technology Division, and the Space Systems Technology Department. The author is the program manager. Thin films and bulk materials are prepared and optimized under the direction of Stuart Wolf. Martin Nisenoff supervises the development of devices such as delay lines, filters, antennas, and high-Q cavities at NRL and by outside contractors. Electrical and structural characterization of devices and materials, by both NRL and contractors, is managed by Robert Soulen. The radiation and space characterization is directed by Geoffrey Summers. The space experiment definition is supervised by George Price. The Naval Center for Space Technology directs the design and construction of the entire space experiment electronics and telemetry starting next year.

HTSSE will be the first comprehensive radiation effects experiment to measure the properties of superconductors in space. Radiation-effects measurements have already been carried out at particle accelerators on high-temperature superconducting materials for this experiment. Initial results show that some

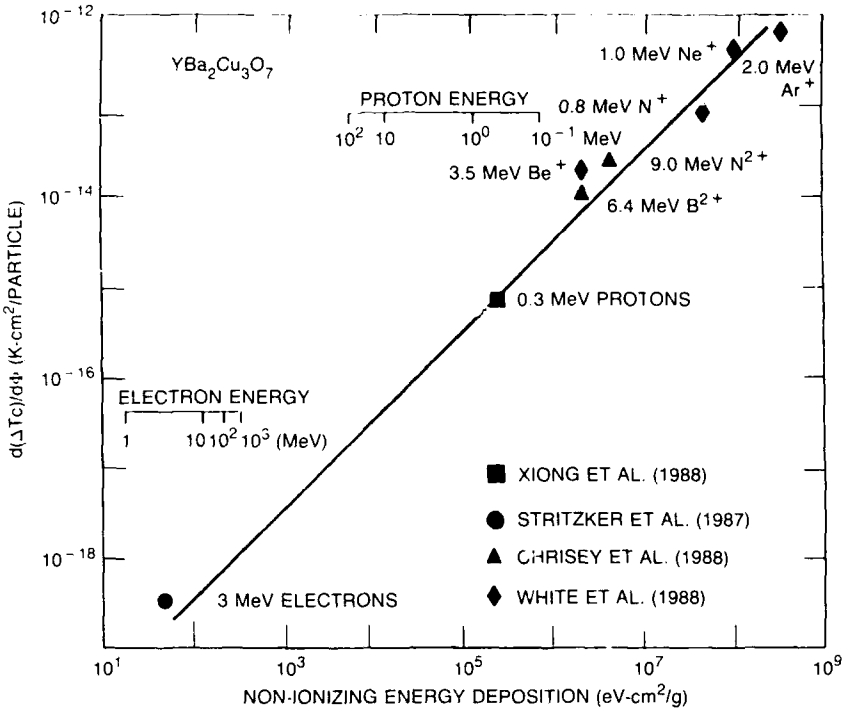

Fig. 10 — Decrease in completion temperature per unit fluence for superconducting $Y_1B_2Cu_3O_7$ as a function of the calculated energy producing displacement damage

superconductors are quite sensitive to radiation and would be damaged in the belts in less than a month, whereas single-crystal materials would survive for over 10 years with negligible damage. Basic superconducting materials are very radiation resistant, but the interface between grains is extremely sensitive. Recent calculations and experiments have shown a very surprising result. Figure 10 shows that when the damage factor, the change in the critical temperature T_c, per unit fluence, is plotted against the nonionizing energy deposition by the particles, a linear dependence exists over nearly 7 orders of magnitude in energy deposition. This indicates that essentially all of the shift in T_c is from atomic displacement, not ionization. These results are strikingly similar to those from the semiconductor materials discussed under displacement damage. It appears that some of the semiconductor radiation effects research of the past approximately 30 years will be directly applicable to superconductors.

Future Challenges

As future microelectronic devices become more complex with smaller feature sizes and higher speeds permitting more to be done on the same size chip, the capability of spacecraft using these devices will increase greatly. Unfortunately, the vulnerability to radiation damage and SEU will also increase greatly. Figure 6 shows how SEU critical charge depends on feature size. At 10 μm the charge necessary to upset the device is about 1 pC, and very few devices with that large a critical charge can be upset even by highly ionizing particles. At 1 μm (the current state of the art) the critical charge has dropped by two orders of magnitude to 0.01 pC, and even lightly ionizing particles can upset the device. When radiation-belt protons can upset devices by direct ionization instead of through a nuclear reaction, then the upset rate will increase by several orders of magnitude. Unfortunately recent experiments have shown that,

with the most sensitive devices, we have already reached that point. A three order-of-magnitude increase in upset rate has been observed. As these new devices are put into spacecraft their SEU problems will truly be astronomical.

As high-temperature superconducting devices are introduced into spacecraft, the spacecraft's capability will increase substantially. There are, however, little consistent radiation effects data on superconductors, and these data will be needed greatly. Furthermore, as superconductors and devices such as IR sensors start to be used on spacecraft more, they will operate at low temperature and will need to be interfaced to conventional electronics. This means that we will need to understand how conventional devices operate and what their radiation damage susceptibility is at low temperature. Currently very little data exist on low-temperature damage or upset rates.

References

1. M.J. Teague, K.W. Chan, and J.I. Vette, "AE:6, A Model Environment of Trapped Electrons for Solar Maximum," NSSDC/WDC-A-R&S 76-04, GSFC, Greenbelt, MD, May 1976.

2. G.W. Singley and J.I. Vette, "The AE-4 Model of the Outer Radiation Zone Electron Environment," NSSDC 72-06, GSFC, Greenbelt, MD, Aug. 1972.

3. D.M. Sawyer and J.I. Vette, "AP-8 Trapped Proton Environment for Solar Maximum and Solar Minimum," NSSDC/WDC-A-R&S 76-06, GSFC, Greenbelt, MD, Dec. 1976.

4. J.H. Adams, Jr., R. Silberberg, and C.H. Tsao, "Cosmic Ray Effects on Microelectronics, Part I: The Near-Earth Particle Environment," NRL Memorandum Report 4506, 1981.

5. J.H. King, "Solar Proton Fluences as Observed During 1966-1972 and as Predicted for 1977-1983 Space Missions," NASA X-601-73-324, Oct. 1973.

6. E.G. Stassinopoulos and J.H. King, "An Empirical Model of Energetic Solar Proton Fluxes with Applications to Earth Orbiting Spacecraft," NASA/GSFC X-601-72-489, Dec. 1972.

7. J.C. Ritter, "Radiation Hardening of Satellite Systems," *J. Defense Res.* **11**(1) (1979).

8. C.J. Dale, P.W. Marshall, E.A. Burke, G.P. Summers, and E.A. Wolicki, "High Energy Electron Induced Displacement Damage in Silicon," *IEEE Trans. Nucl. Sci.* **NS-35**, 1208 (1988).

9. G.P. Summers, E.A. Burke, C.J. Dale, E.A. Wolicki, P.W. Marshall, and M.A. Gehlhausen, "Correlation of Particle-Induced Displacement Damage in Silicon," *IEEE Trans. Nucl. Sci.* **NS-34**, 1134 (1987).

10 P.W. Marshall, C.J. Dale, G.P. Summers, E.A. Burke, and E.A. Wolicki, "Proton, Neutron, and Electron Induced Damage in Germanium," to be published in *IEEE Trans. Nucl. Sci.* (Dec. 1989).

11. G.P. Summers, E.A. Burke, M.A. Xapsos, C.J. Dale, P.W. Marshall, and E.L. Petersen, "Displacement Damage in GaAs Structures," *IEEE Trans. Nucl. Sci.* **NS-35**, 1221 (1988).

12. C.S. Guenzer, E.A. Wolicki, and R.G. Allas, "Single Event Upset of Dynamic RAMS by Neutrons and Protons," *IEEE Trans. Nucl. Sci.* **NS-26**, 5048 (1979).

13. C.S. Guenzer, A.B. Campbell, and P. Shapiro, "Single Event Upsets in NMOS Microprocessors," *IEEE Trans. Nucl. Sci.* **NS-28**, 3955 (1981).

14. P. Shapiro, A.B. Campbell, J.C. Ritter, R. Zuleeg, and J.K. Notthoff, "Single Event Upset Measurements of GaAs E-JFET RAMS," *IEEE Trans. Nucl. Sci.* **NS-30**, 4610 (1983).

15. R. Magno, M. Nisenoff, R. Shelby, A.B. Campbell, and J. Kidd, "Upset Events in Josephson Digital Devices Under Alpha Particle Irradiation," *IEEE Trans. Nucl. Sci.* **NS-28**, 3994 (1981).

16. W.J. Stapor, A.B. Campbell, M.A. Xapsos, R.L. Johnson, Jr., K.W. Fernald, B.L. Bhuva, and S.E. Diehl, "Single Event Upset Temperature Dependence on MOS Static RAMS," *IEEE Trans. Nucl. Sci.* **NS-33**, 1610 (1986).

17. A.R. Knudson, A.B. Campbell, and E.C. Hammond, "Dose Dependence of Single Event Upset Rate," *IEEE Trans. Nucl. Sci.* **NS-30**, 4508 (1983).

18. A.B. Campbell, "Upsets in Error Detection and Correction Circuits," *IEEE Trans. Nucl. Sci.* **NS-29**, 2076 (1982).

19. A.R. Knudson and A.B. Campbell, "Investigation of Soft Upsets in Integrated Circuit Memories and Charge Collection in Semiconductor Test Structures by the Use of an Ion Microbeam," *Nucl. Instrum. Methods* **218**, 625 (1983).

20. A.R. Knudson, A.B. Campbell, P. Shapiro, W.J. Stapor, E.A. Wolicki, E.L. Petersen, S.E. Diehl-Nagle, and P. Dressendorfer, "Charge Collection in Multilayer Structures," *IEEE Trans. Nucl. Sci.* **NS-31,** 1149 (1984).

21. A.B. Campbell, A.R. Knudson, P. Shapiro, D. Patterson, and E. Seiberling, "Charge Collection in Test Structures," *IEEE Trans. Nucl. Sci.* **NS-30**, 4486, (1983).

22. R.S. Wagner, N. Bordes, J.M. Bradley, C.J. Maggiore, A.R. Knudson, and A.B. Campbell, "Alpha, Boron, Silicon and Iron Ion Induced Current Transients In Low Capacitance Silicon and GaAs Diodes," *IEEE Trans. Nucl. Sci.* **NS-35**, 1578 (1988).

23. W.L. Bendel and E. Petersen, "Proton Upsets in Orbit," *IEEE Trans. Nucl. Sci.* **NS-30**, 4481 (1983).

24. E.L. Petersen, P. Shapiro, J.H. Adams, and E.A. Burke, "Calculation of Cosmic-Ray Induced Soft-Upsets and Scaling in VLSI Devices," *IEEE Trans. Nucl. Sci.* **NS-29**, 2055 (1982).

25. E. Petersen, J. Langworthy, and S.E. Diehl, "Suggested Single Event Upset Figure of Merit," *IEEE Trans. Nucl. Sci.* **NS-30**, 4533 (1983).

26. P. Shapiro, "Calculation of Cosmic Ray Induced Single Event Upset: Program CRUP Cosmic Ray Upset Program," NRL Memorandum Report 5171, 1983.

27. J.H. Adams, Jr., "Cosmic Ray Effects on Microelectronics, Part IV," NRL Memorandum Report 5901, 1987.

28. W.J. Stapor and P.T. McDonald, "Practical Approach to Ion Track Energy Distribution," *J. Appl. Phys.* **64**, 4430 (1988).

THE AUTHOR

JAMES RITTER graduated from the University of Colorado with a B.A. (cum laude) in 1957. He received an M.S. in Nuclear Physics from Purdue University in 1962. Before joining NRL in 1962, he worked at Westinghouse and the National Bureau of Standards. Between 1962 and 1971, he pursued basic research in nuclear physics studying photonuclear and neutron capture gamma ray reactions and developing the Neutron Time of Flight facility at the NRL LINAC.

In 1971, Mr. Ritter began performing and directing research in radiation effects on microelectronics. He has worked on the radiation hardening of satellite systems such as FLTSATCOM and UHF follow on. He has participated in revising the Joint Chiefs of Staff (JCS) guidelines for hardening requirements for satellites. He has written an invited review article on radiation hardening of satellite systems published in the Journal of Defense Research. His branch, the Radiation Effects Branch, carries out an extensive program in radiation effects in devices and materials including single-event upset, particle-damage effects and radiation damage in solar cells. He is program manager or principle investigator on space experiments such as the DOD/NASA CRRES Microelectronics Experiment and the High-Temperature Superconductivity Space Experiment (HTSSE)

ACOUSTICS

The Navy's ability to operate effectively in the sea is largely dependent on continuing the development and use of advanced techniques and hardware for sensing acoustic signals generated by surface or submerged vessels. Reported in this chapter is work on acoustic scattering, data processing and display, software for acoustic processes, sonar array calibration, and acoustic stress on space vehicles and hardware.

Contributing to this work are the Acoustics Division (5100), the Spacecraft Engineering Department (8200), and the Underwater Sound Reference Detachment (5900).

Other current research in acoustics includes:

- Unmanned, underwater vehicle communications with ground stations using the FLTCOM satellite
- Flow-noise simulation for sonar array calibration
- Matched field processing in an asymmetric three-dimensional ocean

Spacecraft Vibroacoustic Response Prediction

A. A. Salzberg
Spacecraft Engineering Department

Any payload transported to space is required to survive several structurally threatening environments. Launch and ascent subject a space vehicle to an entire spectrum of vibratory loads. Structure-borne, low-frequency vibrations feed energy into the lower modes of the structure, inducing large system-level stresses. High-order modes, excited acoustically by engine and aerodynamic noise, fatigue components. Early and accurate prediction of a satellite's response to these environments ensures a safe and efficient payload design and is the focus of this research [1].

Several techniques are available for predicting the response of a structure to random vibratory loading. Deterministic analyses, such as the finite-element method, have a proven record of successfully predicting the stresses and displacements in the low-frequency regime. At higher frequencies, however, the models often become complex and require large amounts of computer time.

Recently, statistical energy analysis (SEA) methods have emerged that are more suited to dealing with the high-order modes of a structure. The vibrating system is represented statistically, and the response prediction is based on the average vibrational energy contained within a band of frequencies. The structure and excitation sources are modeled as elements, with empirical theoretical expressions governing the storage, flow, and dissipation of vibrational energy. These sources are then coupled to one another by means of power transmission paths that represent the energy flow through the different structural connections. By using conservation of energy, a finite system of equations can be derived and solved, yielding the total energy within the element. This energy can be related to the acceleration response of a particular structure by using the equations for potential and kinetic energy. With this method, the structure is simply modeled by using its gross structural properties, and the analysis is performed quickly and inexpensively [2].

A program developed by Lockheed, the VibroAcoustic Payload Environment Prediction System (VAPEPS), aids in the construction and analysis of SEA models. This program is being used to develop a methodology for predicting spacecraft responses to acoustic excitation by using the Low-Power Altitude Compensation Experiment (LACE) satellite as a test subject (see Fig. 1).

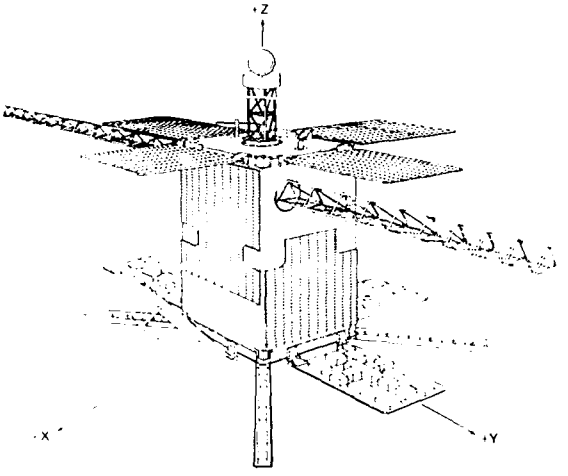

Fig. 1 — LACE spacecraft—on orbit configuration

LACE SEA Model: Within the operating environment of VAPEPS, LACE is represented as an assembly of homogenous plate elements, each joined by weld or point connections. Complex multilayered panels, such as honeycomb sandwich panels with or without rib stiffeners, are reduced to *dynamically equivalent* homogeneous plates by modifying the plate stiffness, density, and thickness to match the dynamic characteristics of the original panel. A methodology was developed that defines the stiffness parameters of ribbed panels for two frequency ranges to accurately represent their observed frequency-dependent dynamic behavior. The discrete frequency that divides these two regimes is determined from the first resonant mode of the panel area between the ribs. Further element characterization includes an

empirical frequency-dependent damping model, the addition of nonstructural mass to represent component weights, and the estimation of bending wave discontinuities.

The plate elements are then assembled and coupled to models of the interior and exterior airspaces. The external airspace is the only excitation element, applying a specified sound pressure level to all external surfaces.

Test Comparison: A system-level acoustic test of the LACE spacecraft was performed at NRL's acoustic test facility (see Fig. 2). The response of the spacecraft was measured at 86 locations and compared to the predicted accelerations. Excellent spectral and overall root-mean-square correlation was observed within the valid operating range of the SEA parameters.

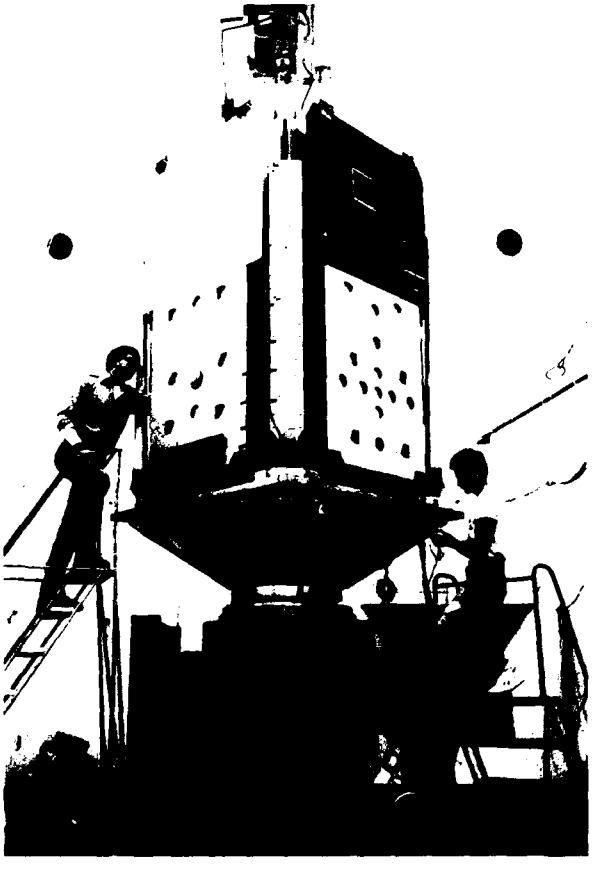

Fig. 2 — Instrumenting LACE for the acoustic test at NRL

Conclusions: A methodology was developed for characterizing a simple spacecraft structure to predict its response to an acoustic excitation by using SEA. The results indicated that, with appropriate modeling techniques developed here and elsewhere, spacecraft structural responses can be predicted accurately, early in the design phase. This allows for an efficient, less conservative, and therefore less expensive, part design.

The Jet Propulsion Laboratory provided the VAPEPS software and support services that made this work possible. This work is an SDIO project spin-off.

[Sponsored by SDIO]

References

1. A.A. Salzberg, "Validation of LACE Spacecraft Vibroacoustic Prediction Model," *J. Environmental Sci.* Jan./Feb. 1989.

2. F.J. Fahey, "Statistical Energy Analysis—A Critical Review," Presented at Colloquium of the Commission Acoustique, W51 du Counceil International du Batiment, Liverpool, England, Oct. 1973.

Prediction of Acoustic Scattering and Radiation from Elastic Structures

L. S. Schuetz, J. Shirron, and J. A. Bucaro
Acoustics Division

Sonar and sonar-related designs require the ability to predict the scattering and radiation of sound by elastic structures in a fluid. Of interest are both the scattered fields owing to a wave incident from the fluid and the radiation produced by mechanical vibrations induced within the structure. When the scatterer (or radiator) is a few wavelengths in size, prediction of the acoustic fields requires accurate modeling of two interacting effects—the loading owing to the fluid and the elastic waves propagating on the structure. Recent algorithmic as well as computational advances have made it possible to treat this

problem numerically, enabling the prediction of target strength and radiated fields of arbitrarily shaped complex structures.

Numerical Model: The model is based on a coupled finite-element/Helmholtz integral formulation. The coupled formulation makes it possible to model a complex structure with varying structural moduli while retaining an exact formulation for the fluid. Thus the model is applicable to three-dimensional targets of arbitrary shape, which may be solids or shells, and may contain complex interior structure, fluids, or evacuated regions. The elastic parameters, including the damping factor, may vary throughout the target. The fluid loading and the elastic waves propagating on the target are modeled as coupled effects. Thus the model becomes a powerful tool for investigating complex target strength issues that have previously been considered only in an approximate sense.

Figure 3 shows the geometry. An arbitrarily shaped, three-dimensional target is assumed to be immersed in an inviscid fluid. The structure is assumed to be excited to linear harmonic vibration, either by an applied mechanical force or by a pressure wave incident from the surrounding fluid.

The coupled formulation divides the infinite three-dimensional domain of Fig. 3 into two regions, separated by the closed surface S, the *wet surface* of the target. The area inside S is modeled by using a conventional finite-element formulation. The exterior (infinite) fluid is modeled by a discretized boundary integral equation that relates the pressure and its normal derivative on S. The resulting coupled equations can be evaluated for the pressure and normal velocity on S, with the field throughout the ambient fluid then also determined from the Helmholtz integral equation.

This coupled, two-domain approach has a number of advantages. The use of the finite-element method to express the target motion makes the formulation applicable to any target amenable to the highly versatile finite-element method. The use of an integral-equation formulation for the fluid makes it possible to reduce the problem from one in an infinite three-dimensional domain to one of a finite two-dimensional surface by use of Green's theorem, greatly reducing the size of the problem and obviating the need for artificial truncation of the fluid region. The resulting integral equation is a Fredholm integral equation of the second kind, a form that has been studied extensively and is known for its numerical tractability.

In the NRL model, this equation is discretized by using quadratic collocation. The elastic structure is modeled by using NASTRAN or specifically developed shell elements, depending on its symmetry.

Results: Results from the model were compared with exact analytical (separation of variables) solutions for scattering from an evacuated spherical shell.

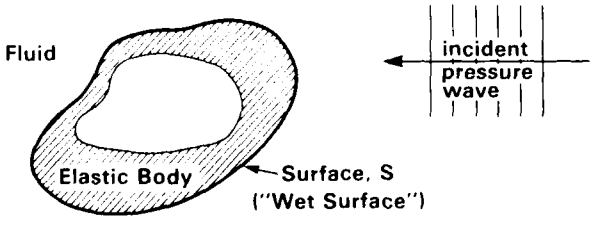

Fig. 3 — Geometry of the finite-element/Helmholtz integral scattering model. The volume is divided into two regions: the scatter and the fluid. The dividing boundary is the *wet surface S* of the scatterer.

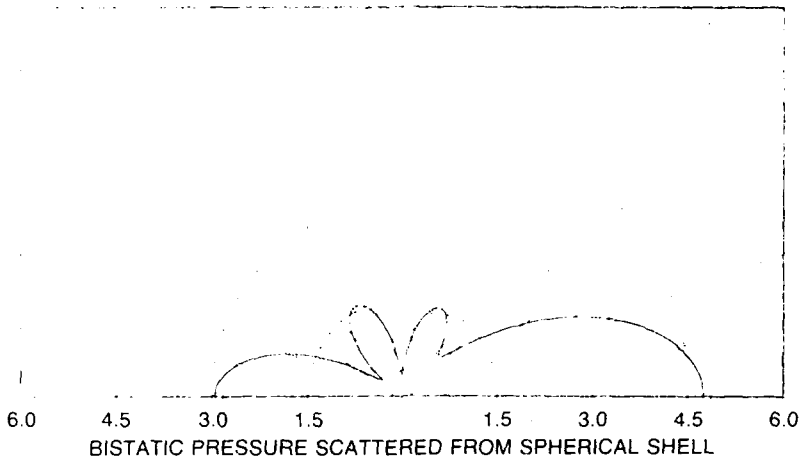

Fig. 4 — Magnitude of the farfield pressure scattered by a spherical shell vs angle. Wavenumber times shell radius = 2. The wave is incident along the positive horizontal axis. —— numerical, ○ exact solution.

Figure 4 is a comparison of the farfield scattered pressure as a function of the angle. The positive horizontal axis is the backscatter direction. The units on the polar axis are linear rather than a dB scale. Equally good agreement was obtained in comparisons with experimental measurements on much more complex geometries.

[Sponsored by ONT and ONR]

Efficacious Methods of Characterizing Active Systems Performance

R. C. Gauss
Acoustics Division

In active sonar systems, acoustic energy—typically, a sequence of broadband finite-duration pulses—is transmitted into the water. The acoustic waves propagate through the medium, scatter off not only the target but also the ocean surface, bottom, and volume, and then propagate to an array of hydrophones where the waves are received as target echo and reverberation, respectively. The goal of active systems is to distinguish target returns from the reverberant returns. By analyzing data from at-sea measurements, we can estimate parameters such as the statistics of reverberant returns in range/azimuth/Doppler/pulse space. With an understanding of the reverberation field, reverberation discriminants can then be developed and applied to these data in an effort to determine the performance potential of active systems. Because of the large computational load associated with active systems data, it is imperative to develop processing and display techniques that allow both a quick overview and detailed analysis of the data.

The processing scheme described here is designed to manage this problem. We also present a technique to process multipulse transmissions and discuss how to use color and other tools to create informative multidimensional displays. These methods have the potential to yield significant improvements in our ability to characterize active systems performance [1].

Data-Compression Technique: Typically, we desire full-range, azimuthal and Doppler coverage for each acoustic transmission. A Doppler-sensitive, broadband, multipulse waveform can provide both high-range and Doppler resolution for each azimuthal look direction. To *optimize* the signal-to-noise ratio, we perform a temporal convolution of the transmitted and received signals, i.e., we *match filter* the data, for each Doppler. The number of matched-filter data points is $T \times N \times M \times D \times P \times S$, where

- T is the duration of the processing (typically the transmission-repetition rate),
- N is the number of samples per second (range resolution $\propto$ 1/bandwidth),
- M is the number of azimuthal look directions (or *beam* channels),
- D is the number of Doppler channels (frequency resolution = 1/(pulse duration)),
- P is the number of normalization schemes, and
- S is the number of pulses per transmission.

For example, if (T,N,M,D,P,S) = (300, 100, 100, 50, 1, 1), then $T \times N \times M \times D \times P \times S = 1.5 \times 10^8$, an unmanageably large number of values for analysis or display.

Our scheme—initially developed by M. E. Weber at NRL—to effectively and efficiently handle these data rates is to segment the time into uniform (e.g., 1-s) intervals. This range window should be chosen to match environmental parameters such as temporal spreading and system parameters such as signal bandwidth; this window should be short enough to isolate acoustic phenomena and long enough to generate an adequate statistical base. As illustrated in Fig. 5, a number of statistics are generated (peak, mean, variance, skewness, kurtosis, distributions, etc.) over each of these range windows, for each Doppler replica (while the data are still in the array processor to avoid additional I/O). This data-compression technique simultaneously reduces the data rate and calculates the statistics of interest in characterizing both targets and the reverberant background without nullifying the resolution and/or extent-of-coverage acquired in previous processing stages.

Minimization: Detection in a reverberation-limited (as opposed to the often-assumed noise-limited) background requires new techniques that can optimize processing of both single pulse and multipulse signals. Furthermore, to maximize use of the finite-source bandwidth (and, hence, maximize the processing gain for each pulse), multipulse signals are often designed where the pulses overlap strongly in frequency, requiring new techniques that can optimize processing of nonorthogonal signals.

Instead of the conventional averaging or multiplying of statistics over pulses to reduce their variance, selecting the minimum over a set or subset of pulses can achieve a similar end, often with an enhanced target-to-reverberation response (Fig. 6(a)) [2]. This will be true whenever the background variance exceeds the target variance. This procedure of minimizing over a set of values is known as *minimization*. Note that this technique has limited success when applied temporally (owing to target and/or source/receiver motions over the pulse duration) unless a windowing scheme (such as described in the previous section) is employed. Furthermore, when the pulses are not orthogonal, minimization can eliminate the cross-replica responses (Fig. 6(b)). We can minimize any statistic (peak, mean, variance, skewness, kurtosis) over any

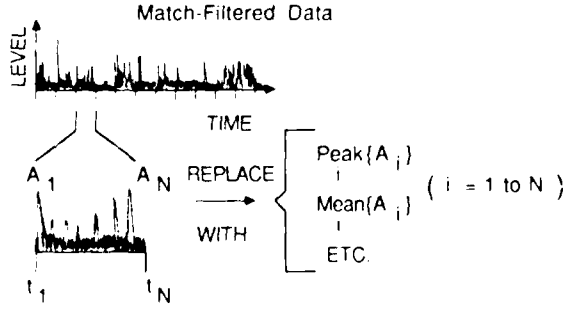

RESULT

Generate desired reverberation/target statistics while reducing data rate and avoiding additional I/O

PROCEDURE

1. Segment time series for each beam/replica into data blocks of equal duration (e.g., 1 sec.)
2. For each data block, replace correlator values with statistics generated from those values:

   Mean — Peak
   Variance — Histogram Values
   Skewness — Range-fluctuation spectra
   Kurtosis — etc.

Fig. 5 — Overview of the data-compression technique

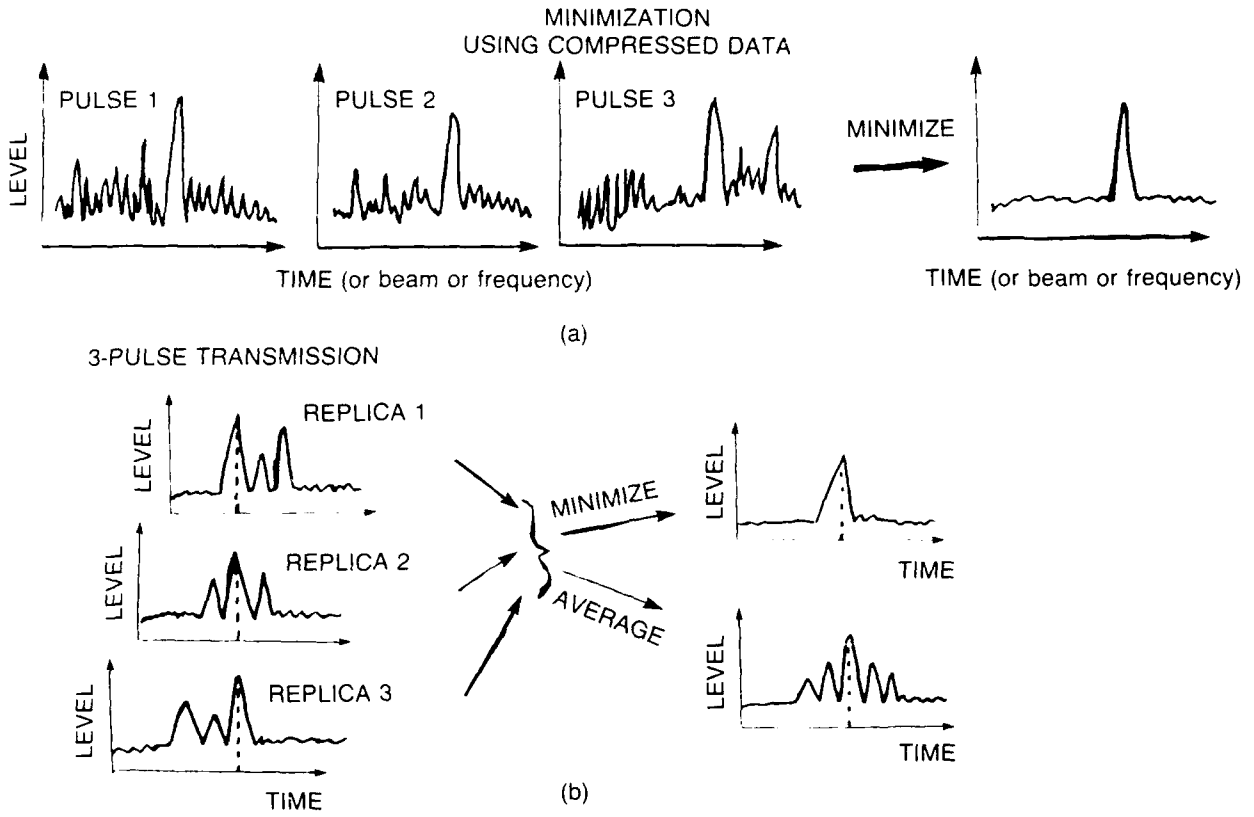

Fig. 6 — Minimization concept applied to (a) compressed-data sequences and (b) time-aligned, nonorthogonal, multipulse matched-filter data

multidimensional space. (Thresholds can be applied after minimization.) A simple example would be a two-stage process for a Doppler-sensitive broadband signal. Here, we can minimize over pulses and then maximize over nonzero Dopplers. We could then do a third stage such as min/maximizing over a statistic (e.g., kurtosis). For a single-pulse transmission, we can apply minimization by: (1) creating subpulses and then minimizing over the subpulses; (2) applying these techniques in the spatial domain either by using a nest of close-by arrays or by forming subapertures of our receiving array, and then minimizing over the set of arrays.

Multidimensional Displays: In attempting to analyze multidimensional data, it is fruitful to be able to add extra *dimensions* to displays both to permit more efficient data examination and to expand or highlight important information.

The use of Doppler-sensitive waveforms in active systems can provide target-speed information and input for detection and tracking schemes that exploit target motion relative to the background. For example, using a Doppler-sensitive broadband waveform, we can use color to represent the Doppler at which the peak correlation value occurred and curve thickness to represent any other classification statistic for each range-beam window (Fig. 7). Thus in one operator display, we are able to present two classification clues that would mutually confirm that a potential target is present. Additional overlays could detail other classification clues. For example, tracking algorithms could place circles around each range-beam cell where potential targets were detected from previous transmissions. Furthermore, we could then color these circles to indicate these potential targets' Dopplers and/or have the circles' radii match the values corresponding to a second classification clue. Similarly, we could use squares, triangles, etc. to represent as many other

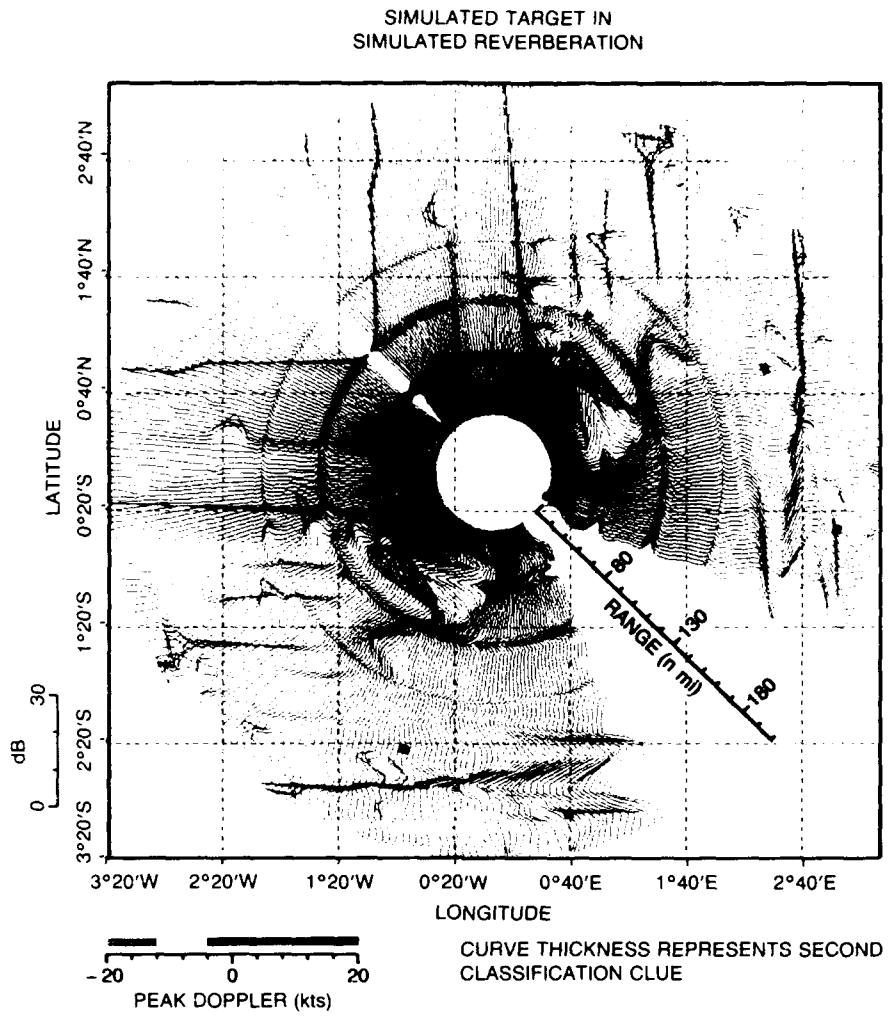

Fig. 7 — Adding extra dimensions of information to a 3-D latitude–longitude simulation of power vs range and beamlook direction (with the spatial ambiguity one sees when receiving on a horizontal-line array); color represents peak Doppler and curve thickness represents a second classification statistic for each pair of range–beam cells

classification clues as the display will allow. In general, by ingenious use of display software packages, an operator can view multiple classification clues on a single display. This would allow the operator to efficiently eliminate most false targets and prioritize the remaining potential targets based on the quantity of clues present.

[Sponsored by ONT]

References

1. R. Gauss, "Efficient Processing and Displaying of Active Systems Data," 7th NATO ASI on Underwater Acoustic Data Processing, Kingston, Ontario, Canada, July 1988.

2. N. Bilgutay, J. Saniie, E. Furgason, and V. Newhouse, "Flaw-to-Grain Echo Enhancement," Proc. Ultras. Intern. '79, Graz, Austria, May 1979.

An Evanescent Wave Generating Array

D. H. Trivett, L. D. Luker, S. Petrie,
A. L. Van Buren, and J. E. Blue
Underwater Sound Reference Detachment

The use of sonar receiving arrays underwater on high-speed platforms involves operating in the presence of significant levels of flow noise

generated by boundary layer turbulence. The successful development of such arrays requires that the degradation of array performance owing to the elevated flow noise levels be eliminated. This may be accomplished only if one is able to evaluate the performance of potential decoupling materials in the presence of flow noise and to determine the sensitivity of candidate transducer modules and arrays to flow noise components. The most straightforward means of satisfying both of these requirements is to use a transmitting array that is capable of generating a nearby pressure field that consists of a single wavenumber component of flow noise over a specified region. However, currently available transmitting arrays generate pressure fields only for the acoustic or radiating portion of the wavenumber spectrum whereas the flow noise spectrum is dominated by nonacoustic or evanescent wavenumbers.

The array described below has successfully demonstrated our ability to design and construct an array that is capable of generating evanescent waves. This capability is expected to have a significant impact on the development of new sonar arrays for the Navy.

Array Design: Our general approach to the design of an array for generating evanescent waves is based on using a sheet of polyvinylidene fluoride (PVDF) as the active element. One side of the sheet contains 20 independently controlled copper electrode stripes, and the other side has a solid copper ground plane. The prototype array (Fig. 8) is designed to generate evanescent waves in water with phase speeds in the 30 to 200 m/s range. To eliminate the excitation of flexural waves in the evanescent generating array, which would contaminate the spectrum of wavenumbers generated by the array, the sheet of PVDF is bonded to a 2.5-cm-thick piece of Lexan. The Lexan shifts the phase velocity of the flexural wave to a value well above 200 m/s in the 500 Hz to 2 kHz operating frequency range of the array while remaining thin enough to be acoustically transparent in this region. This is important since the evanescent waves decay rapidly in the fluid and the receiving array must be placed close to the generating array. The acoustic transparency of the generating array is required to prevent standing waves from being generated between the two arrays, which would interfere with an attempt to obtain a calibration.

The voltage drive for each of the electrode stripes is independently controlled with its own power amplifier. All of the power amplifiers are computer controlled and are driven with individual digitial-to-analog converters operating from the same clock. A computer program sets the frequency of operation. Also, the desired relative amplitudes and phases of the stripes, as determined by a set of computed complex shading coefficients, are inserted into the computer program.

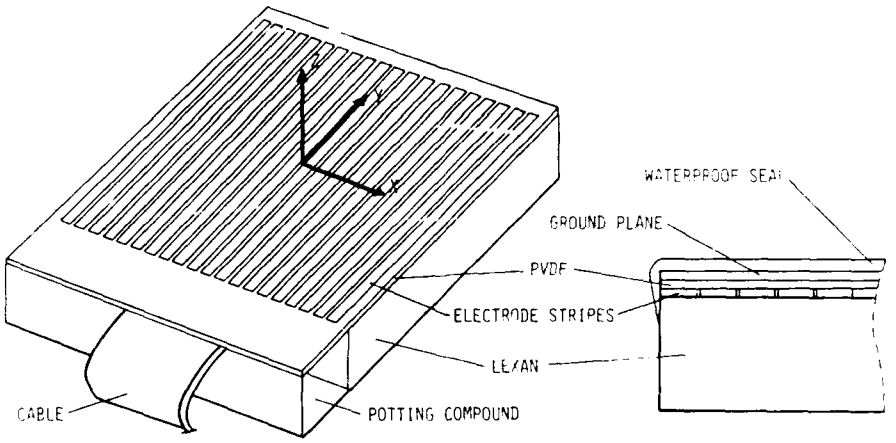

Fig. 8 — Geometry of an evanescent wave generating array

Shading Coefficients: In general, the transfer function of an array may be obtained for a particular frequency by measuring the acoustic field produced by each stripe operating individually. Once the transfer function is obtained, it may be used to generate the shading coefficients for any desired pressure field. This procedure, however, is time consuming and difficult to implement when a large number of stripes are involved. We have found it possible to replace the measurement procedure with a point source numerical algorithm. The numerical procedure generates a set of shading coefficients for a desired pressure field and also ensures that no acoustic wavenumber is generated by the array because of its finite aperture.

Experimental Results: The array was investigated by mounting it in a small water tank and mounting a miniature hydrophone on a positioner to map the pressure field. The stripes were driven with calculated shading coefficients, and the pressure field was mapped 0.65 cm in front of the array with the amplitude and phase recorded. Figure 9 compares the amplitude of the measured field to the calculated amplitude. The field is within 0.5 dB of the calculated value in the window region. Figure 10 compares the measured phase with the calculated and desired phase and indicates that an almost pure 70 m/s evanescent wave was generated.

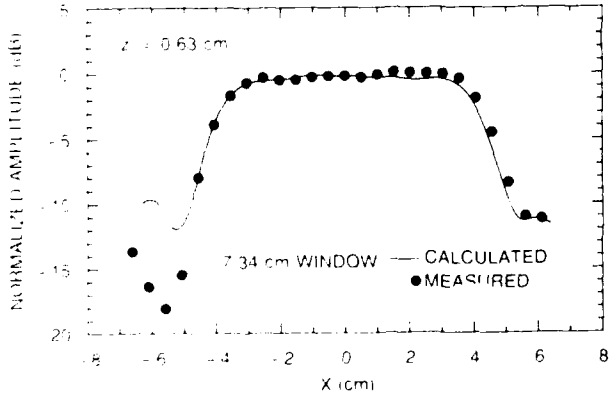

Fig. 9 — Pressure field measured across centerline of array operating at 1 kHz

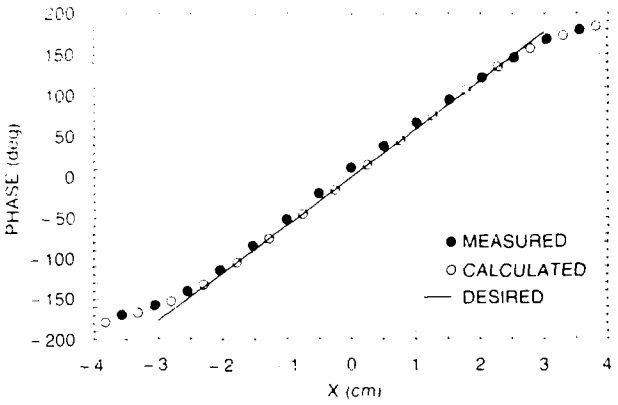

Fig. 10 — Phase measured across centerline of array

The demonstrated ability to generate evanescent waves in water will allow construction of a larger array that will be used to calibrate the wavenumber response of sonar array modules. This will result in the Navy's ability to determine the response of these modules to flow noise and aid in the design of new sonar systems for high-speed platforms.

[Sponsored by ONR and ONT]

The Processing Graph Method

D. J. Kaplan
Acoustics Division

We discuss a new approach to building computer applications that solves some difficult and specific problems associated with real-time signal processing. We believe that this approach solves problems far beyond signal processing.

Needed—Infinite Throughput and Free Software: What the Navy and other users want are computers capable of infinite throughput that never fails, computers that are controlled by free software that contains no errors, and software that is completely reusable and costs nothing to maintain. In pursuit of infinite throughput, two implementation themes occur.

The first implementation theme is approached by increasing central processing unit (CPU)/ memory speed, which is often done through

increased clock speed and decreased circuit size. This idea is exploited in very high speed integrated circuit (VHSIC) technology.

The second theme is approached by building a network of processors and memories that, by operating concurrently and sharing computations among their subelements, makes possible the rapid computation of solutions to complex problems.

Many apparently atomic processors, when examined, are revealed to be processor networks. The Navy's standard signal processors, the AN/UYS-1 (called the advanced signal processor (ASP)) consist of five subprocessors, each with its own local memory, clock, and instruction set along with bulk memory and several busses. The AN/UYS-2 (called the enhanced modular signal processor (EMSP)) is built from multiple arithmetic processors and global memories, a command program processor, a scheduler, some input/output processors, a data transfer network, and many busses.

The Usual Approach: It is very difficult to write real-time programs for processor networks like the ASP and EMSP. The usual approach is to treat the problem something like arranging music for a multipiece orchestra to be played by deaf performers where each player is given a separate score for his/her musical instrument fully defining notes, expression, and timing to be played. If each performer is accurate then something like a performance of the composition will be produced. Imagine now the problem of modifying any one of the player's parts. Because of the synchronous character of the process, every other player's part will also have to be altered. This is an expensive and tedious process and falls quite short of free, completely reusable software containing no errors that costs nothing to maintain.

The Processing Graph Method: We sketch another way of programming processor networks to solve problems. Its name is the processing graph method (PGM), and it is founded on a static data-flow model of programming.

The Programming Model: The concept of processing graph is recursive. Figure 11 shows a processing graph on the left-hand side. The processing graph is built from nodes and directed edges. Each edge carries first-in first-out ordered data along the direction indicated by that edge. Various types of data, integers, floating points, arrays, lists, etc., may be carried along an edge, one type of data per edge. Each node is associated with either

- a computational resource called a primitive or
- a subgraph that is itself a processing graph.

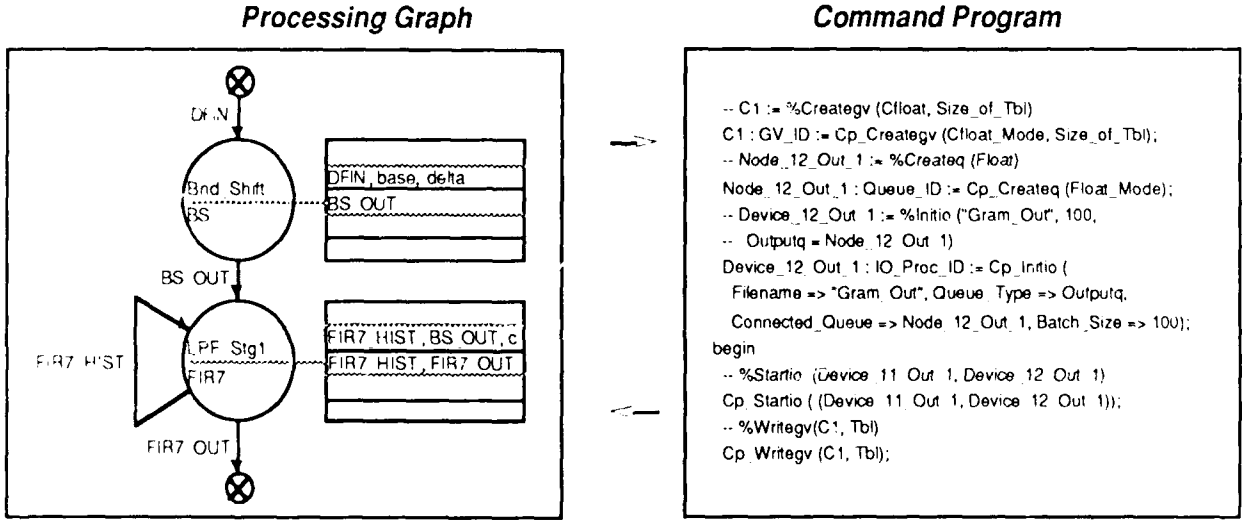

Fig. 11 — A processing graph with its command program

Primitives are irreducible computational procedures such as matrix multiplication routines, sort routines, fast Fourier transforms, and threshold detectors. Any node may execute asynchronously when sufficient data become available on all of its input edges. Some of the data on the node's input edges are used by the node's associated primitive or subgraph to produce new data deposited on the node's output edges. After the new data are deposited, some of the input edges' data are consumed. Since node execution is asynchronous and depends on the availability of sufficient data, any number of nodes may execute concurrently: this process repeating so long as data are available.

A processing graph can be started and, stopped, and its actions can be modified in various ways while it is running. These actions are accomplished through programs written in some specific high-order language making use of procedure calls that provide an interface between the high-order language and processing graphs. Such programs using these procedures are called command programs. Figure 11 illustrates this. At the right in the figure is a simple command program that controls the processing graph shown on the left.

An Outline for Implementation: The transformation of a processing graph into executable code resident in a target is accomplished by three translators. The first translates the pictorial representation that we have been calling a processing graph into a text representation expressed in something called processing graph notation (PGN). The second transforms the PGN form into something called a graph realization. A graph realization becomes resident within the target processor network but is not executable. It serves as a sort of template. The third transforms these templates into machine executable code called graph instances. One realization may be used as a template to form many instances.

Figure 12 outlines the translation process that we have just described. It is also necessary to have a form of inverse translation. When run-time errors occur it is important that the user be informed of them in terms of the original processing graph and command program and not in terms of some machine operation problem at some memory location in some subprocessor.

To supply the proper run-time services to a family of processing graph instances an operating system for the processor family must be built. For the PGM to be useful, the operating system must use the processor family architecture efficiently.

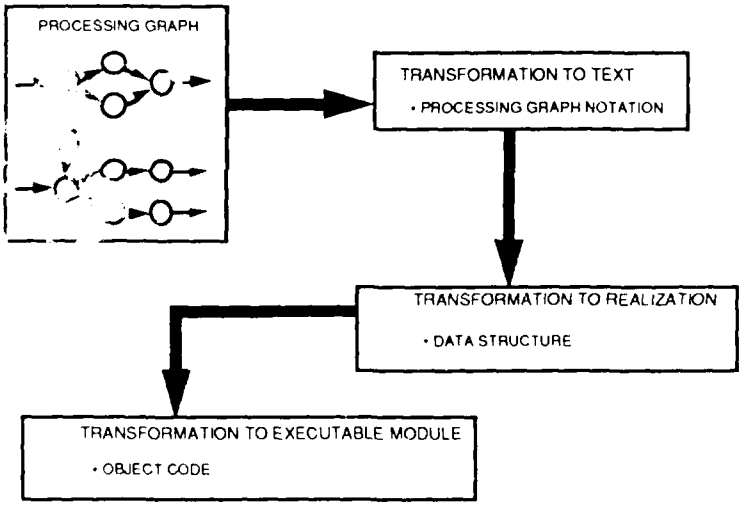

Fig. 12 — The translation process

Processors Using the Processing Graph Method: PGM is now operational on the EMSP with command programs written in CMS2 and on the VAX family of machines (under VMS) with command programs written in Ada; this provides an easy path to any other computer operating with Ada.

The usual control flow representation of a process forces the designer to order the steps of that process; the processing graph approach allows the designer to break away from this rigid ordering to represent any inherent concurrency that may exist within the process.

PGM provides the capability to develop prototypes of systems in a commercial or special-purpose computer or computer network, to work from the top-down, level by level, until the lowest level primitives are designed and tested, always staying within the same paradigm. Furthermore, once a prototype has been developed, it is relatively easy to transport it to any other processor network for which the PGM has been implemented.

[Sponsored by NAVSEA and the Software Technology for Adaptable Reliable Systems (STARS) DoD initiative]

Bibliography

R.S. Stevens, "A Tutorial on the Processing Graph Method," Proceedings of 1987 Summer Computer Simulation Conference, Montreal, Quebec, Canada, July 27-30, 1987.

R. Hillson, "Processing Graph Architectures," Proceedings of 1987 Summer Computer Simulation Conference, Montreal, Quebec, Canada, July 27-30, 1987.

BEHAVIOR AND PROPERTIES OF MATERIALS

The operating Navy is built from a vast array of materials that must withstand the rigors of the world's harshest environments—the sea and space. Much research is performed at NRL relating to the development of new materials—composites, ceramics, alloys, and metals—to name a few—and the determination of their properties, service performance, and reliability. Reported in this chapter is work on corrosion-resistant ceramics, stress-corrosion cracking, high-temperature oxide superconductors, superconducting thin films, ceramic matrix composites, failure of aircraft electrical insulation, and the interactions between interpenetrating fluids.

The Laboratory for Computational Physics and Fluid Dynamics (4400), and the Condensed Matter and Radiation Sciences (4600), Chemistry (6100), and Materials Science and Technology Divisions (6300) contributed to this research.

Other current research in materials includes:

- High-performance permanent magnet materials
- Polycrystalline Fe-C alloys
- Reflective stress wave effects
- Grain growth in metals and alloys
- Polymer/metal isotropic composites
- Silicon carbide fibers

Very Late Time Mixing from the Rayleigh-Taylor Instability

J. P. Boris
Laboratory for Computational Physics and Fluid Dynamics

The Rayleigh-Taylor instability describes how a dense fluid, initially poured over a lower density fluid, becomes dynamically unstable, fragments, and falls through the lighter fluid. In a laboratory, the system eventually approaches a lower energy state with the lighter fluid on top and the heavier fluid on the bottom. The rate of interpenetration at which the final state is approached and the ensuing turbulent mixing rate between the two fluids is crucial to many naval fluid systems with gravity, to combustion systems, to inertial confinement fusion, in some geophysical situations, and to nuclear weapons design.

The rate at which the two fluids interpenetrate and mix has been a subject of intense scientific speculation for decades. Our research has focused extensively on the high-energy laser and pulsed power aspects of the Rayleigh-Taylor instability [1] but the general fluid dynamic question of how fast two fluids of different density interpenetrate has recently been tackled from the more general and fundamental point of view of trying to understand the complex mechanisms that control compressible fluid turbulence [2].

A New Model and New Simulations: Numerical simulations of unprecedented scope using a new description of the problem are being developed to answer this question [2]. These simulations have been performed by using flux-corrected transport (FCT) algorithms (see Ref. 3 and the references therein) on the Laboratory for Computational Physics and Fluid Dynamics' (LCP&FD's) parallel processing Graphical and Array Processing Computer System (GAPS) in a doubly periodic square domain. FCT algorithms are conservative and monotone with fourth-order accuracy to maintain the sharp gradients needed to delineate the interface between the two fluids.

To limit the computational scope of the problem, doubly periodic geometry is attractive, but the problem definition requires some manipulation to remove the average pressure gradient that characterizes the equilibrium configuration of a heavy fluid unstably supported by a light fluid. This average pressure gradient is removed by studying a problem that has no net force. The two fluids are accelerated in opposite directions with two different *gravitational* forces that are inversely proportional to the mass density. Thus these simulations also apply to two oppositely charged fluids in an electrostatic field or, as the usual Rayleigh-Taylor problem, in an accelerated frame of reference. By ensuring that the total force on the system is zero, the net momentum of the system is constant for all time and can be taken as zero. The two fluids are being pulled through each other and thus have a nonzero net interpenetration drift.

Previous theory and numerical modeling of this problem were restricted to the relatively early linear and nonlinear phases when the heavy fluid is still accelerating downward. Experimenters have found it difficult to study a wide enough range of length scales and long enough times for true turbulence to set in. Also, setting up an ideal system having the heavy fluid on top is very difficult. Common sense suggests that the acceleration must end in a constant interpenetration drift of the two fluids when the relative drag of the fluids passing through each other dissipates energy at the same rate as potential energy is being extracted from gravity. Until the new description of this problem, however, it has not been practical, even with supercomputers, to run calculations long enough to determine this steady interpenetration rate.

Results and Application: Figure 1 is a color snapshot of the two fluids taken directly from the GAPS' on-line monitor showing a highly convoluted turbulent state in which the lower density (darker) fluid rises slowly through the higher density (brighter) fluid. The

Fig. 1 — Color mapping of material density in the two-dimensional domain overlaid with regions (in dark green) where the vertical velocity is nearly zero. The low-density fluid, which tends to rise, is mapped into purple and blue colors shading toward red while the high density fluid, which tends to fall, is mapped into yellow and orange colors shading toward red. Regions of predominantly light fluid tend to twist the material interfaces upward and lie across a dark green velocity dividing line from predominantly heavier fluid.

interpenetration drift velocity is only a few meters per second in this case, even though the acceleration is ten thousand times gravity. This result is very surprising, contradicting theories and early-time, short-duration simulations suggesting that the interpenetration drift would increase linearly with time. This strong effect at very late times is caused by the secondary shear flow (Kelvin-Helmholtz) instability, which is generated between the two moving fluids accelerated by the primary Rayleigh-Taylor instability.

The continuing interaction of these two, strong, fluid dynamics modes of instability, leads to a large increase of interfacial surface between the two components of the flow as shown in the figure. This large area interface enhances molecular mixing and, in turbulent combustion, speeds the chemical reactions. This turbulence-driven area increase accounts for many instances where flames transition into explosions and thus is of major importance for safety. With density gradients at these interfaces in the presence of gravity or strong pressure gradients, turbulent vorticity is actually generated as well as rearranged convectively.

The contortion and stretching of the interface between identifiably different phases or components of a fluid is where the currently popular fractial geometry notions probably have their greatest applicability. In the example of Fig. 1, the fractal dimension of the fluid interface varies between 1.45 and 1.55 as the interpenetration drift of the two fluids varies. This *dimension*, a measure of how convoluted the interface curve is, is always somewhat larger than the fractal dimension of the zero-vertical-velocity curve, shown as the dark green overlay, even though these same velocities are responsible for convoluting the interface.

Ted Young of the Laboratory for Computational Physics and Fluid Dynamics is credited with the success of the GAPS computer system and the reactive flow model used for this research. Rob Scott and Ed Reusser of Berkeley Research Associates also made significant contributions to the GAPS.

[Sponsored by ONR and DARPA]

References

1. M.H. Emery, J.H. Gardner, J.P. Boris, and A.L. Cooper, "Vortex Shedding Due to Laser Ablation," *Phys. Fluids*, **27**(5), pp. 1338-1340 (1984).

2. J.P. Boris, "Compressibility in Turbulence Generation and Mixing," Proceedings of the International Workshop on the Physics of Compressible Turbulent Mixing, Princeton University, Princeton NJ, 24-27 October 1988, to be published by Springer-Verlag.

3. E.S. Oran and J.P. Boris, *Numerical Simulation of Reactive Flow* (Elsevier Science Publishing Co., New York, 1987).

High-Temperature Corrosion-Resistant Ceramics

R. L. Jones
Chemistry Division

By the year 2000, advanced ceramics will be a $16 billion-a-year industry in the United States, with equal or greater growth occurring overseas. A major future use of ceramics will be in engines to increase fuel economy and power by improving thermal efficiency and allowing higher operating temperatures. Prototype *ceramic* gas turbine and diesel engines have been already built, and commercial development of ceramics (primarily silicon carbide (SiC) or nitride (Si_3N_4)) for engine components such as turbocharger rotors (now in production in Japan), pistons, and gas turbine vanes, is under way. Ceramic coatings for heat insulation and high-temperature wear applications will also be important. Zirconia (ZrO_2)-based thermal barrier coatings (TBC) are now being developed, e.g., by the Navy and others for use in gas turbines and diesels where they can boost engine power and fuel economy by 10% to 15% by reducing heat transfer from the combustion gas.

Corrosion of Ceramics: All ceramics suitable for oxygen-rich combustion environments are oxides or form protective oxide surface layers (e.g., SiO_2 on SiC or Si_3N_4). Ceramic oxides are highly stable oxides, and it has been supposed in the past that they will therefore not react or *corrode*. This idea is incorrect, and, in fact, current yttria (Y_2O_3)-stabilized zirconia (YSZ) coating applications are limited because YSZ is readily attacked by the trace vanadium contained in many petroleum fuels.

Although ceramic corrosion is becoming recognized as critical, it has as yet received little study. We have recently shown, however, that reactions between ceramic oxides and engine fuel/air contaminants such as sodium, vanadium, and sulfur (which are converted to Na_2O, SO_3, and V_2O_5 in combustion) are explainable by Lewis acid-base concepts. Oxides act as Lewis acids or bases according to their ability to donate (base, e.g., Na_2O) or accept (acid, e.g., V_2O_5) electronic charge, with each oxide having a characteristic acidic (or basic) nature. The various ceramic oxides and vanadate species (Table 1) then give classical acid-base behavior, where the tendency to react is determined by the relative difference in acid-base nature between the reactants. For example, the YSZ corrosion reaction

$$Y_2O_3 \text{ (base)} + V_2O_5 \text{ (acid)} = 2\ YVO_4 \text{ (salt)} \quad (1)$$

occurs with $NaVO_3$ and V_2O_5 but not Na_3VO_4 where the acidity (V_2O_5 activity) is too low.

Table 1 — Vanadium-Ceramic Oxide Reactions

INCREASING ACIDITY →	Na_3VO_4	$NaVO_3$	V_2O_5
Y_2O_3	NR	YVO_4	YVO_4
CeO_2	NR	NR	$CeVO_4$
ZrO_2	NR	NR	ZrV_2O_7 (BUT SLOWLY)
GeO_2	$Na_4Ge_9O_{20}$	$Na_4Ge_9O_{20}$(*)	NR
Ta_2O_5	$NaTaO_3$	$Na_2Ta_4O_{11}$	α-$TaVO_5$

INCREASING ACIDITY ↓

NR = NO REACTION
(*) AS PPT FROM H_2O SOL'N

Development of Corrosion-Resistant Ceramics: The acid-base theory of ceramic corrosion provides a powerful basis for the development of corrosion-resistant ceramics. Table 1 indicates, e.g., that ZrO_2 is virtually nonreactive with even vanadium pentoxide, and that a highly vanadate-resistant, stabilized zirconia should be possible if a stabilizer more acidic than Y_2O_3 could be found. Following this reasoning, we have identified, and are now developing, scandia (Sc_2O_3), the most acidic of the rare earth oxides, as a corrosion resistant stabilizer. In all tests to date, scandia has been superior to yttria against molten vanadate or sulfate/vanadate corrosion. As an example, Fig. 2 shows $NaVO_3$ unreacted on scandia-stabilized zirconia (SSZ) after 475 h at

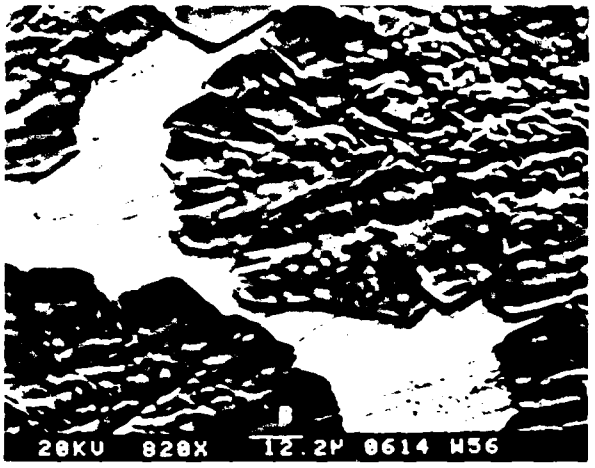

Fig. 2 — Unreacted $NaVO_3$ on SSZ after 475 h at 700°C

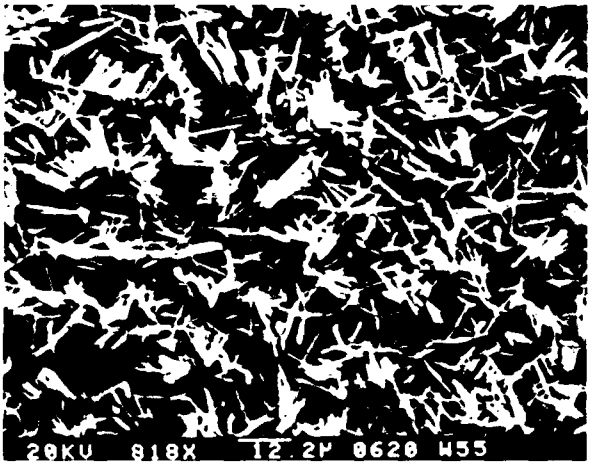

Fig. 3 — Crystalites of YVO_4 produced by reaction of $NaVO_3$ with YSZ after 475 h at 700°C.

700°C, whereas under the same conditions, $NaVO_3$ reacted strongly with YSZ, copiously producing YVO_4 crystals (Fig. 3) and destabilizing the YSZ structure. SSZ appears in fact to resist molten vanadate/sulfate corrosion better than the metallic coatings now used on Navy ship GT blades. Scandia is expensive, but the amounts required are small, and the additional cost (about \$0.15 per cm^2 of coating) is insignificant compared to the benefits possible by the use of SSZ thermal barrier coatings in Navy ship propulsion gas turbines capable of burning low cost, vanadium-containing fuel.

The success of ceramics in engines will depend largely on the development of corrosion-resistant ceramics. The NRL oxide acid-base reaction theory represents a fundamental first step in that quest.

[Sponsored by NAVSEA]

Bibliography

R.L. Jones, "Low-Quality Fuel Problems with Advanced Engine Materials," *High Temp. Technol.* **6**, 187 (1988); also published as NRL Memorandum Report 6252, Aug. 1988.

R.L. Jones, "Scandia as a Corrosion- Resistant Stablizer for Zirconia," NRL Memorandum Report 6332, Sept. 1988.

Fiber–Interphase–Matrix Interactions in Ceramic Matrix Composites

B.A. Bender and D. Lewis III
Materials Science and Technology Division

Many advanced Navy applications require new, high-temperature structural materials, particularly for those applications requiring material temperatures in excess of 1000°C. For these high-temperature structural applications, one of the most promising classes of new materials is that of ceramic fiber-ceramic matrix composites (CMCs). These materials offer unique combinations of lightweight, high strength, high toughness, and the ability to perform in temperatures as high as 1200° to 1500°C.

Reactions: One of the major limitations in employing CMCs in high-temperature applications, and in their fabrication, is that of the deleterious interactions between the various phases. Typically, the matrix, fiber, and fiber-matrix interphases interdiffuse and interreact, degrading the properties of the composite. These deleterious reactions are particularly likely to occur during processing where temperatures are significantly higher than during service, e.g., 1200° to 1700°C vs probable service conditions of <1200°C, as in gas turbine hot sections and hypersonic vehicle skins.

Modeling: The chemistry and physics governing the matrix–interphase–fiber–environment interactions are exceedingly complex. Attempts to model the processes occurring are hindered by the lack of data on high-temperature diffusion, chemical kinetics, and thermodynamic properties, and also by the unknown character of some of the phases present, e.g., amorphous BN films on fibers in the present study. It is thus necessary to base any efforts to model the processes occurring at the fiber–matrix interface in these ceramic matrix composites on a firm base of detailed experimental observations.

Ongoing Research: Current efforts in the Composites and Ceramics Branch on CMCs have focused on such preliminary observations as necessary to subsequent modeling and experimental efforts. This research has begun with the simpler case of fiber–environment and fiber–coating–environment interactions as reported previously [1–3]. Current work involves a relatively well-developed CMC, Nicalon™ SiC fibers with BN or BN/SiC coatings in a $ZrTiO_4$ matrix, for which processing techniques have been previously investigated [4]. These efforts now focus on this more complex system in which a greater variety of diffusion–reaction–recrystallization processes are possible. In this case, the initial constituents include (ignoring possible impurities):

$$\underset{\text{Fiber}}{SiC+C+O} + \underset{\text{Coating}}{BN \text{ or } BN+SiC} + \underset{\text{Matrix}}{ZrTiO_4}$$

$$+ \underset{\text{Processing Atmosphere}}{\text{Vacuum or Argon or } N_2},$$

with possible products:

$$SiC,\ C,\ CO,\ CO_2,\ SiO,\ SiO_2,\ BN,\ B_2O_3,\ Si_3N_4,\ ZrO_2,\ TiO_2,\ ZrTiO_4,\ ZrSiO_4,\ TiC,\ TiN,\ \text{etc.}$$

Note that some possible products are gases at the processing temperatures (CO, CO_2, SiO), some are liquids and possible glass-formers (B_2O_3, SiO_2), and others are expected to be well-defined crystalline compounds (TiC, SiC). The current efforts with regard to CMCs at NRL have investigated the details of these processes by using transmission electron microscopy (TEM), analytical electron microscopy (AEM), and scanning Auger microscopy (SAM). These techniques, while requiring lengthy and difficult sample preparation, provide detailed information on the physical and chemical nature of the interface region. Corollary efforts include measurement of the key mechanical properties of the composite–strength and fracture toughness, as affected by the various material and processing parameters.

Current Findings: Figures 4 and 5 show examples of the strength and toughness measurements. Figure 4 shows the dramatic effect of fiber coatings on both the strength and toughness of the ceramic matrix composite. The single-layer BN coating, a patented NRL development [5], provides on the order of 100% improvements over that obtained with uncoated fibers. This is primarily the result of the reduction in matrix–fiber bonding by the coating, as well as a reduction in the degradation of fiber properties associated with reaction with the matrix. The two-layer BN/SiC coating, in which the SiC overlayer inhibits the reaction of the BN with the oxygen in the matrix, provides even more dramatic improvements, to approximately three times that obtained for uncoated fibers. This coating also has other benefits in applications, since the BN coating is subject to degradation by oxidation. The SiC overlayer tends to protect the underlying BN through formation of a relatively impermeable SiO_2 layer. The CMCs prepared with the two-layer coating exhibit properties for strength and fracture toughness comparable to those for the common engineering metal alloys used in aerospace structures.

Figure 5 shows the effect of the processing atmosphere on the bulk mechanical properties of the composite (with BN/SiC-coated fibers). Here

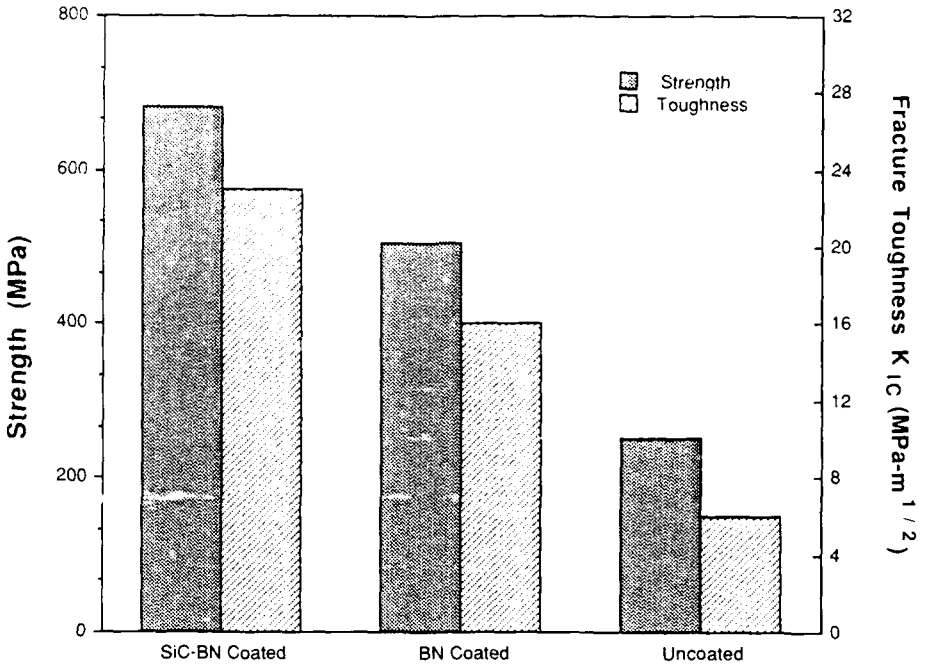

Fig. 4 — Fiber coating

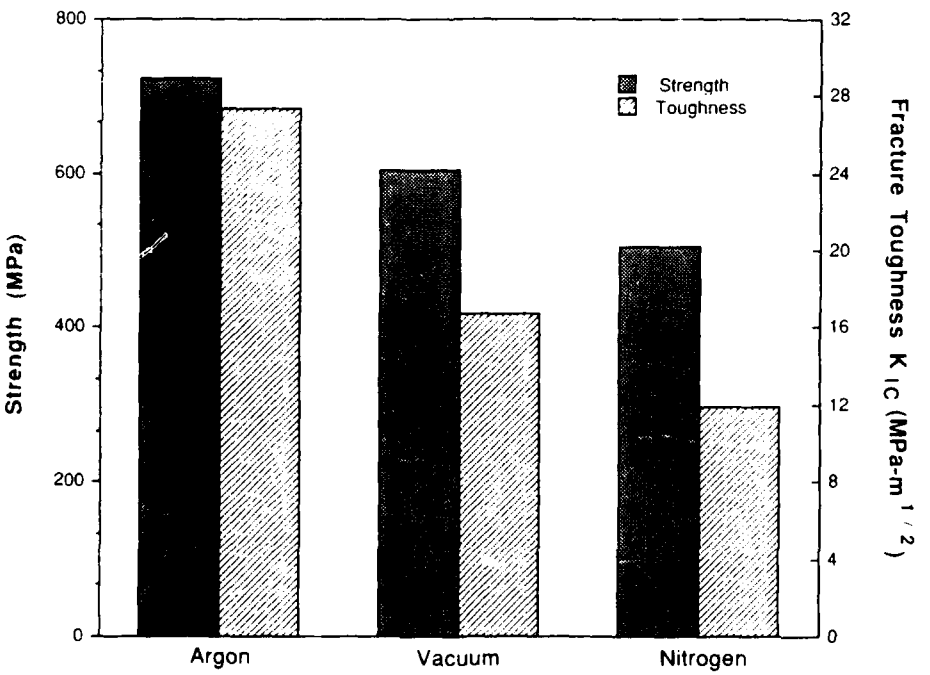

Fig. 5 — Hot pressing environment

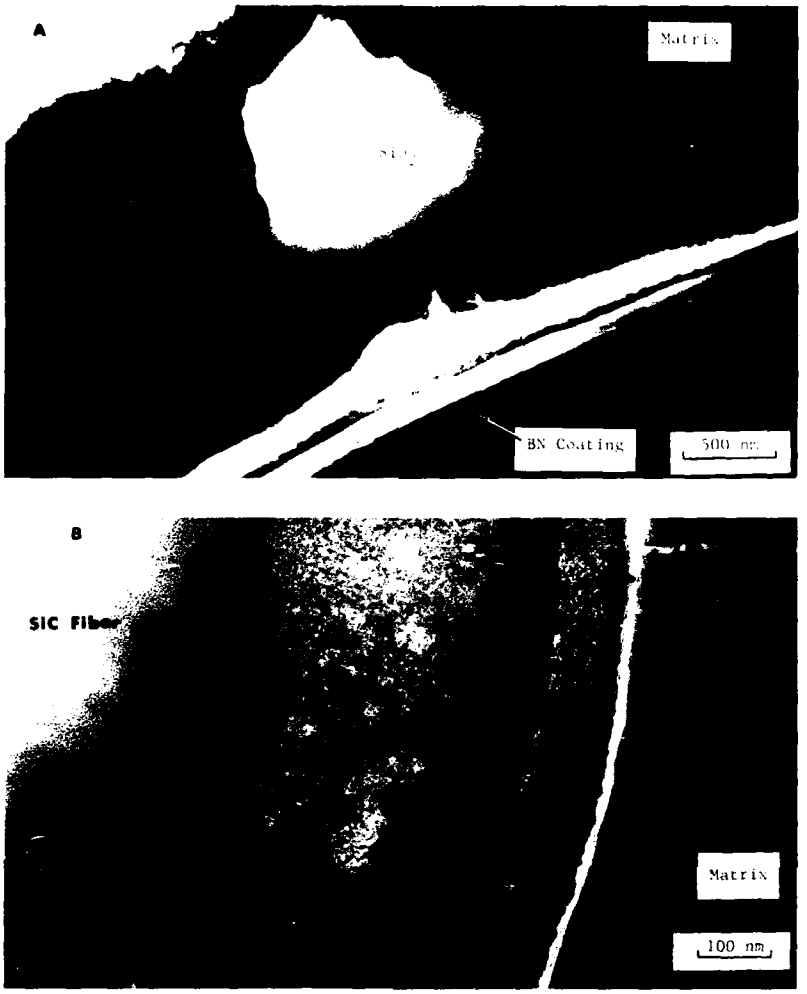

Fig. 6 — TEM of a zirconia titanate/Sic composite interface between the matrix and the coated fiber hot pressed at 1250°

effects would be expected based on possible reactions with the constituents, as noted in a previous *NRL Review* article [3], and on the gaseous nature of some of the reaction products (see above). In this case, the nitrogen atmosphere presumably degrades the composite by some reactions. These would be expected to be those that produce nitride products such as Si_3N_4. However, no such products, e.g., nitrides, have ever been detected by TEM and AEM analysis, indicating that either different processes are responsible for the degradation, or that the nitride products formed are unstable under the conditions in the composite. The vacuum atmosphere tends to promote reactions with gaseous products such as that in the fibers between the SiC, free C and O,

$$SiC + C + O \rightarrow SiO\uparrow + CO\uparrow,$$

and thus tends to encourage degradation of the fibers. The argon atmosphere, which is nonreactive with the composite, but which provides an overpressure to inhibit gas-producing reactions, provides the best results. Possibly other atmospheres, such as those containing a high partial pressure of CO, might prove even better, but practical considerations have prevented trials of such processing conditions.

Figure 6 shows some of the details of the fiber-matrix interface in a composite made with BN/SiC coated fibers. These show the Nicalon SiC fiber with its microcrystalline nature, the

amorphous BN coating and the SiC overlayer, and the crystalline ZrTiO4 matrix. Note also the pocket of amorphous SiO_2 in Fig. 6(a), and the nearly continuous layer of SiO_2 in Fib. 6(b). These result from either oxidation of the SiC coating or from SiO_2 impurities in the matrix precursors (note that most ZrO_2 sources contain significant amounts of SiO_2 since the starting material is typically $ZrSiO_4$ sand). In Fig. 6(b) note also the fine structure of the interfacial region that suggests a number of reaction and diffusion processes are occurring there, e.g., the fine layers at the boundary of the SiC coating and SiO_2 reaction layer. These effects result from processes such as SiO escaping from the fiber and condensing at the fiber coating-matrix boundary. Note also the gap where the fiber has physically debonded from the matrix at the silica/BN coating interface, preventing the silica bonding to the fiber and leading to a significantly tougher composite. The TEM micrograph shows how complex this particular interfacial region is, and how it actually consists of numerous discrete layers that suggest that a number of complex reaction and diffusion processes are occurring at the silica/BN coating interface.

Summary: Preliminary work on a model composite system at NRL has shown the strong effects of the processing environment on the bulk mechanical properties of the composite. Analysis of the details of the interfacial region in this composite suggest very complex interactions between the various phases present and the processing conditions and indicate the need for rather sophisticated modeling to describe the various diffusion and reaction processes occurring.

[Sponsored by NAVAIR]

References

1. B.A. Bender, D.J. Schrodt, and J.S. Wallace, "Thermochemical Treatment of Tyranno Fibers," in *Metal Matrix, Carbon and Ceramic Matrix Composites*, J.D. Buckley, ed., NASA Conf. Publ. 2482, pp. 201-212 (1987).

2. B.A. Bender, J.S. Wallace, and D.J. Schrodt, "Effect of Thermochemical Treatments on the Strength and Microstructure of SiC Fibers," to be published in *Metal Matrix, Carbon and Ceramic Matrix Composites*, J.D. Buckley, ed. (1989).

3. D. Schrodt, B.A. Bender, and D. Lewis III, "Thermochemical Degradation of Polymer-Derived Silicon Carbide Fibers," in *1987 NRL Review*, NRL Publication 112-2630, pp. 91-92 (1988).

4. B.A. Bender, D. Shadwell, C. Bulik, L. Incorvati, and D. Lewis III, "Effect of Fiber Coatings and Composite Processing on Properties of Zirconia-based Matrix SiC Fiber Composites," *Bull. Am. Ceram. Soc.* **65**(2), 363-369 (1986).

5. R.W. Rice, "BN Coating of Ceramic Fibers for Ceramic Fiber Composites," U.S. Patent 4,642,271, 1987.

Prediction of Ripple-Load Effect on Stress-Corrosion Cracking

R.A. Bayles, P.S. Pao, and G.R. Yoder*
Materials Science and Technology Division

Stress-corrosion cracking (SCC) occurs when a susceptible material fails under the conjoint action of a sustained load and a corrosive environment applied for an extended period of time. Subcritical crack growth occurs and leads to failure of a component. High-strength metal alloys are particularly susceptible to SCC, and therefore critical parts of Navy weapons systems are often vulnerable. In a cracked piece, the fracture mechanics parameter K_{Iscc} describes the stress state below which cracking owing to SCC is not anticipated. The present work involves an interpretation of the effect of a small oscillating (ripple) load superimposed upon the high static

*Now at Office of Naval Research

load of a conventional SCC experiment. Direct experiments at NRL [1] and elsewhere have indicated that, in some cases, a severe degradation in strength below K_{Iscc} results from ripple loading, while the effect is absent in other cases. We have predicted the extent of ripple-load degradation in a 5Ni-Cr-Mo-V steel, in good agreement with results of the time-consuming direct experiments. The method also correctly predicted that a 4340 steel would be immune to ripple-load effect.

Corrosion Fatigue: While ripple-load cracking appears to be a perturbation of static SCC, the insight leading to the present predictive capability [2] was obtained by considering ripple-load cracking to be corrosion fatigue occurring at a high load ratio, $R = P_{min}/P_{max}$. Both views are correct, but use of corrosion-fatigue concepts and descriptors permits a straightforward analysis of the process of ripple-load crack propagation.

The data required to predict time-to-failure owing to the ripple-load effect is obtained from a corrosion fatigue experiment that is performed with the appropriate load ratio, frequency, and environment. These same corrosion-fatigue data are used to produce another valuable prediction—the extent of degradation relative to SCC. Additional experiments are run to determine K_{Iscc} for the same material and environment; these results are compared to the ripple-load results. The corrosion-fatigue experiments may be performed in a relatively short time compared to the direct ripple-load experiments. Since the method is based upon fracture mechanics, the prediction using simple laboratory specimens, is applicable to a variety of more complex geometric configurations for which fracture mechanics solutions exist to describe the stress state.

Figure 7 presents the data from a corrosion-fatigue experiment as a plot of crack growth rate per cycle da/dN as a function of the stress-intensity factor range ΔK_I, which is the driving force for cracking. (At the high load ratios considered here, $R \leq 0.9$, closure effects—which can reduce the effect of ΔK_I—are usually absent.) The lower end of the curve represents a threshold value of ΔK_I below which cracking does not occur. Figure 8 shows the maximum stress-intensity factor in a ripple-load cycle; this is related to the stress-intensity factor range by the load ratio

$$K_{max} = \Delta K_I/(1 - R), \qquad (1)$$

so that lowest value of K_{max} that produces cracking is given by substituting the threshold value of ΔK_I into Eq. (1). Comparing this value of K_{max} with K_{Iscc} describes the extent of degradation.

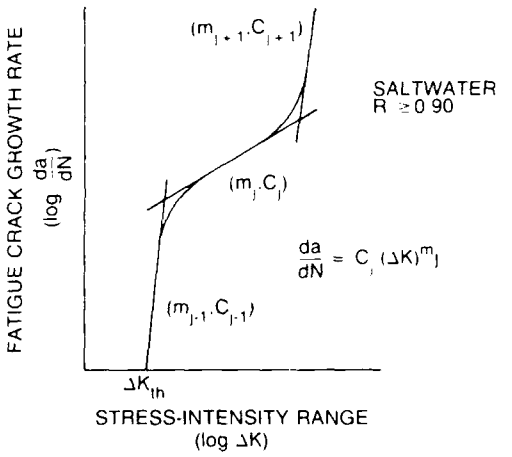

Fig. 7 – Typical appearance of corrosion-fatigue curve. Straight lines represent logarithmic fit used in ripple-load prediction

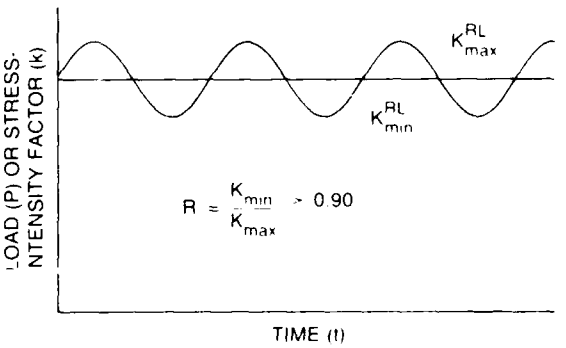

Fig. 8 – Load and stress-intensity factor as a function of time under ripple-load conditions $\Delta K = K_{max} - K_{min}$

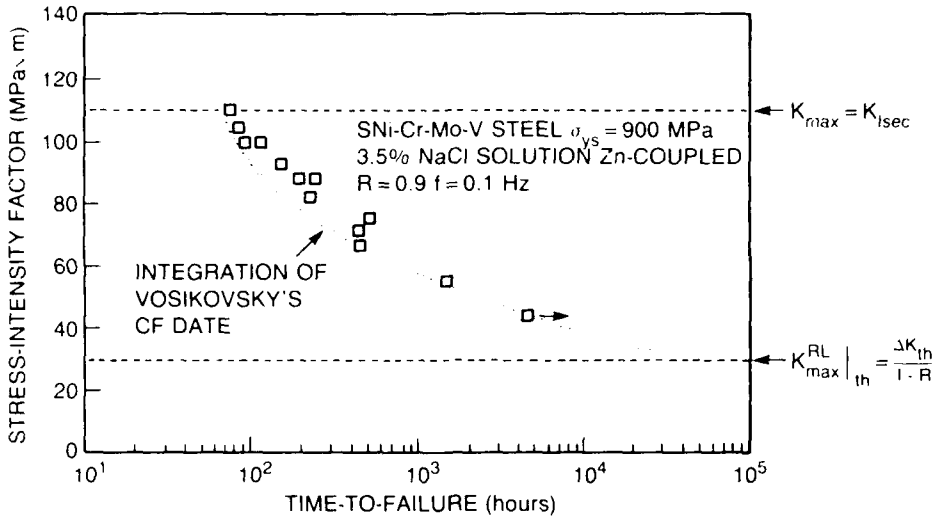

Fig. 9 – Prediction of ripple-load effect (dots) compared to results of the direct experiment (squares). Prediction indicates a lower threshold.

Calculation of the time-to-failure of a cracked structure involves integration of an appropriate portion of the corrosion fatigue curve. In practice, the integration is performed by simulating, in a computer program, the growth of a crack under ripple-load conditions. A starting crack size is assumed. For application to a structure, a good choice of starting crack size is a realistic estimate of the minimum flaw size detectable by nondestructive inspection. For this flaw size, the anticipated maximum applied load, and the geometry of the structure, a value of stress-intensity factor is calculated. The load is assumed to remain constant throughout the simulation. The crack *grows* an increment of length at the rate given by the corrosion-fatigue curve for the calculated value of ΔK_I. The time required for the crack to grow is calculated. Then a new ΔK_I is calculated, and the crack grows another increment for which the time required is calculated. The simulation continues until K_{max} exceeds the critical value for overload fracture. The sum of all the crack growth times is the predicted time-to-failure.

Results for Two Steels: Corrosion-fatigue data from NRL for a 175 ksi yield strength 4340 steel and data from Vosikovsky [3] for a 5Ni-Cr-Mo-V steel, both acquired at R = 0.9, were used to predict the extent of degradation. In the case of the 4340 steel, no degradation was predicted, which is in agreement with direct experiments performed at NRL.

Substantial degradation was predicted for the 5Ni-Cr-Mo-V steel, which also agrees with the results of the direct experiments. Vosikovsky's data were integrated to determine the time-to-failure for many values of load. The dotted curve in Fig. 9 shows the results of these integrations and their excellent agreement with the results [1] of the direct experiments. The direct experiments are nonconservative in that the prediction indicates that after longer times—which are impractical for direct experiments—cracking occurred at lower loads, with the lower limit being determined by the threshold value of ΔK_I. Greater resistance to SCC appears to increase the likelihood of ripple-load cracking in many situations in which the necessary combination of cyclic loading and aggressive environments are present for extended periods of time.

The predictive method described in this article may be applied to a wide variety of materials and environments. Work is underway at NRL to study the basic mechanisms responsible and to quantitatively determine the effect on materials used for construction of ships, aircraft, and offshore structures.

[Sponsored by ONR, NAVAIR, and the Minerals Management Service of the U.S.G.S.]

References

1. T.W. Crooker, J.A. Hauser II, and R.A. Bayles, "Ripple-Load Cracking Effects on Stress-Corrosion Cracking in Steels," Proceedings of Third International Conference on Environmental Degradation of Engineering Materials, M.R. Louthan and R.D. Sisson, Jr., eds. (The Pennsylvania State University Press, University Park, PA, 1987), pp. 521-532.

2. G.R. Yoder, P.S. Pao, and R.A. Bayles, "Theoretical Prediction of Ripple-Load Effect on Stress-Corrosion Cracking," NRL Memorandum Report 6215, May 1988.

3. O. Vosikovsky, "Frequency, Stress Ratio, and Potential Effects on Fatigue Crack Growth of HY130 Steel in Salt Water," *J. Testing and Evaluation* **6**(3), 175-182 (1978).

Reducing Wiring Fires in Naval Aircraft

F. J. Campbell
Condensed Matter and
Radiation Sciences Division

The Navy is experiencing severe aircraft utilization and maintenance problems caused in part by the extensive use of an aromatic polyimide insulated wire (M1L-W-81381) on its fleet of aircraft. The Naval Air Systems Command (NAVAIR) determined that the man-hours spent troubleshooting, repairing, and replacing faulty wiring represents a significant percentage of the yearly avionics maintenance hours. Electrical wiring failure reports have been increasing over the past 5 years, and as a result, NRL was asked to investigate the failure modes and effects of M1L-W-81381 wire and to provide guidance in the selection of replacement types of wire.

The insulating material of M1L-W-81381 wire is Kapton,* a polymer film of the aromatic polyimide class of organic materials selected initially for its light weight, small size, dielectric strength, and its ability to maintain mechanical strength at high operating temperatures. This wire has been used extensively in high-performance aircraft for the past 15 years. The chemical structure of this material is a repeating chain formed by the condensation polymerization of a diamine and a dianhydride; it appears as follows:

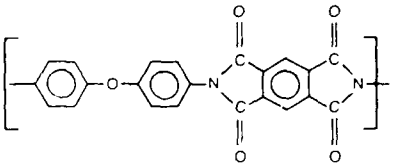

Background: Two major problems with this wiring have appeared in recent years. The most severe problem is the decomposition of Kapton by heat generated by the intense concentration of electric power during arcing. Arcing occurs when a wire is faulted as a result of chafing that produces a short circuit. As a result of the highly aromatic content of the polymer, it tends to pyrolyze into a charry, carbonaceous, graphite-like structure that is a very good conductor of electricity. Before the circuit breaker trips, the heat of the arcing in the initially faulted wire of a harness also pyrolyzes the insulation of adjacent wires to initiate other arcs. The destruction cascades in a short time to pyrolyze the insulation and melt the copper conductors of many wires in the harness. The temperature of an arc of this nature is about 5000°C, and the electrical power in the fault at that instant is about 8 to 10 kW.

Degradation by Reaction with Water: The second major problem with Kapton is its susceptibility to degradation by hydrolysis when exposed to the severe moisture environment encountered in naval service. This reaction reduces the polymer chain length and weakens the initially strong material to one that chafes and cracks readily. Flexing, such as occurs when wings are

*A registered trademark of the Dupont Company

folded and when wires are moved, causes the degraded insulation to crack, baring the conductor. Surface contamination on wires in harnesses caused by salt spray and fluids provides a conductive path between the bare conductors of damaged wires or between the bare conductors and the airframe. Electrical leakage first appears as scintillating arcs that gradually produce carbon tracks across the surfaces of the wires. After time, these become a solid graphite-like path that is highly conductive, and in an instant, a current surge occurs producing the firey arch across the shorted wires. This destructive arcing, as previously described, can sever many wires in a harness.

An Ongoing Program: The research challenges that we are now pursuing at NRL to help NAVAIR minimize the Kapton insulated wiring problems are divided into several programs. One program is dedicated to the development of a laboratory simulation of the arcing flashover phenomena of both chafing faults and wet-wire arc tracking. By using a 400 Hz, three-phase generator to produce aircraft-type electrical power, we evaluate and calculate the effects of circuit impedance changes on the power surges in arcs produced by chafing small wire harnesses. This equipment also serves as a means to evaluate the effects of arcing failures of new experimental insulation materials.

In another program, we are experimenting with methods to detect scintillating arcing in wire harnesses so that they may be replaced prior to catastrophic failure. In this study, we have demonstrated that both the electromagnetic radiation and the ultrasonic waves from electrical arcing can be detected and measured. When the electromagnetic interference from arcing occurs in the laboratory experimental circuitry, it can be readily distinguished from the background electrical noise. The next step is to determine if this measurement is also feasible on harnesses within an aircraft.

Applied Research with a Significant Payoff: The most challenging of these research programs deals with a determination of the chemical kinetics of the hydrolysis reaction that degrades the polymer, and consequently its physical properties, and leads to cracking and a lower resistance to chafing. Thus, by developing the equations for degradation rates under various service conditions of humid environments and physical stresses, we are progressing toward a method to integrate cumulative degradation as a function of time at various environmental and stress factors. Thus we will be able to determine when it is time to overhaul the wiring in a aircraft from its log of service history. Since it is both physically and financially impossible to replace Kapton in all the Navy's aircraft at once, this will permit scheduling to first overhaul those aircraft that are most probable to fail.

[Sponsored by NAVAIR and ONT]

Theory of High-Temperature Oxide Superconductors

W. E. Pickett, D. A. Papaconstantopoulos, and R. E. Cohen
Condensed Matter and Radiation Sciences Divison

The discovery of superconductivity above liquid-nitrogen temperatures in copper oxide materials has generated tremendous scientific excitement as well as technological expectations. The superconductivity results from the pairing of electrons and a subsequent condensation of these pairs into the superconducting state, but there is no consensus on the mechanism of pairing resulting in superconducting transition temperatures T_c up to 125 K (as of the end of 1988).

Since pairing represents an instability in the normal state (i.e., $T > T_c$), determination of the pairing mechanism requires an ability to describe the normal-state properties of these oxides. We

have been successful in describing a number of properties of the superconducting cuprates by use of first-principles calculations of their electronic structure.

Bonding and Electronic Structure: Calculations of the electronic charge density and the important characteristics of bonding have been carried out within a local density approximation for the many body interactions between electrons in the crystal. Clearly, the important interactions are dominated by antibonding combinations of Cu *d* and oxygen *p* states. The *d*–*p* band with lowest binding energy is half occupied, leading to the possibility of strong magnetic correlations and strong electron–phonon interaction, which may result in spin density waves or charge density waves, respectively. The primary feature of both the electronic structure in general and the charge density in particular is the unusual combination of ionic and metallic characters.

Cation Alloying and Oxygen Vacancies: Our tight-binding coherent-potential-approximation (TB-CPA) studies, based on accurate tight-binding representations of the electronic structure, indicate that cation alloying, e.g., replacement of 5% to 10% of the La in La_2CuO_4, with Ba, Sr, or Ca results [1] in an increase by a factor of two in the number of carriers allowed to participate in superconductivity. This prediction corresponds closely with the experimental observation of T_c rising from zero to above 40 K in this range of alloying.

Oxygen vacancies are often present in these ceramic cuprates; indeed the initial fabrication techniques relied on the rapid diffusion of oxygen into the samples at high temperature. This same TB-CPA theory, applied to random oxygen vacancies, predicts [1] a complex behavior in which electrons propagating through the lattice adjust their scattering to accommodate the vacant sites. The resulting shift in Fermi level is quite different from what simple, rigid band arguments would predict.

Ionic Model of Atomic Interactions: A parameter-free ionic model, which takes into account the spherical charge relaxation of the ions, has been found [2] to describe several structural properties of La_2CuO_4. The planar Cu–O breathing mode was predicted to be a high-frequency mode. The displacement corresponding to the tilt mode was found to be unstable, in agreement with detailed neutron scattering data.

Total Energy Frozen Phonon Studies: Both ionic effects and covalent interactions were taken into account by carrying out first-principles total energy calculations. Relaxing the structural parameters led to lattice constants and internal structural parameters in excellent agreement with experiment. By calculating the energy as a function of displacements of atoms, as shown in Fig. 10, several lattice vibrational frequencies were obtained, and in all cases the agreement was at least as good as has been obtained in much simpler materials using the same method. When the energy of the tilt mode (Fig. 10) was calculated vs the amplitude of displacement, it was found that not only was the instability obtained correctly, but the amplitude of the distortion is also predicted correctly. The evidence is clear that our total energy calculations are reliable for these materials.

Electrical Transport Studies: Describing the transport properties correctly requires a knowledge of the wave functions of the charge carriers, and this area presently involves considerable controversy. As a first step, we have supposed that band theory provides the proper eigenstates and that a standard, metallic Fermi liquid approach can be applied. This theory predicts [3] an unexpected anisotropy of the Hall coefficient in $YBa_2Cu_3O_7$, which has subsequently been verified experimentally, and leads to encouraging results in doped La_2CuO_4 as well. Unusual temperature dependences exist in transport coefficients that are not predicted by this approach, at least in the low order that has been carried through so far.

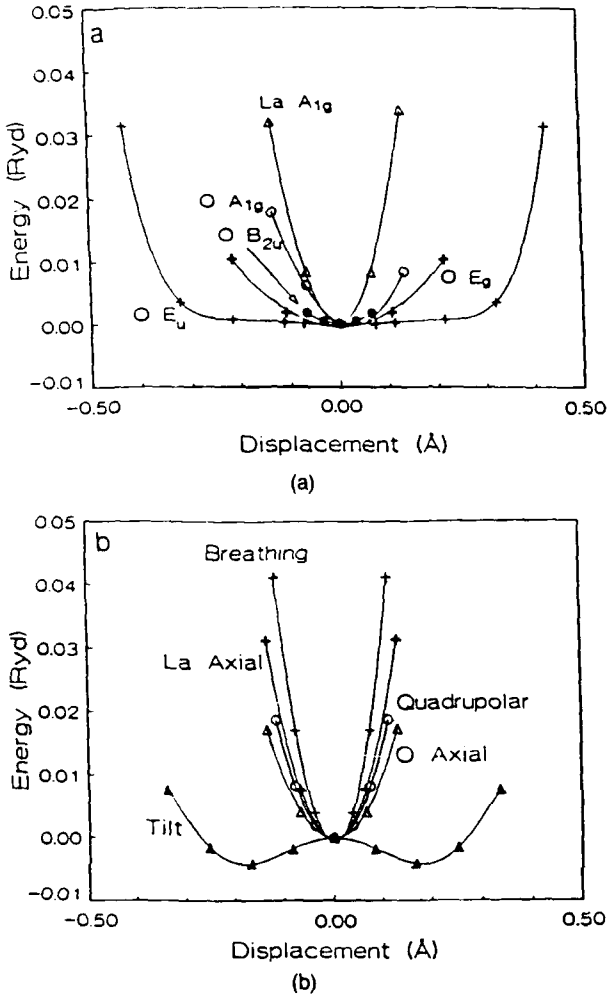

Fig. 10 — Calculated total energy vs amplitude and atomic displacements, for La_2CuO_4. (a) long-wavelength (zone center) modes involving La and O displacements. (b) short-wavelength (zone boundary) modes; downward curvature of the tilt mode around zero displacement indicates the tetragonal-to-orthorhombic instability.

These successes indicate that we have learned a great deal about what is necessary to describe the normal state properties of the novel high T_c superconductors. The future will not only involve improving on these theories, but applying the information to discern the pairing mechanism and the characteristics of the superconducting state in the cuprates. Collaborations with H. Krakauer (College of William and Mary), P. B. Allen (SUNY at Stony Brook), and with L. L. Boyer, B. M. Klein, and M. J. DeWeert in the Complex Systems Theory Branch have been central to this success.

[Sponsored by ONR and NRL]

References

1. D. A. Papaconstantopoulos, W. E. Pickett, and M. J. DeWeert, *Phys. Rev. Lett.* **61,** 211 (1988).
2. R. E. Cohen, W. E. Pickett, L. L. Boyer, and H. Krakauer, *Phys. Rev. Lett.* **60,** 817 (1988).
3. P.B. Allen, W.E. Pickett, and H. Krakauer, *Phys. Rev.* **B37,** 7482 (1988).

Growth of Superconducting Y-Ba-Cu-O Thin Films

P. R. Broussand and M. S. Osofsky
Materials Science and Technology Division

One of the most important applications for the new high-temperature superconductors will be use in electronic such as detectors, logic devices, interconnects, and mixers. Thin superconducting films deposited onto a passive substrate, a semiconducting device, or an intermediate buffer layer are a natural way to produce these devices. Factors such as film stoichiometry, crystalline orientation, homogeneity, surface smoothness, and substrate interaction impact on these applications and must be optimized.

Superconducting Properties: The best known characteristic of a superconductor is the absence of electrical resistance below the transition temperature (T_c). Another property of the superconducting state is its incompatibility with magnetism, that is, magnetic flux is expelled from a superconductor (the Meissner effect), and sufficiently large magnetic fields destroy superconductivity [1]. The self fields generated by large currents can drive superconductors into a state where they dissipate energy, i.e., have a finite resistance. This occurs at the so-called critical current density J_c that is a function of temperature and applied magnetic field. $J_c(T,H)$ is an important quantity for those technological applications where films must carry large currents.

Film Growth by Coevaporation: Thin films of the superconductor $Y_1Ba_2Cu_3O_x$ [2,3] are

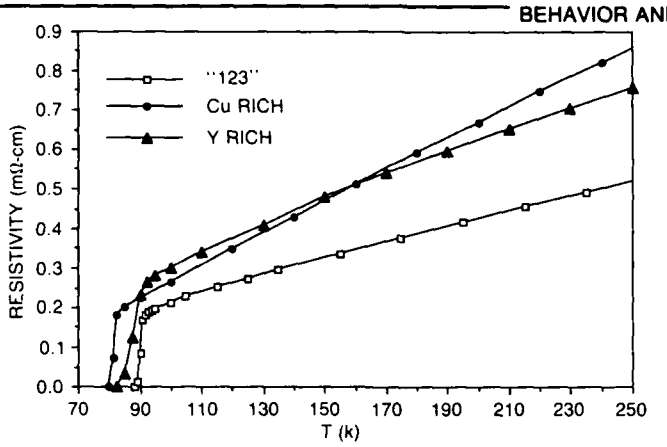

Fig. 11 — Resistivity vs temperature for three films of Y-Ba-Cu-O with different compositions grown on $SrTiO_3$

grown by first coevaporating Y and Cu metal and the insulator BaF_2 in the presence of oxygen. These materials are heated until the vapor pressure is sufficient to boil the material off onto a substrate. At this stage the films do not have the correct crystal structure or sufficient oxygen present to be superconducting. To achieve these conditions, we must anneal the films at 800° to 900°C with a flowing gas mixture of O_2 and H_2O, which decomposes the BaF_2 into BaO and then crystallizes the film. This is followed by a slow cool in dry oxygen, which allows the film to absorb the correct amount of oxygen to form the orthorhombic structure.

To measure the transition temperature of the film, we observe the temperature dependence of the electrical resistivity. Figure 11 shows the resistance trace for three samples on strontium titanate ($SrTiO_3$); one having the correct chemical composition (labeled "123"), one that is Y-rich, and one that is Cu-rich. The "123" film has a T_c of 88 K. The other films show the effect of compositions deviating from the ideal. For the Y-rich film, the T_c is now 85 K. For the Cu-rich film, however, the T_c is depressed to 80 K.

The next important parameter for thin films is the critical current and its dependence in a magnetic field. Such measurements for the sample labeled "123" in Fig. 11 show that this sample was able to carry $\approx 10^6$ A/cm^2 at 4.2 K in zero field without any measurable voltage. In an applied field of 9 T, this value was only reduced by a factor of 10. The other samples referenced in Fig. 11 have correspondingly lower critical currents, showing the importance of achieving the correct chemical composition.

Conclusions: We have shown the importance of chemical composition on the properties of these films, the critical temperature, and the critical current. We have produced films that carry useable current densities at 4.2 K in an applied field of 9 T.

Acknowledgments: The work presented here would never have been possible without the efforts of many people at the Naval Research Laboratory. This group includes J. H. Claassen, L. H. Allen, C. R. Gossett, W. T. Elam, E. Skelton, H. A. Hoff, and B. Bender.

[Sponsored by DARPA]

References

1. A.C. Rose-Innes and E.H. Rhoderick, "Introduction to Superconductivity," in *International Series in Solid State Physics*, (Pergamon Press, New York, 1978), Vol. 6.
2. M.K. Wu, J.R. Ashburn, C.J. Torng, P.H. Hor, R.L. Meng, L. Gao, Z.N. Huang, Y.Q. Wang, and C.W. Chu, *Phys. Rev. Lett.* **58**, 408 (1987).
3. R.J. Cava, B. Batlogg, R.B. van Dover, D.W. Murphy, S.A. Sunshine, T. Siegrist, J.P. Remeika, E.A. Rietman, S. Zahurak, and G.P. Espinosa, *Phys. Rev. Lett.* **58**, 1676 (1987).

CHEMICAL RESEARCH

Chemistry has played an important role in solving many of the Navy's problems relating to polymeric materials, coatings, fuels and combustion, synthesis of materials, firefighting, and surface chemistry; biomolecular engineering holds much promise. Reported in this chapter is work on protein crystalization, cluster science, diamond synthesis, structure–property relationships of a new polyurethane, and the growth of superconductor materials.

Contributing to this work are the Underwater Sound Reference Detachment (5900), the Laboratory for the Structure of Matter (6030), and the Chemistry (6100), Optical Sciences (6500), and Electronics Science and Technology Divisions (6800).

Other current research in chemistry includes:

- High-temperature composite matrix resins
- High T_c superconducting films
- Optical and electronic biosensors
- Fractal-structured soot agglomerates
- Shipboard fire research

Automated Preparation of Protein Single Crystals by Using Laboratory Robotics

W. M. Zuk, K. B. Ward, and M. A. Perozzo
Laboratory for Structure of Matter

A significant concern in the field of protein crystallography is the routine preparation of single crystals suitable for X-ray diffraction analysis. Crystallization techniques developed within the last three decades typically require accurate manipulation of microliter quantities of protein, buffer, and precipitating solutions. The accuracy and reproducibility necessary for such processes and the repetitiveness of the tasks make several of the crystallization methods particularly well suited for automation techniques. We have successfully automated the preparation of protein crystals by the *sandwiched drop* method, described below, using commercially available robotics equipment. The system incorporates a video monitoring station that permits automated inspection of individual crystallization droplets. Results obtained from the automatic monitoring of crystallization experiments will be used to redesign and prepare new experiments. The new experiments will in turn be carried out by the robotics system, thereby allowing a more fully automated system for crystallization.

Crystallization Methods: Several procedures have been developed for growing protein crystals, including the technique most commonly used, the vapor diffusion method [1]. Many procedures designed to grow protein crystals fundamentally involve trial and error and entail accurately and reproducibly mixing small volumes of highly purified protein solutions and solutions of precipitating agents, buffers, and other additives. Since the amount of available protein is often strictly limited, microliter quantities of these solutions must be used. To find optimum conditions for crystal growth, it is necessary to conduct numerous individual crystallization experiments.

We have recently designed an automated system that can be used to prepare protein crystals by using the *sandwiched drop* vapor diffusion technique [2]. Individual experiments are conducted in a single well of a crystallization plate, which contains 15 such wells. A drop (approximately 5 to 20 microliters in volume) containing protein solution, precipitating agents, and buffer is placed between two glass coverslips. The drop is placed to the side of, and close to, a reservoir containing about 0.5 ml of solutions of precipitating agents. The volatile component of the drop (usually water) diffuses from the drop into the reservoir until equilibrium is attained, during which time the droplet slowly becomes more concentrated in both precipitating agent and protein. Under suitable conditions, protein crystals may develop within the drop. Under other conditions, however, protein may precipitate from solution as an amorphous solid, a state that is not desired. To find the optimum conditions of crystal growth, hundreds or thousands of such experiments, each involving manipulations of very small volumes, must be arranged.

Automation of Crystallization Experiments: The automated crystallization system developed in our laboratory uses a Zymate Laboratory Automation system, made by Zymark Corporation, to emulate the manual procedures necessary to grow protein crystals. The Zymark laboratory robot consists of a single arm that operates in a cylindrical work envelope (Fig. 1) with four degrees of freedom (rotary, vertical, reach, and wrist). The Zymate robot performs all the functions required for arrangement of crystallization experiments, including mixing and dispensing of reservoir and droplet solutions, preparation of the crystallization plate, and manipulation of coverslips. These functions are accomplished by using customized hands. Figure 2 shows a syringe hand used for preparing droplets.

Once crystallization droplets have been prepared, they must be monitored periodically to determine the presence of protein crystals. We

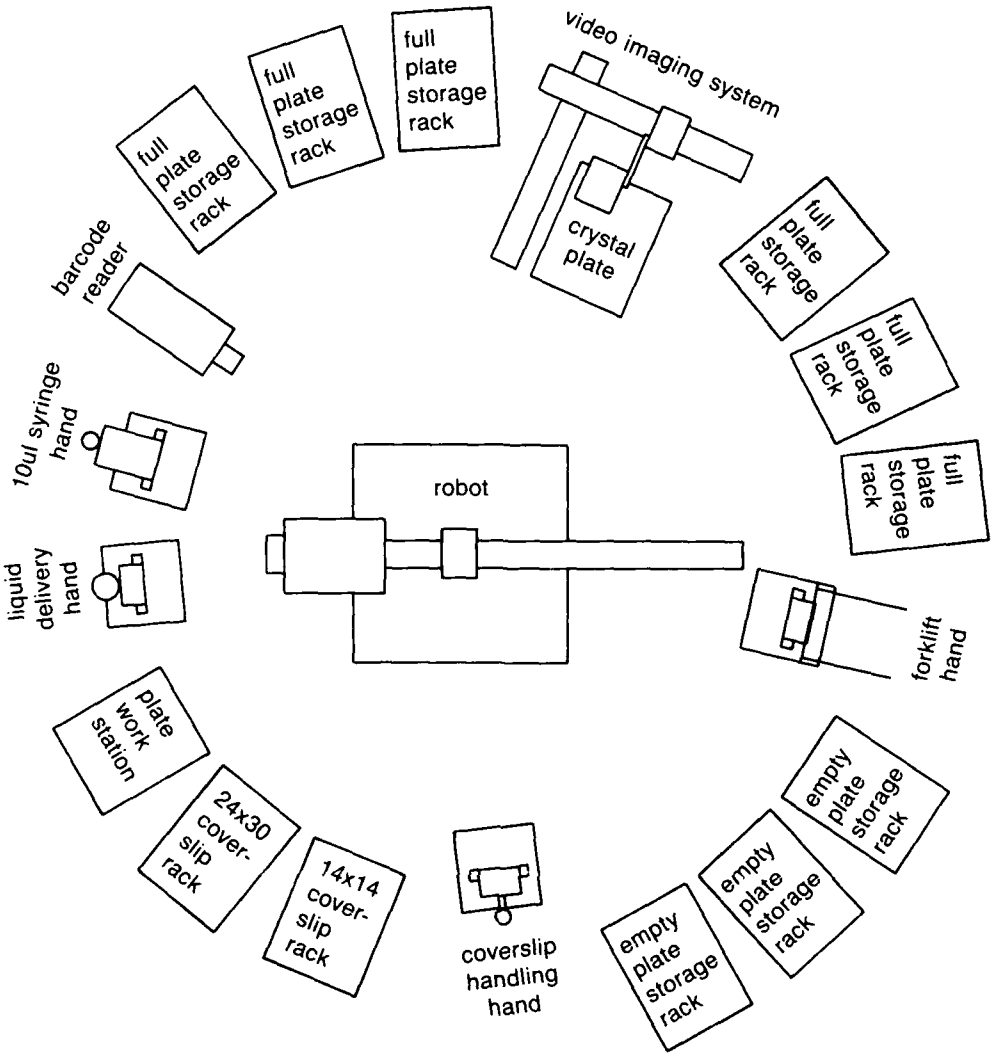

Fig. 1 — Configuration of robotics and image acquisition systems

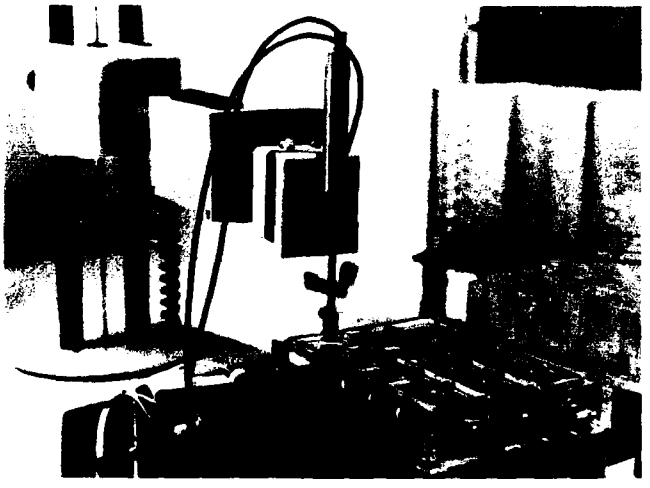

Fig. 2 — Syringe hand of the Zymate robot

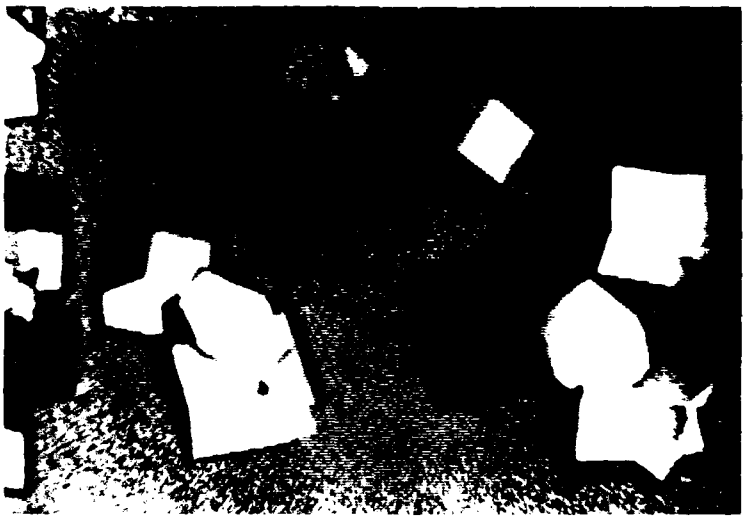

Fig. 3 — Digitized image of lysozyme crystals with the video acquisition system

have integrated an automatic video inspection station and image analysis system into the laboratory robotics system to more fully automate the crystallization procedures. Analog images of the crystallization droplets are obtained with a high-resolution monochrome video camera and are stored on an optical disc using a Panasonic TQ-2025F Optical Memory Disc Recorder. The analog images are subsequently retrieved and digitized by a PCVISION frame grabber installed in a Zenith Z-248 computer, which acts as the host for the entire robotics and imaging system. Figure 3 shows a typical digitized image. The digitized images are then processed and analyzed to determine the contents of each droplet. If solid material is found in the droplet, the host must decide whether the material is crystalline, amorphous, or a particulate impurity.

The goal of our efforts is to more fully automate the vapor diffusion method for protein crystallization. Integration of an automated image acquisition and analysis system into the existing laboratory robotics system allows the host computer to monitor the crystallization volume and then make necessary changes in such experimental conditions as the concentrations or pH values of the solutions. These experimental changes will then be carried out by the robot.

Automating protein crystallization experiments with laboratory robotics provides several advantages over manual methods. Liquid volume delivery is significantly more accurate with the robotics system, permitting routine and reproducible generation of experiments. Automation also permits an experimenter to prepare a greater number of experimental crystallization droplets over lengths of time than would be possible manually. Furthermore, an automated system allows experiments to be easily conducted in hostile environments or with toxic substances.

This work on automated preparation and visual inspection of crystallization experiments has led to our design of related systems that we are currently developing for microgravity experiments. These experiments are to be conducted aboard upcoming space shuttle flights and on the proposed space station.

William M. Zuk is an Office of Naval Technology Postdoctoral Fellow.

[Sponsored by USAMRIID and ONR]

References

1. A. McPherson, *Preparation and Analysis of Protein Crystals* (Wiley, New York, 1982).

2. K.B. Ward, M.A. Perozzo, and W.M. Zuk, "Crystal Growth of Biological Macromolecules," *J. Crystal Growth* **90**, 325-339 (1988).

New Chemicals from Cluster Science

B. I. Dunlap, A. P. Baronavski,
M. M. Ross, and S. W. McElvany
Chemistry Division

Production of Clusters: In the Chemistry Division at NRL and at many other laboratories throughout the world, new molecules with unique properties are being produced by laser or particle bombardment of single- or multielement solid materials. The particles that are ejected from the solid consist mostly of monatomic species, but a significant number of clusters are also formed. Although clusters may bridge the gap between isolated atoms and bulk materials in terms of chemical and physical properties, certain cluster structures exhibit enhanced stability or unusual characteristics. The objective of our work is to develop production and characterization methods and to investigate the potential applications of clusters in areas such as catalysis, electronic materials, composites, and microsensors.

Numerous experimental and theoretical techniques exist that can be used to probe the properties of clusters. These include mass spectrometry, laser spectroscopies, surface spectroscopies, and microscopy. Our studies have focused on production mechanisms, structures, and reactivities of gas-phase clusters by using mass spectrometric methods. The ultimate objective is to collect these unique species as bulk chemicals, although cluster sources presently available do not have the throughput necessary to accomplish this.

We produce clusters by laser vaporization or particle bombardment of solid samples, which are pellets consisting of one or more elemental powders. The distribution of the cluster ions formed depends on the sample and the production method, thus it can be used to provide information on the production mechanism. For example, direct laser vaporization of a graphite sample by using methods developed at NRL produces very large carbon cluster ions (greater than 200 atoms), whereas metal targets yield cluster ions with fewer than 10 atoms. In contrast, particle bombardment of metals yields much larger cluster species [1].

Properties of Clusters: The structures of clusters can be studied by collision-induced dissociation (CID) and chemical reactivity. The CID technique causes ions to break up into fragments, which can be related to the precursor structure. For example, dissociations of cluster ions of bismuth are governed by thermodynamic properties, such as differences in cluster ionization potentials and stabilities [2].

The reactivity of cluster ions is a sensitive probe of cluster structure because the reactivity depends on not only the size but also the geometry of the cluster. For instance, there is a dramatic decrease in the reactivity of carbon cluster ions, between the 9- and 10-atom clusters. This is attributed to a structural change from a linear to cyclic form. Detailed experiments on the 7-carbon atom cluster show than 70% of these clusters have a cyclic (unreactive) structure while the remaining 30% are reactive and presumed to be linear chains. This was the first unambiguous evidence of structural isomers of clusters [3].

The existence of isomers of small carbon clusters leads to the expectation of many isomers of the large carbon clusters. A great deal of experimental and theoretical work has focused on the 60-atom carbon cluster because of its unique postulated spherical structure (soccer ball, called Buckminsterfullerene) and observed anomalously high abundance. The enhanced stability of this cluster has been supported by electronic structure calculations done at NRL [4]. The lowest energy optical absorption features of this isomer are calculated to lie at approximately 2.9 and 3.1 eV, and a single absorption feature has been experimentally observed at 3.2 eV. This special

isomer is clearly an unfamiliar form of carbon. Soot and graphite absorb down into the far infrared, while diamond is transparent up to the vacuum ultraviolet. Furthermore, neither the characteristic diamond structure, nor the layered structure of graphite would suggest a spherical form of carbon molecules. The large carbon clusters (>30 atoms) are found to be unreactive with all reactants studied to date. Therefore we have no indication of the extent of isomerization or the shape of the most abundant single component of these large clusters.

Heteroclusters, those consisting of different elements, are also being studied. Many of these heteroclusters cannot be produced by conventional synthetic methods. We have focused on mixed-metal systems (e.g., BiSb and InAl) and metal-carbide clusters. Nonstoichiometric clusters, those species with elemental ratios different from that of the bulk (e.g., a cluster consisting of two tantalum atoms with 10 carbon atoms while the bulk ratio is 1:1) can be produced and characterized. Many different combinations of the components of heteroclusters exist that allow us to study many new species, some of which may have novel properties.

These studies have enhanced our understanding of the structures and reactivity of gas-phase clusters. Our next goal is to deposit mass-selected clusters on surfaces and into inert matrices for determination of the condensed phase properties; this will be the initial step in developing the capability to produce thin films with specific, desirable chemical properties.

[Sponsored by NRL and ONR]

References

1. S.W. McElvany, M.M. Ross, and A.P. Baronavski, *Anal. Inst.* **17,** 23 (1988).

2. M.M. Ross and S.W. McElvany, *J. Chem. Phys.* **89,** 4821 (1988).

3. S.W. McElvany, B.I. Dunlap, and A. O'Keefe, *J. Chem. Phys.* **86,** 715 (1987).

4. B.I. Dunlap, *Int. J. Quantum Chem.* **22,** 257 (1988).

Diamond Synthesis in Flames

L. M. Hanssen and K. A. Snail
Optical Sciences Division

J. E. Butler
Chemistry Division

Although diamond is well known for its hardness, it has many other superlative properties that give it great technological value. These properties include a thermal conductivity five times that of copper, optical transparency from the ultraviolet to the far infrared, a frictional coefficient near that of Teflon, and high tolerance to radiation exposure. Many applications are envisioned for diamonds synthesized in flames and low-pressure processes. These include: high-speed, high-temperature electronic devices; low-cost abrasive grit; infrared domes and coatings; heat sinks for integrated electronics; X-ray windows; and tool coatings.

Previous Diamond Research: The first reproducible synthesis of diamond at very high temperatures and pressures (50,000 atm) occurred at General Electric during the late 1950s. At the same time, a low-pressure technique was discovered at Union Carbide, however the growth rate and cost of this process rendered it commercially unviable. In the 1970s and 1980s, a series of breakthroughs by Soviet and Japanese researchers increased the growth rates of the low-pressure (0.01 to 0.1 atm) technique into the 1 to 10 μm/h range. The improvements included the use of hot filaments, RF coils, and microwave cavities to activate mixtures of hydrocarbon, oxygen, and hydrogen gases. Substrate temperatures were typically in the 700° to 1100°C range. In 1988, researchers at Fujitsu demonstrated a plasma-jet process operated at high temperatures (3000°C) and flow rates that yielded diamond growth rates over 200 μm/h.

Fig. 4 — Close-up of oxygen-acetylene torch deposition of diamond. The silicon sample is situated in the acetylene feather region of the flame.

Fig. 5 — Scanning electron photomicrograph of a continuous film of diamond crystallines deposited with an oxygen-acetylene torch. The magnification and scale (dotted bar) are shown below the photo.

Flame Synthesis of Diamond: In March 1988, Y. Hirose at the Nippon Institute of Technology in Tokyo reported the synthesis of diamond in an oxygen-acetylene flame, without revealing many details of the experiment. From NRL's experience with the hot-filament technique, it was felt that cooling the substrate into the 700° to 1100°C range would be critical to achieving diamond growth in a flame. Thus a water-cooled substrate mount was built and a two-color optical pyrometer (insensitive to the flame's emissions) was used to monitor the substrate temperature. Experiments with an oxygen-acetylene brazing torch (see Fig. 4) then began. NRL confirmed that diamond could be synthesized in an oxygen-acetylene flame. The diamond crystallites were analyzed with an optical microscope, a Raman spectrometer, a scanning electron microscope (see Fig. 5), and an X-ray diffractometer (with Dr. E. Skelton, from the Condensed Matter and Radiation Sciences Division).

Further experiments determined the range of parameters over which diamond could be grown. It was found that diamond could only be synthesized in an acetylene-rich flame and that growth only occurred in the inner acetylene feather region of the flame. It was also determined that substrate temperatures from 650° to 1150°C and oxygen-acetylene gas flow ratios of 0.9 to 1.2 are required [1]. Diamond can be grown on a variety of materials including silicon, copper, molybdenum, titanium carbide, and boron nitride [1], as well as in flames of oxygen-ethylene, oxygen-ethane, and oxygen-acetylene-hydrogen [2]. We have shown that the addition of hydrogen to an oxygen-acetylene flame improves the quality of deposited diamond, as measured by Raman spectroscopy.

In summary, we have investigated and defined the range of operational parameters associated with diamond growth in oxygen-acetylene flames. Growth rates exceeding 100 μm/h and single crystals larger than 300μm have been achieved. The low cost and high growth rates associated with this technique may lead to improved abrasive grit manufacturing techniques, tool coatings, and other diamond products. Future efforts will be directed toward identifying the chemical species and surface processes responsible for diamond growth.

This work was performed in collaboration with Mr. William Carrington of the University of Virginia and Dr. Davis B. Oakes, an ONT Postdoctoral Fellow.

[Sponsored by ONR]

References

1. L. M. Hanssen, W. A. Carrington, J. E. Butler, and K. A. Snail, "Diamond Synthesis Using an Oxygen-Acetylene Torch," *Mater. Lett.* **7**, 289 (1988).

2. K. A. Snail, L. M. Hanssen, W. A. Carrington, D. B. Oakes, and J. E. Butler, "Diamond Growth in Combustion Flames," Proceedings of the 1st International Conference on the New Diamond Science and Technology, Tokyo, Oct. 24-26, 1988, p. 142.

Investigation of the Structure-Property Relationships in Polyurethanes Based on Tetramethyl Xylene Diisocyanate

G. M. Stack and R. N. Capps
Underwater Sound Reference Detachment

Polyurethanes are block copolymers that are typically made by first reacting diisocyanate molecules with a high molecular weight polyol to form a prepolymer terminated with reactive isocyanate groups. Diamines or dialcohols are then used to cure this castable intermediate into a high molecular weight elastomer. Changes in the composition of the formulation components give large variations in the properties of the cured elastomer, which makes polyurethanes promising materials for underwater acoustic applications where specific dynamic mechanical properties are required.

To design polyurethanes with specific acoustic properties, it is necessary to understand the effects of compositional parameters on the dynamic mechanical behavior of the resultant polyurethane. To this end, a series of model polyurethane compounds based upon tetramethyl xylene diisocyanate (TMXDI) have been prepared. The diisocyanate exists in two structural forms, a meta and a para isomer. This aliphatic isocyanate forms linear, segmented polyurethanes and is ideal for studies of structural isomerism, phase segregation, and hydrogen bonding in polyurethanes. A series of model polyurethane compounds based on the two isomers of TMXDI was prepared. The compositional parameters varied included isocyanate content, type of curative, and cure stoichiometry. Also, the polyurethanes contained soft segments based on a nonpolar polyether, hydroxy-terminated polybutadiene (HTPBD), or the polar polyester, polycaprolactone (PCL). Characterization techniques used included dynamic mechanical spectroscopy, tensile and tear testing, differential scanning calorimetry (DSC), and Fourier transform infrared spectroscopy (FTIR).

Dynamic Mechanical Behavior: The first polyurethanes studied were based upon PCL, m-TMXDI, and a diamine curative, diethyltoluenediamine (DETDA). Little effect on dynamic mechanical properties was observed when the amount of DETDA was varied. Increasing the isocyanate content caused a significant increase in the frequency-dependent Young's storage modulus, as shown in Fig. 6. In the cured polyurethane, the urethane portions of the chains will phase separate into regions of greater order known as hard segment phases. These provide mechanical reinforcement similar to carbon black in compounded rubbers. Increasing the isocyanate content increases the amount of hard segments and causes the observed higher modulus. Conversely, the loss tangent was lowered (cf. Fig. 6). The major loss mechanisms lie in the soft segments, and increasing the hard segment concentration decreases the relative amount of soft segment available to contribute to the loss tangent.

For polyurethanes of the same composition based on the meta and para isomers of TMXDI,

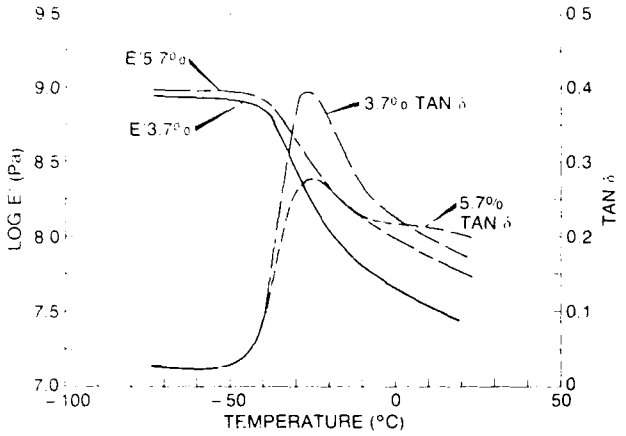

Fig. 6 — Effect of isocyanate content on dynamic Young's modulus (E' is storage Young's modulus) and the loss tangent (tan δ) at 1 Hz of PCL and m-TMXDI based polyurethanes cured with DETDA

respectively, the para isomer gave a higher Young's storage modulus and a lower loss tangent. This is attributed to the fact that the para isomer forms more ordered hard segments, resulting in greater phase segregation between the hard and soft segments. This conclusion is supported by DSC measurements.

Use of the polar PCL soft segment, in contrast to the nonpolar HTPBD, gave polyurethanes with much more phase mixing between hard and soft segments. This was observed in both DSC and dynamic mechanical spectroscopy experiments, which showed that the observed low-temperature, soft-block glass transition was shifted upward and broadened in the PCL-based material. These results, in conjunction with those discussed earlier, indicate that changes in dynamic mechanical behavior can be explained in terms of the stucture of the polyurethane. This suggests that the polyurethanes can be tailored to give specific acoustic properties for a given application.

Annealing Experiments: It was initially thought that use of the symmetric para isomer of TMXDI would result in the formation of crystalline hard segments. This was found not to be the case when DETDA was used as a curative. Use of the symmetric dialcohol, butanediol, resulted in the formation of actual crystalline hard segments, as revealed by high-temperature DSC melting peaks. It was found that annealing these polyurethanes at temperatures from 100° to 180°C, resulted in an increase of over 40° in the DSC peak melting point (Fig. 7). Low-temperature DSC scans were later made on these annealed samples. No significant change in the low-temperature glass transition point existed. This indicates that no significant change in phase segregation occurred in these polyurethanes.

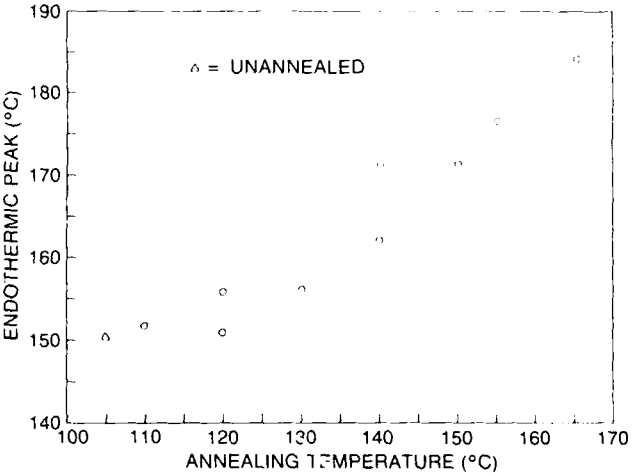

Fig. 7 — Effect of annealing temperature on high-temperature melting peak of PCL-p-TMXDI-butanediol polyurethane

FTIR spectra indicated differences in the type and extent of hydrogen bonding in these materials, as compared to polyurethanes synthesized from DETDA and/or the meta isomer. Experiments are in progress to clarify whether the observed thermal behavior is due solely to morphological changes or if hydrogen bonding plays a role.

Dr. Eugene Chang of the American Cyanamid Company made significant contributions to this research.

[Sponsored by ONR]

Bibliography

E.Y. Chang and R. Saxon, "Novel Cast Polyurethane Elastomers Based on p-TMXDI, An Aliphatic Diisocyanate," *Elastomerics* **117**(6), 18-24 (1985).

R.N. Capps, G.M. Stack, E.M. Dodd, and E.Y. Chang, "Relationship Between Polyurethane Composition and Viscoelastic Properties of Model Urethane Systems," presented at the 114th Meeting of the Acoustical Society of America, Miami, FL, Nov. 1987.

Growth of Superconductor Materials by Spray Pyrolysis

R. L. Henry, E. J. Cukauskas, and A. H. Singer
Electronics Science and Technology Division

Reproducible growth of high-quality oxide superconducting films is a goal that is important for many potential applications of the high-transition temperature (T_c) superconductor materials. Spray pyrolysis of aqueous nitrate solutions enables good reproducibility of a homogeneous composition from film to film. One of the advantages of spray pyrolysis for film growth is that desired concentrations of dopants can be incorporated simply by adding the nitrate of the dopant as either a substitution for, or in addition to, the component nitrates when preparing the aqueous solution. This is a relatively simple and reproducible procedure for incorporating dopants into films. In this article we report the preparation and properties of Y-Ba-Cu-oxide:Ag composite films formed by spray pyrolysis of aqueous nitrate solutions.

Sample Preparation: The solutions used for growth of the Y-Ba-Cu-oxide films are made by dissolving yttrium oxide, barium carbonate, and cupric oxide in dilute nitric acid such that the solution is equivalent to having dissolved 0.05 mole of the Y-Ba-Cu-oxide per liter. Quantities of silver nitrate are added to yield from 0.02 to 0.05 molar solutions. These solutions are sprayed onto a heated MgO substrate, using oxygen as the propellant gas, then transferred to a tubular furnace and annealed under flowing oxygen for 10 min at 960°C.

Characterization and Discussion: X-ray diffraction patterns for Y-Ba-Cu-O:Ag composite films on MgO show that the (001) reflections are by far the most predominant reflections with the other reflections for Y-Ba-Cu-O having relatively low intensity. The presence of silver in the film increases the tendency for preferential orientation. Although preferential orientation has been occasionally observed in our other Y-Ba-Cu-O films, the relative changes in intensity of the (001) peaks relative to all others has not been as consistent nor as extensive prior to the addition of silver.

Figure 8 is a scanning electron micrograph (SEM) showing an edge view of a Y-Ba-Cu-O:Ag film at the cleaved substrate. The addition of silver results in a film that contains fewer voids and adheres better to the substrate. One possible reason for the increased uniformity and density of the silver-containing films is that the silver, which was initially dispersed throughout the film, diffused and coalesced at the grain boundaries upon annealing. The diffusion of silver from and through Y-Ba-Cu-O grains may aid in the fusion of the individual grains into a more uniform material containing fewer voids. The morphology and the preferential orientation exhibited by the silver-containing films suggest that a liquid may have been present during the annealing, possibly as a result of partial melting or dissolution of Y-Ba-Cu-O in molten silver.

Figure 9 shows a plot of resistance vs temperature for a film of Y-Ba-Cu-O:Ag on MgO. The superconducting T_c for this film is 85 K with a transition width of 3 K. The values of T_c for films without silver are slightly lower at 74 K. An initial measurement of the critical current density at 4.2 K shows a value of approximately 1000 A/cm^2. Studies are under way to investigate the critical current density dependence on the concentration of silver and other slight changes in the stoichiometry.

[Sponsored by ONR]

Fig 8 — SEM showing an edge view of a Y–Ba–Cu–O:Ag film

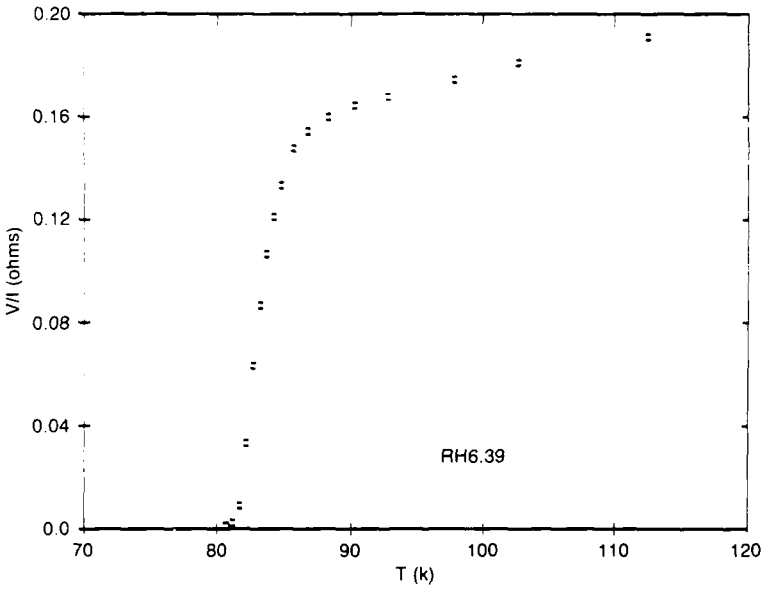

Fig. 9 — Plot of resistance vs temperature for Y–Ba–Cu–O:Ag/MgO

ELECTROMAGNETIC SYSTEMS AND SENSING

Radar commands an important position as a major sensor and detection system for the Navy, and radar research continuously focuses on advanced sensor concepts to upgrade this technology. Electromagnetic radiation is also used for applications in the areas of countermeasures, signal simulation, jamming, and decoys. Reported in this chapter is work on HF radar calibration, unmanned research aircraft (moving platform), electromagnetic wave reflection and scattering, X-band clutter radar, space-borne radar imagery, and an underwater communications link.

This work was performed by the Acoustics Division (5100), the Radar Division (5300), and the Tactical Electronic Warfare Division (5700).

Other current research in electromagnetic systems and sensing includes:

- Radar sea scatter measurements
- Reduction of radar electromagnetic interference
- Doppler frequency estimation
- Monopulse radar simulation

Development of the Low Altitude/Airspeed Unmanned Research Aircraft (LAURA)

R. J. Foch and P. L. Toot
Tactical Electronic Warfare Division

Introduction: The Low Altitude/Airspeed Unmanned Research Aircraft (LAURA) is being developed to address operational requirements of small unmanned air vehicles (UAVs) for Fleet EW missions [1]. LAURA is a remotely controlled, highly instrumented test-bed aircraft. The modular fuselage was designed to accept the installation of several wing/tail combinations having various airfoils. Flight test research involving low Reynolds number (LRN) airfoils is critical for the development of high-performance, unmanned EW aircraft. Additional requirements for a Navy UAV that drive research include long flight endurance while flying at shiplike speeds, flying in a gusting wind, and storage in a low-volume canister as protection against the saltwater spray environment prior to shipboard launch. The LAURA will ultimately provide inflight measurements of airplane characteristics and performance under realistic environmental conditions. Correlation will then be possible between LRN theory, wind tunnel measurements, and flight test data, thus greatly enhancing our ability to design and develop advanced performance UAVs for Navy EW missions.

LAURA Preliminary Design: The LAURA fuselage carries the flight data system, command control system, power plant, and landing gear. An 18 to 20 kg gross vehicle weight range was selected to allow the use of an *off-the-shelf* 3 hp internal combustion engine developed for radio-controlled model aircraft use. Based on a weight estimate of 12 kg for the fuselage and subsystems, the wing/tail combination was limited to 8 kg. Performance specifications include a 13 to 28 m/s speed range and a rate of climb of 2 m/s.

Wing/Tail Configuration Descriptions: Figure 1 shows the four distinct wing/tail configurations that emerged as candidates for the LAURA program; the hinged wing, joined wing, three surface, and tandem wing.

The hinged wing (Fig. 1(a)) consists of a monoplane wing that is capable of folding the outer tip panels. When folded, the wing has approximately 60% of the wing area of the unfolded planform. The wing is deployed purely aerodynamically by use of a trailing edge control surface. This simple and lightweight system may have several applications for both unmanned and manned aircraft.

The joined wing (Fig. 1(b)) is fundamentally a very high aspect ratio, swept flying wing. Additional stiffness is obtained from the attachment of the rear wing, which acts as a stabilizer, lift strut, and trim surface. The resulting configuration achieves lower structural weight for a given strength and stiffness. The joined wing can be packaged in the least volume of the four candidates and has high resistance to loads applied during catapult launch.

The three surface (Fig. 1(c)) uses an advanced, laminar flow LRN airfoil developed by NASA Langley specifically for the LAURA program. High performance is obtained by using the airfoil and wing planform, which was designed to have a large reduction in section drag coefficient compared to other LRN airfoils.

The tandem wing configuration uses the technology developed by NRL during the Long Duration Expendable Decoy (LODED) program. For stability requirements, the forward wing develops most of the aircraft's lift and thus has the highest aspect ratio to minimize induced drag (drag owing to lift). The rear wing has a relatively low aspect ratio and lightweight structure for weight and balance considerations. Directional stability is achieved by NASA/Whitcomb winglets at the rear wing tips, which provide stability without a reduction in performance.

Wind Tunnel Testing: All four configurations showed maximum lift/drag (L/D) values greater than 20/1, much higher than the 7/1

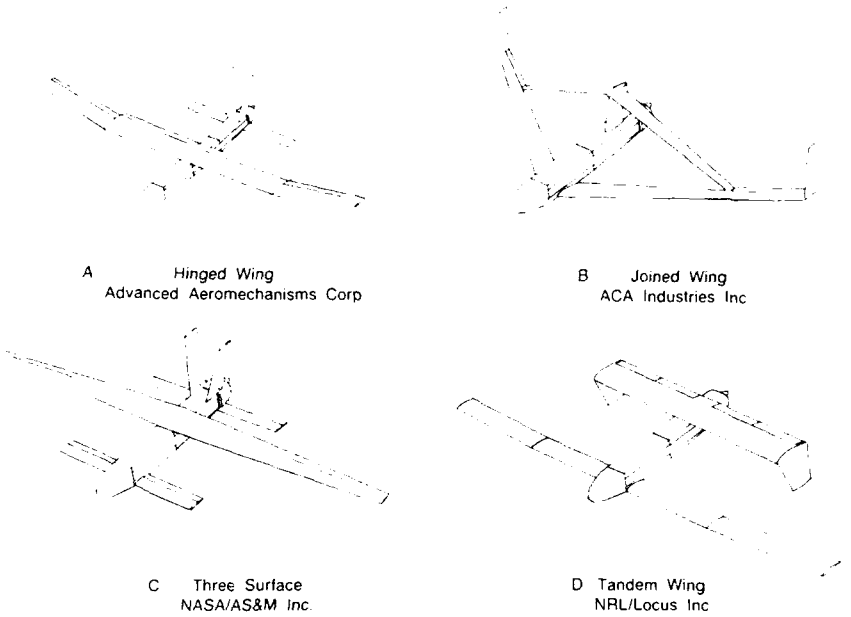

Fig. 1 — LAURA vehicle configurations

to 10/1 values currently achieved by military UAVs that operate at LRN flight conditions. The tandem wing offered a wider speed range at best endurance, which may be representative of more stable performance in areas of changing velocity, such as wind gusts.

The simultaneous development and testing of four distinctly different aircraft configurations designed to one specification provided direct comparisons of their aerodynamic qualities under matching experimental conditions. Interestingly, despite a wide range of design features, each configuration was able to meet the performance specifications—indicating that configuration played a more dominant role in stability and control, structures, and packaging than did aerodynamic performance. Each design surpassed the original velocity range specification of 13 to 28 m/s by achieving even slower speeds, which could significantly enhance their EW mission effectiveness. All four configurations showed significant aerodynamic performance improvement over previous Navy UAV designs. These improvements can be attributed to the use of airfoils that operate efficiently in the LRN range; high aspect ratio wings, now possible by applying state-of-the-art structures; and a design methodology that exploits LRN effects.

[Sponsored by ONR]

Reference

1. R.J. Foch and R.E. Wyatt, "Low Altitude/Airspeed Unmanned Research Aircraft (LAURA) Preliminary Development," Aerodynamics at Low Reynolds Numbers, Proceedings, Volume III, The Royal Aeronautical Society, London, Oct. 1986.

HF Radar Calibration Through Land-Sea Boundaries

B. T. Root
Radar Division

The ionosphere reflects electromagnetic radiation in the HF spectrum (3 to 30 MHz). Thus it can act as a mirror at these frequencies and enable us to *see* far beyond the horizon, something no other radar can do. However, uncertainties concerning the characteristics of the ionosphere cause uncertainties in our interpretation of the

radar returns. In particular, we cannot directly read the ground range of targets, but must resort to a guess, an approximation, or a deduction based on laborious analysis of the data. The identification of known land-sea boundaries in the data offers a relatively easy way of calibrating the radar for ground range. We performed an experiment, in cooperation with other scientists from the United States and from the United Kingdom, to investigate the practicality, accuracy, and reliability of this idea.

The equipment used in this experiment consisted of an experimental ionospheric sounder with a 10-kW HF transmitter, a small, steered, filled-array receiving antenna; an automated *frequency management system* to aid in frequency selection; and a data collection system. Therefore, results and conclusions from this experiment represent a lower bound on the capability of an actual operational radar system.

Signal Processing: Land and sea are discriminated in the sounder data through Doppler analysis. It is well known that radiation is shifted in frequency when reflected from a moving target. This effect is called Doppler shift. Now the ocean surface can be analyzed into water waves of many different wavelengths. Those water waves, whose length has a certain simple relationship to the wavelength of the incident electromagnetic energy, reflect that energy. (This is similar to Bragg reflection in crystals; the water wavelength—i.e., the separation between the peaks of the water waves—corresponds to the separation of the atoms in the crystal.) This reflected energy is Doppler shifted because of the radial velocity of the reflecting water waves. (The water waves always have a known velocity, because of the relationship between water wavelength and phase velocity for gravity waves on deep water.) In brief, the sea surface reflects the transmitted energy with a Doppler shift, and the stationary land reflects the energy without a Doppler shift. In this way, we can discriminate between land and sea.

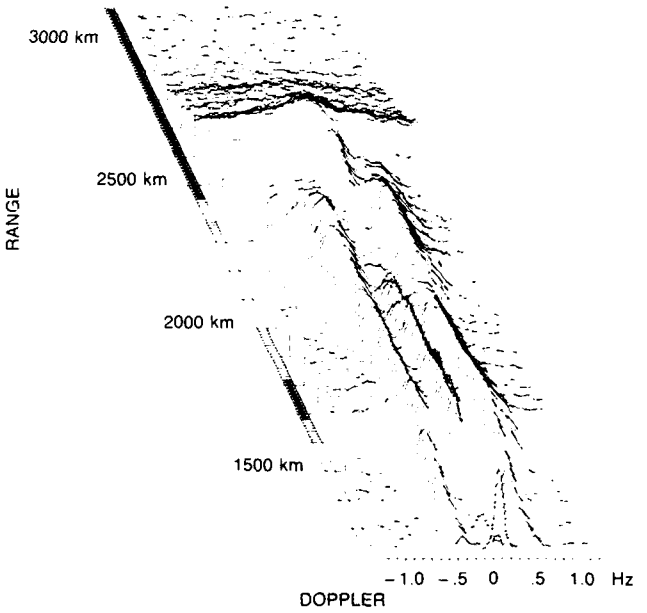

Fig. 2 — An amplitude–range–Doppler map showing Iceland and southern Greenland

To process the sounder data and extract the Doppler information, we must use Fourier analysis to transform the data to the frequency domain. This is accomplished by computer with the use of the fast Fourier transform (FFT). Figure 2 shows the result displayed on an amplitude-range-Doppler (ARD) map. This is a simulated, three-dimensional plot. The horizontal or x axis gives the Doppler frequency shift. The receding or y axis gives an approximation to ground range. We cannot measure ground range directly, but instead measure *slant* range, which is the distance that the energy would have traveled in free space. We obtain this quantity simply by multiplying the time delay of the reflected signal by the speed of light in free space. Since the rays of the propagated beam are nearly horizontal, and since they are only briefly in the ionosphere, the slant range of the various targets is close to ground range. To give a crude approximation to ground range, we simply subtract 150 km from slant range. Our experiment essentially consisted of determining the further small correction necessary to accurately calibrate for ground range. Finally the vertical or z axis (not shown on the figure) corresponds to the power amplitude of the return signal. We expect to see

sharp peaks at zero Doppler frequency where there is land and at plus and minus the Bragg frequency where there is sea. (The thin bar along the left-hand side of the map gives the ground range of land and sea for comparison with the radar returns. The dark part represents land, the light part sea, and the gray part a mixture of land and sea. To avoid confusion, remember that the range axis means slant range minus 150 km for the radar data and ground range for the geographical bar.)

A Particular Case (Denmark Strait): We are looking at a geographical area corresponding to the box labeled by the number 2 in Fig. 2. This area covers Iceland, the Denmark Strait, and the southern coast of Greenland, thus providing us with three land-sea boundaries. The geographical bar on the ARD map (Fig. 2), is based on this box. If we look at the ARD map we clearly see long tracks of sea and land peaks, and comparison with the geographical bar shows that they are at the right locations. There is one long land track at 0 Hz on the Doppler axis extending from about 1500 to about 2000 km, which is where Iceland should be. (The southern coast of Iceland is at 1600 km ground range. So we see that we must add 100 km to our original subtraction of 150 km, to give a total correction of minus 50 km.) The land track resumes at about 2300 km, which is the southern coast of Greenland. A pair of sea tracks symmetrically placed in Doppler with respect to the land tracks runs up and down the map. (There is sea where Iceland is located because of the relative broadness of the beamwidth of our small experimental sounder. The width of the box on Fig. 3 is based on the 3 dB points of the beam. Also, there may be a tilt in the reflecting layer of the ionosphere causing the beam to deflect to the west.) Note that there is a slight positive bias to the Doppler frequencies of the tracks because of the motion of the ionosphere.

We locate a coast by setting a threshold for the amplitude of the land peaks with respect to the sea peaks. For instance, if the threshold is 0 dB, then the coast is simply the (corrected) slant range at

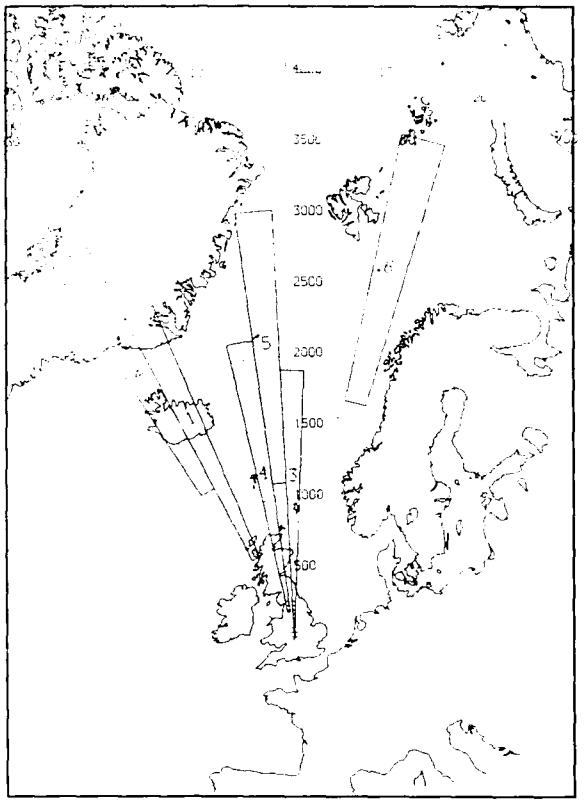

Fig. 3 — Sounder coverage areas, range in kilometers, azimuth in degrees

which the land peaks rise above the sea peaks. We then compare this range with the true ground range of the coast and thus calibrate the system. Usually, the 0 dB threshold works well. We have developed a computer algorithm to automatically select the *best* threshold, and it seems to work will if the data are of decent quality.

We collected 7 days of data, spread over the months of March, April, May, and August, 1988. About 7 hours of data were collected per day. The basic conclusion of our experiment was that the land-sea boundaries could be clearly discriminated most of the daytime, at least at ranges less than about 2500 km, provided that the operating frequency was *reasonably well chosen*. Frequency management, or the proper selection of operating frequency, is one of the main difficulties of HF radar operation, owing to the variability and unpredictability of the ionosphere. Occasionally the ionosphere is too turbulent to provide useful returns, but this is far less of a problem than

incorrect frequency management. At ranges longer than 2500 km, the data were generally poor; this was probably due to magnetic auroral activity characteristic of these northern latitudes.

[Sponsored by USAF]

Physical Optics and Plane-Stratified Anisotropic Media

H. J. Bilow
Radar Division

Introduction: The physical optics technique is an approximation frequently used to determine the electromagnetic scattering cross section of perfectly conducting bodies. The technique applies to bodies that can be decomposed into sections that are large and smooth, i.e., into sections whose dimensions and radii of curvature are both very large in comparison to the wavelength of interest. The technique approximates the currents induced at each point on the scattering body by the incident wave with the currents that would be induced on an infinite, perfectly conducting plane tangent to the body at each point of interest (but with the scattering body absent). The technique is especially efficient to apply if the scattering body can be decomposed into planar sections.

We desire to be able to extend the physical optics technique to allow scattering cross section predictions to be made for coated, perfectly conducting bodies as well as uncoated ones; coatings of anisotropic materials are of particular interest. The following describes the work done to allow a physical optics treatment of bodies composed of large, planar, perfectly conducting sections with multilayer coatings. Each layer of a coating is taken to be uniform in both thickness and electrical properties; the latter may be anisotropic.

Problem Description: Figure 4 illustrates the problem that needs to be solved to apply physical optics to a body composed of coated planar sections. We have a monochromatic plane wave of a given frequency and incidence direction impinging on an infinite planar structure composed of N uniform layers, and we wish to compute the reflected wave. Parameters $\bar{\bar{\epsilon}}_n$, $\bar{\bar{\mu}}_n$, and t_n are the permittivity tensor, the permeability tensor, and the thickness, respectively, of the nth layer; the region $z > 0$ is taken to be free space. At $z = z_N$, the bottom of the Nth layer, the surface impedance (the relation between the tangental E and H fields) is characterized by a four-component tensor $\bar{\bar{\eta}}_N$ (equivalent to a 2×2 matrix). This impedance tensor is a function of wave vector components k_x, k_y, and is assumed known a priori. For a perfect conductor the components of the impedance tensor are all zero.

Solution Procedure: The first step in solving the problem is to determine the propagation modes that can exist in the various layers. Once we have found these modes we can use a matching procedure is determine the impedance tensor for the top surface of a layer in terms of the layer impedance tensor at the bottom surface. By starting at the lowest layer, where the impedance tensor at the bottom surface is specified a priori, we proceed upward layer by layer to ultimately determine the impedance tensor at $z > 0$. Knowledge of the impedance tensor allows us to calculate a reflection tensor for the layered structure, and hence to determine the reflected wave. The procedure is analogous to finding the impedance by looking into a set of transmission lines of various lengths and characteristic impedances connected in series and terminated by a known impedance.

After the reflected wave has been determined, we compute the equivalent electric and magnetic surface currents that would produce a wave identical to the reflected wave. In the physical optics approximation these currents are taken to be the same as those that would be induced on a similarly coated and oriented finite planar section of a scattering body. This allows us to calculate the contribution of the section to the total scattered electromagnetic field of the body. Summing the contributions of the various body sections (each of which may have a different coating) yields the total

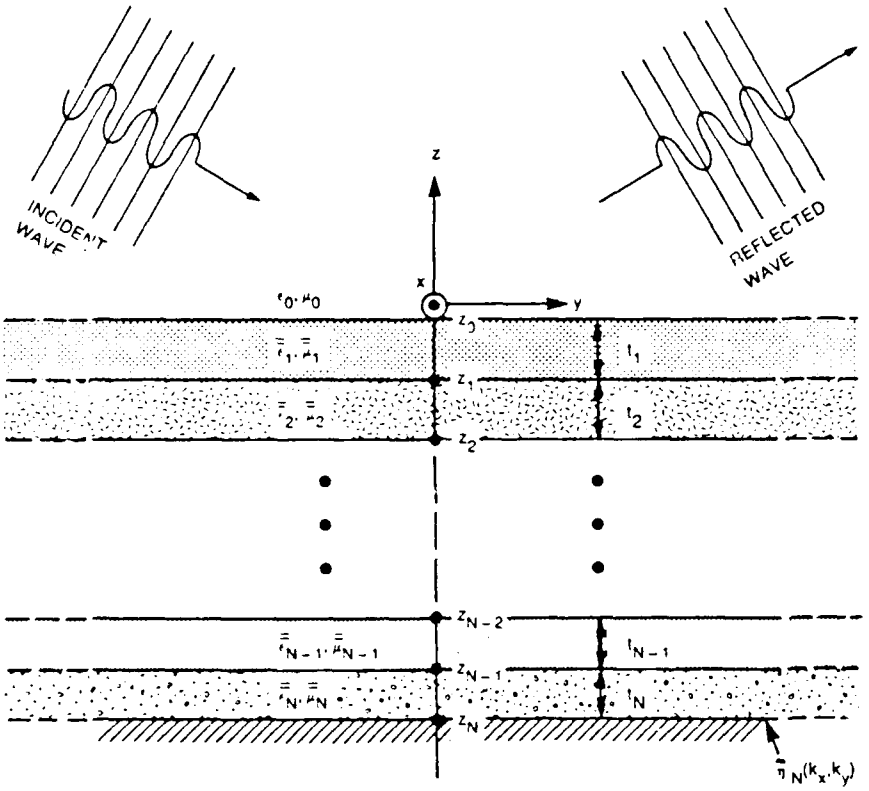

Fig. 4 — Stratified anisotropic region with incident and reflected plane waves

scattered field of the body, from which the scattering cross section is readily obtained.

Sample Results: As an example of the type of results that can be obtained with this physical optics technique, we compute the scattering cross section of a perfectly conducting square plate coated with a material with a lossy anisotropic dielectric. The relative dielectric tensor is taken to be diagonal with $\epsilon_{xx} = \epsilon_{zz} = 1 + i2.5, \epsilon_{yy} = 1 + i5$. The relative permeability tensor is taken to be the identity matrix. The computation is performed at 3 GHz for a plate that is 1 m (10 wavelengths) on a side. The thickness of the coating is taken to be 2 cm.

The results can be seen in Fig. 5, which shows plots of the bistatic cross section in the specular direction vs θ for $\phi = 0°$ and $\phi = 90°$. The E-field in both cases is linearly polarized in the θ-direction. For comparison, the result for an uncoated plate is also shown; this results is the same for both values of ϕ. The effect of the anisotropy is clearly seen in the difference in the plots for the values of two ϕ, since for isotropic materials these plots would be identical.

[Sponsored by ONR]

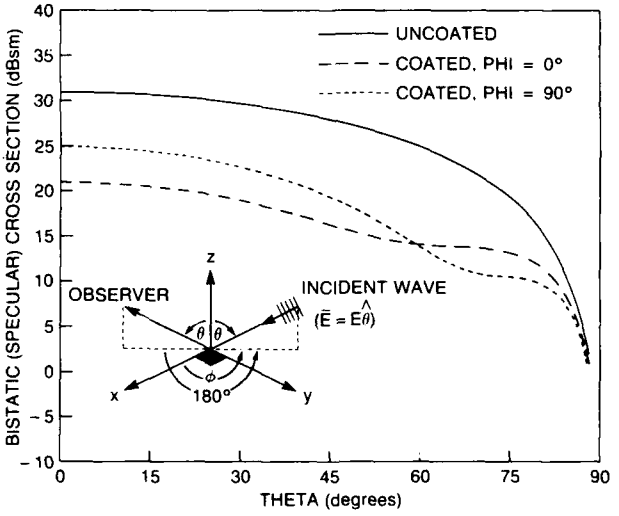

Fig. 5 — Bistatic cross section of a square plate, with and without a lossy anisotropic dielectric coating, in specular direction

Bibliography

H.J. Bilow, "Electromagnetic Wave Reflection and Scattering from a Plane-Stratified Anisotropic Region," NRL Report 9029, April 1987.

High Resolution X-Band Clutter Radar

J. P. Hansen
Radar Division

An understanding of the basic scattering mechanisms of radar clutter sources such as the sea surface is important for both remote-sensing and target-detection applications. Many simultaneously occuring surface features such as windblown ripples, facets, breaking waves, wedgelike crests, and even splashing raindrops have been tentatively identified as contributors to surface backscatter. Extensive experimental measurements have been made in the past, but unfortunately, the measuring systems have lacked versatility in such parameters as spatial resolution and polarization, which are required to help sort out contributions from the various features. In response to this experimental need, a dual polarization, X-band radar system has been configured for performing backscatter measurements. The radar features a single-phase, shifter polarization switch that allows pulse-to-pulse changes in transmit polarization.

System Characteristics: This new radar incorporates the mount and antenna structure (Fig. 6) from a TPQ-27 Marine radar combined with reconfigured transmit, receive, and record electronics. Table 1 lists the system parameters.

Transmitter: The radar transmitter uses an X-band local oscillator whose output is gated to the desired pulse length and linearly amplified by a high-power travelling wave tube (TWT). Transmit polarization is switched between linear horizontal, linear vertical, or right or left circular by the combination of a polarization switch assembly and

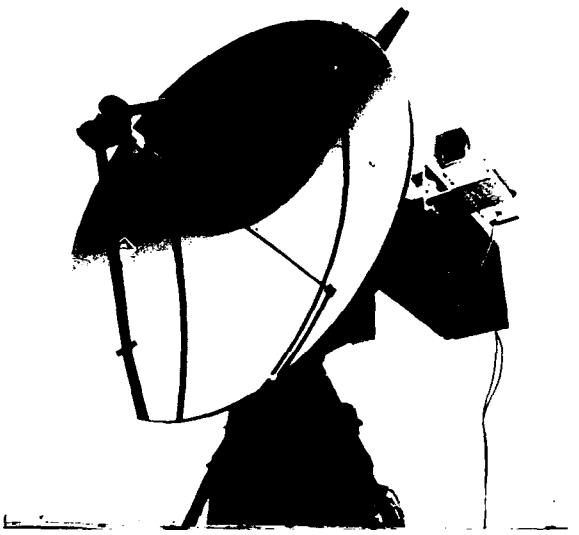

Fig. 6 — High-resolution, X-band clutter radar antenna

two polarization orthogonal feed ports, which have been physically rotated by 45° (Fig. 7). The switch assembly uses a power divider and a single phase shifter. When the phase shifter is set to a relative 0°, the vectorally combined output of the two rotated feed ports becomes linear vertical in polarization. When the phase shifter is set to a relative 150°, the combined output of the two ports becomes linear horizontal in polarization. Right or left circular polarization is achieved by using relative 90° or 270° phase shifts. The advantages of this arrangement are that the phase shifter is much faster than the electromechanical, high-power switch used in alternative configurations and the use of dual feeds minimizes power loss as compared to attenuator based configurations.

Receiver: Receive functions are also performed by using the two rotated polarization orthogonal feed ports. Scattered signals are simultaneously received on the two antenna ports and are then recombined and phase shifted at intermediate frequency. The resulting orthogonal receive channels (linear vertical, linear horizontal, or left and right circular) are simultaneously processed with the original local oscillator signal and detected as quadrature base band components.

Table 1 — Radar Characteristics

Frequency	- X-band, 9.3 GHz
Antenna	- 1° beamwidth, 26 dB sidelobe
Pulse Repetition Rate	- up to 5 kHz
Peak Power	- 50 kW
Pulse width	- 40 to 200 ns
Polarizations	
Transmit	- Switchable in 20 μs Linear or Circular
Receive	- Dual orthogonal, Linear or Circular
Receive Processing	- Quadrature Channel coherent, up to 100 MHz digitization rate at 8 bits.

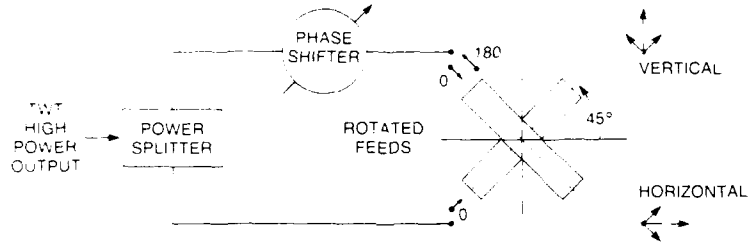

Fig. 7 — Polarization switch

These components, containing the phase and amplitude information of the scattered signals for each polarization, are then digitized by high-speed analog-to-digital converters and stored in memory for further processing. The convertors are gated so that the digital outputs represent the time varying characteristics of received scatter from radar illuminated features at selected ranges from the radar. Transmit polarization may be switched on a pulse-to-pulse basis while simultaneously observing backscatter in both orthogonal receive polarizations. Finally, a split-screen video system is used to visually record both the radar illuminated target area, as seen by an antenna mounted TV camera, and the power detected received signal as seen by another TV camera observing a range display.

Capability: In summary, this dual polarization, X-band measurement radar now combines the features of high resolution, coherency, and pulse-to-pulse transmit polarization switching, which are required for ongoing experimental investigations of high-resolution radar clutter from the sea surface.

[Sponsored by ONR]

Data Compression for Spaceborne SAR Imagery—The SARCOM System

S. A. Mango
Radar Division

One of the highest data rate, highest data volume remote sensing systems for the 1980s and projected for the 1990s is the spaceborne synthetic aperture radar (SAR). The needs for (a) real-time distribution of SAR imagery to researchers and operational users; (b) limited bandwidth links; (c)

limited time to transmit on shared links; as well as (d) more efficient archiving, demand data compression techniques with compression factors as high as 10-to-1, 100-to-1 or even higher. The data compression technique(s) must not only achieve the desired compression factor but also produce the highest fidelity, reconstructed imagery.

A SAR system's equivalent output image rate is typically 10 to 80 megabits per second (Mbps) when a modest quantization level of 8 bits/pixel is employed; whereas the links to the users are usually over data-rate-limited lines, usually at most 1.5 Mbps, or more typically 56 or 9.2 kbps. A variable compression factor is needed because the same SAR imagery may be used by various users who often have significantly different geometric and radiometric resolution requirements.

The NRL Digital Image Processing Laboratory (DIPL) studied the various data compression techniques by using SEASAT SAR and Shuttle Imaging Radar (SIR-B) imagery of ice, land, and sea [1]. A special emphasis was placed on the compression of SAR ice imagery in the compression factor range of 8-to-1 through 45-to-1 required by the SAR communications (SARCOM) system being developed at NRL for the National Oceanographic and Atmospheric Administration (NOAA) Ice Center and discussed below.

Some of the techniques evaluated and/or developed in both nonadaptive and adaptive forms included spatial techniques such as new linear, bilinear, and quadratic interpolative techniques; a new, linked polynomial technique; a block truncation coding (BTC); and a few variations of vector quantization (VQ), as well as transform techniques such as the discrete cosine transform (DCT) and the Hadamard transform (HT). The evaluation criteria used were the fidelity of the reconstructed imagery determined by subjective polling, the normalized-mean-square-error (NMSE) of the reconstructed image with respect to the original image, and the arithmetic burden imposed on the processing system by the compression process.

Results: The study results indicated that the DCT technique yielded excellent results, and a new variation of an older adaptive DCT (ADCT) technique [2] was found to increase further the fidelity of the reconstructed imagery. Figure 8 diagrams the transform-type data compression technique such as the DCT. The DCT and ADCT techniques were found to be well matched with the predominant multiplicative (speckle) noise characteristics of a coherent sensor system such as a SAR.

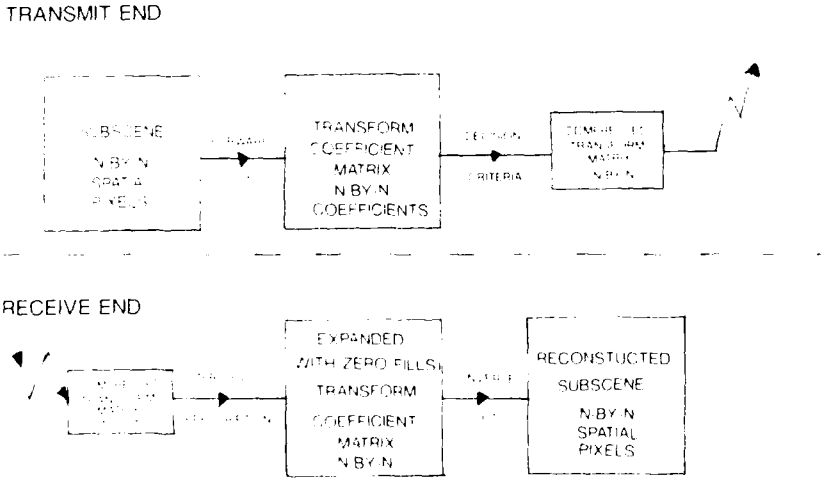

Fig. 8 — Data compression schematic for DCT technique

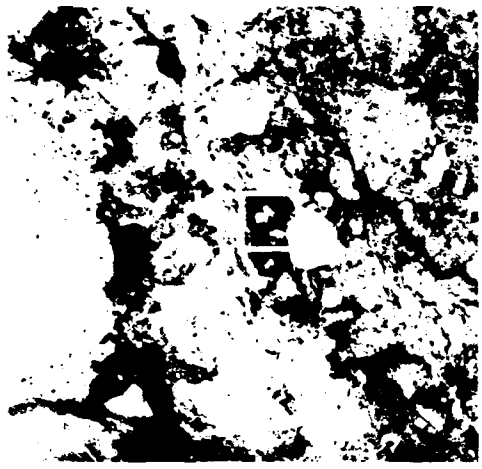

(a) Original
3968 by 3712 pixels

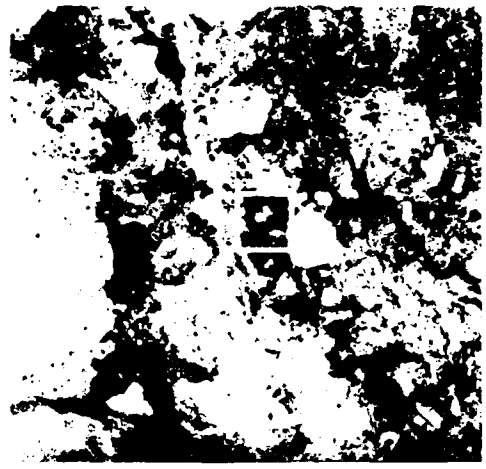

(b) Reconstructed (C.F. = 32)
Blocksize = 128 by 128

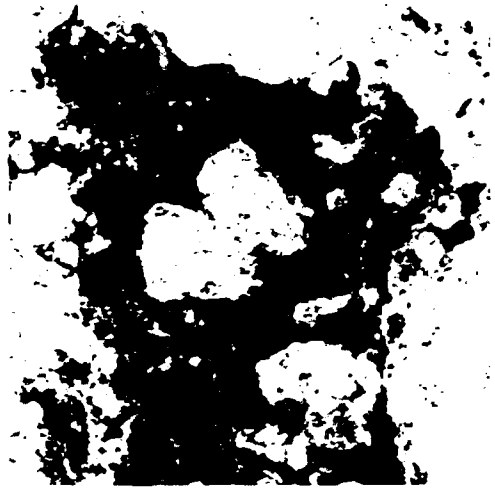

(c) Zoom (64-to-1) of central region of (a)
512 by 512 pixels

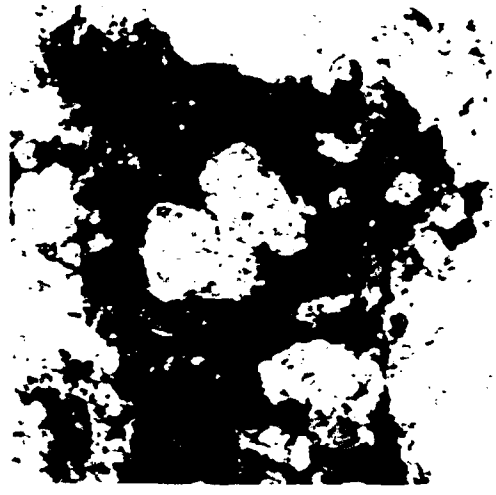

(d) Zoom (64-to-1) of central region of (b)
Blocksize = 128 by 128

Fig. 9 —Data compression (compression factor (C.F.) = 32) using an ADCT technique on a SEASAT SAR image of the Banks Island area with shore-fast and mobile ice fields in the Arctic basin. Scene size is 50 by 46 km.

Figure 9 displays the effective ADCT technique. The reconstructed image (compression factor (C.F.) = 32) is presented side-by-side with the original image (25-m resolution) at an approximate map scale of 1:500,000. The scene is a SEASAT SAR ice image collected in 1978 of a portion of the Beaufort Sea in the Arctic basin. Banks Island occupies the left one-quarter of the image from top to bottom, shore-fast ice occupies roughly the next one-quarter, and much more mobile ice (5 to 6 km per day) occupies the right half of the image. To emphasize the fidelity of the reconstructed image, the small ice floe region within the white box is zoomed from 64-to-1 in area to a more demanding map scale of approximately 1:62,500. The technique yielded an NMSE of the intensities of the entire reconstructed scene with respect to the original of 0.021 or 2.1%.

Even at this scale, all of the essential ice features including edges of the floes, subfloes, and filamentary new ice forming in the low-contrast, open-water areas are preserved and essentially indistinguishable from the original, even though only 3.1% (1/C.F. = 32) of the original amount of data were transmitted as compressed ADCT coefficients.

Figure 10 shows a second example of the ADCT technique for a C.F. = 100 applied to a SEASAT SAR scene with three small ships and their wakes navigating in deep water off Cape Canaveral. For this scene, the NMSE = 0.051 or 5.1%. Surface wave patterns, ships, and ships' wakes signatures are all well preserved.

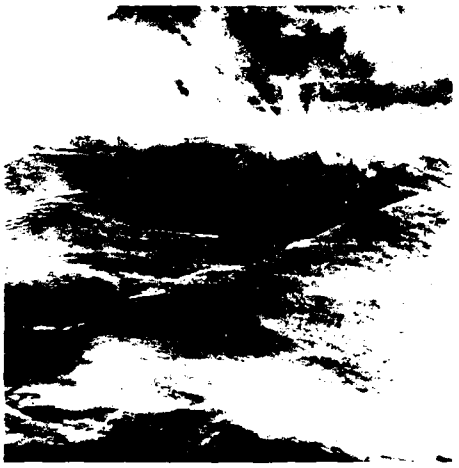

(a) Original
3200 by 3200 pixzels

(b) Reconstructed (C.F. = 100)
Block Size: 128 vy 128

Fig. 10 — Data compression: ADCT technique; SEASAT SAR ship and ship-wake image-Rev 407

Application of Results—The SARCOM System: The Systems Research and Control Branch applied the results of its data compression research in their design of the SARCOM system. SARCOM will provide a real-time operational demonstration of the transmission of spaceborne SAR imagery of Arctic ice over a bandwidth-limited satellite communications link. The transmit end of SARCOM will be collocated with and interfaced to the Alaska SAR Facility (ASF) located at the Geophysical Institute of the University of Alaska in Fairbanks (UAF). The ASF is sponsored by the National Aeronautics and Space Administration (NASA) and developed by the Jet Propulsion Laboratory (JPL). The SARCOM imagery will be transmitted from the ASF by way of a DOMSAT satellite link to the SARCOM receive end at the NOAA Ice Center (NIC) in Suitland, Maryland (Fig. 11(a)). A spaceborne SAR is portrayed viewing a portion of the Arctic basin operating in a strip map mode indicated by dashed lines that delineate the edges of the data-collection swathwidth.

To achieve the real-time capability, SARCOM will apply data compression techniques [1] to the SAR imagery prior to the transmission through the satellite link. The effective real-time SAR image rate will be as high as 60 Mbps while the satellite link maximum bandwidth is 1.33 Mbps. Therefore, compression ratios as high as 45-to-1 must be employed.

The SARCOM system will handle, at minimum, the SAR imagery from three spaceborne SARs:

1. E-ERS-1 (European Space Agency) September 1990 launch
2. J-ERS-1 (Japan) 1992 launch
3. RADARSAT (Canada) 1994-1995 launch.

These three intended SAR platforms will be in a polar orbit, providing excellent opportunities to provide synoptic coverage of the Arctic regions.

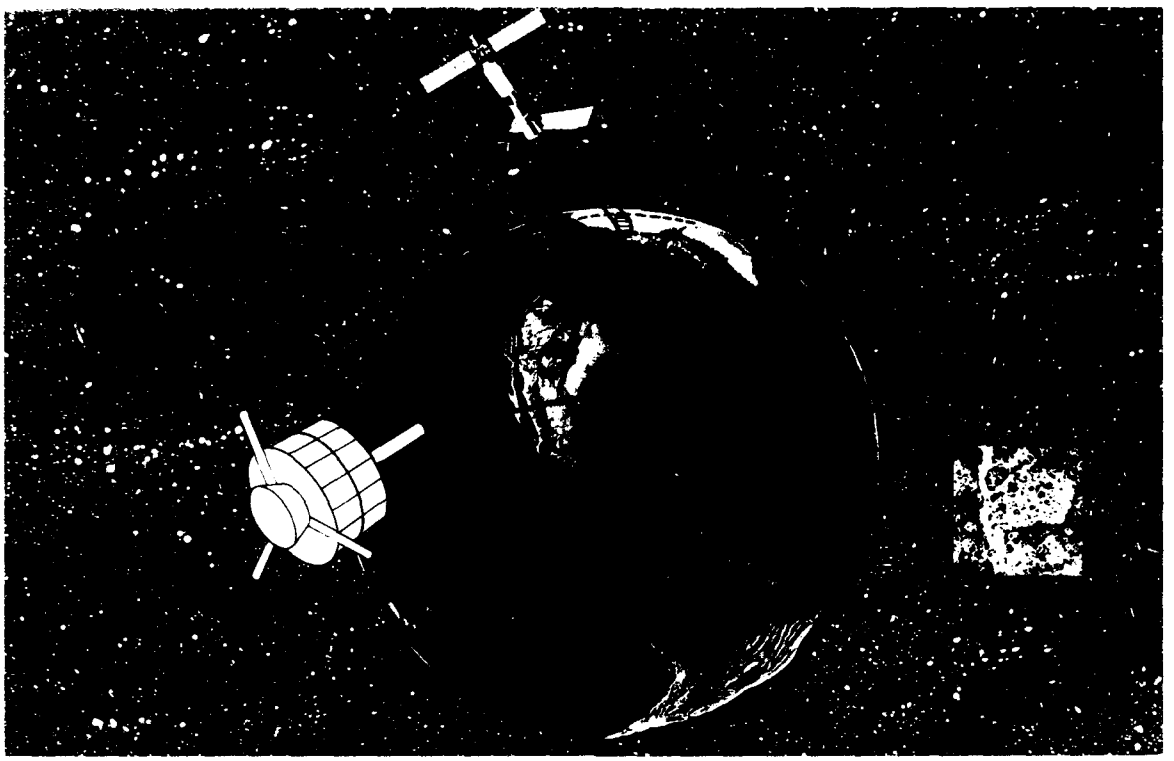

(a)

(b)

Fig. 11 — (a) SARCOM data path from ASF at UAF to the NOAA CDA station in Gilmore Creek, Alaska by way of DOMSAT communications satellite to NIC; (b) SARCOM system elements—elements at ASF shown in green box

Overlaps in the operating lifetimes of the three systems should provide unique, spaceborne observations of these regions at multiple frequencies, polarizations, and look angles. The day-night, essentially all weather capability of the SAR and its high resolution, typically 25 to 30 m on the ground, even at satellite altitudes, makes it an ideal sensor for operational uses such as ice monitoring.

The SARCOM applications' goal is to provide SAR ice imagery to enhance and expand the ice forecasting capabilities and services of the Ice Center. SARCOM will especially cater to the quick-turnabout imagery, that is *fresh* ice imagery less than 6-h old. These imagery will serve as both quick forecasting and synoptic data bases for direct ship support operating in these Arctic regions and for longer term sea ice data bases for ice modeling and research. These data will be used in research to determine ice concentration; to classify ice types (ice morphology); to determine ice motion as a means of understanding the kinematics of ice fields and its incorporation into ice dynamics modeling; and to study the deformation of ice.

Figure 11(b) shows the SARCOM system as an augmentation to the ASF system with the two data umbilical cords between the two systems. Once the data are captured from the ASF system, SARCOM is in autonomous operation. SARCOM performs the data compression at real-time rates with a throughput of up to 8 Mpixels per second and at sustained arithmetic rates of 160 to 200 MFLOPS (million floating point operations per second).

The compressed imagery will be transmitted by satellite between the two NOAA Command and Data Acquisition (CDA) stations in Alaska and Maryland. At the NIC receive-end SARCOM will perform the inverse of the data compression algorithms applied at the transmit-end to reconstruct the SAR imagery with the highest fidelity possible. The reconstructed high-resolution imagery will then be analyzed for information extraction for the NIC operational applications.

K. Hoppel, P. Bey, and M. Grunes of the Bendix Field Engineering Corporation have made significant contributions to the data compression study portion of this research.

[Sponsored by the Office of the Oceanographer of the Navy, SPAWAR, and NOAA]

References

1. S.A. Mango, "Alaska SAR Facility (ASF) SAR Communications (SARCOM) Data Compression System," Proceedings of the NASA Scientific Data Compression Workshop, Snowbird, Utah May 1988, pp. 393-417.

2. W. Chen and C.H. Smith, "Adaptive Coding of Monochrome and Color Images," *IEEE Trans. Commun.* **COM-25**, 1285-1292 (1977).

High-Speed, Long-Range, Unmanned Underwater Vehicle Communications Link

J. G. Eskinzes
Acoustics Division

J. R. Bashista
Information Technology Division

Introduction: Unmanned underwater vehicles (UUVs) have the potential to accomplish many important present and future Navy missions. However, much technology must be developed before UUVs can accomplish many of the required Navy tasks. One of the key technologies required is long-range, high-bandwidth, two-way communications/telemetry between a UUV and a surface station so that operational data and instructions can be transmitted at long distances. NRL is being tasked by the Office of Naval Technology (ONT) to develop a long-range radio frequency (RF) satellite communications link for

this purpose. UUVs generally have similar constraints as torpedoes; that is, they are space and energy limited. Therefore, the transceiver used aboard the UUV must be small and have low energy requirements. The transceiver built by NRL for the AN/BSQ-5 Towed Communications Buoy Project had all the salient features and was successfully adapted for this project. The UUV satellite communications system was designed, installed, and successfully tested on the Sea Lion semisubmersible vehicle in September 1988.

Background: Communication systems between UUVs and surface stations are using fiber-optic technology, acoustic techniques, and rf line-of-sight transmissions. Fiber-optic systems are not practical for long range UUVs since they are limited to the length of the fiber that often becomes severed or broken. High-frequency acoustic communication systems are severely range and/or multipath limited. Low-frequency acoustic underwater communications limit the data rates that can be used. RF transmissions to surface ships and aircraft are limited to line of sight with distances typically less than 10 nmi for surface ships and 200 nmi for aircraft. These distances greatly decrease as a function of sea state. An RF link to a satellite used as a relay station between the UUV and a surface station is the best alternative. Sea-state effects only affect the link when the satellite is visible at the lower elevation angles.

Project Description: A long-range communications link between a UUV and a surface station was designed. The transceiver used on the vehicle was designed to be compact and operate with minimum power consumption. The UUV used was the semisubmersible Sea Lion, (Fig. 12), which uses a diesel engine and snorkel. The shore-based system was a self-powered Winnebago recreation vehicle (Fig. 13) modified to accept equipment racks. This configuration allowed maximum flexibility in selecting an operating area. The Sea Lion was designed to be

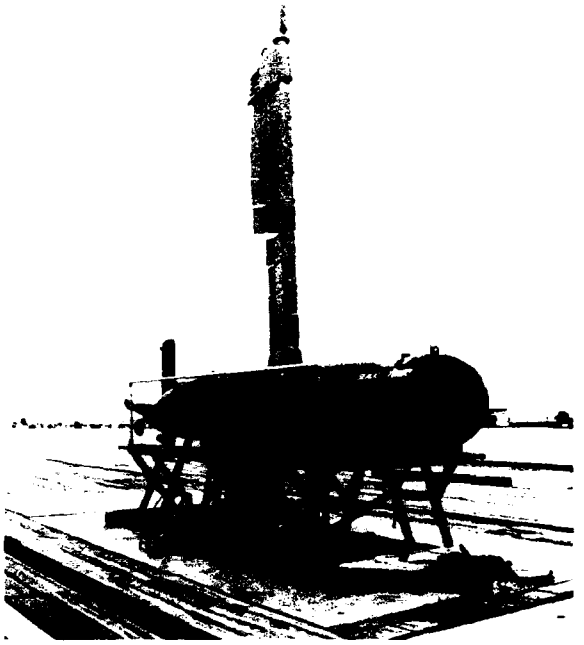

Fig. 12 — Sea Lion, a semisubmersible vehicle with a special resonant helix antenna on its mast

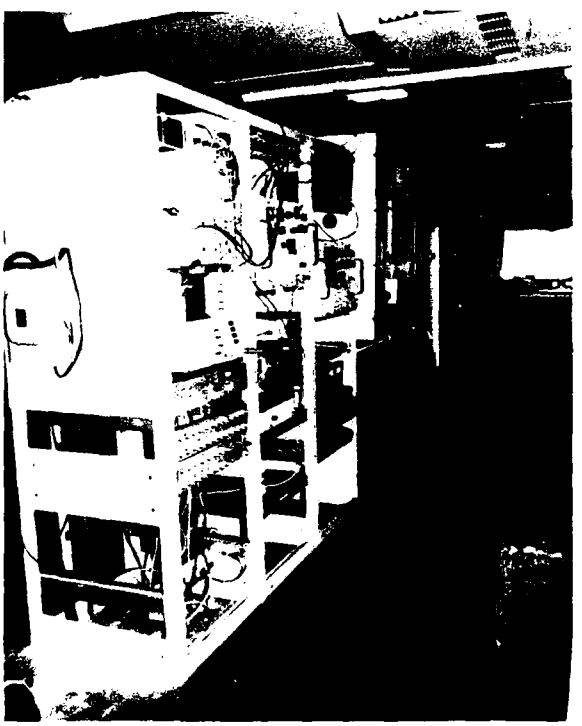

Fig. 13 — Interior of specially instrumented, shore-based Winnebego system showing satellite communication equipment and Sea Lion control console

controlled through an RF telemetry link. The telemetry electronics of the vehicle were modified to allow operation from a shore-based station by using the satellite link. Also, the vehicle control programs were modified to reflect slower response effects of the increased path length of the satellite link.

The communications link was tested in September 1988 on the Patuxent River with the shore-based station located at the Naval Air Station in Patuxent River, Maryland. The UUV (Sea Lion), under control of the shore-based station, was directed to submerge to a prescribed depth with the antenna positioned above the water surface. The vehicle was maneuvered over a variety of turns within the constraints imposed by the river with the link operating successfully without serious dropouts and/or loss of monitor and control of the vehicle.

Future Goals: The initial demonstration adapted existing control links requiring limited data rates for use in a satellite application and did not attempt to match information transfer to available satellite channel capacity. Future tasks are proposed to modify the existing vehicle control links to operate at higher data rates to match the satellite channel capacity. Also various sensors will be mounted on the body of the Sea Lion to demonstrate the remote collection of environmental information and the delivery of that data to a shore station by using a satellite relay. Navigation systems will be included to allow operations over long periods of time without direct control by a remote station.

[Sponsored by ONT]

ELECTRONICS RESEARCH

Electronics research embraces, in part, work on microwave techniques; thin films; semiconductor microstructure, interfaces, and surfaces; vacuum electronics; and solid state circuitry and sensors. Reported in this chapter is work on lithography and processing for nanoelectronics and on light detection with superconducting materials.

The Materials Science and Technology (6300) and Electronics Science and Technology Divisions (6800) contributed to these research efforts.

Other current research in electronics includes:

- Gyro-peniotron amplifier
- Single crystal GaAs preparation using a liquid encapsulant
- Microelectronic artificial neural networks
- Ion implantation

Microfabrication for Nanoelectronics

E. A. Dobisz and C. R. K. Marrian
Electronics Science and Technology Division

Introduction: We address advanced concepts in the basic science and technology of semiconductors on the nanometer scale. As device sizes become comparable to the carrier mean free path (≤ 500 nm) and quantum wavelength (≤ 100 nm), a new type of quantum electronic device has become feasible.

The growth of layered semiconductor materials has presented exciting new possibilities for electron waveguides through engineering the band gap and the refractive index of the semiconductor. However, to make useful devices, these materials must be patterned perpendicular to the growth direction. Patterning on the nanometer scale has been possible only recently, and then only in a few research laboratories. Typically a pattern is first written into a resist material by a lithographic process and then transferred into the semiconductor. As a major advance in lithography, a novel monomer resist system has been developed in which metal selectively electroless plates onto the resist [1]. The utility of material removal for pattern transfer is questionable at these dimensions owing to etch isotropy and carrier depletion because of band pinning by surface states. (Carrier depletion lengths can be as large as 500 nm.)

An example of a novel electronic device exploiting the physics of the nanometer regime is the ballistic transport split gate field-effect transistor (SFET), with a 50-nm space between the gates. Preliminary calculations predict the gain of this device to be more than double that of a conventional field-effect transistor. A further example, an interdigitated photodetector with spacings of less than 100 nm, is expected to have a frequency response of 500 GHz.

Pattern Transfer: We have identified compositional disordering of superlattices or quantum well structures as a means of pattern transfer. Certain impurities or implanted damage can enhance the interdiffusion between the layers in the heterostructure during annealing. By patterning the location of the *diffusion enhancers* one can locally change the band gap and refractive index of the structure without interrupting the crystal structure with an interface, as is created in etched material. We have discovered that the Si diffusion enhanced mixing of a GaAs-AlAs superlattice is anisotropic, which enables resolution of better than 100 nm. Anisotropic diffusion was found in samples in which the Si was diffused from a stripe, shown in Fig. 1 [2], and in samples in which the Si was introduced by ion implantation [3]. A distributed feedback laser, with a 250-nm spacing grating, has been designed that uses this patterning technique.

Fig. 1 — Transmission electron micrograph of a GaAs-AlAs superlattice compositionally mixed by diffusion from an Si stripe. The mixed region extends to a depth of 400 nm, while the lateral spread away from the Si stripe is less than 100 nm.

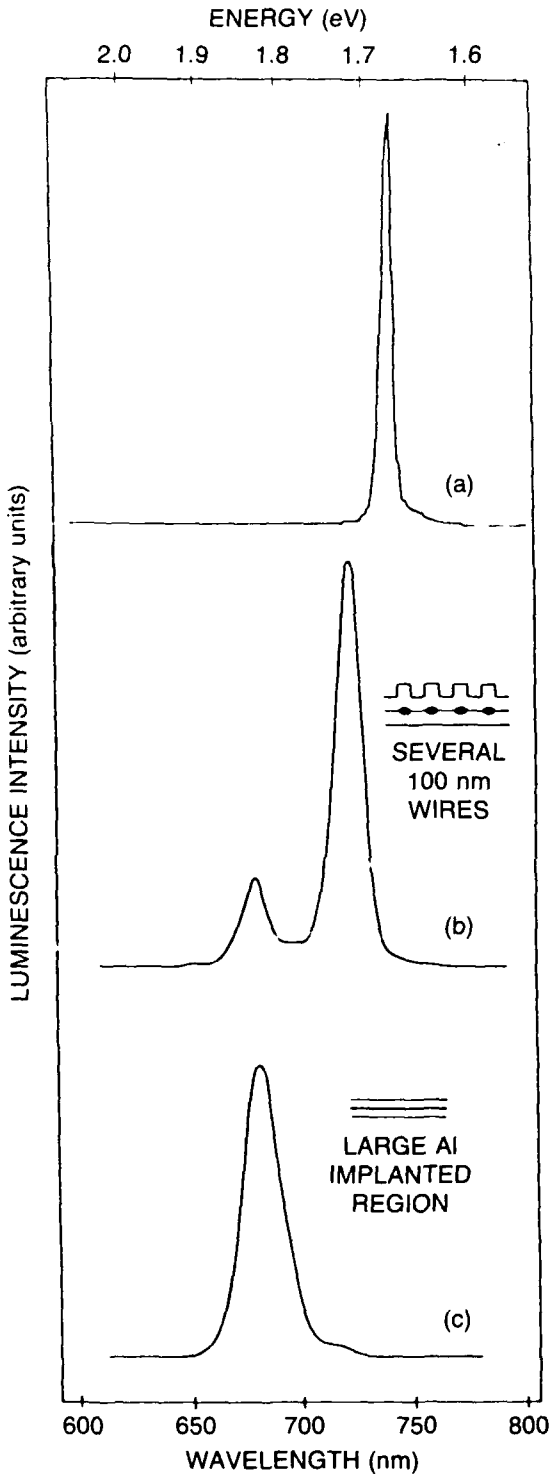

Fig. 2 — Cathodoluminescence spectra, at 60 K, of single 4.5-nm GaAs quantum well sample with Al(.6)Ga(.4)As barriers and top layer of 300-nm GaAs, which has been patterned to form the ion implant mask [5]. The sample was implanted with Al and annealed at 800°C for 2 h. (a) Large unimplanted region under mask. (b) Quantum well wires under several 100-nm wide GaAs mask lines. (c) Large implanted region.

Because of the control in depth and lateral dimensions, the use of implantation to introduce impurities is being examined extensively. An investigation of the effects of implant damage on compositional disordering concentrates on two areas: the effect of implant damage on impurity induced compositional mixing [4] and the implant-damage-induced interdiffusion. Ion channelling, transmission electron microscopy (TEM), and electrical measurements are focusing on the effects of implant temperature on the crystal damage and the diffusion of the Si. Hall measurements show that the percent activation of Si in GaAs, implanted at 77K, is one half that in GaAs implanted at room temperature [4]. However, previous work has shown that the superlattice samples, implanted at 77 K, exhibited the most uniform and extensive mixing [3].

For implant-damage-assisted compositional mixing, the sample is implanted with a nondopant and the layers interdiffuse as the damage is annealed out of the crystal in subsequent thermal annealing. Although the interdiffusion is not as complete, the advantage of this method is that a dopant is not introduced. Cathodoluminescence spectra of a 6-nm quantum well interdiffused following Al implantation (Fig. 2(c)) shows that the well exhibits 130 meV increase in the exciton peak energy (approximately the magnitude of change in the band gap) from that of the unimplanted sample shown in Fig. 2(a). Furthermore the cathodoluminescence spectrum (Fig. 2(b)) demonstrates that quantum well wires of dimensions ≤ 100 nm can be successfully patterned by this technique.

The collaboration of Professor M. Nathan and Professor M. Shur, at the University of Minnesota and of the Microelectronics Processing Facility for the SFET is gratefully acknowledged.

[Sponsored by ONR and ONT]

References

1. J. Calvert, J. Georger, C.R.K. Marrian, P. Schoen, M.C. Peckerar, and J. Schnur, U.S. Patent Application #07/182,123.

2. E.A. Dobisz, C.R.K. Marrian, and S. Hues, presented at the Electron, Ion, and Proton Beam Meeting, 1989.
3. E.A. Dobisz, B. Tell, H.G. Craighead, S.A. Schwarz, M.C. Tamargo, and J.P. Harbison, *Mater. Res. Soc. Proc.* **77**, 423.
4. E.A. Dobisz, H.B. Dietrich, and A.W. McCormick, presented at the MRS Spring Meeting, 1989.

Light Detection with Granular Superconducting Films

U. Strom and J. C. Culbertson
Electronics Science and Technology Division

S. A. Wolf
Materials Science and Technology Division

Introduction: With the discovery of a new class of high-temperature superconductors, it has become feasible to operate superconducting components at temperatures that are above the boiling point of liquid nitrogen. This fact has removed a primary objection to the potential use of superconducting films as detectors of infrared radiation [1].

Superconducting devices, such as tunnel junctions (which are based on the conventional low-temperature type of superconductors) are presently used as extremely sensitive microwave radiation detectors. The use of superconductors to detect the much higher energy infrared radiation is less well established.

Bolometric Detection: For the bolometric detection mechanism, the temperature of the superconducting film is biased near the steep transition to the superconducting state. Incident light, which is modulated by a mechanical chopper, induces small temperature variations in the film. These in turn result in a change in resistance and hence the voltage drop across the film for a given bias current. This bolometric mode of operation is particularly attractive for the new superconductors such as $Y_1Ba_2Cu_3O_{7-x}$ because of their high temperature of operation. Figure 3 shows the bolometric response for a film of $Y_{0.65}Ba_{1.44}Cu_{3.0}O_{7-x}$. The somewhat nonstoichiometric composition of this film, compared to the stoichiometric 1-2-3 composition, has lowered the superconducting transition temperature from 93 to 70 K. As expected for a bolometric mechanism, the peak in the photoresponse (solid line) corresponds to the maximum value of the slope in the resistance vs temperature curve (dashed line). The peak response of this device can be increased by reducing the width of the superconducting transition. Transition widths less than 1 K have been achieved at NRL and elsewhere near 93 K. For infrared wavelengths greater than 20 μm this type of bolometer, operating at 90 K, is estimated to be competitive with semiconductor detectors that are cooled to 4.2 K [2].

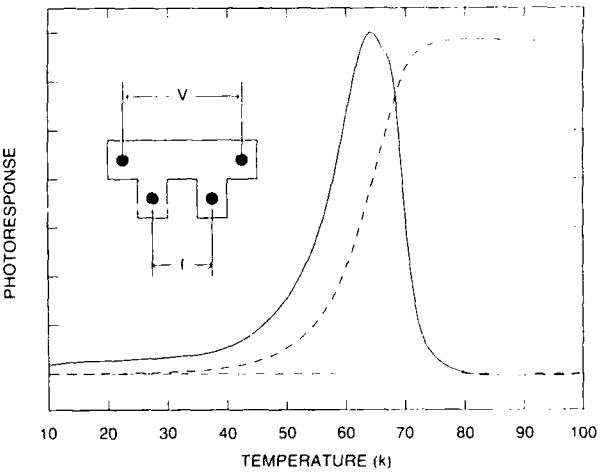

Fig. 3 — Resistance (dashed curve) and photoresponse (solid curve) of a film of Y-Ba-Cu-O, illuminated by an HeNe laser, chopped at 100 Hz

Nonbolometric Detection: The chief disadvantage of the bolometer detector is its relatively slow response time (on the order of milliseconds or longer). However, a second mode of operation exists that is intrinsically faster. This mode of operation, which has been pioneered by

NRL researchers, relies on the two-dimensional (2D) character of the transition to a state of zero resistance of a thin granular superconducting film. The resistance vs temperature dependence for such a film is indicated by the dashed line in Fig. 4. There is a distinct onset of superconductivity near 80 K. But because of its granularity, the film does not reach the superconducting state until about 10 K. Theory describing this 2D transition near 10 K for this particular film predicts a quadratic dependence of the photoresponse on bias current near 10 K, as is actually observed [3] (see Fig. 4). Note that the bolometric response for this film (the peaks near 30, 60, and 80 K) is linearly dependent on bias current.

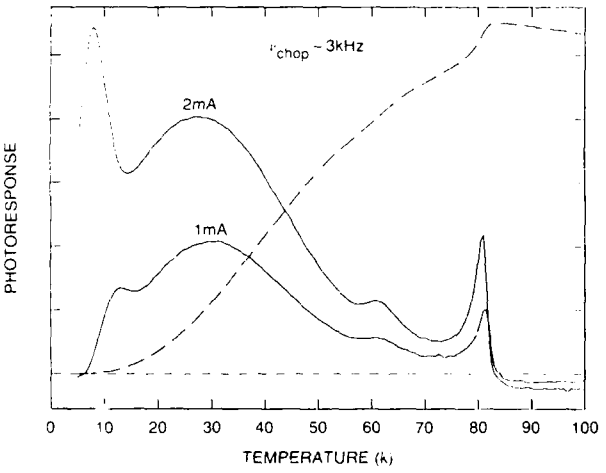

Fig. 4 — Resistance (dashed curve) and photoresponse (solid curve) for a highly granular Y-Ba-Cu-O film, illuminated by an HeNe laser, chopped at 3 kHz

The low-temperature response, corresponding to the quadratic current dependence, is intrinsically fast. Figure 5 shows temperature dependence of the response to a 10-ns long laser pulse. The slower, higher temperature bolometric peaks, which were observed in Fig. 4, are not observed in the pulsed data.

Conclusion: These preliminary results are encouraging for the development of usable superconducting detectors. When operated as a bolometer, the new high-temperature superconductors are likely to become competitive bolometric detectors of infrared radiation when high response speeds are not a consideration. The nonbolometric detector response can lead to the development of useful, fast, superconducting infrared detectors, provided that their operating point (i.e., near the 2D transition temperature) can be increased to near the boiling point of liquid nitrogen (77 K).

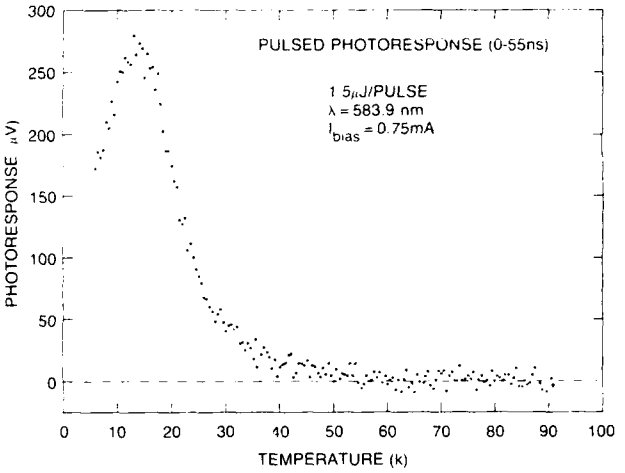

Fig. 5 — Temperature dependence of photoresponse for same granular Y-Ba-Cu-O film, illuminated by a pulsed (10 ns) visible laser.

[Sponsored by SDIO]

References

1. M. Leung, P. R. Broussard, J. H. Claassen, M. Osofsky, S. A. Wolf, and U. Strom, "Optical Detection in Thin Granular Films of Y-Ba-Cu-O at Temperatures Between 4.2 and 100 K," *Appl. Phys. Lett.* **51,** 2046 (1987).

2. P. L. Richards, J. Clarke, R. Leoni, Ph. Lerch, S. Verghese, M. R. Beasley, T. H. Geballe, R. H. Hammond, P. Rosenthal, and S. R. Spielman, "Feasibility of the High T_c Superconducting Bolometer," *Appl. Phys. Lett.* **54,** 283 (1989).

3. J. C. Culbertson, U. Strom, S. A. Wolf, P. Skeath, E. J. West, and W. K. Burns, "Nonlinear Optical Response of Granular Y-Ba-Cu-O Films," to be published.

ENERGETIC PARTICLES AND BEAMS

More compact energetic beam sources with a higher energy output continue to be developed at NRL where research is performed in the areas of plasma, laser, and advanced beam technology and how such energetic beams react with, and affect, matter. Reported in this chapter is work on the laboratory production of plasmas with extremely high energy densities, photopumping X-ray lasers, and the pulse reponse of AlGaAs laser diodes.

The Laboratory for Computational Physics and Fluid Dynamics (4400), the Plasma Physics Division (4700), and the Space Systems Development Department (8300) contributed to this work.

Other current research in energetic particles includes:

- Quasi-optical gyrotons
- Plasma chemistry
- Plasma microwave electronics
- Magnetic fusion
- High-energy charged particle beams

Laboratory Laser-Plasma Space Experiments

B. H. Ripin, C. K. Manka, and J. D. Huba
Plasma Physics Division

An understanding of the space environment is crucal to proper operation of Navy and DoD space assets, such as military communications (C^3I) and surveillance systems. The most direct way to study space physics is with actual satellite or space probes. However, such experiments are expensive, infrequent, and rarely have enough diagnostics for a thorough investigation. Moreover, space phenomena tend to occur sporadically and nonreproducibly, making it difficult to understand the underlying processes. Laboratory expertments, on the other hand, are relatively inexpensive, accessible, and can be made reproducible and very diagnosable. Laboratory parameters can be varied at will, enabling definitive investigations and tests of theory. Complementary laboratory and space experimentation is clearly the most *effective* approach.

Laser-produced plasmas provide a unique laboratory test bed for investigation of many space and astrophysical processes because they can span a wide range of parameters of interest. For instance, laser-produced plasmas can have energy densities from gigajoules/cc down to strongly coupled plasma conditions, where plasma kinetic energy is less than interparticle potential energies; plasma-βs (the plasma-to-magnetic energy density ratio) can range from much less than one to hundreds; temperatures can range from one to thousands of eV; and directed velocities can range over 1000 km/s (supernova-like). These conditions can be generally achieved with good control, reproducibility, and diagnosability.

Recently, the PHAROS III, high-power glass laser facility at NRL was used to create space and astrophysical-like plasma phenomena in the laboratory. Two examples are given here: (1) the large Larmor radius instability (originally seen in the Active Magnetospheric Particle Tracker Experiment (AMPTE) space experiment) in which a dramatic flutelike structure is formed, and (2) plasma cross-magnetic-field jetting in which a plasma mass can travel large distances across magnetic fields reminiscent, perhaps, of intergalactic jets. However, we first describe the general characteristics of laser-produced plasmas and their relevance to space and astrophysical plasmas.

Laser-Produced, Space-Like Plasmas: When a high-power laser beam is focused onto millimeter-sized solid targets with irradiance up to hundreds of TW/cm^2, the resulting ablation plasma has tremendous energy density and a temperature comparable to the sun's corona (~ 1 kV). As this plasma expands away from the target, it behaves very similarly to the solar wind that emanates from the sun. In both cases, the flows are highly supersonic (with speeds of several hundreds of km/s), relatively cold (eV) plasma. The complex interactions of the solar wind with Earth's dipole magnetic field form Earth's magnetosphere, bow shock, neutral sheet, aurora, and ionospheric phenomena. Laser ablation plasmas can also emulate other space and astrophysical situations, such as supernova shocks.

An ambient background plasma can be formed simultaneously with the energetic ablation component, if desired, by bleeding gas into the experimental chamber; the gas is photoionized by laser-target interaction radiation in the vicinity of the target and forms a cold stationary target plasma through which the ablation plasma streams. A magnetic field of up to 10 kG is often imposed by using a set of coils; this field corresponds to Earth's dipole field. Interstreaming plasma interactions occur when the fast ablation plasma flows into the ambient media. At low background gas pressures ($<<1$ Torr) collisionless phenomena, such as the solar wind, impinge on the magnetosphere, ionosphe- and obstacles, such as comets, moons, and planets. Similarly, at higher pressures (>1 Torr), collisional effects such as blast-wave shocks

dominate; these shocks behave much like supernova shocks.

Other types of laser-produced plasma are useful for other studies. Shock waves set up in the solid target interior by the high-pressure laser/plasma impulse create a dense and slow component that expands much like the ablation plasma; this plasma is useful in the study of plasma jetting. Plasma jets, or plasmoids, are plasma masses that can travel unexpectedly large distances across magnetic fields (such as many gyroradii or magnetic confinement radii); they may be involved in astrophysical jetting, solar disruption plasma transport, bipolar stars, and active release or beam space experiments. Finally, an especially low energy-density (strong-coupled) plasma can also be formed by laser irradiation of thin films. Strong-coupled plasmas exist naturally in solar interiors, white dwarfs, and Jupiter.

Large Larmor Radius Instability: The large Larmor radius (LLR) instability is an example of a new effect that has been investigated in the laboratory. Unexpected observations of plasma striations in the March 1985 AMPTE barium release experiment in the tail of the magnetosphere [1] led NRL theorists to develop a stability theory for sub-Alfvenic expansions in the large ion-Larmor radius (LLR) limit [2]. In this theory, the electrons are magnetized, since their orbits are quite small, but the ions are effectively unmagnetized, since they have Larmor radii that are large compared to characteristic dimensions. The LLR instability is analogous to the conventional, totally magnetized, plasma Rayleigh-Taylor (or interchange) instability, but has a much faster growth rate and other properties distinct from the known case. The NRL laser-plasma experiment verified the existence and basic properties of this new instability [3]. Figure 1 shows two examples of the resulting unstable plasma structure: Fig. 1(a) is an example of structure near the end of the LLR linear growth phase showing the well-developed fluting; Fig. 1(b) is an example of the very large and unusual structure characteristic of later, nonlinear stages. The nonlinear structure development does not really saturate, but rather, it continues to expand outward at approximately the original plasma velocity even though it is well beyond the nominal magnetic stopping distance for the plasma. The flutes become erratic and even appear to bifurcate. It appears that individual flute tips eventually act like independent plasma jets. We find, therefore, that the LLR instability is extremely robust and can be expected to appear in a variety of space and man-made (e.g., magnetic fusion) plasmas.

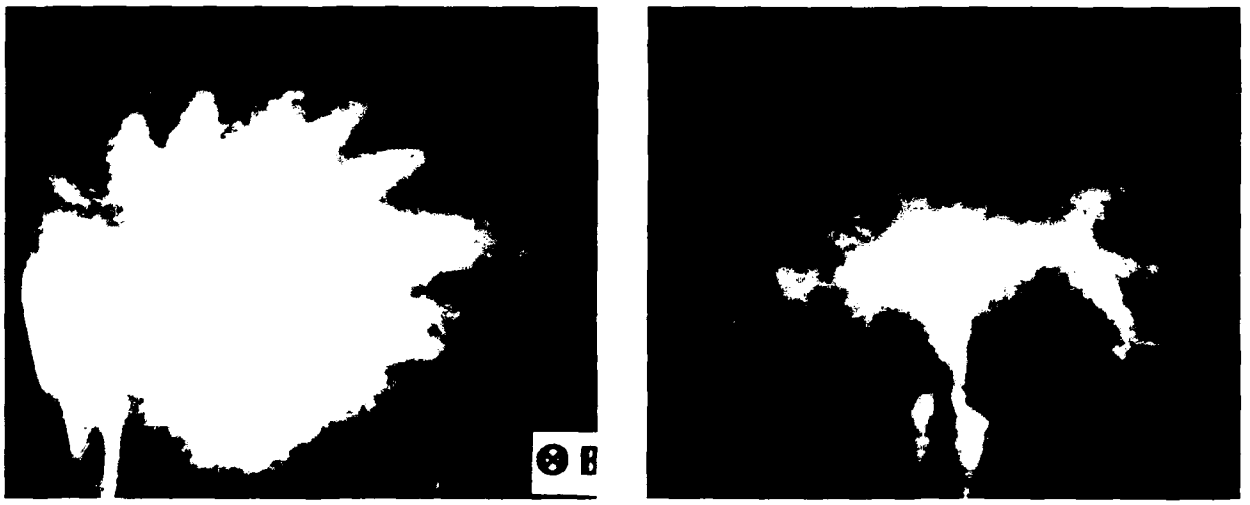

(a) (b)

Fig. 1 — Two examples of the LLR instability seen in the NRL experiment. (a) Instability near the end of its linear stage (10 kG, 376 J, 99 ns). (b) Some fascinating bifrucationlike structures appearing in the nonlinear stage (10 kG, 30 J, 90 ns).

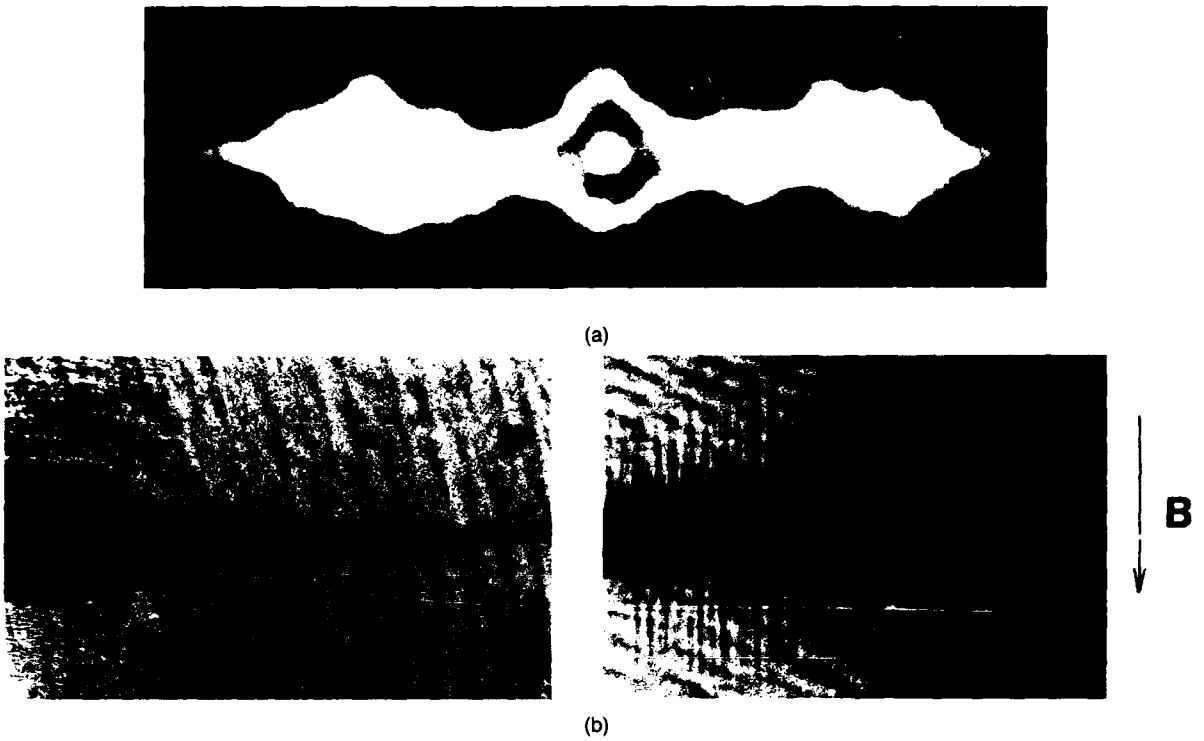

Fig. 2 — Examples of cross-field plasma jetting. (a) Cylindrical target jet, $V_o \sim 5 \times 10^6$ cm/s, B_o = 10 kG, observed at 1 μs. (b) Barium-jet with $V_o \sim 10^6$ cm/s, B_o = 10 kG, observed at 1 μs; note field-aligned structure in the cross-field view.

Plasma Jets: Clumps of plasma can move large distances across magnetic fields, distances much greater than either the magnetic confinement radii or the ion gyroradii, in many space and laboratory situations. This cross-field motion is not possible for isolated charged particles, but a plasma can act collectively to overcome the magnetic field force. What happens is that forces on charged particles in a plasma moving across magnetic field B_o with speed V_o causes an internal polarization electric field E_p to form. Then, the plasma responds according to $E_p \times B_o = V_o$, and the plasma continues its crossfield motion at its original velocity. Of course, charge is continually depleted at the boundaries and the process will eventually terminate.

Figure 2 shows several examples of cross-field jetting observed in our experiments. Figure 2(a) shows a $\beta \sim 1$ jet produced by firing the laser into the ends of a small glass cylinder and allowing the plasma to squirt out its ends across the magnetic field. Figure 2(b) shows a $\beta << 1$ barium plasma jet also squirting across the B-field [4]. Several common features are found in these NRL laboratory jet experiments: they occur if the plasma is asymmetric; they propagate great distances across the magnetic field at nearly their initial speed; they tend to pinch down at their leading edge owing to curvature of the internal polarization electric fields; and they often form field-aligned structures on there boundaries, presumably resulting from instability.

Summary: Laser-produced plasmas can be made with parameters of space and astrophysical interest. This allows many space phenomena to be studied in the laboratory.

Collaborators in these experiments include: E.A. McLean, A.N. Mostovych, and J.A. Stamper of NRL, A.B. Hassam of the University of Maryland, and T.A. Peyser of Science Applications International Corp.

[Sponsored by DNA]

References

1. P. Bernhardt, et al., *Geophys. Res.* **92,** 5777 (1987).
2. A.B. Hassam and J.D. Huba, *Geophys. Res. Lett.* **14,** 60 (1987).
3. B.H. Ripin, et al., *Phys. Rev. Lett.* **59,** 2299 (1987).
4. A.N. Mostovych, J.A. Stamper, and B.H. Ripin, *Rev. Sci. Insts.* **59,** 1497 (1988).

An Efficient Pulsed-Power Source for Photopumping an X-ray Laser

F. C. Young and J. P. Apruzese
Plasma Physics Division

The Gamble II pulsed-power generator at NRL was used to develop an intense pulsed source of kilovolt sodium X-ray line radiation. This sodium radiation can be used to selectively photopump an appropriately preformed neon plasma with the potential to produce a soft X-ray laser.

Resonant Photopumping: Currently, laboratory X-ray lasers use powerful but inefficient optical or infrared lasers to create a plasma lasing medium through electron-ion collisions in the plasma. By using a pulsed-power driver to create an intense source of X rays, which are concentrated in a single line, the lasing medium can be formed by resonant photopumping with much higher efficiency.

One of the most promising schemes to achieve a photopumped X-ray laser involves a naturally occurring X-ray line coincidence between the n = 2 to 1 transition in helium-like sodium and the n = 4 to 1 transition in helium-like neon. This wavelength match allows X rays from a hot, dense, helium-like sodium plasma to resonantly photopump a cooler, more tenuous neon plasma. Under proper conditions lasing would occur at wavelengths of approximately 230, 82, and 60 Å, respectively. However, this scheme requires an intense sodium x-ray pump source.

Pulsed-power generators were initially developed by the Defense Nuclear Agency to produce bremsstrahlung radiation sources by using intense electron beams. More recently, the generators produced powerful sources of lower energy X rays by driving a cylindrical annular gas puff or wire array with a megampere- (MA-) level current in a Z-pinch implosion. For example, sodium atoms are stripped of all but one or two electrons in Z-pinch implosions on the Gamble II generator. As these hydrogen-like or helium-like sodium ions collide with ambient electrons, K-shell X rays are radiated in a few strong lines with energies near 1 keV.

Sodium Pump Source: An intense sodium pump has been developed at NRL by imploding a sodium-bearing plasma produced with a capillary-discharge source [1] on the Gamble II generator. Since sodium is not suited to a gas puff or wire array, a capillary discharge of sodium fluoride (NaF) was developed to inject an NaF plasma across the anode-cathode gap of Gamble II. A 4-cm long, 1.5-cm diameter cylindrical column of plasma with ion density of about 10^{17} cm^{-3} is imploded with a 1-MA peak current pulse to produce sodium K-shell X rays. The radiation is optimized by adjusting the initial diameter and mass per unit length of the NaF plasma to match the Gamble II driving current. The measurements in Fig. 3 indicate that the implosion occurs after the peak of the current when an intense X-ray burst is emitted. The peak power of the sodium K-shell X-ray emission is nearly 80 gigawatts (GW), and about half of that power (39 GW) is in the n = 2 to 1 pump line (labeled He-α in Fig. 3). The total energy in this line is about 700 J. Pinhole camera images and K-shell line spectra of X rays from such implosions are measured and analyzed to determine that the imploded plasmas reach electron densities of about 4×10^{20} cm^{-3} (ion density 4×10^{19} cm^{-3}) and temperatures of about 3×10^{6} K [2].

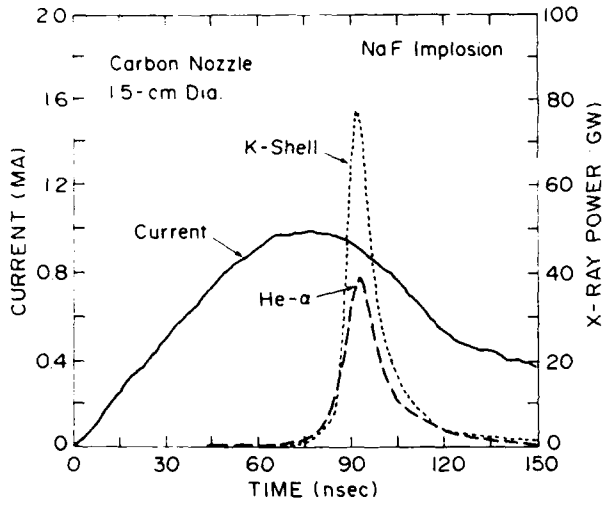

Fig. 3 — Driving current and X-ray traces for an NaF implosion on Gamble II. The K-shell trace includes all the sodium K-shell X rays. The He-α trace includes only the n = 2 to 1 helium-like sodium pump line.

The production of 700 J of X rays concentrated in a single pump line is a major step toward a resonantly photopumped sodium/neon X-ray laser. This source is being used to study the photopumping of a nearby neon plasma. There is experimental evidence for fluorescence of the n = 4 to 1 line of neon when pumped by sodium [3]. Further research is required to prepare the neon plasma with the optimum density, temperature, and uniformity required for lasing. Also, to achieve lasing the pump power must be increased to more than 200 GW by driving the NaF implosion with 2 to 3 MA from a larger pulsed-power generator. However, the higher efficiency associated with a lasing medium produced by ion-photon collisions should lead to X-ray laser outputs measured in joules, rather than in millijoules as in present systems.

[Sponsored by IS&T/SDIO]

References

1. F.C. Young, S.J. Stephanakis, V.E. Scherrer, B.L. Welch, G. Mehlman, P.G. Burkhalter, and J.P. Apruzese, *Appl. Phys. Lett.* **50,** 1053 (1987).
2. J.P. Apruzese, G. Mehlman, J. Davis, J.E. Rogerson, V.E. Scherrer, S.J. Stephanakis, P.F. Ottinger, and F.C. Young, *Phys. Rev. A* **35,** 4896 (1987).
3. S.J. Stephanakis, J.P. Apruzese, P.G. Burkhalter, G. Cooperstein, J. Davis, D.D. Hinshelwood, G. Mehlman, D. Mosher, P.F. Ottinger, V.E. Scherrer, J.W. Thornhill, B.L. Welch, and F.C. Young, *IEEE Trans. Plasma Sci.* **16,** 472 (1988).

Modal Transients in Pulsed Laser-Diode Arrays

W.L. Lippincott, A.E. Clement, and W.C. Collins
Space Systems Development Department

Our group has been involved in studying the properties of gain-guided, multiquantum-well AlGaAs single-stripe and ten-stripe laser diodes. Recent advances in laser-diode technology have led to the development of low-cost, long-lived, high-power devices that have excellent potential as transmitters for satellite communication systems [1]. However, we have found that these multimode devices exhibit intermodal power sharing that can continue for up to 70 ns during modulation.

Longitudinal optical modes are separate discrete frequencies of radiation that set up standing waves in the laser cavity. In a typical laser-diode cavity, several modes can be amplified. In an optical link that transmits from a laser coupled to a fiber, a speckle pattern is produced at the output. Intermodal power sharing in the pulsed laser causes instability of the projected speckle pattern, which results in waveform distortion if a receiver samples only part of the beam. Our investigation of this behavior has involved examining the pulse response of the individual modes of each stripe of the laser arrays and analytically modeling the thermal behavior of the laser with a finite element code.

Experimental Work: The experimental setup shown in Fig. 4 was used to focus the laser light onto an echelle grating that separates the modes.

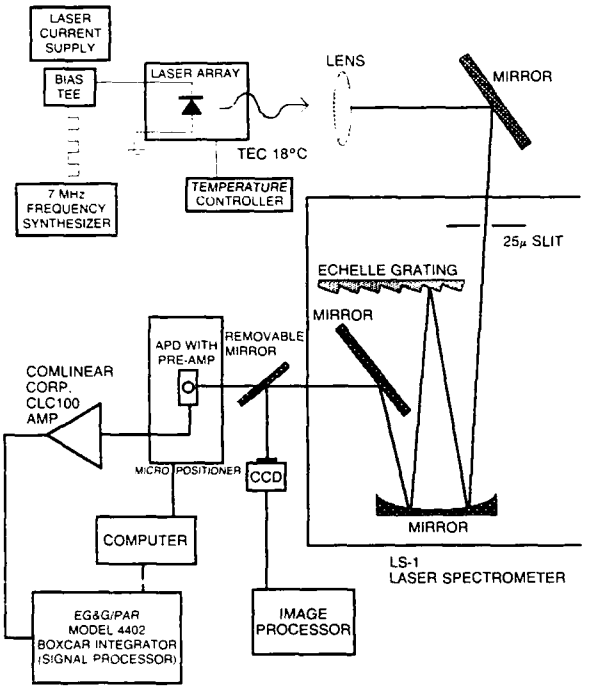

Fig. 4 — Experimental configuration for examining modal transients in pulsed laser-diode arrays

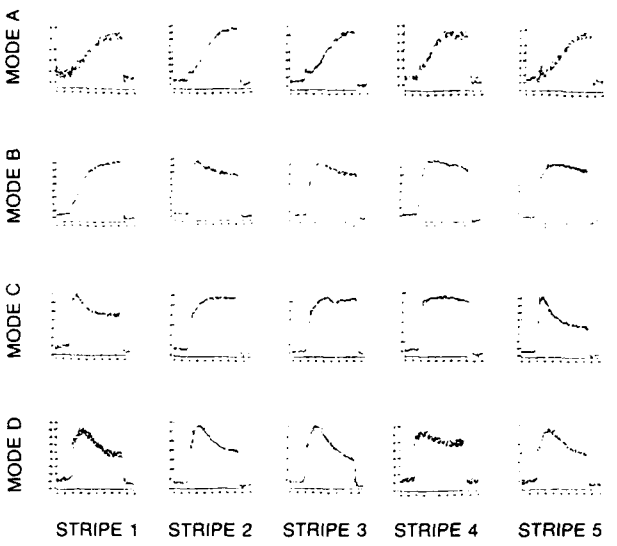

Fig. 5 — Pulse response from a 10-stripe laser-diode array. The four main modes are shown for five of the stripes

With this configuration, we can see the time-integrated, three-dimensional intensity profile of each mode on a charged-coupled device (CCD) camera as well as capture their time response during the period of a pulse with scanning avalanche photodiode (APD). Figure 5 shows the effect of intermodal power sharing in the four ›minant modes of a ten-stripe array. Each stripe has modes that are gaining intensity, losing intensity, and that remain fairly constant over a 70-ns pulse.

To fully characterize the intermodal behavior, the laser was pulsed at different modulation depths and bias currents. Using the standard deviation from a square pulse as a figure of merit for comparison between waveforms, we found that the distortions increased significantly at higher modulation depths. This indicates the instability is due to thermal transients in the active area of the laser.

Computer Simulation: The NASTRAN finite element code on the CRAY computer was used to model the temperature transients within the active area of the diode arrays [2]. Temperature changes affect the refractive index of the laser and cause the modal output to change. In this model, the diode is divided into a two-dimensional grid of cells (Fig. 6). The conductivity, density, and heat capacity of the material within each cell are specified as well as any heat generated from photon absorption, nonradiative recombination, or ohmic heating. The distribution of heat generated in the diode's active area was determined by imaging the laser facet at threshold current onto a CCD camera and by using an image processor to plot the intensity distribution of the spontaneous emission. The model uses the given thermodynamic information and the assumption that heat can flow out only through a constant-temperature heat sink to determine the thermal distribution in the laser during modulation or in steady-state operation.

The theoretical steady-state temperature distribution in the lasers correlated well with experimental thermal impedance measurements. The temperature transients obtained from the model can be translated into modal transients and compared to experimental data by performing gain calculations to determine the spectral-distribution curve shift.

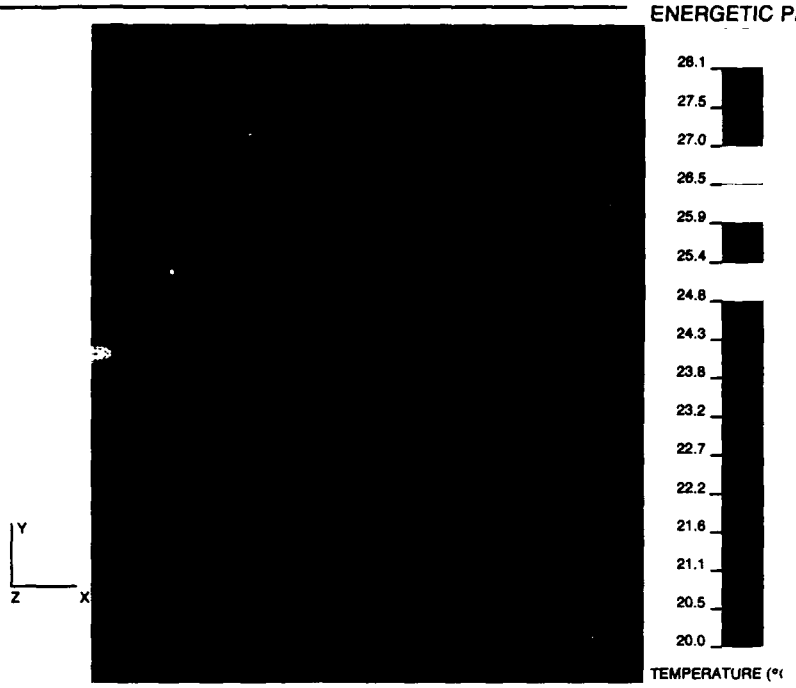

Fig. 6 — Finite element grid structure for thermal modeling of a laser diode. The temperature distribution during steady-state operation of a single-stripe laser diode is depicted.

References

1. D.R. Scifres, R.D. Burnham, and W. Streifer, "High Power Multiple Stripe Quantum Well Injection Lasers," *Appl. Phys. Lett.* **41**(2), 118-120 (1982).
2. W.L. Lippincott and A.E. Clement, "Finite Element Analysis of Thermal Transients in Laser Diode Multi-Stripe Arrays," Proceedings of the SPIE Conference on Lasers and Optics, Los Angeles, CA. Jan. 1989.

The Ablative Rayleigh-Taylor Instability in Three Dimensions

J. P. Dahlburg and J. H. Gardner
Laboratory for Computational Physics and Fluid Dynamics

When a powerful laser beam illuminates a laser target, a low-density plasma forms and blows off the irradiated target surface. By conservation of momentum, the ablating plasma accelerates the target away from the laser. Because the accelerated target is heavier than the low-density blow-off plasma, the illuminated target surface is Rayleigh-Taylor (RT) unstable. Practically, this means that small irregularities on the target surface grow at the interface between the accelerating target and the ablating plasma, causing the target surface to deform and hot plasma to mix with the cooler target material. For some RT perturbation wavelengths, growth of the instability is so rapid that an entire target can be destroyed in a few nanoseconds. The research reported here is motivated by the desire to understand the RT instability in directly driven laser fusion. For direct-drive laser fusion to be feasible, this instability must be understood and controlled. Although much work has been performed on the laser-driven, ablative RT instability in two dimensions (2D), ablative RT evolution in three dimensions (3D) has just begun to be studied.

FAST3D Computation: NRL scientists have recently performed the first, fully 3D simulations of the ablative RT instability, using the newly developed NRL *FAST3D* laser-matter interactions (LMI) code, an extension of our *FAST2D* [1]

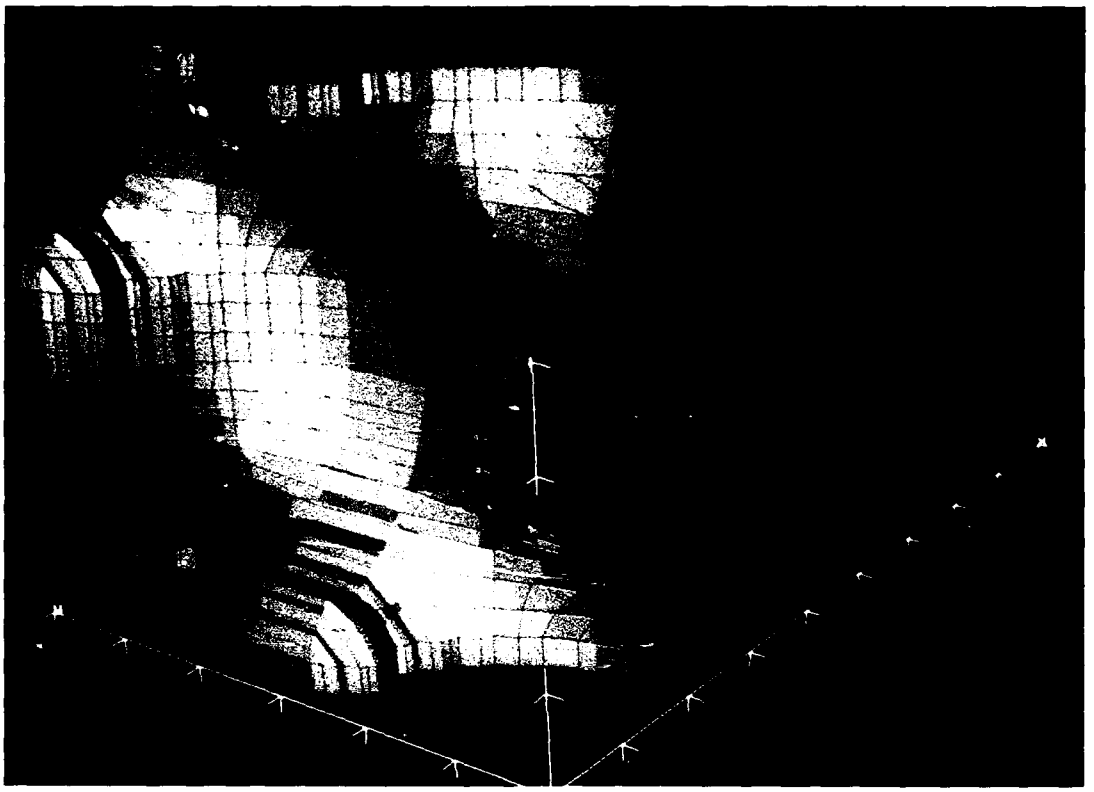

Fig. 7 — The laser-irradiated, RT unstable target surface at 4.5 ns looking toward the laser from the interior of the target

algorithm. This code solves the 3D Euler equations of compressible flow, coupled with an energy transport through the plasma by classical Spitzer thermal conduction. Laser energy is deposited in the plasma by inverse bremsstrahlung. The present simulations are of a 100-μm thick plastic target irradiated by a uniform red (1.054-μm) laser beam at an intensity of 3×10^{13} W/cm^2.

3D Results: Comparison of these new 3D results with previous 2D RT simulations [2] shows that although the 3D instability evolves identically with its 2D counterpart during the linear phase, nonlinear evolution differs significantly. In the linear phase, ring vortices grow up around each of the 3D target protrusions (spikes) and indentations (bubbles), where vorticity is the curl of the velocity flow field. Early in nonlinear development, the ring vortices begin to interact with each other and also with the streaming blow-off plasma. These interactions lead to vortex tilting and stretching that are intrinsically 3D hydrodynamic mixing mechanisms. The evolving vortices significantly alter the flow pattern near the target. Subsequently, the 3D RT spikes are observed to be wider in cross section and extend further toward the laser than do the 2D spikes at identical times in the nonlinear evolution. Figure 7 shows a plot of the 3D irradiated target surface after 4.8 ns. For this simulation the target was initialized with a 3.5% single mode perturbation. The viewpoint is as if one is looking from the interior part of the target towards the laser. The RT "spike" is the broad, gentle concavity in the center of the surface. The "bubbles" are the convex regions circled in blue.

The difference between the 2D spike and the 3D spike indicates the presence of a 3D mass transfer or mixing mechanism. Direct evidence of this mechanism is displayed in Fig. 8, a plot of vorticity lines at the same time, spatial region and viewpoint as in Fig. 7. The coral side vortices and

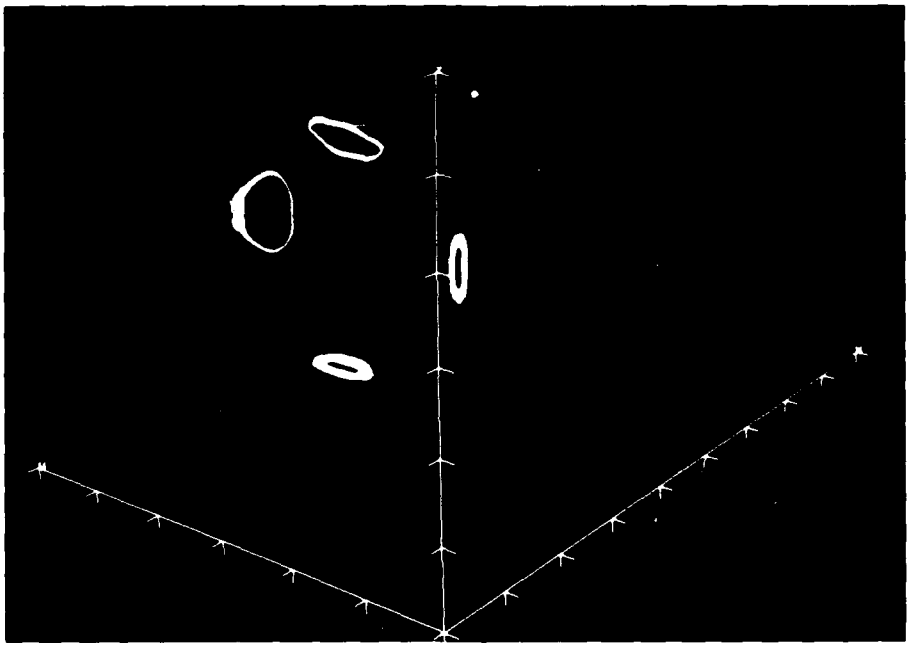

Fig. 8 — Vortex lines for the same time, spatial extent, and perspective as in Fig. 7. The coral and gold vortices have tilted to be parallel to the evolving RT spike.

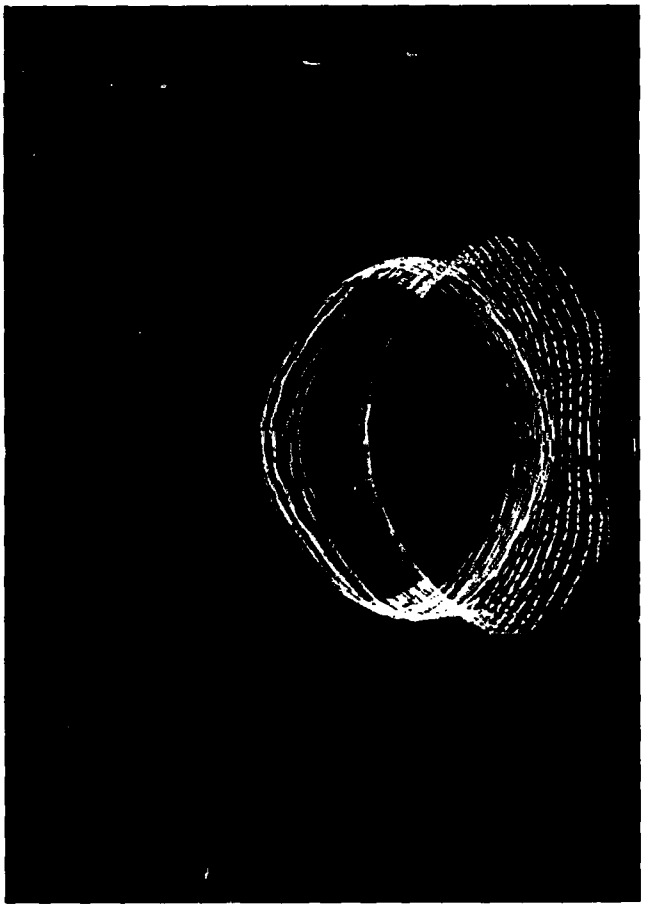

Fig. 9 — An enlargement of the green vortex of Fig. 8, looking from the laser. This vortex is undergoing a rippling instability.

gold top and bottom vortices are tilting into planes parallel to the spike surface, thereby entraining more mass from the bubble and feeding it to the spike. In a strictly 2D situation, these vortices are unable to tilt out of planes initially parallel to the target, and mass transfer from bubble to spike is reduced.

Figure 9 shows another hydrodynamically interesting transition mechanism. This figure depicts an enlargement of the green vortex ring of Fig. 8 looking from the laser side. The ring vortex has been convected away from the RT unstable interface and has a diminishing influence on the target hydrodynamics. However, the interaction of the various vortex rings has introduced 3D perturbations to this vortex ring, which is now undergoing rippling and stretching. These lead to additional 3D instabilities that will eventually break up the flow into turbulent behavior.

Significance: By means of *FAST3D* LMI simulation results reported here, we have observed evidence of the basic 3D hydrodynamic rippling instability to which a ring vortex is subject. More importantly, we have identified a new ablative RT mass transfer mechanism that arises through vortex tilting. These results thus have application to both basic hydrodynamic research and to the design of laser fusion pellets.

[Sponsored by ONR and DOE]

References

1. J.H. Gardner, M.J. Herbst, F.C. Young, J.A. [illegible]nper, S.P. Obenschain, C.K. Manka, L.J. [illegible]rney, J. Grun, D. Dustin, and P.G. Burkhalter, *Phys. Fluids* **29**, 1305 (1986).
2. M.H. Emery, J.P. Dahlburg, and J.H. Gardner, *Phys.Fluids* **31**, 1007 (1988).

INFORMATION TECHNOLOGY

Modern battle management is composed of a number of integrated components; one is communication. Secure transmission of battle information and its subsequent timely processing is paramount to battle success and related research addresses artificial intelligence, parallel computing, information security, and human-computer interactions. Reported in this chapter is work on the analytical evaluation of special function integrals, software for controlling mission-critical real-time processes, and human-computer communications.

The Information Technology (5500) Division and the Underwater Sound Reference Detachment (5900) contributed to the work presented here.

Other current research in information technology includes:

- Competition-based learning systems
- SDI network technology
- Intratask force tactical communications

New Interaction Techniques for Human-Computer Communication

R. J. K. Jacob
Information Technology Division

As computers become more powerful, the critical bottleneck in deploying computer-based systems is now often in the user interface, rather than the computer processing. Providing rapid, natural, and convenient techniques for users to indicate their intentions to a system is especially important in time-critical military applications.

At the Human-Computer Interaction Laboratory, we are studying hitherto-unused methods by which users and computers can communicate information. We are presently focusing on obtaining input from the user's eye movements. That is, the computer will identify the point on its display screen at which the user is looking and use that information as a part of its dialogue with the user. For example, if a display showed several ships, a user might request additional information about one of them. Instead of requiring the user to indicate which ship was desired by pointing to it with a mouse or by entering its name with a keyboard, the computer can determine which ship the user was looking at and give the information on it immediately.

Input from the Eyes: People can move their eyes extremely rapidly and with rather little conscious effort. A user interface based on eye movement inputs therefore has the potential for faster and more effortless interaction than current interfaces. However, people are not accustomed to operating devices in the world simply by moving their eyes. Our research focuses on the careful design of new *interaction techniques* to ensure that they are not only fast but that they use eye input in a natural and unobtrusive way.

A further problem arises because people do not normally move their eyes in the same slow and deliberate way they operate conventional computer input devices. Eyes continually dart from point to point, in rapid and sudden *saccades*. Even when users think and view a single object, the eyes do not remain still for long. It would therefore be inappropriate simply to plug in an eye tracker as a direct replacement for a mouse. We must instead develop techniques to extract some higher level intentions of the user that make sense in a user-computer dialogue from the noisy, jittery stream of position data produced by the eyes. In particular, we use a model of eye motions (fixations separated by saccades) to process the eye-tracker data into a stream of input *tokens* that are meaningful to a user-computer dialogue. These tokens are passed on to our User Interface Management System, along with tokens generated by the other, more conventional input devices being used simultaneously, such as the keyboard or mouse.

Inventing New Interaction Techniques: As a specific, but simple example of the kind of interaction technique that might be used with eye input, consider the use of a multiwindow display: Selecting the *listener* window, that is, the context in which keyboard input is to be interpreted, is normally done by using a mouse to point to the window, but this requires sharing the use of a hand between the keyboard and mouse. A less obtrusive approach might be to make the window at which the user is looking implicitly the current focus for the dialogue. Some filtering would be incorporated so that the user could look at other windows briefly without causing excessive context shifts. As another simple example, if the computer presented an output requiring urgent action from the user, it could use recent eye position history to determine whether the user saw it (and perhaps intentionally ignored it) or simply failed to look at it. The latter case would then trigger an audio output.

The interaction techniques currently being studied in our laboratory include: object selection (by dwell time and/or by command button); continuous display of attributes of an eye-selected object (instead of explicit user commands to request display); moving an object by eye selection, then pressing a button down, *dragging*

the object by moving the eye, and releasing the button to stop dragging; moving an object by eye selection, then dragging with the mouse; pull-down menu commands using dwell time to select or look away to cancel the menu, with an optional accelerator button; and forward and backward eye-controlled text scrolling.

We have built a testbed for developing and studying eye-movement-based interaction techniques and installed an Applied Science Laboratories model 3250R eye tracker. We have been developing the filtering and calibration methods needed to extract useful user-computer dialogue tokens from the eye-tracker data, and we are currently developing and experimenting with a range of new interaction techniques.

[Sponsored by ONR]

Symbolic Integration of Special Functions

J. C. Piquette
Underwater Sound Reference Detachment

Theoretical solutions to scientific and engineering problems are frequently formulated in terms of integrals over special functions. It is always desirable to evaluate such integrals analytically, when possible, since numerical integration is not straightforward, and can be costly in terms of computer time. The potential increase in computation speed obtainable by evaluating such integrals analytically might enable certain essential processing to be performed in real time (such as might be required in a combat situation).

General Form of the Integral: An analytical technique has been developed for evaluating integrals of the form

$$I = \int f(x) \prod_{i=1}^{m} R_{\mu_i}^{(i)}(x)\, dx, \qquad (1)$$

where $R_{\mu}^{(i)}(x)$ is the ith type of special function of order μ_i obeying a set of recurrence relations of the general form

$$R_{\mu+1}^{(i)} = a_{\mu}(x)R_{\mu}^{(i)}(x) + b_{\mu}(x)R_{\mu-1}^{(i)}(x) \qquad (2a)$$

and

$$DR_{\mu}^{(i)}(x) = c_{\mu}(x)R_{\mu}^{(i)}(x) + d_{\mu}(x)R_{\mu-1}^{(i)}(x). \qquad (2b)$$

The function $f(x)$ in Eq. (1) can be any reasonably well-behaved function. Special functions that obey the relations of Eq. (2) include most of the special functions of physics, such as Bessel functions, Legendre functions, Hermite functions, and Laguerre functions.

The Method: The approach is based on assuming that the integral (Eq. (1)) can be represented by a *finite* sum over special-function products that are similar to the product term of the integrand. The unknown coefficient functions of these product terms are found to satisfy a coupled set of ordinary, linear differential equations. A method for analytically uncoupling the set is available. This produces expressions for all of the unknown expansion functions in terms of one particular expansion function. This one expansion function is determined by finding *any particular solution* of its differential equation. An important feature of the method is that this uncoupled equation does not contain any special functions. Thus, the method reduces the problem of evaluating Eq. (1) to the problem of finding any particular solution of an ordinary, linear differential equation that contains no special functions.

Symbolic-Mathematics Implementation: The procedure is well suited to implementation in a symbolic-mathematics computing environment. That is, analytical expressions that can algorithmically transform the original integral into the uncoupled differential equation have been derived. The search for a solution of this equation is quite amenable to symbolic-mathematics

calculations. The algorithm obtains the required solution by substituting various standard candidate functional forms to determine whether they can satisfy the differential equation.

This algorithm has been implemented in a fully automatic computer program based on the SMP™ symbolic-mathematics language. Hence, even a user who is unfamiliar with the method can implement it by using this computer program.

For example, a user interested in evaluating the integral

$$I = \int xH_\nu(x)\ dx,$$

where H_ν is the Hermite function of order ν, merely enters the integrand $xH_\nu(x)$ into the SMP symbolic operator defined by the program and the result

$$I = \frac{H_\nu(x) + xH_{\nu+1}(x)}{2(\nu + 2)}$$

is automatically produced. This calculation requires approximately 10 s on a VAX 11/780.

Potential Impact: The algorithm described here has produced analytical results for integrals that have been previously tabulated. Hence, integrals that are not available in standard tables, but that are required in a computer simulation, might be capable of analytical evaluation. Any technical computer program that involves numerical evaluation of integrals over special functions can be potentially operate at much greater computational speed if these integrals can be analytically evaluated by the present method.

[Sponsored by ONR]

Managing Uncertainty in Target Classification Problems

L. B. Booker
Information Technology Division

Classifying targets on the basis of sensor returns and other evidence is a very complex process. The details of this process depend heavily on the characteristics of the sensors being used and on the specificity required of the final classification decision. However, some basic issues must be addressed in all target classification problems regardless of which sensors are involved. Perhaps the most important of these issues is the management of uncertainty. Uncertainty has many potential sources in target classification problems. The uncertainty associated with sensor data and other evidence must be carefully accounted for to help assure that inferences about the implications of that evidence are plausible. Clearly, the reliability of these inferences is critically important in all Navy target classification problems.

The research discussed here has investigated computational schemes for managing uncertainty in target classification problems. This investigation has led to the development of a computer program called the Bayesian Reasoning Tool (BaRT) that efficiently and rationally computes the impact of uncertain evidence on target hypotheses.

Reasoning Under Uncertainty: The key issue in uncertain reasoning is how to represent and compute the many ways belief in one uncertain hypothesis affects belief in other hypotheses. A fundamental assumption made by many computational approaches to uncertainty is that uncertain inferences can be modularized just like logical inferences. An inference of the form "*A implies B with strength S*" is modular in the sense that belief in *B* is updated no matter how our belief in *A* was derived, and no matter what else is known about the problem. This point of view has recently been questioned, however, as it has become clear that uncertain reasoning often must handle dependencies among hypotheses that are inherently not modular. Accounting for these dependencies requires reasoning capabilities that can be difficult to implement by using a collection of modular rules of inference.

An alternative approach to this problem is to abandon the modularity of rule-based updating and represent the relationships among hypotheses

explicitly. This type of representation is available in computational schemes that use probabilistic *belief networks* [1]. A belief network is a graphical representation of the dependencies among hypotheses. Each node in a belief network designates an uncertain variable having a set of mutually exclusive and exhaustive values. The current opinion about which value is correct is summarized by a probability distribution at each node that characterizes the belief for every value. The links between nodes in a belief network use conditional probabilities to quantify how the belief in one node influences the belief in another. Paths through the network efficiently summarize the direct and indirect relationships among hypotheses. The information needed to update the belief in a node is available from the links coming into that node. This makes it possible to use distributed, message-passing computations to propagate the effects of changes in belief. These computations update belief everywhere in the network in a manner that is in strict compliance with probability theory and Bayes' Rule.

BaRT—A Bayesian Reasoning Tool: The primary goal of the BaRT project is to make these state-of-the-art techniques for uncertain reasoning available to Navy researchers building target-classification decision aids. The thrust of our research has therefore been to design and implement a generic tool for hierarchical Bayesian reasoning [2]. BaRT brings together several theoretical ideas about belief networks in a way that is efficient and practical for Navy applications. Decision aids properly constructed using BaRT have the advantage of a solid rationale for the inferences they compute. Moreover, a tool like BaRT will make it convenient to build systems that solve large-scale Navy problems in a coherent way.

Figure 1 shows the overall BaRT architecture. The system is designed to be used interactively as a stand-alone decision aid or as the reasoning component of a more automated target-classification system. Because the belief network updating procedure is inherently parallel, a version of BaRT has been implemented on a parallel computer that is attractive for some real-time applications. Preliminary releases of BaRT have been used as a decision aid for classifying ship images and as the reasoning component for systems doing target tracking and situation assessment.

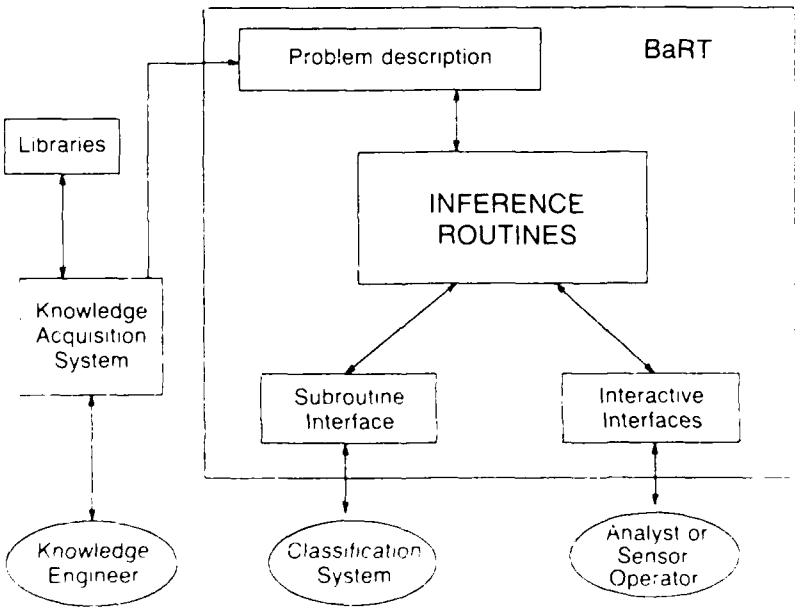

Fig. 1 — BaRT system architecture

Naveen Hota of JAYCOR, Gavin Hemphill of DREA (Canada), and Connie Ramsey have all made significant contributions to this research.

[Sponsored by ONT]

References

1. J. Pearl, *Probabilistic Reasoning in Intelligent Systems: Networks of Plausible Inference* (Morgan Kaufmann, San Mateo, CA, 1988).

2. L. Booker, "Plausible Reasoning in Classification Problem Solving," in *Image Understanding in Unstructured Environments*, S. Chen, ed. (World Scientific Publishing Co., Teaneck, NJ, 1988).

NUMERICAL SIMULATION

Reflecting the age of computers, much fundamental and applied research is performed at NRL around the Cray X/MP supercomputer and the ubiquitous desktop personal computer. This research includes simulation and modeling to interface with the Navy's real-world problems. Reported in this chapter is work on the application of simulation language to communications systems design, techniques for visualizing electronic warfare simulations, and the verification and analysis of electronic warfare scenario environments by visualization and animated graphics displays.

Some of the research performed by the Information Technology (5500) and the Tactical Electronic Warfare Divisions (5700) is presented here.

Other current research in numerical simulation includes:

- Combat management information systems
- Artificial intelligence
- Advanced numerical simulation techniques

Applications of Simulation Languages to Communications System Design

J. Choi
Information Technology Division

Many situations exist, especially for military communications, where explicit performance evaluation defies system analysis and meaningful experimental results can be obtained only through either actual hardware system evaluation or digital computer simulations. While the former approach yields accurate results, it is generally cumbersome, expensive, time consuming, relatively inflexible, and difficult to pursue detailed parametric studies for subsystem specifications. The latter approach is less time consuming and very flexible, but greater care must be taken to verify the accuracy of the result.

Deployed electronic warfare (EW) systems often do not have the capability required to match current and emerging operational requirements, and the continuing effort to upgrade them is expensive and time consuming. Because future communication systems are expected to be more complex and adaptive, it is critical that the future EW systems be designed to be rapidly reprogrammed in response to the changing battlefield threat. To reduce these costs, time, and challenges, it is necessary to design and build both flexible and general-purpose threat communication simulation and countermeasure systems that are accurate, unobtrusive, and easy to use.

Objective: The main purpose of the interactive communication systems simulation model (ICSSM) implementation at NRL is to support, enhance, and extend the present capability of NRL's Counter C^3 Communication Laboratory; problems can then be solved by using analysis without making extensive hardware changes to the existing counter C^3 facilities. ICSSM also supports high-level system design concepts by use of quick-look simulations for advanced system design and development, performs rapid comparison studies for alternative system configurations, supports detailed subsystem or unit specifications and performance characteristics by means of detailed parametric studies, and validates measured imperfections of system design for further implementation.

Simulation Capabilities: ICSSM simulation language consists of executive control programs, model definition and configuration programs, postprocessing programs, and a library of communication systems modeling elements and analysis subroutines. The software structure of the ICSSM has the following characteristics.

- It is general enough to allow virtually any system to be simulated that is reducible to a block diagram.
- It provides a flexible, expandable, general, and easy-to-use means to configure specific communication systems requirements, to evaluate new techniques, and to assess the performance of existing or proposed systems and equipments.
- It defines a communication systems simulation model as a network of connected preprogrammed subroutines and modules representing functional elements of communication links or measurement devices.
- It includes a convenient means to alter or expand a previously configured simulation model, to execute portions or submodels of a more elaborate model, to drive a model with data obtained from sources external to the simulation, and to checkpoint and monitor simulation executions.

Libraries of mathematics, statistics, and special functions have been implemented to strengthen the simulation capabilities. These libraries also extend its applications to control system analysis and digital filter design/digital signal processing for radar, optical data transmission, and underwater acoustics applications. The simulation facility consists of a

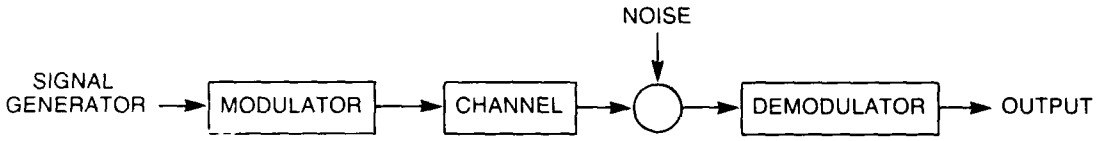

Fig. 1 — Communication system model

VAX station II with extended 230-megabytes memory hard disk, TK50 tape cartridge driver, and RX50 dual diskette driver.

Simulation Test Models: Figure 1 shows one of the simplest communication system models. This model is configured and simulated by the sequential process of generating a signal, modulating it, corrupting it by artificial noise (jamming) and natural channel noise, demodulating it, and analyzing the received signal in various ways. During the simulation process, several parameters can be characterized by observing the demodulator output results or error detector outputs and comparing the input and output signals. *Those parameters are:*

- signal characteristics (such as signal duration, amplitude, number of information bits, sampling period, number of samples per chip, or duty cycle),
- modulation types (such as ASK, PSK, FSK, QPSK, BPSK, or MSK) and parameters (such as modulation, bandwidth, amplitude, reference frequency, or sight frequency),
- channel characteristics (such as signal-to-noise ratio, peak input signal amplitude, or normalized IR/RF bandwidth),
- demodulator/error detectors (such as number of reference bits, reference increments, number of decoder bits, or decoder increments), and
- postprocessor output (such as waveform plots, continuous/sampled IQ plots, eye diagram, error histogram, or symbol error statistics).

Figure 2 shows the output spectra of a PSK modulator and PSK demodulator interrupted by artificial and natural channel noise when a triangular signal is applied to the system.

Conclusions: The formulation or processing of electronic countermeasure (ECM) simulation modeling is readily feasible with minor adjustments or modifications depending on specific mission requirements and applications. ECM techniques implementation using digital computer technology are more generic in nature and are sufficiently flexible to allow new techniques to be implemented by means of software modifications rather than costly and time-consuming hardware changes. Future EW systems, thus, will be more adaptive in nature, allowing countermeasures tactics to be modified during an engagement, based on measured effectiveness, thereby increasing the probability of survival. Future counter C^3 communication systems research areas are: (1) the study of more intelligent, high-leverage jamming techniques; (2) the identification and definition of techniques for exploitation of communication signals with emphasis on deception techniques and real-time countermeasure assessment algorithm; (3) the analysis of the interaction of simultaneous operation among antijamming communications systems, counter-communication systems, and communication exploitation systems; (4) the evaluation of system performance with parametric values and comparison between actual systems test results and simulation results; and (5) the development of measure of ECM and counter-ECM effectiveness for both existing and proposed techniques. The application of simulation languages to communication system design and analysis holds great promise and may be extended to wide applications such as communication

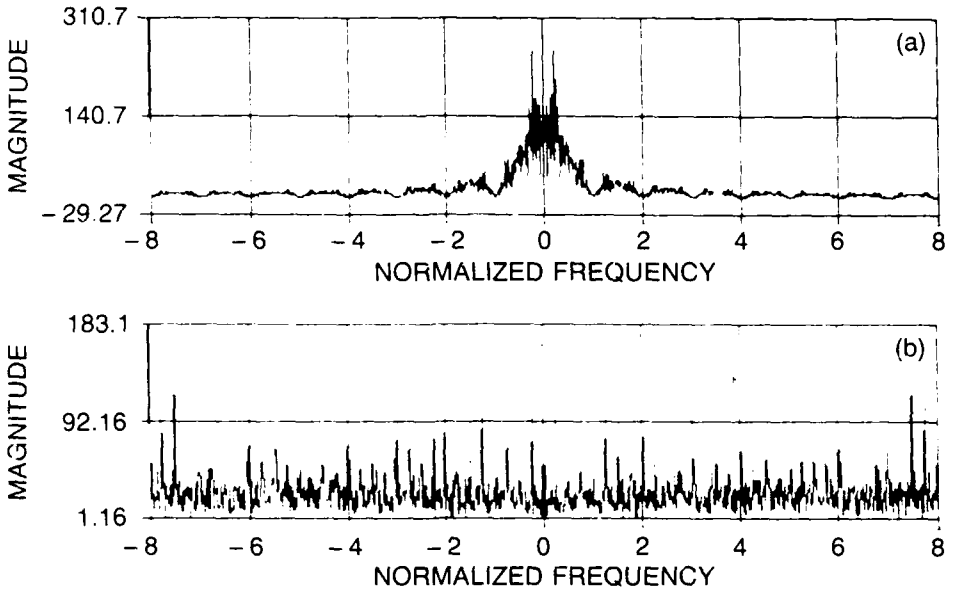

Fig. 2 — Waveform after an application of triangular signal

networks, satellite communication, radar system design, signal analysis, and many advanced signal processing areas.

[Sponsored by NAVAIR]

Bibliography

W.D. Wade, M.E. Mortara, P.K., Leong, and V.S. Frost, "Interactive Communication Systems Simulation Model-ICSSM," *IEEE J. Selected Areas Commun.* **SAC-2**(1), 102-128 (1984).

User Manual for Interactive Communications Systems Simulation Model (ICSSM), published by the ICSSM User's Group, Rome Air Development Center, RADC/DCLF, Griffiss AFB, Rome, NY, July 1988.

Visualization Enhanced EW Simulations

A. A. Di Mattesa
Tactical Electronic Warfare Division

Understanding the role and effects of EW in the combat process is a problem frequently assigned to simulation. As EW assumes a multidimensional responsibility throughout the battle timeline (warning and targeting, force projection, and terminal defense), visual analytical methods are needed to assess the effectiveness of various EW concepts, systems, and tactics. The application of the computer-based field of visualization in scientific computing (ViSC) to EW provides insight into the complex processes resulting from the introduction of electronic countermeasures (ECM) into the tactical engagement area. Visualization computation transforms the symbolic into the geometric, enabling researchers to observe their simulations and computations—in essence, to see the unseen. It embraces both image understanding and image synthesis [1].

Research is being conducted to model complex engagement scenarios featuring EW and to develop methods whereby the large amount of data produced can be readily examined and analyzed. The latter efforts are conducted under an exploratory research and development (R&D) task titled Electronic Warfare Visualization Laboratory (EWVL) (Fig. 3), in support of a larger EW simulation project referred to as Coordinated EW Simulations (CEWS). The thrust of the EWVL is twofold; first to develop tools for interpreting the

Fig. 3 – R. Normoyle, of Quest Research Corporation, develops a real-world graphics representation of a tatical missile/EW engagement using an E&S PS300 series graphics display system that is part of the EWVL

data produced by use of simulations and, second, to generate a database of geometric images for use in EW R&D.

Early Efforts: The Central Target Simulation (CTS) Facility has proven itself as a valuable tool in determining the effectiveness of ECM against missile threats. This facility, where hardware-in-the-loop tactical engagement simulations are conducted, includes the physical means to exercise actual ECM and missile systems under simulated tactical situations to develop, test, and evaluate the relative merits of various countermeasures. The real-time nature of the simulations produces large quantities of data that typically required an inordinate amount of time to analyze effectively. A natural requirement existed to develop a method for presenting the engagement process from a real-world perspective as it unfolded in the simulation. This requirement precipitated the early research into scientific visualization. By viewing the real-time simulation data in various representations and from different real-world perspectives, the researcher could achieve an intuitive understanding of the resulting interactions. Thus the researcher would be able to analyze more information at a faster rate and determine instantaneously the relative advantages and disadvantages of the EW concept without requiring countless hours of postrun analysis. The utility of this effort was demonstrated by using an Evans and Sutherland (E&S) PS-300 series interactive graphics system. The resulting work allowed researchers involved in EW simulations to employ sophisticated computer graphics to optimize design solutions. Figure 4 is an illustration of the early graphics developed for real-time display of CTS simulations. Today this capability is employed in the CTS facility to test and evaluate new EW concepts and designs.

Current Research: Current efforts are focused in three major areas. The first involves hardware upgrades that only recently have become available to fully exploit visualization capabilities. The second addresses the development of visualization software and data bases, while the third focuses on applications. Graphics work-stations, which offer the power of high-speed computations combined with sophisticated

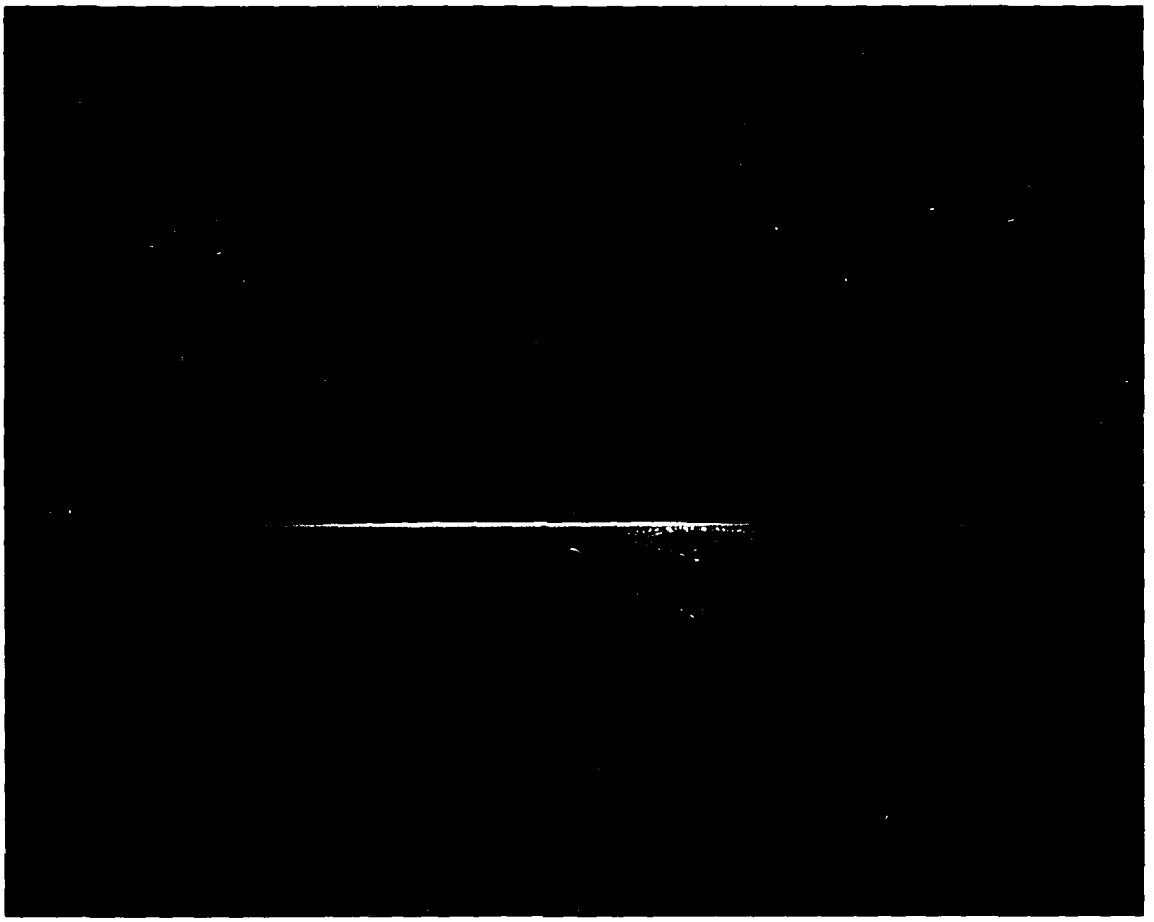

Fig. 4 – Early representation of a tactical missile/EW engagement simulation conducted in the CTS. An E&S PS330 graphics system is used to display in real-time geometrically accurate images of a ship, chaff, and missile.

graphics displays, are being incorporated into EWVL. A Silicon Graphics IRIS-4D Superworkstation is being integrated into the CTS and CEWS projects to provide the visualization capabilities previously performed on the E&S system. Existing geometric shapes and platforms and other relevant data are being converted for real-time, nonreal-time, and video taping of simulation results. The goal of this thrust is to standardize a common workstation configuration where individuals are able to share the visualization software that has been developed. Visualization software for image development is being directed toward achieving the proper mix of interactivity vs photorealism to create the desired effect for maximum insight into complex EW engagement processes. This entails developing methods to display multidimensional, unpredictable, real-time dynamic data in an artistically appealing and easy to comprehend manner, while simultaneously showing the overview of the simulation results and the importance of any fine detail in the simulation as it is occurring. Too much detail about a specific model's attributes such as color or intensity is not valuable to a researcher interested in the interaction of ships, aircraft, and decoys against a missile. Conversely, a researcher interested in radar cross-section (RCS) reduction would have a keen interest in a model's fine grain detail. The geometry of nature (fractals) offers a powerful solution to ViSC problems. Fractals allow complex structures such as those found in

Fig. 5 – Improved graphics of a tactical missile engagement simulation featuring a realistic view of the ship, missile, and chaff. The natural scene of the ocean and clouds is formed by using fractal geometry.

nature to be reduced to a simple compact equation that can be stored, reproduced, and modified to represent graphically these structures in astonishing detail. Figure 5 shows visualization graphics of an ocean and clouds by using fractal equations. The most beneficial aspect of these efforts involves the application of ViSC products to EW problems. As illustrated in Figs. 4 and 5, the insight into examining these simulations from an interactive real-world perspective provides the researcher with the ability to achieve an intuitive understanding of the EW problem. A direct benefit is also provided to the training community where solutions to complex problems are readily illustrated and easily understood by nontechnical personnel.

The research discussed is applicable to all three services and is supported by the Joint Directors of Laboratories (JDL) Technology Panel for Electronic Warfare (TPEW). To maximize service interaction, a Memorandum of Agreement (MOA) had been drafted that will partition ViSC efforts between each service on the basis of their specific interests and thereby serve to eliminate duplication.

R. Normoyle of Quest Research Corporation and B. McGhee and T. Ricci of NRL continue to provide significant contributions to this ongoing research.

[Sponsored by ONT]

Reference

1. B.K. McCormick et al., ed. "Visualization in Scientific Computing," *Computer Graphics* **21**(6) (1987).

Visualizing Electronic Warfare Simulations

M. R. Bracco and M. J. Davis
Tactical Electronic Warfare Division

Electronic Warfare: Controlling the electromagnetic spectrum for the use of friendly forces and preventing or hampering its use by hostile forces is the goal of electronic warfare (EW). In the battlefields of today and tomorrow the use of sophisticated radars, radar jammers, decoys, and deception techniques will be the deciding factor between victory and defeat.

The Effectiveness of the Naval Electronic Warfare Systems (ENEWS) program of the Tactical Electronic Warfare Division was established to provide the Navy with accurate, unbiased projections of the effectiveness of proposed and actual EW systems. In pursuit of this goal, computer, laboratory and Fleet simulations are conducted. Large-scale computer simulation of both the actual systems to be evaluated and the environments in which they may be operated were developed. The technique of separating the environments from the systems allows multiple systems to be fairly evaluated in identical environments and allows the evaluation of a single system in multiple environments.

Scenarios: The situations modeled in a multiple engagement scenario are often at an overwhelming level of complexity to the users of the scenario. Imagine starting with five-hundred land sites, then adding the movement and tactics of several hundred land sites, then adding the movement and tactics of several hundred ships, submarines, aircraft, and missiles; each of which contains a number of electronic emitters that switch operating modes according to how they perceive the environment. Attempting to remember and comprehend all of these interactions would tax even the most experienced EW specialist.

To solve this problem, a series of tools has been developed that provides the ability to view and interact with a scenario in a way that takes full advantage of the visual nature of the human mind. Also, the tools provide the user with intelligent assistance in the retrieval, modification, and integration of the detailed information available from the scenario.

VIEWER and TRACKER: EW simulations are developed and run on the ENEWS dual VAX 8650 computer cluster. Connected to each VAX is a Ramtek 4225 color graphics display, an intelligent graphics workstation. The scenario VIEWER program makes use of the Ramteks to provide a full color, animated presentation of the scenario. Figure 6 shows an Eastern Mediterranean scenario in which a carrier task force is being engaged by hostile aircraft armed with antiship cruise missiles. Navy Tactical Data System (NTDS) symbology is used to represent the platform positions and these symbols are color coded *blue* for friendly and *red* for hostile. An on-screen menu on the right-hand side of the display permits the operator to control the program with a mouse. This operator control extends to all aspects of the display including the size of the viewed area, the animation speed, and the highlighting or thinning of selected platforms. When more than a visual overview is required, the user has a wide range of options to call up detailed information about individual or entire classes of platforms.

The TRACKER program, a second generation extension of the VIEWER, can generate the motion of any platform interactively on the map display while viewing the relative position and motion of all other platforms. Artificial intelligence techniques are incorporated to check that the motion created is valid and to suggest alternatives when inconsistences are detected in the input. This frees the scenario builder from the time consuming and error-prone tasks of calculating speed, acceleration, turning radius, and Earth surface position. Figure 7 shows the motion of an aircraft being created with the TRACKER program.

With the introduction of a means to interactively view and modify an electronic

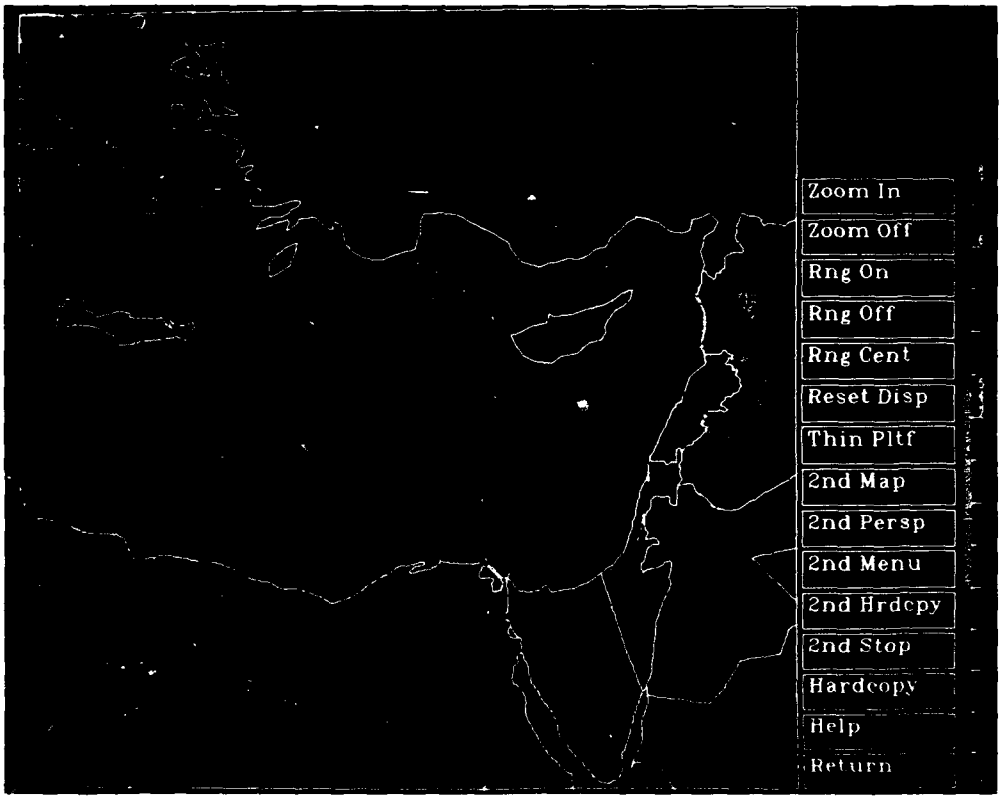

Fig. 6 — An Eastern Mediterranean scenario; a friendly carrier task force engaged by hostile, antiship cruise missiles

Fig. 7 — The creation of an aircraft's motion with the TRACKER program

environment, we have provided an important tool for the visual verification of scenarios. A common frame of reference now exists for the exchange of ideas between the scenario builders, system modelers, and program sponsors. VIEWER and TRACKER have enhanced the ENEWS program's ability to simulate the complex environments that tomorrow's Navy may face.

[Sponsored by NAVAIR]

OPTICAL SYSTEMS

Research in optical sciences is directed, in part, toward holography, optical warfare, optical data processing, space optics, laser-matter interactions, wave guide technology, and IR surveillance. Fiber optics research and improved versatility and powers of lasers are also addressed. Reported in this chapter is work on the stability of material for use in space optics; high-frequency, wide-bandwidth spectrum analysis; and multiplexing for fiber optic sensors.

This work is performed by Optical Sciences Division (6500).

Other current research in optical systems includes:

- Amplification of weak optical signals
- Electro-optic probing of high-speed electrical circuits
- Laser chemical kinetics
- Solid state lasers
- UV countermeasures

Dimensional Stability of Materials for Space Optics

P. L. Higby, C. G. Askins, and E. J. Friebele
Optical Sciences Division

Background: Mirrors used in space applications such as surveillance have very strict surface figure and finish requirements. Simply stated, the surface of the mirror cannot deviate from its specified optical figure by more than the equivalent of 1 in. over 2000 mi (or 7 parts per billion) [1]. Therefore, the materials used for fabricating the mirrors must be dimensionally stable throughout the mirror's on-orbit lifetime, which may involve thermal cycling from moving in and out of the sun's rays, bombardment by atomic oxygen, exposure to ultraviolet solar radiation, and ionizing radiation from cosmic rays, charged particles, etc. The materials of choice should have very small coefficients of thermal expansion (CTE) so that they will maintain their dimensions under temperature gradients, even after they have been exposed to the various kinds of radiation present in space.

The Optical Materials Research Group has designed and implemented a high-sensitivity apparatus to measure the CTE of candidate mirror substrate materials. Since ionizing radiation is known to result in changes in the atomic arrangements, which are sufficient to cause densification in most nonmetallic materials, the study had two objectives: (1) to observe and characterize the change in length of the low-CTE samples as the temperature is cycled from ambient to 150 K; and (2) to measure how the expansion characteristics change when the sample is exposed to ionizing radiation.

CTE Apparatus: The high-sensitivity measurement of the change in length is performed with a double Michelson interferometer (Fig. 1). The vacuum chamber containing the critical optical paths is sealed and evacuated after proper alignment. The temperature of the sample is then decreased by allowing cold nitrogen gas to flow

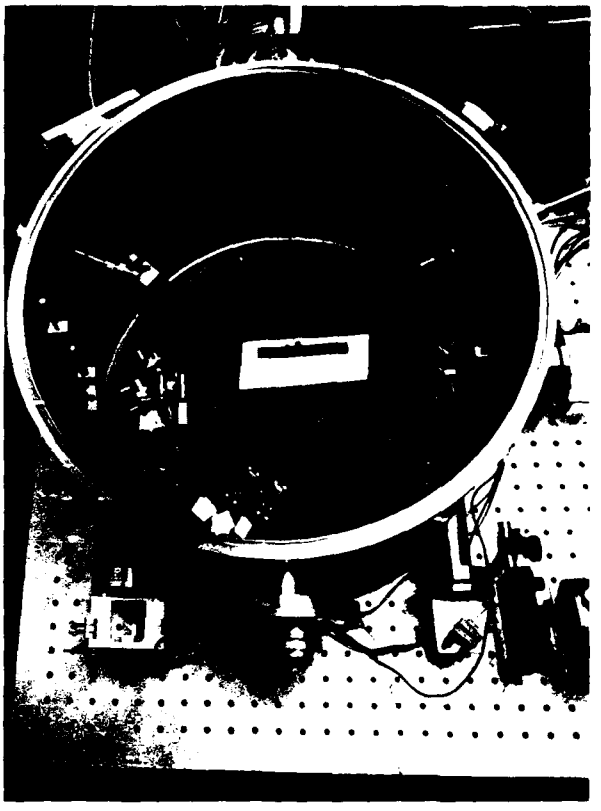

Fig. 1 — NRL double Michelson interferometer

though a cylindrical jacket that surrounds the sample. Each interferometer compares the distance from a beam splitter to one end face of the sample with the distance from that beam splitter to a reference mirror common to both interferometers. As the relative path lengths between the reference and sample arms change, the fringe motion is monitored by computer; the sum of the change in the lengths measured by the two interferometers is the net change in length of the sample. The NRL instrument has at least 20 times the sensitivity of similar interferometric dilatometers [2] owing to innovative signal processing and improved optical design. A length change smaller than 1 nm is detectible, with absolute accuracy better than 6 nm.

Results: The raw data were collected in the form of change in length Δl as a function of temperature and must then be normalized by the starting length l of the sample to obtain $\Delta l/l$. The CTE is the derivative of $\Delta l/l$ vs temperature.

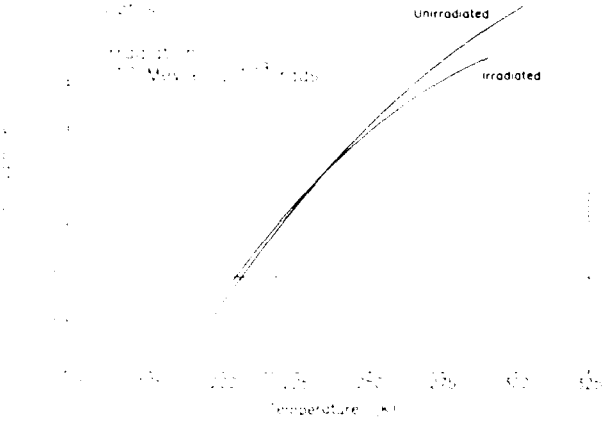

Fig. 2 — CTE of unirradiated and irradiated vitreous silica

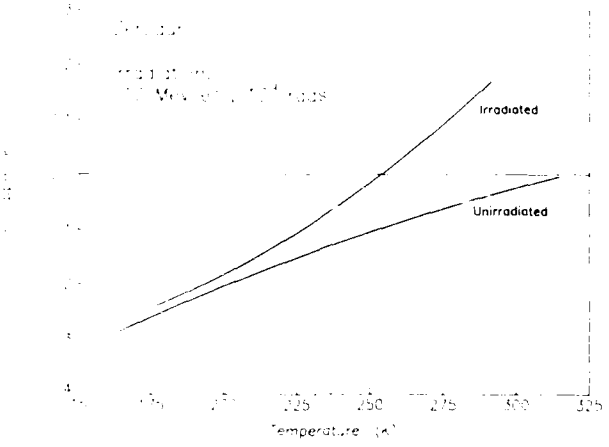

Fig. 3 — CTE of unirradiated and irradiated low-CTE glass-ceramic

Figures 2 and 3 show typical results of experiments performed by use of the NRL apparatus. Optosil, the material in Fig. 2, is vitreous silica made by fusing natural quartz in an oxygen-hydrogen flame; the temperature at which its CTE equals zero is approximately 205 K. A radiation dose of 1 billion rads, which is typical of that experienced by an unshielded mirror during 10 years in orbit, causes a negligible change in the CTE between 150 and 300 K. The material in Fig. 3 is Zerodur, a low-CTE glass-ceramic containing two phases: a crystalline phase having a negative CTE, and a glassy phase with a positive CTE. The composition and relative concentrations of the two phases are optimized so that the net CTE of the composite material is near zero at room temperature. Note that a radiation dose of 1 billion rads results in a large change in the expansion behavior of Zerodur.

The dimensional stability of space optics becomes more and more crucial as an increased amount of information is needed from space surveillance. The method described here is a reliable way to perform research on low-CTE materials and to screen such materials for suitability for use in space before a large, expensive mirror is fabricated and might possibly fail under test. We have demonstrated that the CTE of some materials is affected by high radiation doses, and optics fabricated from them must be shielded from the space environment if they are to maintain their optical figure. However, we have also been able to demonstrate that certain materials appear to be fairly dimensionally stable in the space radiation environment.

Ms. Jackie A. Ruller of Sachs/Freeman Association contributed to this work.

[Sponsored by the Rome Air Development Center]

References

1. C.J. Pelleerin, F. Ayer, Y. Mehrotra, and A.K. Hopkins, "New Opportunities from Materials Selection Trade-offs for High Precision Space Mirrors," *SPIE Optical Fabrication and Testing Workshop: Large Telescope Optics* **542**, 5-18 (1985).
2. E.G. Wolff and R.C. Savedra, "Precision Interferometric Interferometer," *Rev. Sci. Instrum.* **56**, 1313-1319 (1985).

Time-Division Multiplexing for Fiber Optic Sensors

A. D. Kersey and A. Dandridge
Optical Sciences Division

Background: Fiber-optic sensors offer many advantages over conventional sensors including high sensitivity, light weight, immunity to

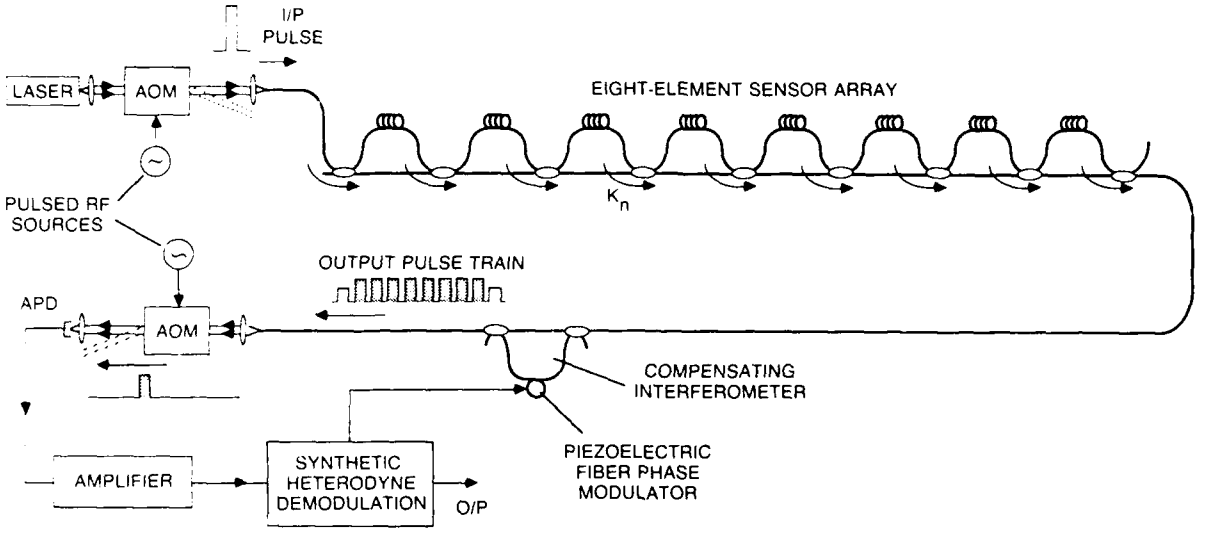

Fig. 4 — Eight-element telecommunications system architecture (TSA) multiplexed sensor system

electromagnetic interference (EMI), and ease of fabrication. A major effort has been underway since 1978 to develop fiber-optic sensors for a variety of Navy systems including tactical and ASW surveillance systems, shipboard damage control, and various process and motor control applications. Many of the applications for fiber-optic sensors require multisensor systems, for example, high-sensitivity acoustic sensor arrays. Currently, research is being directed toward the development of all-optical, multisensor systems that combine optical fiber sensing with a means to telemeter sensor information along fiber links. Such an all-fiber, multisensor network has several advantages over conventional electrical multiplexing/data collection schemes. First, because of the large transmission bandwidths of optical fibers, the telemetry system is, technically, capable of supporting a large number of sensors. Second, the network operates passively without the need for electrically active components and thus the whole network retains a low intrinsic susceptibility to EMI. The ability to couple fiber sensor technology and fiber telemetry to form passive all-optical networks is crucial to the successful development of fiber-optic acoustic sensor technology in a broad range of application areas.

Multiplexing techniques: We have developed a number of multiplexing techniques that have the potential to service 30 or more sensors by using a single pair of fibers. These approaches use different forms of remote interrogation of the interferometric sensor, the output of which is proportional to the energy of the field to be measured. Both time- and frequency-division multiplexing (TDM, FDM) have been investigated; however, most of the developmental work has been on TDM-based schemes. Figure 4 shows one array architecture that has been developed. Pulsed light from a laser source is launched into the input fiber and coupled to the series of sensor elements each of length L. A small fraction κ_n of the optical power in this fiber is tapped off to an output fiber bus at points between each sensor element and at points before the first and after the last elements. If the width of the input pulse is less than the optical propagation delay τ in each sensor element, the output obtained from the array consists of a series of $N + 1$ pulses that are separated in the time domain. Apart from weak cross-talk effects these pulses carry no direct interferometric information. Applying this output pulse train to a compensating interferometer of optical path imbalance L coherently mixes pulses obtained from consecutive tap points. A series of

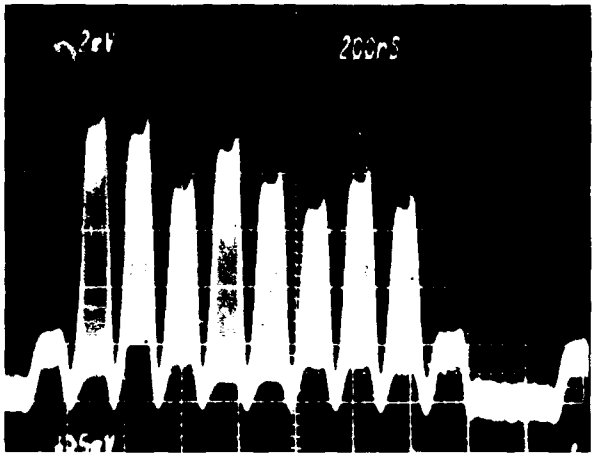

Fig. 5 — Optical pulse train at the compensator output without demultiplexing (note central 8 pulses carry interferometric information from the sensors)

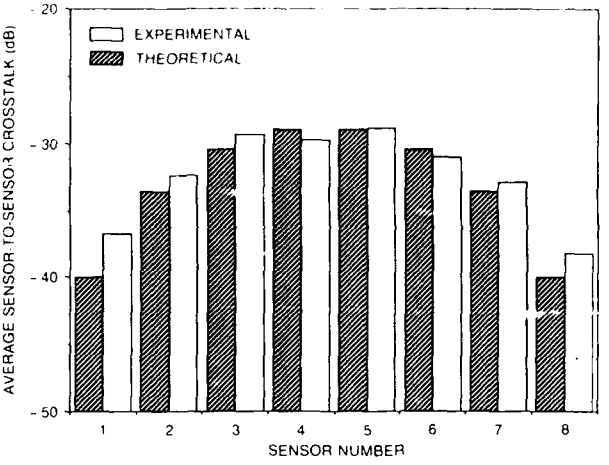

Fig. 6 — Comparison of theoretical and experimentally observed average cross talk level for each sensor

$N + 2$ output pulses is thus generated at the output of the compensating interferometer, the central N of which carry information generated by the N sensor elements. Time-division demultiplexing of this output pulse train can then be used to address individual sensors.

Operation: An eight-sensor system has been constructed and tested; the optical pulse train produced at the output is shown in Fig. 5. These signals are then time demultiplexed and demodulated to allow each sensor to be separately interrogated. This array architecture is optically efficient, has low noise, and uses commercially available fiber optic components.

Most multiplexing architectures exhibit no direct optical cross talk. The system shown in Fig. 4, however, is subject to direct intrinsic optical cross talk between the sensors in the array owing to the multiple cross-coupling of optical pulses between the sensor fiber and the output collection fiber. This cross talk in the array has been both theoretically analyzed and experimentally determined. Figure 6 shows the good agreement between the measured average cross talk experienced by each sensor and those theoretically predicted by our models.

[Sponsored by ONT]

Bibliography

A.D. Kersey, K.L. Dorsey, and A. Dandridge, "Demonstration of an Eight-Element Time-Division Multiplexed Interferometric Fiber Sensor Array," *Elec. Lett.* **24,** 689 (1988).

A.D. Kersey and A. Dandridge, "Distributed and Multiplexed Fiber-Optic Sensor Systems," *J. Inst. Elect. Radio Eng.* **58,** S99 (1988).

SPACE RESEARCH AND TECHNOLOGY

NRL has been involved for many years with various aspects of space research in the fields of astrophysics and astronomy, atmospheric science, and solar-terrestrial interactions, as well as with spacecraft engineering and systems development. Reported in this chapter is theoretical and observational work relating to plasma clouds, space chemistry, solar phenomenon, weather predictions, and the development of space hardware.

This work was performed in the Space Science Division (4100), the Laboratory for Computational Physics and Fluid Dynamics (4400), the Plasma Physics Division (4700), and the Space Systems Technology Department (8300).

Other current research in space and technology includes:

- Solar spectrograph development
- Oriented scintillation spectrometry
- Space testing of solar cells and concentrator systems
- Instrumentation for shuttle missions

3D Dynamics of Ionospheric Plasma Clouds

S. T. Zalesak, J. D. Huba, and
M. J. Mulbrandon
Plasma Physics Division

Many military systems, such as C^3I and surveillance, operate in the plasma (ionized gas) environment that surrounds earth. This plasma may be naturally produced, as in the case of earth's ionosphere, or may be artificially created, as in the case of a nuclear explosion. The degradation of these systems depends critically on the degree to which the plasma is structured (i.e., electron density irregularities). This degradation occurs because of electromagnetic wave scattering and absorption. An understanding of the structuring process, the process by which these irregularities are generated and maintained, is critical to being able to predict the environment under which a military system will have to operate. A significant effort has been undertaken at NRL to understand these processes.

Two key questions relevant to the structuring process are the following: First, what are the mechanisms and time scales by which large plasma structures attain scale sizes that adversely effect military systems? And second, what are the physical parameters that determine the long-term persistence of these structures once they are formed? The first question is reasonably well understood. Large plasma structures break up (i.e., bifurcate) into smaller ones because of the onset of plasma instabilities (such as the gradient drift, Rayleigh-Taylor, current convective, and/or Kelvin-Helmholtz instabilities). The question regarding plasma irregularity persistence remains unanswered. Strong evidence exists that when an ionospheric plasma structure is smaller than a few hundred meters in diameter (transverse to earth's magnetic field), further reduction in size by these instabilities ceases. This phenomenon is known as *freezing*. The physical mechanisms contained in existing two-dimensional (2D) theoretical and computational models of plasma structuring predict diameters of a few tens of meters and cannot explain this large transverse diameter. The goal of our research is to develop new models that can describe the freezing phenomenon.

Improved Structuring Models: Most of the models of plasma structuring are based on two approximations. The first is that the magnetic field lines can be approximated as equipotential lines. This is because the electrical resistivity along the magnetic field is extremely small in the ionosphere. Effectively, all plasma along a given magnetic field is electrically connected, and the plasma can be thought of as having been collapsed onto a single 2D plane perpendicular to the magnetic field. The second approximation follows from the first. It can be shown that for a 2D plasma, plasma pressure has no effect on plasma evolution and hence can be neglected.

The equipotential approximation is extemely good for transverse scale sizes larger than a kilometer but starts to break down for scale sizes of several hundred meters, which are sizes relevant to the freezing phenomenon. The work we describe here involves (1) the elimination of the equipotential approximation, i.e., we consider three-dimensional (3D) plasma dynamics, and (2) the introduction of the pressure into the equations of motion. We find that a consideration of these two pieces of improved physics yields fertile ground for an explanation and understanding of the freezing phenomenon.

Analytic 3D Models: We have developed an analytic model of 3D ionospheric plasma clouds (man-made plasma structures) based on an idealized model [1,2]. The purpose of this research is to understand the underlying 3D physical processes that can lead to cloud stability, i.e., resistance to bifurcation. We consider a spheroidal cloud of constant plasma density immersed in a uniform plasma of a lower density. We impose a uniform neutral wind on the cloud transverse to the magnetic field, perturb the surface of this cloud, and monitor the evolution of these perturbations. If all of these perturbations damp in time, then the

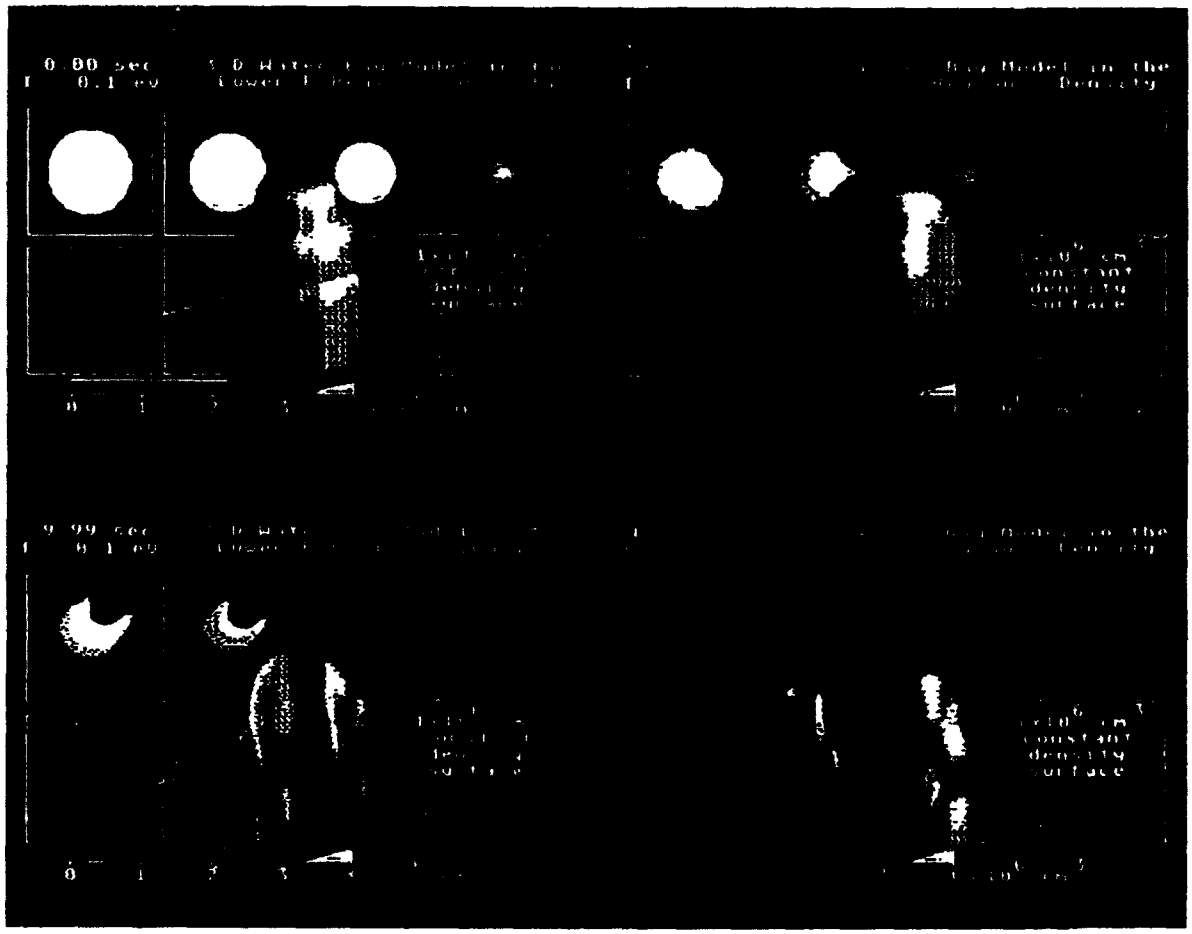

Fig 1 — 3D simulation of a *cold* ionospheric barium cloud where T = 0.1 eV

cloud is stable or *frozen*. We find that for sufficiently small clouds (along the magnetic field), or sufficiently large pressures (i.e., temperatures), stabilization is achieved by means of a shearing mechanism that wraps the imposed perturbation around the cloud in a pattern similar to that on a barber pole. This pattern is the result of a shear in plasma flow, both radially transverse to the magnetic field and vertically along the field, which is caused by an imperfect balance between electric field and pressure gradient forces acting on the plasma. This stabilization only occurs because of the 3D dynamics included in the analysis. However, the model does leave something to be desired since the plasma cloud density model is oversimplified, and since ion inertia has been neglected.

3D Numerical Simulation Results: Having determined that 3D dynamics and finite pressure effects can profoundly affect cloud stability, we upgraded the capabilities of our numerical simulation codes to account for the additional physics. This involved developing and running a fully 3D simulation code [3]. Perhaps not so obvious was the need to also develop new 3D graphic capabilities to help understand the output of the code. Figures 1 and 2 show results from both of these efforts. Shown in each figure is a series of isodensity surfaces at various times of a cloud initially 100 m in transverse radius, at 160 km altitude in earth's ionosphere. Figure 1 is for a plasma temperature of 0.1 eV, and Fig. 2 is for 0.2 eV. The results clearly show the stabilizing effects of plasma pressure in a 3D geometry, specifically,

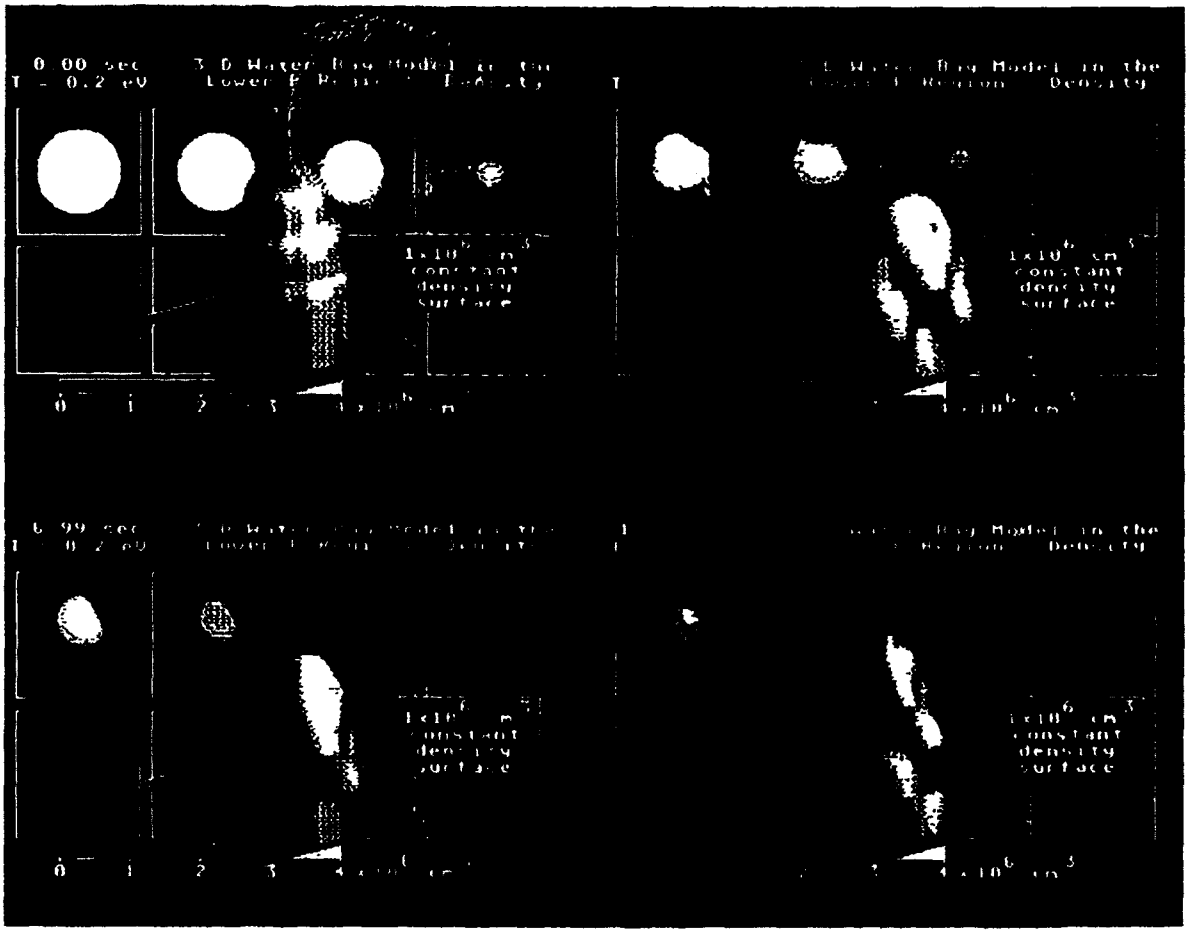

Fig 2 — 3D simulation of a *hot* ionospheric barium cloud where T = 0.2 eV

the lower pressure cloud bifurcated (Fig. 1), whereas the higher pressure cloud did not (Fig. 2). Animations of figures similar to these show the stabilization mechanism to be related to plasma cloud rotation and shear.

Conclusions: A combination of analytical models, 3D numerical simulations, and computer graphics/animation have enabled us to make significant progress in the understanding of ionospheric structuring processes important in the reliable operation of military systems.

Dr. J. F. Drake of SAIC and the University of Maryland has made significant contributions to this research, and Dr H. G. Mitchell of SAIC has contributed to the graphics.

[Sponsored by ONR and DNA]

References

1. J.F. Drake and J.D. Huba, *Phys. Rev. Lett.* **58,** 278 (1987).
2. J.F. Drake, M.J. Mulbrandon, and J.D. Huba, *Phys. Fluids* **31,** 3412 (1988).
3. S.T. Zalesak, J.F. Drake, and J.D. Huba, *Radio Science* **24,** 591 (1988).

Space-based Tethered Array Antenna

M. S. Kaplan and C. A. King
Space Systems Technology Department

Space-based radar (SBR) technology may, in the future, enable the Navy to detect, track, and identify small targets such as aircraft and cruise

missiles. To provide the SBR with a large enough signal-to-noise ratio to allow reliable target detection, large aperture antennas with large gains and narrow beamwidths are usually required. Large antenna aperture usually means that the SBR will be an expensive system to build because of the large antenna mass and the complexity of designing and deploying the large antenna. The Advanced Concepts and Processing Branch has developed a new antenna concept that may be capable of obtaining the desired aperture for less mass and at a lower cost than more conventional approaches. This antenna concept is called the tethered array antenna.

The tethered array antenna (Fig. 3(a)) can be considered a collection of antenna elements connected in a nonrigid manner to form a dynamic, quasi-linear phased array antenna. Gravity-gradient forces tend to force this configuration into an Earth-pointing orientation. The tether forms a *spine* for this nonlinear phased array antenna. Figure 3 illustrates the tethered array antenna. The antenna can act either as a dual transmit/receive antenna for a monostatic radar or as a separate transmit or receive antenna for a bistatic radar system. Phase information is passed through the tether (Fig. 3(b)) to steer the resultant beam in the desired direction.

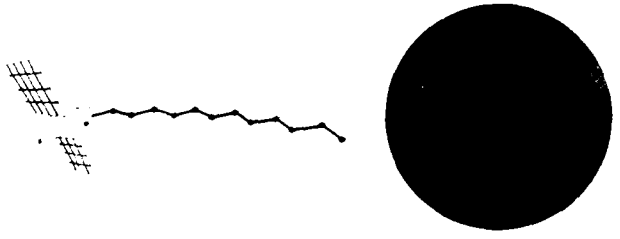

Fig. 3(a) — Space-based tethered array antenna concept

To understand the electromagnetic behavior and the utility of the tethered array antenna, one has to understand the antenna's dynamics. The following sections briefly describe dynamics and electromagnetic considerations for the antenna.

Dynamic Characteristics: The dominant force driving the dynamics of the tethered array

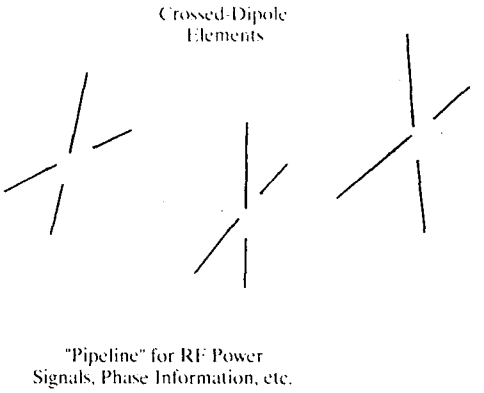

Fig. 3(b) — Detailed view of space-based tethered array antenna

antenna is the gravity-gradient force. This force has both in-plane and out-of-plane components. Gravity-gradient forces induce librations on the antenna with a periodicity of $\sqrt{3}$ and 2 times the orbital period for in-plane and out-of-plane librations, respectively. Other forces that are present but are less significant include solar and lunar gravitational forces, solar radiation pressure, atmospheric drag, Lorentz forces, and thermal expansion and contraction.

As an illustration of the dynamics experienced by a tethered array antenna, consider the following example. A computer-generated case of a 200-m tether in a 1000-km circular orbit, inclined 63.4° with 20 discrete uniformly spaced masses was run to obtain estimates on the magnitude of the tether's librations. Each mass was assumed to be 67 kg, and the mass of the spacecraft deploying the tether was assumed to be 60,000 kg. Preliminary conclusions are that for this case, the magnitudes of the librations are less than 20 cm in-plane, 50 cm out-of-plane. Figure 4 illustrates this motion for several time-steps that are 30 s apart. (For sake of clarity, the deformations are exaggerated for them to be visible.) These preliminary results could be used as a basis for determining the feasibility of the antenna. For example, consider an antenna operating at 1 GHz (30-cm wavelength); librations on the order of 1 to 2 wavelengths are obtained. It is believed that this is an amount significant enough to merit correction by means of signal processing.

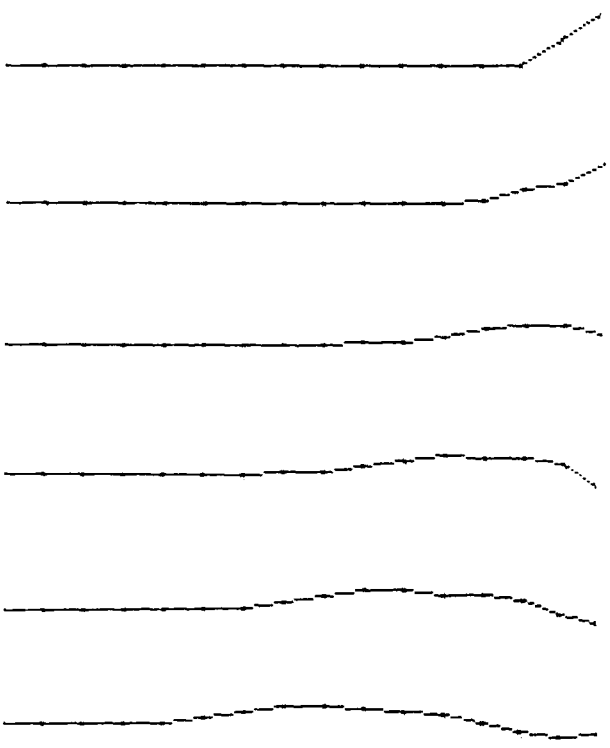

Fig. 4 — Tether configurations for six time-steps, 30-s apart

Electromagnetic Characteristics: Given the types of dynamics that will be present, it is anticipated that the tethered array antenna will be most useful at frequencies below 1 GHz because the magnitude of the librations become smaller in terms of wavelengths. Unfortunately, the gain of the antenna decreases as well. One way to alleviate this gain reduction is to design the antenna to be longer with more elements. However, this solution may introduce other problems; if a serial feed topology is used and the antenna is to have some usable bandwidth, then an upper bound must be placed on the number of elements for the antenna. For example, an SBR at 1 GHz, using a waveform requiring 5 MHz bandwidth, needs 0.5% bandwidth. This means that an antenna with a beamwidth narrower than 0.5° is unusable. At 100-km altitude, a 0.5° beam has a spot size on the ground of 8.7 km. Thus for this sample case, the maximum size for a tethered array antenna is 3.3 km, with 22,228 elements providing an array gain of 47 dB. (Note that these are theoretical upper bounds from a bandwidth constraint and probably are not achievable in practice.)

It is believed that most applications of this antenna will require a radiation pattern with symmetry with respect to the tether. An element design that is capable of producing such a pattern is a crossed-dipole. To steer the beam, phase information would be passed up and down the antenna by using fiber optics. DC power might be distributed by using *twisted-pair* cable to minimize inducing Lorentz forces on the tether.

Current and Future Research Activity: The Advanced Concepts and Processing Branch is currently addressing the primary technical issues pertaining to the antenna's feasibility—predicting tethered array antenna dynamics and characterizing the resulting antenna radiation patterns. Once these issues are better understood, attention will be focused on beam steering, antenna construction, and space deployment. Eventual program goals include a space-based demonstration of key aspects of this technology, perhaps as part of the DARPA LIGHTSAT program.

[Sponsored by DARPA]

Bibliography:

R.E. Colin, *Antennas and Radiowave Propagation* (McGraw-Hill, New York, 1985).

D.A. Arnold, "The Behavior of Long Tethers in Space," *J. Astronautical Sci.*, **35**(1), 3 (1987).

NRL Predicts the Great Snow Storm of 1983

S.W. Chang and R.V. Madala
Space Science Division

Accurate predictions of fast-developing, rapidly moving adverse weather systems are very important for naval operations, because they carry with them great energy and severe atmospheric and oceanic states. These adverse weather systems are

sometimes difficult to forecast because of the scarcity of observations at early stages. One such system is the midlatitude, wintertime storms that develop rapidly off the east coast of the North American and Asian continents, right over our major shipping routes to Europe and Asia. These familiar winter storms also cause havoc along the major U.S. urban corridor from Washington, DC to Boston. Because of their very rapid intensification rate—the central pressure can drop more than 1 mbar (0.03 in.) per hour—these systems are given the name *meteorological bombs*. These bombs, with a typical lifespan of 3 days and a radius of gale force wind of 250 km, can develop in 6 to 12 hours and move at a speed of 30 knots with a maximum surface wind of 50 m/s generating waves that are 30 to 40 ft high. Because of their destructive force and potential for disruption of naval operations, a special effort has been made at NRL to develop a computer software system to predict the bombs.

Prediction Model: Predictions of global atmospheric circulation with simple numerical models have been in existence since the birth of high-speed, digital computers. The technology of weather prediction on the time and space scale of the bombs (mesoscale) has proceeded rapidly with the advance of supercomputers in the last decade. The technique used basically solves the appropriate hydrodynamic equations as an initial-value problem. An accurate, three-dimensional (3D) description of the atmospheric state, in terms of wind vector, pressure, temperature, and humidity, is obtained from the global observational network. By using this state as the initial condition, the future atmospheric state can be obtained by integrating in time a set of equations governing the atmospheric motions for the appropriate scale—mesoscale in this case.

The governing model consists of equations of motions in all three space dimensions: a thermodynamic equation, a conservation equation for the humidity, and the equation of state of the air. Many of the atmospheric processes, owing to their complexity and interactions, cannot always be resolved by the model and need to be parameterized. These processes include the release of condensation heating in cumulus clouds, solar and terrestrial radiative transfer, and surface boundary layer effects. Also, in a realistic prediction model, the terrain and sea-land distribution have to be considered. The fact that modern numerical weather prediction still is not very successful for extended ranges is attributed to the inaccurate description of the initial state, the uncertainty in parameterization of the physical processes, and errors in computational techniques.

The NRL mesoscale weather prediction system consists of four major components: a data analysis component, an initialization component, a prediction model, and an output package [1]. We use a successive-correction method to obtain the initial analysis from the unevenly distributed observation sites, retaining the important mesoscale information and discarding the noise. A normal mode initialization is then applied to the initial analysis to get the best dynamically consistent initial state for the prediction model. Our prediction model uses primitive equations, a terrain-following vertical coordinate, and a relaxation lateral boundary treatment. The parameterized physics include the Kuo's cumulus scheme and a $1+1/2$-order turbulence model for detail surface boundary layer processes. The numerical technique in the model is 4th-order conserving in space and 2nd-order (split-explicit) conserving in time.

Prediction: To test the forecast system, we selected the great east coast snowstorm that occurred February 10 to 12, 1983 and let our forecast system *hindcast* the event. At 00Z (midnight, Greenwich mean time) of February 10, 1983 (7 pm EST February 9), the surface pressure analysis showed only a weak low-pressure area over the Texas-Louisiana border. Twenty-four hours later a low-pressure center with closed isobars formed over southern Georgia. At this

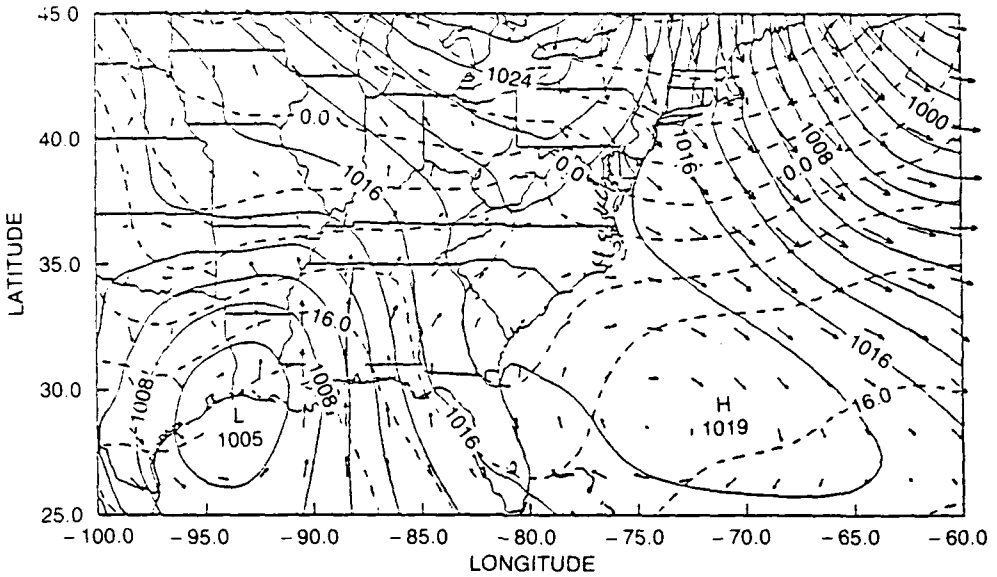

Fig. 5 — The surface analysis, containing isobars of sea-level pressure, surface wind vector, and 1000-mbar-level isotherms, at 00Z, February 12, 1983

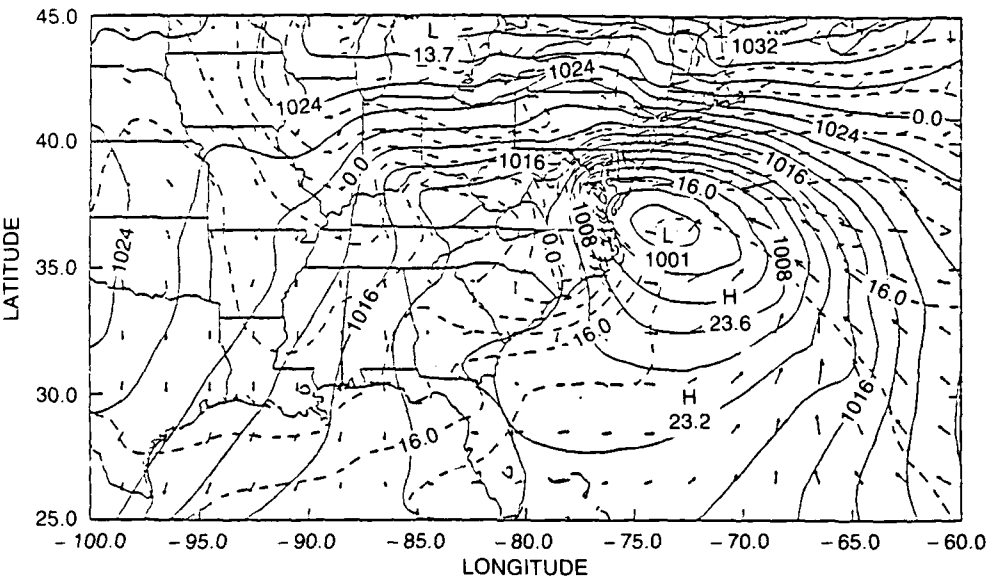

Fig. 6 — The 48 h forecast made by the NRL prediction system for 00Z, February 12, 1983

time, as the Canadian colder air was transported southward to the east of the Appalachian mountains, mixed rain and snow started to fall over the higher elevations of the Carolinas. At 00Z of February 12, a well-defined low pressure located about 150 km offshore at the Virginia and North Carolina state line (Fig.5) developed. The position of the low-pressure center produced easterly flows over the mid-Atlantic and New England states, which is most inductive for snowfalls for this region. Major metropolitan areas on the East Coast from Richmond to Boston had snowfalls of 6 to 12 in. on February 12 to 13, which caused great disruptions. The Washington metropolitan area had 12 to 18 in. of snow accumulation and NRL was closed for two days. This particular storm is thus called the megalopolitan snowstorm of 1983.

The NRL prediction system produces an excellent hindcast of this snow storm. Figure 6 shows the 48 h prediction by the NRL prediction

system. The model was able to pinpoint the location of the center and misses the central pressure by merely 1 mbar. The model also makes a remarkably accurate snowfall forecast, correctly pointing out the maximum snowfall of 2 ft in West Virginia and central Pennsylvania.

Future: The NRL forecast system will be subjected to more case testing, particularly with the ERICA field experiment data, which are collected during the 1988–89 winter, focusing specifically on the meteorological bombs. As we gain more confidence with the forecast system, some of the techniques used in the system will hopefully be transferred to the operational community.

Keith Sashegyi of Science Applications International Corporation and Katherine Brehme of North Carolina State University have contributed to the development of the prediction system.

[Sponsored by ONR]

Reference

1. S. Chang, K. Brehme, R. Madala, and K. Sashegyi, "A Numerical Study of the East Coast Snow Storm of Feb. 10–12, 1983," *Monthly Weather Review*, July 1989.

QPOs: A New Astronomical Mystery

J.P. Norris and P. L. Hertz
Space Science Division

Quasi-periodic oscillations (QPOs) were discovered recently in the X rays emitted by bright, low-mass X-ray binaries (LMXBs, Fig. 7). LMXBs are close binary stellar systems in which a neutron star (in the QPO case) or black hole accretes matter from a normal stellar companion. Up to 10^{31} W in X rays are produced in the accretion process through conversion of the gravitational potential energy of infalling matter into radiation. Unlike the coherent signal of a pulsar, which appears as a narrow spike in a Fourier power spectrum, long-term averages of QPO signals appear as broad bumps, indicating some form of incoherent temporal modulation of the time-varying X-ray flux from the accreting neutron star.

Discovery of QPO Modes in Neutron Star Binaries: In early 1985 the X-ray star GX5-1 was found to emit QPOs with centroid frequencies from 20 to 36 Hz [1]. Their coherence length is approximately two cycles (giving a width of several hertz and a $Q \sim 1$), and the rms intensity strength is 1% to 5%. Although manifested intermittently, QPOs have now been observed in at least ten of the bright LMXBs and appear to be a common mode for these stellar systems. QPOs with centroid frequencies up to ~150 Hz have been observed in one LMXB system.

A beat frequency model (BFM) has been advanced to explain some of the QPO behavior [2]. The neutron star's magnetosphere, spinning with frequency Ω_s, gates accreting blobs of plasma orbiting at the Keplerian frequency Ω_K. The hot plasma hits the star at the beat (QPO) frequency, producing on the average a weak modulation of the total X-ray luminosity. Higher accretion pressure pushes the plasma farther into the magnetosphere, Ω_K increases, resulting in higher QPO frequencies and production of more X rays. The stellar magnetic fields are weak, allowing the accreting matter to communicate spin-up torque to the neutron star surface. Spin periods in the range of 1 to 10 ms are predicted, yet coherent pulsations from rotation are not observed in LMXBs.

Stable Five Hertz Mode: Shortly after the original QPO discovery, a distinct QPO mode was found in Cygnus X-2 by using data from the NRL's HEAO A-1 experiment. A relatively stable 5 to 6 Hz QPO was observed, in which the correlation of X-ray intensity and QPO frequency is absent, arguing against the BFM as a universal explanation for QPOs [3]. Also, NRL experimenters found that another prediction of the BFM, correlation of spectral power in low-frequency noise (LFN) and in the QPO, was evidently not present during the 5 Hz mode (Fig. 8). LFN is significant power above

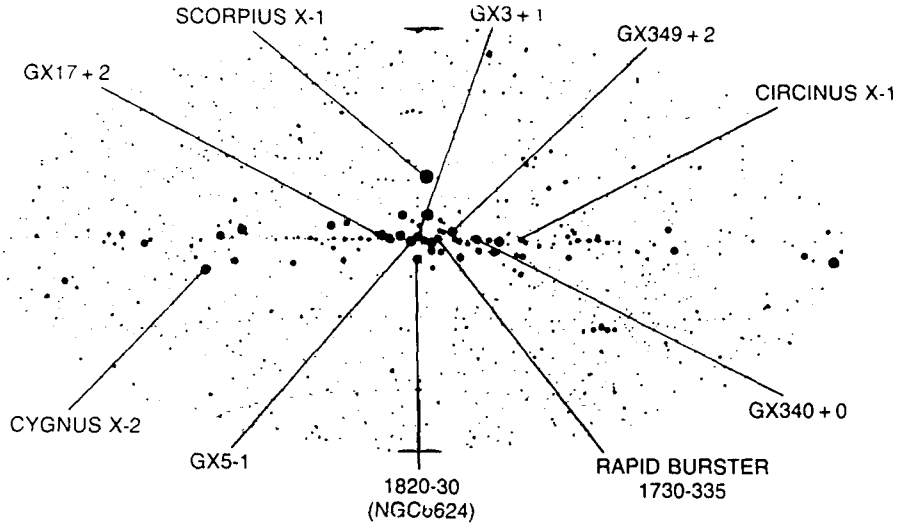

Fig. 7 — The X-ray sky in galactic coordinates. Among the most luminous galactic X-ray sources, and the brightest as seen from Earth, are the QPO sources, which cluster near the galactic center. X-ray brightness is indicated by radius of plotted disk (quasi-logarithmic scale). From NRL's HEAO A-1 catalog [4].

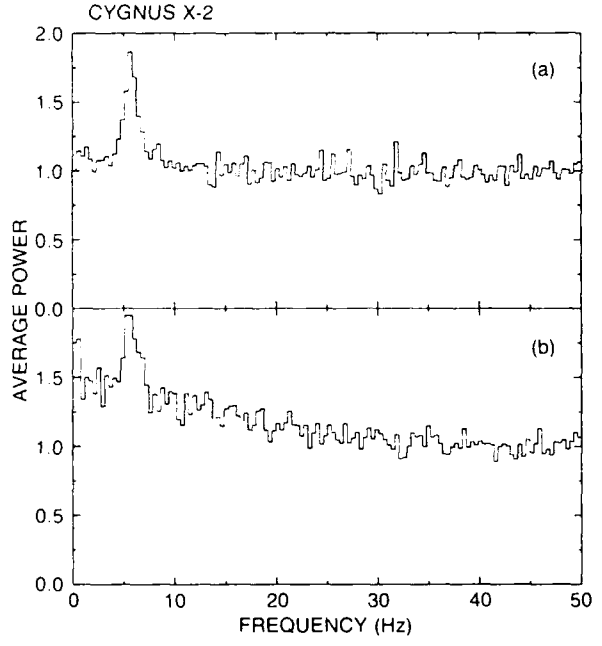

Fig. 8 — Fourier power spectra of Cygnus X-2 during intervals of strong 5 Hz QPOs, observed by NRL's HEAO A-1 experiment; (a) no LFN is observed; (b) LFN accompanies QPOs. From Ref. 3.

white noise, observed near and below the QPO bump and above ~0.1 Hz. The QPO-LFN correlation was expected since the temporal envelope of the accreting matter, which is reflected in the LFN signature, is the effective carrier of the QPO modulation. Eventually, the stable 5 Hz mode was observed in most of the QPO sources, and in each case where the signal was sufficiently strong to warrant detailed analysis the NRL findings for the 5 Hz mode were corroborated.

Investigations in progress at NRL (in collaboration with scientists from Japan's Institute for Space and Astronautical Science using the Large Area X-ray Counter aboard the Ginga satellite) indicate that, in the high-frequency QPO mode of GX5-1, significant QPO amplitude fluctuations are not accompanied by LFN fluctuations on the short timescales during which QPO is expected to be coherent; this further constrains the popular BFM. Also, these statistical studies appear to indicate that in some strong shots the instantaneous QPO strength may range as high as 30% to 40% of the total X-ray luminosity, an indication that QPOs are probably related to processes near the neutron star surface where most of the gravitational potential energy of the accreting matter is released.

Future Observations—Large Area Detectors: The QPO wavetrains are too short to study individually with present X-ray instrumentation. Thus it is virtually impossible to determine which kind of modulation(s) (frequency, amplitude,

shots, etc.) may be producing the short QPO coherence length and the LFN. The most sensitive searches for the suspected weak pulsars in LMXBs have been carried out employing coherence recovery techniques developed at NRL [3] on data from the HEAO-1 and Ginga satellites (collecting areas of 1800 and 4500 cm^2, respectively), yielding upper limits as low as 0.1% on the fraction of the flux that is pulsed; the pulsed flux is expected by many theorists to be even weaker. An experiment that could see individual QPO cycles and detect the pulsars is the X-ray Large Array (XLA), a 100-m^2 X-ray proportional counter array. Originated by Dr. K. Wood of NRL's Space Science Division, XLA was recently proposed for the NASA Space Station. The payoffs of this experiment relevant to QPO sources include detection of the suspected weak pulsars QPO sources, which could lead to detection by gravitational wave experiments tuned to the known pulsar frequency; probing the environment of extreme magnetic and gravitational fields; and understanding the turbulent mechanisms that give rise to the fragmented QPO wavetrains.

[Sponsored by ONR and NASA]

References

1. M. van der Klis, F. Jansen, J. van Paradijs, W.H.G. Lewin, E.P.J. van den Heuvel, J. Trumper, and M. Sztajno, "Intensity-Dependent Quasi-Periodic Oscillations in the X-ray Flux of GX5-1," *Nature* **316,** 225 (1985).

2. M.A. Alpar and J. Shaham, "Is GX5-1 A Millisecond Pulsar?," *Nature* **316,** 239 (1985).

3. J.P. Norris and K.S. Wood, "Discovery of 5 Hertz Quasi-Periodic Oscillations in Cygnus X-2," *Astrophys. J.* **312,** 732 (1987).

4. K.S. Wood, J.F. Meekins, D.J. Yentis, H.W. Smathers, D.P. McNutt, R.D. Bleach, E.T. Byram, T.A. Chubb, H. Friedman, and M. Meidav, "The HEAO A-1 X-ray Source Catalog," *Astrophys. J. Suppl.* **56,** 507 (1984).

Michelson Interferometry—Fifty Years Later

K.J. Johnston, D. Mozurkewich, and R.S. Simon
Space Science Division

Introduction: Long baseline optical interferometry (LBOI) is the use of discrete receiving elements to obtain detailed spatial structure of celestial objects. Angular resolution achieved by this technique can be 60,000 times that of the human eye and is much higher than can be obtained with a monolithic mirror, i.e., the Hubble space telescope has a 2.4-m mirror that has a resolution 700 times that of the human eye. This increase in resolution is necessary to study celestial and near-Earth objects in detail to identify them and investigate their kinematic motions and the energy sources that power them. For example, this technology will allow one to determine with unprecedented accuracy all the fundamental parameters such as the size, shape, and distance of a star. Taken with a star's apparent luminosity as a function of frequency, there is all the information to deduce a detailed picture of the star and allow an estimate of a complete stellar evolutionary model.

The technology of LBOI allows the use of independent apertures to be combined coherently into a single aperture. Since the spacing of the apertures is proportional to the angular resolution, the highest angular resolutions can be reached to image objects that have enough intensity per angular resolution element. To image objects, a sufficient number of spatial frequencies must be sampled to form a true image. In cases where there is insufficient sampling, detailed models of the image may be obtained.

Previous Research: This technology was first developed by Albert Michelson, who formed his early ideas while an instructor at the U.S. Naval Academy. His initial experiments were made in 1890 when he measured the angular diameters of the Galilean satellites of Jupiter. He surpassed these measurements in 1920 by making the first measurement of the diameter of a star other than the

sun. With a 20-ft. separation of the apertures, he was able to determine that the diameter of the star Betelgeuse was 0.047 arc second. Thus the size of this star was almost as large as the orbit of Mars.

All of Michelson's measurements were made by simply separating two mirrors and measuring the combined signal. Thus he sampled very few spatial frequencies. Since stars are roughly spherical only a few critical measurements are necessary to measure stellar diameters. To make these measurements, the path lengths the light travels must be equal to a fraction of the wavelength of light. Further, the atmosphere distorts the optical path length to the different apertures making it difficult to obtain a stable correlated or a combined signal. Michelson made his measurements of stellar diameters at Mount Wilson, California where the atmosphere is very stable. The diameters of only a few stars were measured by Michelson before his death in the 1930s. Other scientists, namely Hanburry-Brown using the amplitude interferometer at Narribri, Australia and Labeyrie and his colleagues at CERGA, have determined the diameters of about 100 bright stars. These are mainly very large stars or, in astronomical jargon, giant or supergiant stars.

NRL, with the United States Naval Observatory (USNO), the Smithsonian Astrophysical Observatory, and the Massachusetts Institute of Technology have developed the technology of optical interferometry for astrometry and imaging. The initial driver for the program was USNO's need to determine precisely the positions of stars over large angles. The presently available technology using transit circles measures the meridian passage of a star. The accuracy of this determination is of the order of 0.1 arc second. Measurements of star positions could be made with pairs of apertures, allowing the technology for a two-element interferometer to be developed.

Mt. Wilson Optical Interferometer: An interferometer (Fig. 9) was developed at Mount Wilson, California and is located approximately 80 m east of the 100-in. telescope where Michelson made his first measurements of stellar diameters. This interferometer has the capability for a north-south baseline of 12 and 20 m, a NE-SW baseline of 8 and 12 m, and has several other novel features developed under this program. It is the first optical interferometer capable of measuring the total combined or cross-correlated signal from a star. This signal, though complex,

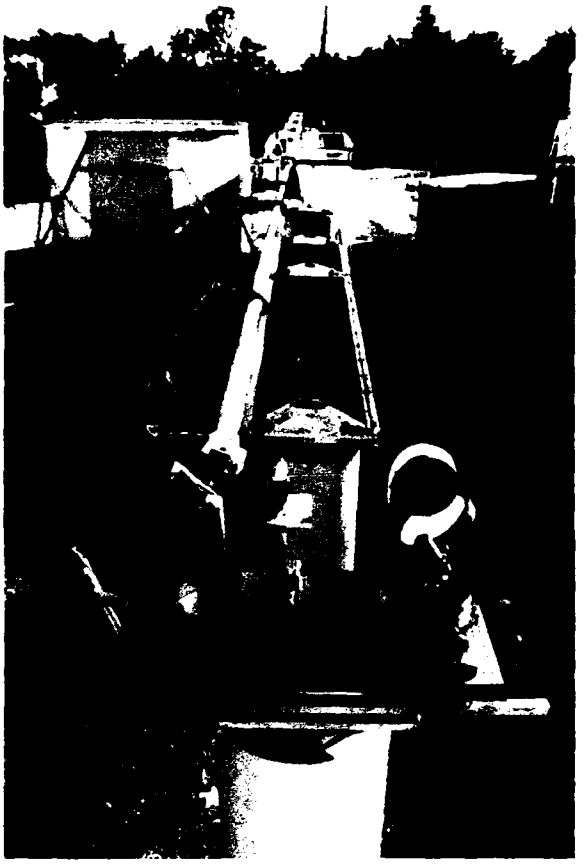

Fig. 9 – A view of the longest north-south baseline of the Mount Wilson Optical Interferometer. At each end of the interferometer starlight is directed by flat mirrors (the mirror for the near end is visible in the foreground) into the long vacuum pipe. The two light beams are then directed into the optical laboratory on the right where they are interferometrically combined and detected. The total length of the baseline pictured is 29 m; baselines up to 32 m in length are available with this instrument. This north-south baseline is used primarily for imaging of stellar systems and determining stellar diameters. The small octagonal shed in the upper left is one end of an alternative east-west baseline used primarily to measure stellar positions by astrometric interferometry.

has an amplitude and phase. Previous measurements were capable of measuring only the magnitude or phase of the cross-correlated signal.

A major innovation in this instrument is a dither delay line that vibrates at a frequency of 1 KHz with an amplitude of one wavelength of the light being observed. Once a correlated signal is detected from a star, the dither delay line allows the signal to be tracked at the millisecond time level. Thus the effects of atmospheric path length distortions can be tracked, and the resulting data can be fed into a computer allowing for a totally automated system with a fast response time. Also a delay line was developed to equalize the overall path lengths to 10% of the observed wavelength of the light.

This system is totally automated in that it acquires the stars, obtains a cross-correlated signal, and outputs the resulting signal to a computer. This was necessary for USNO's application as the measurement of star positions requires the observation of a large number of stars over as short a timescale as possible. Measurements made in 1988 indicate that by observation of stars in two colors, formal accuracies of 0.01 arc second have been achieved. These measurements must be repeated over several years to determine the systematic errors of these measurements. On the basis of these successful observations, USNO has initiated a program to fabricate an operational interferometer to replace the transit circles now in use.

This program was also successful in measuring the diameters of many stars from the position measurements. A new program is being undertaken to image celestial and near-Earth objects. It will demonstrate that by using a multiaperture system images of objects can be made, thus extending the work on stellar diameters. This will result in detailed images of objects at milliarcsecond wavelengths and will extend by a millionfold the resolution of optical ground-based measurements that are at present limited by the atmosphere.

[Sponsored by ONR]

Understanding the Evolution of the Sun's Large-Scale Magnetic Field

N. R. Sheeley, Jr., A. G. Nash, and Y. M. Wang
Space Science Division

C. R. DeVore
Laboratory for Computational Physics and Fluid Dynamics

The sun's magnetic field differs drastically from Earth's 1 G dipole field with which we are familiar. Fields of several thousand gauss are concentrated in sunspot groups that come and go in a matter of weeks, and large-scale fields of several gauss evolve on time scales of months to years. Magnetic fields with strengths of at least 5 G exist at the sun's poles near sunspot minimum but weaken and reverse their polarities approximately at the time of sunspot maximum in each sunspot cycle. These complicated time-varying magnetic fields give rise to a variety of energetic phenomena including solar flares, coronal mass ejections, and coronal holes, which disturb Earth's space environment and affect Navy systems.

Solar Magnetic Phenomena: Recently, we have been conducting a research program designed to understand these terrestrially important solar magnetic phenomena. It is based on the idea that all of the sun's magnetism originates in sunspot groups and in the subsequent months spreads out on the surface to form the observed large-scale patterns. Because the sun rotates differentially with a period that ranges from 27 days at the equator to 34 days near the poles, these magnetic patterns become sheared as they expand. A poleward meridional flow assists the effective diffusion in transporting the evolving fields toward the poles.

Simulating Magnetic Fields: By using a procedure developed in a collaboration between the Space Science Division and the Laboratory for Computational Physics and Fluid Dynamics, we have been simulating the evolving magnetic fields on the sun. Beginning in 1976 at the start of sunspot cycle 21, we enter the magnetic fields from each

new sunspot group as input to our simulation, and we redistribute these fields at the measured rates of diffusion, differential rotation, and meridional flow. During the 11-year sunspot cycle, more than 2000 sunspot groups contribute to the formation and evolution of the large-scale fields. We display these simulated magnetic field patterns in synoptic maps at approximately 27-day intervals.

Figure 10 compares a map of the simulated field during November 1982 (below) with a map of the corresponding field observed at the National Solar Observatory (NSO) at Kitt Peak. Here field intensities are represented by a logarithmic gray scale, with contours ranging from −50 G (black) to +50 G (white), positive fields being directed out of the sun toward the observer and negative fields pointing inward. The agreement is generally good, except near the poles where the simulated fields of negative polarity in the north and positive polarity in the south are stronger than the corresponding observed fields, which are poorly observed at high latitude and are not shown all the way to the poles.

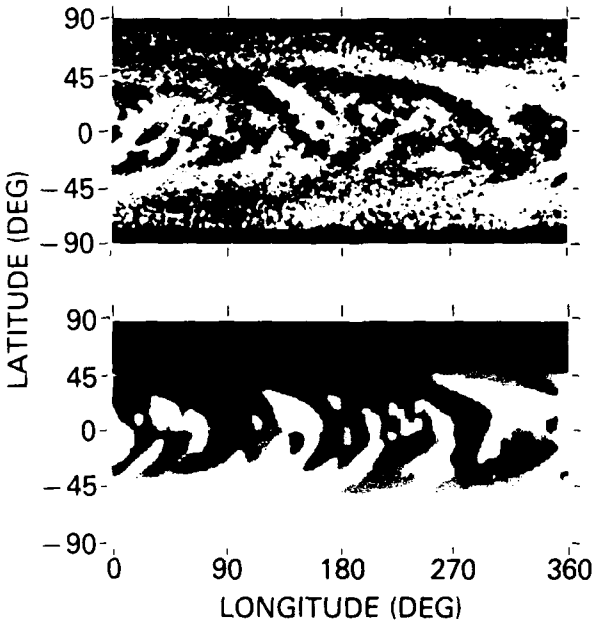

Fig. 10 — Photospheric magnetic field distribution during November 1982. Top: Synoptic map showing field strengths measured by NSO (Kitt Peak). Bottom: Synoptic map of the numerically simulated field. The curved patterns result from the combined action of differential rotation, supergranular diffusion, and meridional flow.

Poleward Diffusion and Meridional Flow: In each hemisphere, large slanted patterns are clearly visible extending poleward from their origins in low-latitude sunspot groups. It has long been known that these patterns rotate more rigidly than the surface layers in which they are embedded. Now, by conducting experiments with our numerical model, we have learned that poleward diffusion and meridional flow are responsible for this paradoxical effect. The poleward motion offsets the eastward drift owing to differential rotation so that the individual small-scale elements move along slanted paths that are stationary in the coordinate system that rotates rigidly at the equatorial rate. Thus, the slanted field patterns rotate rigidly, while their individual small-scale elements exhibit the differential rates of the latitudes they are drifting across during their poleward journey.

Such rigidly rotating patterns would appear as spirals if observed from above the corresponding pole of the sun. Such spirals are shown in Fig. 11, which is a colored display of the NSO observations during August 1983 as they would appear from above the north pole. Positive polarity is indicated by shades of red and yellow, and negative polarity is indicated by shades of blue. Viewed in time lapse, these patterns would rotate rigidly like a giant pinwheel while the individual small-scale fields move steadily poleward along their spiral paths.

Forecasting: Our numerical model has proved to be useful not only for solving such problems in solar physics, but also for forecasting the evolution of solar magnetic fields and their associated coronal, interplanetary, and terrestrial phenomena. We simply use the most recent map of the observed field as input to our simulation and then run the simulation forward in time by several months. Although the resulting forecast obviously will not include the effects of new fields that erupt after the initialization, they will still give a fairly accurate representation of the large-scale fields for a few months until the recent eruptions have had time to evolve. However, the longer we extend the

Fig. 11 — Northern-hemisphere magnetic field distribution during August 1983, as viewed from above the sun's north pole. The magnetic flux migrates from the sunspot regions toward the pole, forming a rigidly rotating spiral pattern (data provided by NSO (Kitt Peak).

forecast, the more important these subsequent eruptions will become.

We illustrate this forecasting procedure by using observations during the declining phase of the sunspot cycle when the eruption rate is becoming relatively low and will therefore have little immediate effect on the forecasts. As an example, we consider the evolution of coronal holes, which are regions of *open* magnetic field extending outward from the sun. They are the sources of high-speed, solar-wind streams that sweep past Earth as the sun rotates and induce geomagnetic and auroral activity. Because these terrestrial disturbances affect a variety of Navy and other systems, their forecasts are of practical interest.

Figure 12 compares coronal holes observed at NSO (Kitt Peak) with coronal holes simulated with our model. The observed coronal holes are indicated by lighter-than-average areas in the NSO helium images (right). The simulated holes were determined from a current-free extension of the field on the sun's surface, either as it was observed in September 1984 at the Wilcox Solar Observatory, or as it was simulated two and four solar rotation periods later. The resulting coronal holes are indicated by dotted areas on the simulated maps (left). Closed-field regions of relatively high field strength may be expected to correspond to darker-than-average helium features and are indicated by triangles or plus signs depending on their magnetic polarity.

Conclusions: Comparing these observed and simulated holes, we find generally good agreement, not only initially when the observed

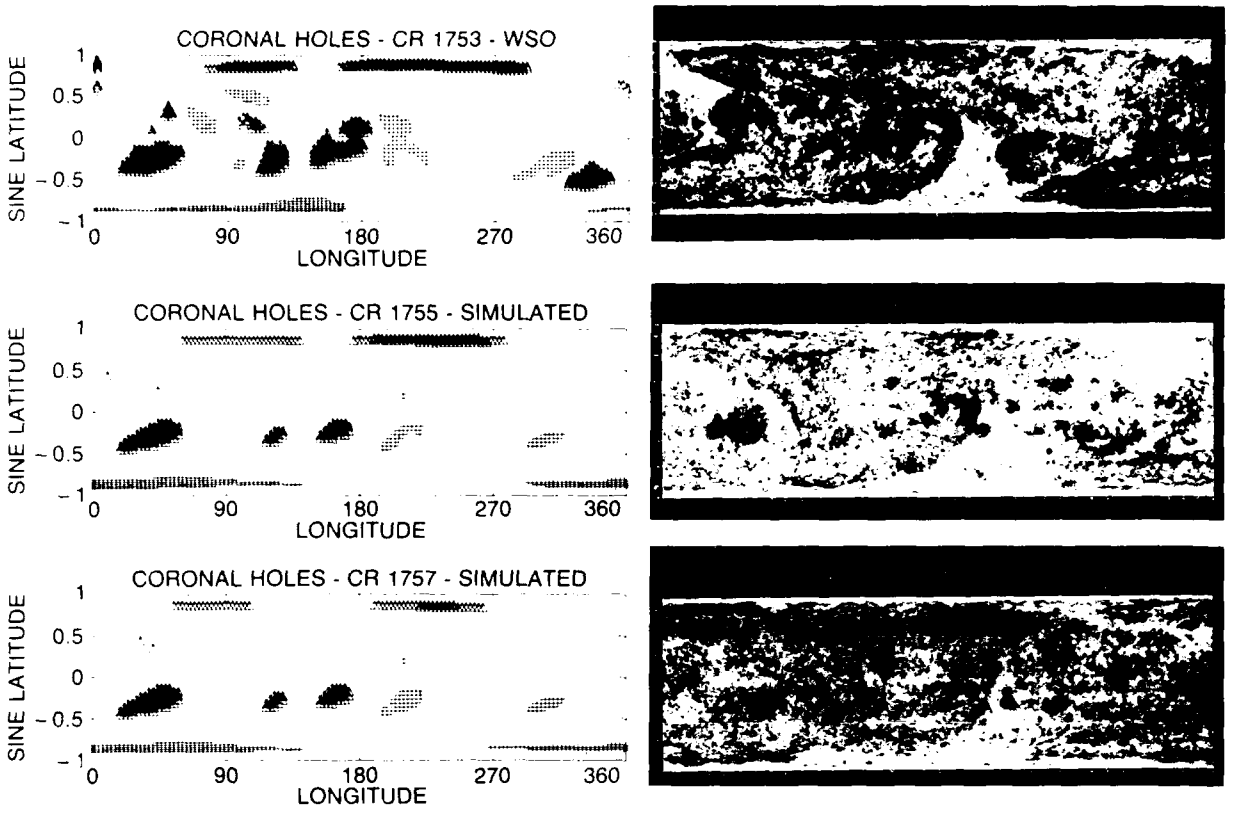

Fig. 12 — Comparison between numerically simulated coronal holes (left panels: stippled areas) and coronal holes seen on He I images (right panels: light areas). The photospheric maps are spaced two months apart and cover the period September 1984 to January 1985. The crosses and triangles on the simulated maps represent regions of strong positive- and negative-polarity field where the field lines are closed.

field was used to calculate the holes, but also two and four rotations later when the simulated field was used. Discrepancies, such as the somewhat larger and more equatorward extension of the observed hole in the southern hemisphere, may be due to systematic errors in the observed field used as input to the simulations as well as inaccuracies in the model itself.

By the mid 1990s when the declining phase of sunspot cycle 22 arrives, we expect that such forecasting techniques will be used routinely for forecasting the evolution of coronal holes and their associated geomagnetic and auroral activity. Such long-range forecasts will be available for helping a wide variety of users not only in the Navy and DoD, but also in other organizations whose operations are affected by conditions in Earth's space environment.

[Sponsored by ONR and NASA]

Theory of Origin of the Elements Confirmed

M. D. Leising and G. H. Share
Space Science Division

In 1949, NRL scientists performed remote measurements of radioactivity resulting from a nuclear explosion, confirming that the Soviet Union had exploded a nuclear weapon. In 1988, NRL scientists again made remote measurements of the radioactive debris of a nuclear explosion—a supernova 170,000 light years away in the Large Magellanic Cloud, a companion galaxy to our own Milky Way.

Supernova Theories· A massive star, in this case equivalent to 20 suns, burns all of its nuclear fuel in a few million years. With no interior energy source, the star can no longer support its own

weight and the inner core collapses upon itself. The tremendous gravitational energy release heats this core, only kilometers in size, to temperatures of nearly 10^{11} K. This thermal soup of particles and photons cools by the emission of 10^{53} ergs of neutrinos in a few seconds and becomes a neutron star or black hole. Through an unknown mechanism, about 1% of the energy released in the collapse is transferred to the stellar envelope, the outer layers that have not yet collapsed very far. The absorption of this energy heats some of the material to about 5×10^9 K and propels it outward at escape velocity. At these temperatures nuclear fusion substantially rearranges the elemental and isotopic composition.

Nucleosynthesis: There is much evidence that the observable universe began in a Big Bang, and that the resulting matter was mostly hydrogen and helium. This implies that the other elements, including the metals of Earth and the carbon of all life, originated since that time, probably in stars. The heavier elements could only have formed at extremely high temperatures, apparently in supernova explosions.

Gamma-Ray Astronomy: There was much indirect evidence that this picture was correct, but for 20 years gamma-ray astronomers have tried to observe directly the short-lived radioactive nuclei produced in the thermonuclear fusion in a supernova. The Solar Maximum Mission (SMM), launched in 1980, included the Gamma-Ray Spectrometer (GRS) built by scientists at the University of New Hampshire and the Max Planck Institute in Garching, FRG to observe gamma rays from solar flares, which it has done successfully. NRL scientists endeavored to used the GRS to observe extrasolar sources and have succeeded in detecting gamma-ray emission from the Galactic plane and from otherwise unseen sources called gamma-ray bursters [1].

Supernova 1987A: On February 23, 1987, optical astronomers discovered the brightest supernova seen from Earth since the invention of the telescope, providing unprecedented opportunities for studying supernovae. About 20 of the neutrinos mentioned above interacted in large underground detectors on Earth, a clear signal of the stellar collapse and the birth of neutrino astronomy.

SMM GRS Observations: NRL researchers began studying the SMM GRS data, looking for evidence of gamma-ray lines from radioactive decay in the supernova debris. This was not easy because part of the instrument's shield blocks the supernova, and background rates in the detector are about 1000 times greater than the expected signal. Beginning in August 1987 increases were seen in the counting rates at two specific energies, and by early 1988 it was undeniable. They were detecting gamma-ray lines at 0.847 and 1.238 MeV from radioactive ^{56}Co as it decayed into stable ^{56}Fe, the abundant isotope found all around us [2]. The ^{56}Co, with a half-life of 77 days, was itself the daughter of radioactive ^{56}Ni (half-life 6 days), the most tightly bound nucleus. It had been predicted that ^{56}Ni would be the most abundant product of the nuclear burning at several billion degrees.

A gamma-ray spectrum of SN1987A can be constructed from the SMM GRS data by doing multiple subtractions of background spectra. Figure 13 shows the resulting spectrum, summed from August 1987 to December 1988. Also shown is a fit of lines at the instrumental width at the energies expected from the strongest lines of ^{56}Co decay. Some evidence also exists for weaker lines in parts of the spectrum not shown here.

These gamma rays were detected much earlier than expected, indicating that the massive envelope ejected above the region of thermonuclear burning was somehow breaking up, or that the radioactive material produced in the inner regions was accelerated outward. Researchers are still working to understand how this occurred.

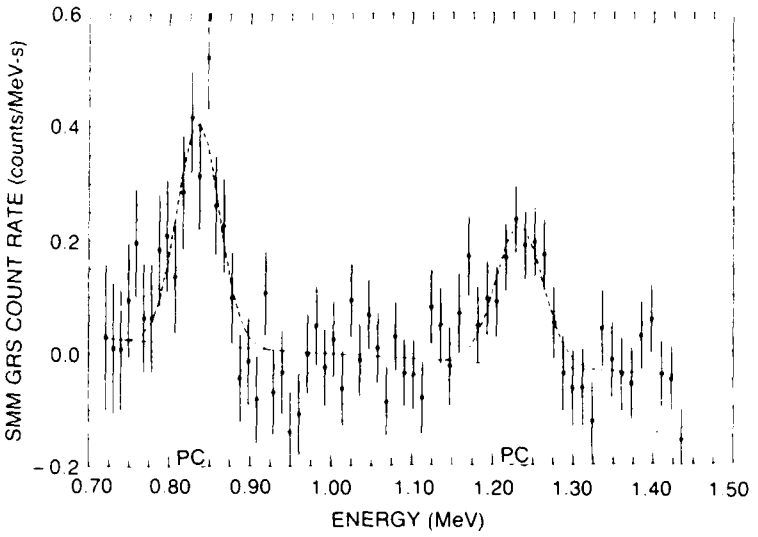

Fig. 13 — The SMM gamma-ray spectrum at the energies of the two strongest lines from ^{56}Co decay. This spectrum is the mean accumulations from August 1987 through December 1988.

From this work, theories of the origin of the elements have been largely verified. Search of the SMM GRS data for other gamma-ray emission from the supernova continues, but the satellite is doomed to crash to Earth in late 1989. The Oriented Scintillation Spectrometer Experiment, built by NRL scientists to be launched in 1990 on NASA's Gamma Ray Observatory can perhaps detect other gamma-ray emission from Supernova 1987A or new supernovae. In particular, the likely detection of gamma rays from the decay of radioactive ^{57}Co would yield crucial information on the composition of the nuclear burning regions.

[Sponsored by NASA]

References

1. G. Share and R. Kinzer, 1986 NRL Review, p. 41.
2. S.M. Matz, G.H. Share, M.D. Leising, E.L. Chupp, W.T. Vestrand, W.R. Purcell, M.S. Strickman, and C. Reppin, *Nature* **331**, 416 (1988).

AWARDS AND RECOGNITION

"We should ask ourselves, 'Are we, as an in-house laboratory, performing our job as Mr. Edison thought we should?' I believe the answer is that we are doing considerably better than he ever imagined we would. We have been responsive to Navy problems, we have maintained sustained technical competence over the many fields of Navy interest, and we have managed to maintain our intellectual independence."

"In the final analysis, these awards recognize exceptional commitment to continued productivity, intellectual integrity, and forefront work in science and technology."

Dr. Alan Berman, former Director of Research
10th Annual Research Publication Awards Presentation

SPECIAL AWARDS AND RECOGNITION

NRL is proud of its many distinguished scientists and engineers. A few of these have received exceptional honors for their achievements.

Dr. Timothy Coffey
Director of Research

PRESIDENTIAL RANK OF DISTINGUISHED EXECUTIVE IN THE SENIOR EXECUTIVE SERVICE

"...For sustained extraordinary accomplishment in management of programs of the United States Government and for leadership exemplifying the highest standards of service to the public, reflecting credit on the career civil service."

Peter G. Wilhelm
Naval Center for
Space Technology

PRESIDENTIAL RANK OF MERITORIOUS EXECUTIVE IN THE SENIOR EXECUTIVE SERVICE

"...For sustained superior accomplishment in management of programs of the United States Government and for noteworthy achievement of quality and efficiency in the public service."

PRESIDENTIAL RANK OF MERITORIOUS EXECUTIVE IN THE SENIOR EXECUTIVE SERVICE

"...For sustained superior accomplishment in management of programs of the United States Government and for noteworthy achievement of quality and efficiency in the public service."

Dr. Jay P. Boris
Laboratory for Computational Physics and Fluid Dynamics

PRESIDENTIAL RANK OF MERITORIOUS EXECUTIVE IN THE SENIOR EXECUTIVE SERVICE

"...For sustained superior accomplishment in management of programs of the United States Government and for noteworthy achievement of quality and efficiency in the public service."

Dr. John A. Montgomery
Tactical Electronic Warfare Division

1988 E.O. HULBURT AWARD FOR SCIENCE

"...For his contributions to the understanding of combustion processes, and most specifically, for the application of this knowledge and expertise to the solution of an urgent Navy decoy problem."

Dr. Jimmie R. McDonald
Chemistry Division

THE REAR ADMIRAL WILLIAM S. PARSONS AWARD

Dr. Isabella L. Karle
Laboratory for Structure
of Matter

"...For her outstanding accomplishments while serving as head of the x-ray diffraction section at the Naval Research Laboratory (NRL) for the Structure of Matter. ...Dr. Karle has conducted innovative scientific research which has led to the exponential increase in the spread and facility with which key questions of identification and structural configuration could be answered."

THE GREGORI AMINOFFS PRIZE

"...For her beautiful crystallogic studies of complicated natural products."

FEDERAL LABORATORY CONSORTIUM 1988 AWARD FOR EXCELLENCE IN TECHNOLOGY TRANSFER

Dr. Norman C. Koon
Condensed Matter and
Radiation Sciences Division

"For his novel research, development, and technology transfer on rare earth magnetic alloys and their application in a variety of fields."

THE 1988 WOMEN IN SCIENCE AND ENGINEERING AWARD FOR SCIENTIFIC ACHIEVEMENT

Dr. Elaine S. Oran
Laboratory for Computational
Physics and Fluid Dynamics

"...She leads a broadly based program of theoretical and computational research that resulted in the creation and application of a spectrum of unique models and techniques for predicting reactive flows in use in hundreds of major research facilities and universities throughout the world,...has provided career guidance to young women involved in research, and has been instrumental in bringing women...into the Naval Research Laboratory, and has assisted students in securing jobs in other laboratories."

THE NRL–SIGMA XI PURE SCIENCE AWARD FOR 1988

"For pioneering work in condensed matter theory developing *ab initio* electronic structure models and applying them to calculations of equations of state and lattice instabilities in ionically bonded solids."

Dr. Larry L. Boyer
Condensed Matter and
Radiation Sciences Division

THE NRL–SIGMA XI APPLIED SCIENCE AWARD FOR 1988

"For pioneering contributions to the physics of intense laser–plasma interactions. These investigations have made fundamental advances in plasma physics, space science, the understanding of high–altitude nuclear effects, and towards achieving confinement fusion."

Dr. Barrett H. Ripin
Plasma Physics Division

INTERNATIONAL ACADEMY OF ASTRONAUTICS BASIC SCIENCES BOOK AWARD

"For outstanding achievement as evidenced by the publication of *Sun and Earth*."

Dr. Herbert Friedman
Space Science Division

Grace C. Burroughs
Engineering Services Division

1987 OFFICE OF THE CHIEF OF NAVAL RESEARCH CLAIMANCY AWARD FOR ACHIEVEMENTS IN THE FIELD OF EQUAL EMPLOYMENT OPPORTUNITY

"In recognition of her outstanding contributions to the Equal Employment Opportunity (EEO) goals of the Navy Research Laboratory (NRL). ...Through her demonstrated performance, Ms. Burroughs has exhibited the strongest possible commitment to the EEO as a supervisor ..."

Harold G. Eaton, Jr.
Chemistry Division

1987 COMMANDING OFFICER'S AWARD FOR ACHIEVEMENTS IN THE FIELD OF EQUAL EMPLOYMENT OPPORTUNITY (EEO)

"In recognition of the many contributions he has made to promote Equal Employment Opportunity at the Laboratory. ...Mr. Eaton has been very instrumental in implementing the many activities of the NRL Community Outreach Program. ...He enthusiastically encourages local students to pursue careers in math and science, as well as support careers, and effectively promotes career opportunities. ...His leadership abilities have served to inspire some...employees to explore other career options as well as developmental opportunities. Through Mr. Eaton's dedicated commitment to the promotion of Equal Employment Opportunity, better opportunities for minorities have been realized."

Gabrielle T. Peace
Materials Science and
Technology Division

1987 COMMANDING OFFICER'S AWARD FOR ACHIEVEMENTS IN THE FIELD OF EQUAL EMPLOYMENT OPPORTUNITY (EEO)

"In recognition of her significant accomplishments and exemplary contribution to the Equal Employment Opportunity (EEO) Program. Mrs. Peace is presently chairperson of the Community Outreach Program...has been a member of the EEO Committee since 1977...has diligently worked with NRL employees as an EEO counselor since 1979...and has been involved with the local chapter of Federally Employed Women for approximately six years..."

CHICAGO MUSEUM OF SCIENCE AND INDUSTRY FEATURED SCIENTISTS IN THE BLACK ACHIEVERS IN SCIENCE AND ENGINEERING EXHIBIT

Dr. Carruthers is one of 12 featured scientists and engineers chosen to present positive role models to minority children.

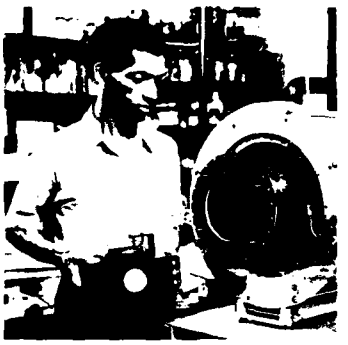

Dr. George Carruthers
Space Science Division

CHICAGO MUSEUM OF SCIENCE AND INDUSTRY FEATURED SCIENTISTS IN THE BLACK ACHIEVERS IN SCIENCE AND ENGINEERING EXHIBIT

Dr. Holmes is one of 112 special achievers, chosen by the museum's selection panel, who are representative of people who have pursued careers in science and engineering.

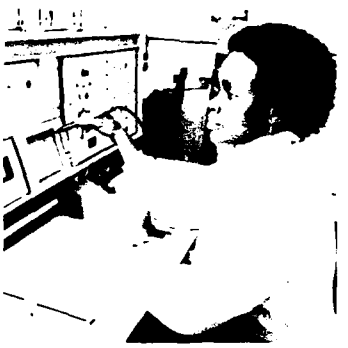

Dr. Brenda S. Holmes
Chemistry Division

NAVY MERITORIOUS CIVILIAN SERVICE AWARD

"For his significant contributions to the conceptualization and development of Naval Infrared Technology for surveillance and electronic warfare applications. Other areas where Dr. Takken excelled were in providing the first analysis showing how and to what extent infrared plane arrays will be able to answer most operational requirements; in conceiving, analyzing and verifying a form of random-pulse jam code for use against reticle-type threats; and in developing the pre-threshold clutter filtering technique now being used in the Navy's first shipboard IR Search and Track System."

Dr. Edward Takken
Optical Sciences Division

AMERICAN ASSOCIATION FOR MEDICAL INSTRUMENTATION 1988 ANNUAL MEETING MANUSCRIPT AWARD

Biomolecular Engineering Branch

A manuscript co–authored by researchers in the Biomolecular Engineering Branch was selected to receive the American Association for Medical Instrumentation Annual Meeting Manuscript Award. The recipients pictured from left to right are Dr. Frances Ligler, Keith Seib, Mary Ayers, Dr. John Smuda, Dr. Alok Singh, Dr. Patrick Ahl, and Dr. Thomas Fare. Co–authors not pictured are Dr. Adam Daiziel and Dr. Paul Yager.

NAVY AWARD OF MERIT FOR GROUP ACHIEVEMENT

A Team Effort

A 13 member team of scientists from the Tactical Electronic Warfare Division and the Chemistry Division won the Navy's Award of Merit for Group Achievement. Pictured from left to right on the bottom row are: Dr. Allen Saunders, Arthur Allshouse, Dr. Jimmie McDonald, Dr. William Howell, John Dries, Mary Ann Snapp, and Dr. Gerald Friedman. Top row (left to right): Rudy Prevatt, Dr. Robert Evans, Dr. Herbert Nelson, Stanley Moroz, Elmer Williams, and Dr. Harold Ladouceur.

INDIVIDUAL HONORS

Laboratory employees received numerous scientific medals, military service awards, academic honors, and other forms of recognition, including election and appointment to offices in technical societies. The following is an alphabetical list of persons who received such recognition in 1988.

President Ronald Reagan presents Dr. Timothy Coffey with the Distinguished Presidential Rank award.

Abraham, G., Board of Managers, Washington Academy of Sciences, Engineering Research and Development Committee, IEEE; U.S. Technology Policy Committee, IEEE; IEEE Delegate to Section B (Physics), AAAS; DoD Nonvolatile Memory Coordinating Committee.

Aggarwal, I.D., Member, Editorial Board, Journal of Optical Communications; Editor, Infrared Transmitting Glasses and Filters.

Baer, R.N., Fellow, Acoustical Society of America.

Bassel, R.H., Fellow, American Physical Society; Fellow, AAAS.

Bishop, S.G., Member, Technical Advisory Committee, Center for Compound Semiconductor Microelectronics, University of Illinois; Member, Program Committee, Gordon Research Conf. on Point Defects, Line Defects and Interfaces in Semiconductors; Member, Technical Review Committee, Joint Services Electronics Program; Member, Natl. Science Foundation Panel on Light Wave Technology; Member, External Review

Panel, Center for Electronic and Electro-Optic Materials, State Univ. of New York at Buffalo; Adjunct Professor, State University of New York at Buffalo and University of Utah.

Bodner, S.E., Invited Member of British Science and Engineering Research Council Panel to Review the Central Laser Facility at Rutherford Appleton Laboratory; Fellow, American Physical Society.

Bogar, F.D., Member, Young Author's Award Committee, Electrochemical Society.

Bolster, R.N., First prize for poster entitled "Friction Coefficients: How Low Can They Go?" at Gordon Conference on Tribology, June 1988.

Boos, J.B., Committe member, First International Conference on Indium Phosphide and Related Materials for Advanced Electronic and Optical Devices.

Boris, J.P., NRL Chair of Science in Computational Physics, 1979—present; Fellow of the American Physical Society, 1977—present; Executive Committee Chairman, American Physical Society Topical Group on Computational Physics, 1987—present; Panel for NBS Computing, Board of Assessment of NBS Programs, National Research Council, 1986—present; Member of ONR Advisory, Selection, and Program Review Panels, 1980—present; Committee Member/Panel Chairman, DoD, NASA, and DARPA Topical Review on Computational Fluid Dynamics, 1988; Member of the External Advisory Panels for the University of California at San Diego and Brown University URI Programs in Turbulence and Fluid Dynamics, 1986—present; Editor, Numerical Approaches to Combustion Modelling, to be published by American Institute for Aeronautics and Astronautics, 1989, Meritorious Senior Executive Award, U.S. Department of the Navy Senior Executive Service, September 1988.

Borsuk, G.M., Member of the Editorial Board of the IEEE Proceedings.

Dr. Larry Boyer and his son show the 1988 Sigma Xi Pure Science award

Boyer, L.L., NRL—Sigma Xi Award for Research in Pure Science.

Bradley, D.L., Head, Underwater Acoustics Technical Committee, Acoustical Society of America.

Brady, R.F., Jr., Chairman, Admissions Committee, American Chemical Society; Editorial Boards, Journal of Coatings Technology and Journal of Protective Coatings and Linings.

Bruce, W.C., Achieved Profession Registration—Professional Engineer (P.E.) Registered with the state of Maryland.

Brueckner, G.E., Corresponding member, International Academy of Astronautics.

Burns, W.K., Committee member, Topical Meeting Integrated and Guided Wave Optics 1989 (IGWO '89)

Butler, J.W., Member, Organizing committee and session chairman, Tenth Conference on the Application of Accelerators in Research and Industry, Denton, Texas.

Campbell, F.J., Member, IEEE, Nuclear and Plasma Sciences Society; Member, IEEE, Power Engineering Society; Member, IEEE, Dielectrics and Electrical Insulation Society's Awards Committee, Fellows Committee, Radiation Effects Committee, and

Transactions Review Committee; Member, ASTM, D-09 Electrical Insulation Materials's Subcommittee on Electrical Tests, Subcommittee on Hookup Wire, Subcommittee on Thermal Capabilities, and Subcommittee on International Standards; Member, American Chemical Society's Division of Polymeric Materials; Member, American Institute of Chemists, Member, Joint Board on Science and Engineering Education of Washington Area; Member, Independent Living for the Handicapped; Member, Naval Aerospace Vehicle Wiring Action Group; Member, NRL Space Technology Study Group; Fellow, Institute of Electrical and Electronics Engineers; and Fellow American Institute of Chemists.

Campbell, P.M., Invited paper at fall meeting of Electrochemical Society: "Heteroepitoxy of Compound Semiconductors and Its Parallels to the Semiconductor-Insulator System."

Carlos, W.E., Member of Program Committee of Semiconductor Interface Specialists Conference.

Carruthers, G.R., Editor, Journal of the National Technical Association.

Christou, A., Chairman of 1987 International GaAs and Related Compounds Symposium; Editor of 1987 Proceedings on GaAs and related Compounds.

Cole, R. Jr., Appointed to the West Virginia University Department of Electrical and Computer Engineering Advisory Committee.

Colton, R.J., Elected and served as chairman of the Applied Surface Science Division of the American Vacuum Society; third year as First Vice-Chairman of the ASTM E-42 Committee on Surface Analysis; appointed to the Editorial Board of Applied Surface Science.

Commisso, R.J., Elected to Executive Committee of the Standing Technical Committee on Plasma Science and Applications of the IEEE Nuclear and Plasma Sciences Society, Selected to serve on the Technical Program Committee for the 1987 IEEE Conference on Plasma Science (Seattle, WA).

Cooper, J.C., Selected by the University of Nebraska as a 1988 "Master," part of a leadership program.

Cooperstein, G., Elected fellow of the American Physical Society.

Cruddace, R.G., NASA Review Panel on use of the Japanese Ginga satellite; NASA Review Panel on the AXAF focal-plane instruments.

Dahlburg, J.P., Second year as Member of the (DOE-sponsored) Sherwood Theory Program Executive Committee; Member of the team selected as one of the 1988 R&D 100 Competition winners (sponsored by Research & Development Magazine) for development of the "Lattice Gas Algorithm."

Davis, J., Guest Editor—IEEE Transactions of Plasma Science—Special Issue "X-ray Lasers."

Dicus, R.L., Election to Sigma Xi Honorary Research Society.

Dobisz, E.A., DARPA National X-ray Lithography Coordinating Committee.

Donovan, E.P., Became member of Optical Society of America; Member of Materials Research Society, Sigma Xi; Condensed Matter and Radiation Sciences Division Computation Committee Chairman.

Dozier, C.M., ASTM E10:07 (Nuclear Technology and Applications Committee, Ionizing Radiation Dosimetry and Radiation Effects on Materials and Devices); ASTM F1:11 (Electronics/Quality and Hardness Assurance Subcommittee).

Elam, W.T., Charter member, Committee on Standards and Criteria for XAFS; External Advisory Committee (continuing membership); Biostructure PRT (X9); National Synchrotron Light Source.

Fernsler, R.F., Elected to Sigma Xi, May 1988.

Fisher, A.D., Invited to be on Technical Program Committee, OSA Topical Meeting On Optical Computing, Salt Lake City, Utah, 3/89;

Invited to teach course on Spatial Light Modulators at FLO Optical Computing Meeting, Toulon, France, 8/88; Coeditor, Special Issue on SLMS of Applied Optics (to appear 12/88); Invited to write article for Optical Computing Newsletter to appear in Laser Focus Magazine, 12/88; Chaired Optical Computing Session, OSA Annual Meeting, Rochester, NY, 10/87; Co-Author, Invited paper at OSA Topical Meeting on SLMS, Lake Tahoe, 3/88; Became IEEE Senior Member; and Invited to participate in DARPA Neural Network Study, 10/87-2/88.

Fitzgerald, J.W., Elected to a second 4-year term on the Committee on Nucleation and Atmospheric Aerosols of the International Commission on Cloud Physics.

Fliflet, A.W., Appointed to DoD/DOE Panel on Mode Converters for High Power Microwave Sources.

Fox, R.B., American Chemical Society: Elected Member of Council; Member of Society Committee on Publications; Nomenclature Committee; Vice-Chair of Joint Divisional Polymer Education Committe; Member of Polymer Division Program Committee, International Activities Committee, and Nomenclature Committee; Associate Member Council Committee on Meetings and Expositions.

Friebele, E.J., Fellow of the American Ceramic Society (continuing); Member of SDIO Optics Coordination Commitee (continuing); Chairman of Tri-service Fiber Optics Coordination Structure Committee on Radiation Effects; NATO Panel IV RSG 12 member.

Fritz, G.G., Member, High Energy Astrophysics Panel, Explorer Concept Review, NASA Headquarters, 20-22 October 1987.

Gaber, B., Member of Executive Committee for the North American Chapter of the Molecular Graphics Society; Senior Editor of "Biotechnological Applications of Lipid Microstructures."

Gardner, J.H., Member, National Aerospace Plane CFD Technical Support Team; Member, National Aerospace Plane Technology Maturation Team.

Garroway, A.N., Elected to chair 1989 Experimental NMR conference.

Giallorenzi, T.G., Chief Editor, IEEE/Optical Society of America, Journal, Lightwave Technology; Committee, IEEE Conference, Lasers and Electro-optical (CLEO); Member, Board of Editors, Optical Society of America; Member, Technical Committee, IEEE Ultrasonic Conference; Chairperson, Tri-service Fiber Optics Committee; Member, National IRIS Executive Committee, Industrial Advisory Boards of University of New Mexico and University of Virginia; Member, National Research Council Panel on Photonics Science and Technology Ass ment.

Gold, S.H., Guest Editor of the IEEE Transactions on Plasma Science Second Special Issue on High Power Microwave Generation; Associate Editor of the IEEE Transactions on Plasma Science.

Goodman, J.M., Guest editor for Radio Science (May-June issue); Guest editor for Radio Science (July-August issue); Editor-in-Chief, "Effect of the Ionosphere on Communication Navigation System," Proceedings of IES '87.

Gossett, C.R., Reviewer for Applied Physics Letters, Journal of Applied Physics, and Nuclear Instruments and Methods, Series B.

Grabowski, K.S., Co-chairman and co-editor for proceedings of symposium on "Environmental Degradation of Ion and Laser Beam Treated Surfaces" held at the TMS Fall 1988 meeting in Chicago.

Griffin, O.M., Editorial Board Member and Associate Editor, Journal of Fluids and Structures, Academic Press, London; Committee, International Symposium on Flow-Induced Vibration and Noise, ASME, Chicago, IL, December 1988.

Griscom, D.L., Editorial Advisory Board, Journal of Non-Crystalline Solids; Fellow of the American Ceramic Society; Appointed to NASA Universities Space Research Association Glasses and Ceramics Discipline Working Group.

Groshans, R.G., Re-elected (third year)—Class Secretary United States Military Academy Class of 1953.

Gubser, D.U., Editor, Journal of Superconductivity; Program Committee, Applied Superconductivity Conference; Session Chairman, Applied Superconductivity Conference; Co-chairman, Gordon Conference on Superconducting Films; Chairman, Naval Consortium for Superconductivity; Plenary Lecturer, Navy IRAD Conference (High-Temperature Superconductivity); Manager, SDI High-Temperature Superconductivity Program; Committee member for study of "High Magnetic Field Facilities in the USA."

Gruber, P.L., Election to Sigma Xi Honorary Research Society.

Haftel, M.I., CMRSD Colloquium Committee (Chairman 1987-1988).

Hellrich, F.V., Member, Space-based Elements Study, Strategic Defense Initiative Organization (SDIO).

Hera, P.L., Member, High-Energy Astrophysics Review Panel for NASA Astrophysics Data Program

Holmes, B.S., Selected to participate in 1988-1989 Women's Executive Leadership Program; Featured Scientist, Chicago Museum of Science and Industry Black Achievers in Science Exhibit.

Hoppel, W.A., Appointed to the Editorial Board of the journal, Aerosol Science and Technology of the American Association for Aerosol Research; Member, Awards Committee of the American Association for Aerosol Research.

Hsu, D.S.Y., Elected Fellow, American Institute of Chemists.

Hubler, G.K., Member, International Committee, Conference on Surface Modification of Metals by Ion Beams; Member, Joint Services Committee on Laser Eye Protection Program.

Hui, C.M.T., Invited speaker at the 13th Annual Meeting of the Plasma Physics Division of the American Physical Society —"Key Physics Issues Associated with Free Electron Lasers"; Program Committee Member for the 1989 Particle Accelerator Conference.

Hurdle, B.G., Acoustical Society of America (Membership Committee).

Jacob, R.J.K., Tutorials Chair for the ACM CHI'88 Conference on Human Factors in Computing Systems.

Kabler, M.N., Fellow, American Physical Society; Member, National Synchrotron Light Source PRT Council; Member, LASS/BASS Technology Assessment Subpanel of Balanced Technology Initiative HPM Program Implementing Panel.

Kailasanath, K., Member, AIAA Propellants and Combustion Technical Committee; Elected, Senior Member, American Institute of Aeronautics and Astronautics (AIAA).

Kapetanakos, C.A., Fellow, APS (Continuing); Fellow, Washington Academy of Science (Continuing).

Kaufman, B., Elected Chairman of Astrodynamics Technical Committee of the American Institute of Aeronautics and Astronautics (AIAA) for 1988-1989; Technical chairman of Astrodynamics Specialists conference Aug. 1988 of the American Institute of Aeronautics and Astronautics and the American Astronautical Society; Selected as a member of Program Committee for the 1989 Goddard Space Flight Center's International Symposium on orbital mechanics and mission design.

Keramidas, G.A., Editor-in-Chief, HYDROSOFT, International Journal for Hydrodynamics and Hydraulics.

Kim, C., Appointed to Manuscript Board of Review, Journal of Materials Engineering; Elected Vice President of the Korean American Scholarship Foundation; Elected Councillor (Group I, Materials Sciences) of the

Korean Scientists and Engineers Association of America, Inc.

Klein, B.M., Member, Session Organizing Committee for the March, 1988 American Physical Society Meeting; Member, NRL Incentives Awards Committee; Chairman, Peer Review Committee, Pittsburgh Supercomputer Center and National Center for Supercomputer Applications.

Klein, P.H., Guest Editor of the Journal of Crystal Growth special issue on purification of materials for crystal growth and glass processing; Associate Editor of Materials Letters; Fellow, American Institute of Chemists.

Krowne, C.M., Member of the Technical Program Committee for the 1988 IEEE MTT-S International Microwave Symposium.

Knudson, A.R., Member of NRL Space Warfare Working Group of Space Technology Study.

Lambert, J.M., Reviewer, Physical Review Letters, National Science Foundation, American Association for the Advancement of Science, and American Institute of Physics; Appointed to Executive Council, College of Arts and Sciences, Georgetown University; Continuing as Chairman, Department of Physics, Georgetown University; Director, Georgetown University Bicentennial Lecture Series "Frontiers in Science," Organizing Committee, International Symposium on the Three-body Force in the Three-nucleon System, 1986; Organizing Committee and Cochair of Plenary Sessions of the 1988 Conferences of the Applications of Accelerators in Research and Industry.

Lamontagne, R.A., Appointed to NATO AC/225 (Panel VII/Naval Subpanel) Ad Hoc Working Group on Standardization of Ship NRC Filters.

Lampe, M., Editor of series of review articles on charged particle beams, to appear in special issue Journal of Defense Research.

Landwehr, C.E., Chairman, IEEE TC on Security and Privacy; Chairman, IFIP Working Group 11.3 on Database Security; Chairman, TTCP XTP-1 on Trustworthy Computing Technologies, IEEE Distinguished Visitor.

Lau, Y.Y., Invited speaker at the 13th Annual Meeting of the Plasma Physics Division of the American Physical Society—"New Results on the Theory of Beam Break-Up Instabilities."

Lee, J.N., Treasurer of the IEEE Steering Committee for the IEEE-OSA Journal of Lightwave Technology; Member of the Joint IEEE-OSA Coordinating Committee for the Journal of Lightwave Technology; A Navy Representative on the Optical Signal Processing Tri-service Advisory Group for the Office of Secretary of Defense; Member, Aerospace Industry Association Panel on Optical Information Processing; Senior Member of the IEEE.

Lessoff, H., Presidential Letter of Commendation January 88; Member, Electronic Material Committee; Metallurgical Society of AIME, Conference Committee Member; 1st International Conference on InP and Related Materials (1989); Member, Organizing Committee, 6th Semi-Insulating Semiconducting Materials Conference (Toronto, 1990); Coordinating Committee, Multi-Lateral Export Control (COCOM); Member, Technical Working Group 5 and Technology Transfer Group F.

Mr. Howard Lessoff and his wife show his letter of commendation from President Ronald Reagan for research work that saved the government significant money.

CAPT William Clautice (right) presents Dr. Frances Ligler with a 1987 Annual Research Publication Award

Dr. Philip Selwin (right) of the Office of Naval Technology presents the President's Meritorious Rank Award for Senior Executives to Dr. John Montgomery

Ligler, F.S., 3-M Medical-Surgical Division AAMI Annual Meeting Manuscript Award presented to F. S. Ligler, T. L. Fare, K. D. Seib, J. W. Smuda, A. Singh, M. E. Ayers, A. Daiziel and P. Yager.

Marrian, C.R.K., DARPA National X-ray Lithography Coordinating Committee.

McCafferty, E., Member, Executive Committee, Corrosion Division of the Electrochemical Society; Member, Technical Affairs Committee, the Electrochemical Society.

McGrath, K.J., Participant in the NRL Edison Program for graduate study at Georgetown University.

McMahon, J.M., Member, Ground-Based Free Electron Laser Technical Advisory Group; Member, Pilot Near-Term Applications Study Team (USAF-AFWL); independent consultant to Department of Energy on solid state lasers for inertial confinement fusion and review of LLNL Inertial Confinement Fusion Program; Member, Steering Committee on High Average Power Burst Neodymium Laser (Defense Nuclear Agency); Common Module Laser Committee advisory to JDL-Technical Panel on Electronic Warfare; Advisory Committee on Basilisks and MPSSL Programs.

Mehl, M.J., Member, Sigma Xi; Member, American Physical Society; Member, American Geophysical Union.

Metzbower, E.A., Member, Board of Directors of the Laser Institute of America; Chairman of the Electron and Laser Beam Committee of the Joining Division Council of ASM International; Cochairman and Coeditor of International Conference on Power Beams.

Michel, D.J., Member, Technical Program Committee, Third International Symposium on Environmental Degradation of Materials in Nuclear Power Systems—Water Reactors; Member, Task Force on Crack Propagation Technology, Metals Properties Council and American Society of Mechanical Engineers, Boiler and Pressure Vessel Code Subcommittee on Properties of Metals; Professional Lecturer, The George Washington University.

Molnar, B., Chairman of the Processing Technology Section of the 14th International Symposium on GaAs and Related Compounds; Invited Talk, "Optically Detected Magnetic Resonance Studies in Shallow Impurities in Heteroepitaxial Laser of $Al_xGa_{1-x}As$ on GaAs," by E. Glasser, T. A. Kennedy, and B. Molnar, at the 3rd International Conference on Shallow Impurities in Semiconductors.

Moniz, W.B., U.S. Navy Representative, Technical Panel 3 (Organic Materials), Subgroup P of the Technical Cooperation Program; Advisory Board, National Center

for Composite Materials Research, University of Illinois.

Mueller, G.P., Member, Organizing Committee for the 7th DoD Conference on DEW Vulnerability, Survivability, and Effects: Member, Organizing Committee for the 10th Annual Lasers in Modern Battlefield Conference; Subpanel chairman for the International Information Exchange Agreement IEP UK-III.

Murday, J.S., Member, Board of Directors, American Vacuum Society; Member, American Institute of Physics governing board.

Murtagh, E.B., Professional Engineer, registration with state of Maryland.

Nagel, D.J., Chairman, X-UV Technical Group Optical Society of America 1986-1987; Member, Program Advisory Committee National Synchrotron Light Source Brookhaven National Laboratory Department of Energy; Member, Program Review Committee National Laser Users Facility Laboratory for Laser Energetics University of Rochester; Chairman, Technology Panel High Power Microwave Program Balanced Technology Initiative; Member, Proposal Review Committee X-ray Lithography Program Very High Speed Integrated Circuits (VHSIC) Program, Defense Advanced Research Projects Agency; Member, Lethality Assessments Group Defense Nuclear Agency; Member, Program Committee Ninth International Conference on Vacuum Ultraviolet Radiation Physics; Chairman, NRL Committee on Technology Transfer.

Namenson, A., DNA Advisory Committee on Military Standards, Hardness Assured Device Specifications.

Natishan, P.M., Chairman for the Symposium on Marine Corrosion, 1989 NACE Northeast Regional Meeting; Program Chairman, Baltimore-Washington Section of NACE; Treasurer, National Capital Section of the Electrochemical Society; Representative to the Individual Membership Committee, the Electrochemical Society.

Neihof, R.A., Steering committee member, International Association for Stability and Handling of Liquid Fuels.

O'Grady, W.E., Appointed editor of physical electrochemistry for the Journal of the Electrochemical Society.

Olin, I.D., Fellow of the IEEE.

Oran, E.S., National WISE Award in Science; Editorial Board, Progress in Energy and Combustion Science; Vice Chairman, Division of Fluid Dynamics, American Physical Society; Member, Committee on the Status of Women in Physics, American Physical Society; Chairman, Committee in Status and Bylaws, American Geophysical Union; Publications Committee, American Institute of Aeronautics and Astronautics, Chairman, Subcommittee on Technical Information Services.

Ossakow, S.L., Organizer, Special Session on High Latitude Ionospheric Turbulence at the 1988 MIT Cambridge Workshop in Theoretical Geoplasma Physics; Advisor, ONR Ionospheric Research.

Pande, C.S., Member of Newly Formed Superconducting Materials Committee of TMS Metallurgical Society; Chairman, Electrical, Magnetic and Optical Phenomena Committee of American Society of Metals.

Papaconstantopoulos, D., Member, organizing committee of the 20th International Conference on the Physics of Semiconductors.

Parker, R.K., Navy member of the OUSD (Acquisition) Advisory Group on Electron Devices, Working Group A: Microwaves; Member of the Executive Board for the Air Force Thermionic Research Initiative at the University of California at Los Angeles.

Pauls, T.A., Fellow, American Astronomical Society; Fellow, Royal Astronomical Society (London); Fellow, International Astronomical Union.

NRL EEO award winners for 1988 are (left to rignt) Ms. Garbrielle Peace, Mr. Harold Eaton, and Ms. Grace Burroughs. Ms. Burroughs is also the first recipient of the Office of the Chief of Naval Research EEO Supervisor of the Year Award.

CAPT William G. Clautice, USN, NRL's Commanding Officer, R.E. Reynolds, head of the Video Services Section, and J.W. Gately, head of the Information Services Branch and NRL's Public Affairs Officer accept NRL's award for Best Audio–Visual Presentation for 1988 from the Combined Federal Campaign.

Peebles, D.L., Chairman, Condensed Matter and Radiation Sciences Division Colloquium Committee, 1988–1989.

Pickett, W.E., Appointed to the Editorial Board of Journal of Superconductivity.

Petersen, E.L., Program Area Reviewer for DNA Neutral Particle Beam Program; Editor, Journal of Radiation Effects, Special Issues, Technical Program Chairman for DNA DARPA Single Event Upset Symposium.

Rath, B.B., Chairman, Surfaces and Interfaces Committee; ASM–International; Editorial Board, International Materials Review; Co–organizer, Interface Design Conference; TMS Representative, American Association of Engineering Societies; Member, ASM–International Fellow Selection Committee; Adjunct Professor, Colorado School of Mines; Member, Advisory Board, Light Metal Center, University of Virginia.

Reinecke, T.L., Secretary, Steering Committee of the Greater Washington Solid State Physics Colloquium; Member, National Science Foundation Evaluation Committee for Centers of Science and Technology; Member, Solid State Sciences Committee of the National Research Council of the National Academy of Sciences.

Rife, J.C., Division 4600 COMSPEC Committee.

Ritter, J.C., Tutorial Short Course Instructor at the 1989 IEEE Nuclear and Space Radiation Effects Conference short course on Radiation Effects; Invited to address the International Commission on Radiation Units & Measurements at its 1988 meeting in Helsinki, Finland; Selected by the Defense Nuclear Agency (DNA) to serve on the editorial board to prepare a special issue of the Journal of Defense Research (JDR) on System Generated Electromagnetic Pulse (SGEMP); Session Chairman, DNA/DARPA Single Event Upset Symposium; Member of the Air Force Space

Ronald Beard (left), head of Sigma Xi presents Dr. Barry Ripin with the 1988 Sigma Xi Applied Science Award

Technology Center, Space and Missiles Environment Interaction Strategy Panel.

Roland, C.M., Editorial Advisory Board, American Chemical Society Symposium Series and Advances in Chemistry Series.

Ruhnke, L.H., Elected President, International Commission on Atmopsheric Electricity of the International Association of Meteorology and Atmospheric Physics. (Member organization of IUGG).

Sadananda, K., Member, American Society of Materials; Program Chairman, Conference on Stress Induced Microstructural Instability; Vice-chairman—Flow and Fracture committee; Member of Physical Metallurgy, Mechanical Metallurgy and Structural Metallurgy committees of the AIME; Member of the Board of Review of Metallurgical Transactions Journal.

Sadeghi, H.R., CM&RSD Division Colloquium Committee.

Saenz, A.W., Chairman and Co-organizer of Invited Speaker Session on "Dynamical Systems," Spring 1988 Meeting of the American Physical Society; Editor of "Method and Applications of Nonlinear Dynamics."

Sandlin, G.D., Major contributor and editor of the film "The Universe," that appeared in the videotape volume, "Achievements in Space" and that was voted best science film of the year.

Sartwell, B.D., General Chairman, 16th International Conference on Metallic Coatings; Editor, Journal of Surface and Coatings Technology; Executive Committee Member, Vacuum Metallurgy Division of the American Vacuum Society.

Schmidt-Nielsen, A., Newsletter Editor, Division 21; American Psychological Association Member; Technical Committee for Speech Communications, 1986–1988; Acoustical Society of America.

Schnur, J.M. (DR), Senior Editor of "Biotechnological Applications of Lipid Microstructures;" Chairman of Gordon Conference on Organic Thin Films (Feb. 1990).

Share, G.H., Co-editor of American Institute of Physics Conference Proceedings 170, "Nuclear Spectroscopy of Astrophysical Sources."

Sheinson, R.S., Combustion Institute, Eastern Section Secretary.

Singer, I.L., First prize for poster entitled "Friction Coefficients: How Low Can They Go?" at Gordon Conference on Tribology, June 1988.

Skelton, E.F., Spokesperson for High Pressure Insertion Devices Team at National Synchrotron Light Source, Brookhaven National Laboratory.

Sleger, K., Technical Vice Chairman 1988 IEEE GaAs IC Symposium; International Advisory Committee, 2nd International Conference on Amorphous and Crystalline Silicon Carbide and Related Materials; Committee Member, First International Conference on Indium Phosphide and Related Materials for Advanced Electronic and Optical Devices; Deputy member, Advisory Group on Electron Devices, Working Group A.

Smidt, F.A., Fellow, ASM International; NRL-FABTECH Committee, Chairman Materials and Coatings Working Group, NRL

Space Technology Study; Navy Council on Materials and Structures, U.S. Government-TTG-A, Subgroup C (Technology Export Control Advisory Group on Coatings); American Society for Materials (National Committee)—Technical Awareness Advisory Committee; American Society for Materials—Cochairman, Organizing committee for symposium on Engineered Materials for Advanced Friction and Wear Applications; Materials Research Society—Cochairman, Symposium A—organizing committee, "Processing and Characterization of Materials Using Ion Beams," Fall '88 MRS meeting; cochairman—organizing committee for International Conference on Surface Modification of Metals by Ion Beams.

Sprangle, P., Member 1988 Program Committee for the APS Division of Plasma Physics; Panel Member, Magnetic Fusion Advisory Committee (MFAC) XXI on Electron Cyclotron Heating (ECH); Invited speaker, 13th Annual meeting, Plasma Physics Division of American Physical Society, "Coherent Radiation Sources."

Stolovy, A., Chairman, Energetic Materials Panel, Particle Beam Weapons, S.D.I.; Member, Lethality Assessment Panel, Particle Beam Weapons, S.D.I.

Strom, U., Program Committee Member, 13th International Conference on Infrared and Millimeter Waves.

Summers, G.P., Served as Session Chairman for IEEE Radiation Conference; Head, Physics Department, University of Maryland, Baltimore, MD.

Tatem, P.A., Combustion Institute, Eastern Section, Meeting Arrangements Chairman.

Teitler, S., Fellow of the American Physical Society (continuing).

Tolstoy, A.I., Federal Women's Program Subcommittee.

Trzascoma, P., Vice Chairman Council of Local Sections (Electrochemical Society); Member, Ad Hoc Committee on Publicity (Electrochemical Society); Member, Publications Committee (Electrochemical Society); Officer, National Capital Section of the Electrochemical Society.

Dr. Edward Takken, recipient of the 1988 Navy Meritorious Civilian Service Award is pinned by CAPT William G. Clautice as his family looks on.

Turner, N.H., Continuing as an Alternate Counselor for the Chemical Society of Washington (Washington Section of the American Chemical Society). Membership Secretary, Division of Colloid and Surface Chemistry, American Chemical Society.

Vandermeer, R.A., Inducted as Fellow of American Society for Metals International; Vice-Chariman of the Recovery and Annealing Committee of ASM International.

Valenzuela, G.R., Member, Ad-Hoc Group on the International Geosphere Biosphere Program (IGBP) of the International Union of Radio Science (URSI); Cochairman, Office of Naval Research Workshop on "The Modulation of Gravity-Capillary Waves by Nonuniform Currents."

Venezky, D.L., Alternate Councilor to represent the Chemical Society of Washington; Member, Committee of Nominations and Elections, American Chemical Society.

Wagner, R.J., Program Committee Member, 1989 U.S. Workshop on the Physics and Chemistry of Mercury Cadmium Telluride; Member,

Program Committee of the IRIS Specialty Group on Infrared Materials; Member, Program Committee, International Conf. on Narrow Gap Semiconductors and Related Materials.

Walker, D.H., Chairperson, Interagency Advanced Power Group (IAPG) Solar Working Panel 1988–1989.

Webb, D.C., Member, Technical Program Committee, 1988 Ultrasonics Symposium, IEEE; Member, Technical Program Committee, 1988 International IEEE Microwave Theory and Techniques Symposium.

Weller, J.R., Member, Program Committee, Optical Fiber Communication; Chairman, Tri-service Fiber Optic Subcommittee on Sources and Detectors; Associate Editor, Optical Letters.

Whitlock, R.R., Invention Disclosure Evaluation Board.

Wieting, T.J., Member, Organizing Committee, 4th National Conference on High-Power Microwave Technology; Program Chairman, 4th National Conference on High-Power Microwave Technology; Editor, Proceedings of the 4th National Conference on High-Power Microwave Technology; Member, DoD Microwave Effects Panel; Member, DoD Systems Assessment Subpanel; Member, DoD Team on Project Tiger Grip; Member, Review Group on AF Project Seek Needle.

Wilhelm, P.G., 1987 Presidential Meritorious Rank Award.

Willet, J.C., Associate Editor, Journal of Geophysical Research, Atmospheres.

Williams, F., Member, Government Board, Combustion Institute, Eastern Section.

Zedd, M.F., Secretary, American Institute of Aeronautics and Astronautics Guidance, Navigation, and Control Technical Committee.

ALAN BERMAN RESEARCH PUBLICATION AWARDS

The Annual Research Publications Awards Program was established in 1968 to recognize the authors of the best NRL publications each year. These awards not only honor individuals for superior scientific accomplishments in the field of naval research, but also seek to promote continued excellence in research and in this documentation. In 1982, the name of this award was changed to the Alan Berman Research Publications Award in honor of its founder.

There were 1378 separate publications published in 1988 that were considered for recognition. Of those considered, 32 were selected. These selected publications represent 112 authors each of whom received a publication awards certificate, a bronze paperweight, and a booklet of the publications receiving special recognition. In addition, NRL authors share in their respective division's monetary award.

The winning papers with their respective authors are listed below by their research units. Non-Laboratory coauthors are indicated by an asterisk.

Office of Director of Research

Aqueous Channels Within Apolar Peptide Aggregates: Solvated Helix of the α-Aminoisobutyric Acid (Aib)-Containing Peptide Boc-(Aib-Ala-Leu)$_3$-Aib-OMe·2H$_2$O·CH$_3$OH in Crystals
Isabella L. Karle, Judith L. Flippen-Anderson, Kuchibhotla Uma,* and Padmanabhan Balaram*

Space Science Division

The Application of Radio Interferometry to Surveillance at Low Radio Frequencies
Kenneth J. Johnston, Richard S. Simon, John F. Meekins,
John H. Spencer, and John A. Waak

Gamma-Ray Line Emission From SN1987A
Steven M. Matz, Gerald H. Share, Mark D. Leising, Mark S. Strickman,
Edward L. Chupp,* William T. Vestrand,* William R. Purcell,* and Claus Reppin*

Laboratory for Computational Physics and Fluid Dynamics

On Evaluating the Reaction Path Hamiltonian
Michael J. Page and James W. McIver, Jr.*

Ocean and Ship Wave Modification by a Surface Wake Flow Pattern
Owen M. Griffin, George A. Keramidas, Thomas F. Swean, Jr., Henry T. Wang
Richard A. Skop,* and Yvan Leipold*

Condensed Matter and Radiation Sciences Division

The Development of Non-Uniform Deposition of Holes in Gate Oxides
Ralph K. Freitag, Charles M. Dozier, Dennis B. Brown,
and Edward A. Burke*

Ionic Contributions to Lattice Instabilities and Phonon Dispersion in La_2CuO_4
Ronald E. Cohen, Warren E. Pickett, Larry L. Boyer,
and Henry Krakauer*

Plasma Physics Division

Development of a Sodium-Pump/Neon-Lasant Photopumped Soft X-Ray Laser
Stavros J. Stephanakis, John P. Apruzese, Gerald Cooperstein, Jack Davis,
David Mosher, Paul F. Ottinger, Victor E. Scherrer, J. Ward Thornhill,
Frank C. Young, Philip G. Burkhalter,[1] David D. Hinshelwood,*
Germaine Mehlman,* and Benjamin L. Welch*

Externally Modulated Intense Relativistic Electron Beams
Moshe Friedman, Yue Ying Lau, Victor Serlin, and Jonathan Krall*

Radar Division

On the Design and Test of an Advanced Instrument Landing System
William M. Waters and George J. Linde

Measurement and Interpretation of North Atlantic Ocean Marine Radar Sea Scatter
Dennis B. Trizna

Acoustics Division

Experimental Confirmation of Horizontal Refraction of CW Acoustic Radiation from a Point Source in a Wedge-Shaped Ocean Environment
R. Doolittle, Alexandra I. Tolstoy, and Michael Buckingham*

Target Classification Based on Form Function Representations Derived from Scale Model Measurements
Nai-Chyuan Yen, Louis R. Dragonette, and Charles F. Gaumond

Information Technology Division

Credit Assignment in Rule Discovery Systems Based on Genetic Algorithms
John J. Grefenstette

A Distributed Reservation-Based CDMA Protocol That Does Not Require Feedback Information
Jeffrey E. Wieselthier, Julie Ann B. Tarr, and Anthony Ephremides*

1 Condensed Matter and Radiation Sciences Division

Tactical Electronic Warfare Division

Electronic Warfare Unintentional-Modulation Processors: System Definition Considerations
Robert L. Goodwin

Underwater Sound Reference Detachment

Resistivity of Rubber as a Function of Mold Pressure
Corley M. Thompson, Timothy W. Besuden,* and Linda L. Beumel*

Chemistry Division

High Molecular Weight Boron Oxides in the Gas Phase
Robert J. Doyle, Jr.

Hyperfine Interactions in Cluster Models of the P_b Defect Center
Michael Cook and Carter T. White

Materials Science and Technology Division

The Relation of Tensile Specimen Size and Geometry Effects to Unique Constitutive Parameters for Ductile Materials
Peter Matic, George C. Kirby III, and Mitchell I. Jolles

Crystallography of the ζ to β' Massive Transformation in Ag-50 at. % Cd
Jack D. Ayers, Peter G. Moore, and Robert A. Masumura

Optical Sciences Division

Narrow-Linewidth Unstable Resonator
David G. Cooper,* Lawrence L. Tankersley,* and John F. Reintjes

Ultrahigh Electron and Hole Mobilities in Zero-Gap Hg-Based Superlattices
Jerry R. Meyer, Craig A. Hoffman, Filbert J. Bartoli, Jr., Jeong W. Han,* James W. Cook, Jr.,* Jan F. Schetzina,* X. Chu,* Jean-Pierre Faurie,* and Joel N. Schulman*

Optimization and Stabilization of Visibility in Interferometric Fiber-Optic Sensors Using Input-Polarization Control
Alan D. Kersey, Michael J. Marrone, Anthony Dandridge, and Alan B. Tveten

Electronics Science and Technology Division

Growth and Structure of Aluminum Films on (001) Silicon Carbide
Victor M. Bermudez

Magneto-Optical Properties of Highly Anisotropic Holes in HgTe/CdTe Superlattices
Jose M. Perez, Robert J. Wagner, Jerry R. Meyer, Jeong W. Han,* James W. Cook, Jr.,* and Jan F. Schetzina*

Space Systems Development Department

The Figure-of-8 Librations of the Gravity Gradient Pendulum and Modes of an Orbiting Tether
Peter J. Melvin

Two-Wave Mixing Photorefractive Diffraction Efficiency
G. Charmaine Gilbreath and Fred M. Davidson*

Spacecraft Engineering Department

Implementing Recurrent Back-Propagation on the Connection Machine
Etienne M. Deprit

LIPS III: An Effective and Existing 'Lightsat'
Robert H. Towsley, David A. Hastman, and Michael E. Mook

Space Systems Technology Department

Reduction of Cavity Pulling in a Passive Hydrogen Maser
William M. Golding,* Vincent J. Folen, Alick H. Frank, Joseph D. White, and Ronald L. Beard

IFF Interrogation Without Directional Antennas: A Proposed Method
Richard J. Blume

PROFESSIONAL DEVELOPMENT

NRL has established many programs for the professional and personal development of its employees so that they may better serve the needs of the Navy. These programs develop and retain talented people and keep them abreast of advanced technology management skills. Graduate assistantships, fellowships, sabbatical study programs, cooperative education programs, individual college courses, and short courses for personal improvement contribute to professional development.

Programs are also available for non-NRL employees. These enhance the Laboratory research program by providing a means for non-NRL professionals to work at the Laboratory and thus improve the exchange of ideas, meet critical short-term technical requirements, and provide a source of new, dynamic scientists and engineers. The programs range from two-year graduate fellowships, faculty and professional interchanges, and undergraduate work to an introduction of gifted and talented high school students to the world of technology.

PROGRAMS FOR NRL PEOPLE

During 1988, under the auspices of the Employee Development Branch, NRL employees participated in about 5000 individual training events. Many of these were presented as either videotaped or on-site instructed courses on diverse technical subjects, management techniques, and enhancement of such personal skills as efficient use of time, speed reading, memory improvement, and interpersonal communications. Courses are also available by means of computer-based training (CBT) and live television courses for monitoring nationwide.

One common study procedure is for employees to work full time at the Laboratory while taking job-related scientific courses at universities and schools in the Washington area. The training ranges from a single course to full graduate and postgraduate programs. Tuition for training is paid by NRL. The formal programs offered by NRL are described here.

GRADUATE PROGRAMS

• The **Advanced Graduate Research Program** (formerly the Sabbatical Study Program) enables selected professional employees to devote full time to research or pursue work in their own or a related field for one academic year at an institution of their choice without the loss of regular salary, leave, or fringe benefits. NRL pays all educational costs, travel, and moving expenses for the employee and dependents. Criteria for eligibility include professional stature consistent with the applicant's opportunities and experience, a satisfactory program of study, and acceptance by the institution selected by the applicant. The program is open to paraprofessional (and above) employees who have completed 6 years of Federal Service, 4 of which are required at NRL. Since the program began in 1964, 164 employees have participated.

• The **Edison Memorial Graduate Training Program** enables employees to pursue advanced studies in their fields at local universities. Participants in this program work 24 hours each workweek and pursue their studies during the other 16 hours. The criteria for eligibility include a minimum of 1 year of service at NRL, a bachelor's or master's degree in an appropriate field, and professional standing in keeping with the candidate's opportunities and experience.

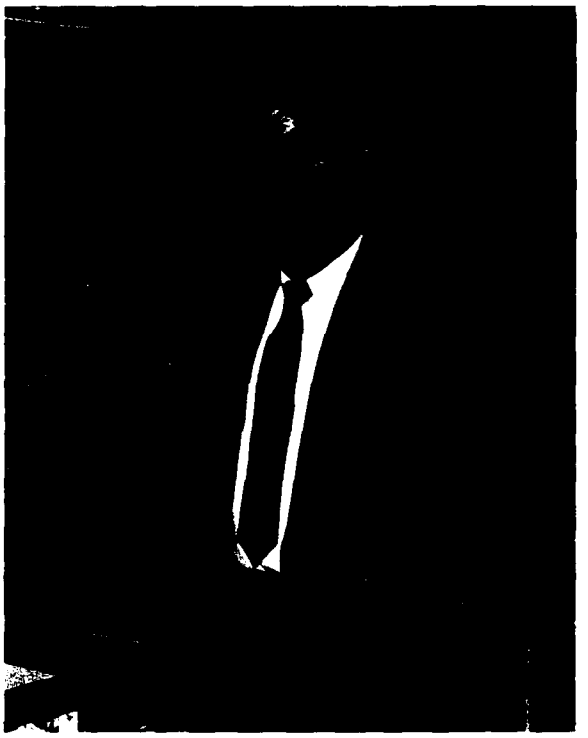

Dr. Philip R. Schwartz, head of the Infrared and Millimeter-Wave Astronomy Section, spent a summer with the Institute for Applied Physics at the University of Bern, Bern, Switzerland as part of the NRL Advanced Graduate Research Program.

• To be eligible for the **Select Graduate Student Program**, employees must have a college degree in an appropriate field and must have maintained at least a B average in undergraduate study. Students accepted in this program devote a full academic year to graduate study. While attending school, they receive one half of their salary, and NRL pays for tuition, books, and laboratory expenses. During the summer, they work at the Laboratory and receive normal pay and fringe benefits. Forty-one staff members have enrolled in the program since it began in 1967.

Laura Loechler, Systems Engineering and Analysis Branch, completed her Master of Science in aerospace engineering at the Massachusetts Institute of Technology while participating in the Select Graduate Student Program

• Research conducted at NRL may be used as **thesis material for an advanced degree.** This original research is supervised by a qualified employee of NRL who is approved by the graduate school. The candidate should have completed the required course work and should have satisfied the language, residence, and other requirements of the graduate school from which the degree is sought. NRL provides space, research facilities, and supervision but leaves decisions on academic policy to the cooperating schools.

• The **Alfred P. Sloan Fellows Program** is designed for competent young executives whose job performance indicates senior management potential. The Sloan Fellows spend 1 year with the Massachusetts Institute of Technology faculty and with policymakers in industry and government. They study the theory and practice of effective and responsible management in a rapidly changing society.

• The **Education Program for Federal Officials** is directed to the needs of a small group of Federal employees who have demonstrated high competence and unusual promise. The Woodrow Wilson School of Princeton University has developed this program to enable selected mid-career officials to enlarge their knowledge in particular disciplines, to relate their fields of specialization to the broader concerns of government, and to sharpen their capacity for objective analysis of governmental problems.

• Federal Executive fellowships are available each year to employees who want to study in the **Brookings Institute Advanced Study Program**. In the program, the fellow is exposed to and participates in planning, developing, and conducting educational conferences on public policy issues for leaders in public and private life.

• The **Fellowship in Congressional Operations for Executives** provides an opportunity for some of the most promising young, technically oriented Federal executives to participate in a variety of assignments designed to develop their knowledge and understanding of Congressional operations.

• The **Maxwell Midcareer Development Program** of the Maxwell Graduate School of Citizenship and Public Affairs, Syracuse, New York, is designed to increase the managerial knowledge, ability, and skills of experienced

Government officials who have been identified by their agencies as having potential for advancement to positions demanding progressively greater managerial and executive responsibilities.

• The **Practicing Engineer Advanced Study Program** of the M.I.T. Center for Advanced Engineering, Cambridge, Massachusetts, enables experienced engineers and applied scientists to work in-depth in technological areas pertinent to their professions.

• The **Science and Technology Fellowship Program**, a subsidiary of the Commerce Science Program, includes a variety of special events, lectures, seminars, visits, conferences, field trips, and interactions with key persons from both the public and private sectors. Participants spend one week on Capitol Hill in an intensive, congressional orientation, and one week at the Brookings Institute Science Policy Conference. They also take two week-long field trips for on-site inspection of scientific institutions and industrial complexes.

• The **Stanford-Sloan Program of the Graduate School of Business**, Stanford, California, offers exceptional young executives an opportunity to make an intensive study of new concepts in business, to develop a top management perspective, and to broaden their intellectual horizons.

• The **Naval Postgraduate School** (NPS) in Monterey, California, provides advanced graduate study to selected Federal civilian employees who meet NPS academic requirements for the program in which they are interested, and whose employing agency is willing to act as sponsor.

CONTINUING EDUCATION

• Local colleges and universities offer **undergraduate and graduate courses** at NRL for employees interested in improving their skills and keeping abreast of current developments in their fields. These courses are also available at many other DoD installations in the Washington, DC area.

• The Employee Development Branch at NRL offers to all employees **short courses** in a number of fields of interest including technical subjects, computer operation, supervisory and management techniques, and clerical/secretarial skills. Laboratory employees may attend these courses at nongovernment facilities as well. Interagency courses in management, personnel, finance, supervisory development, and clerical skills are also available.

For further information on any of the above programs, contact the Employee Development Branch (Code 1840) (202) 767-2956.

TECHNOLOGY TRANSFER

• The **Navy Science Assistance Program** establishes an information loop between the Fleet and the R&D shore establishments to expedite technology transfer to the user. The program addresses operational problems, focuses resources to solve specific technical problems, and develops a nucleus of senior scientific personnel familiar with the impact of current research and system performance on military operations.

• The **Office of Research and Technology Applications Program** ensures the full use of the results of the Nation's federal investment in research and development by transferring federally owned or originated technology to state and local governments and the private sector.

The Navy's Scientists-to-Sea program offers Navy researchers and R&D managers the opportunity to learn firsthand about factors that affect shipboard system design and operations. The program includes personnel from NRL. A first allotment of 25 embarkation opportunities was completed in September 1987 with trips lasting from three to ten days. Because of the success of the first experiment, the Scientists-to-Sea program has been scheduled to continue indefinitely

with new embarkations offered on a quarterly basis.

Inquiries concerning NRL's technology transfer programs should be made to Dr. George Abraham (Code 1003.2), at (202) 767-3744.

PROFESSIONAL DEVELOPMENT

NRL has several programs, professional society chapters, and informal clubs that enhance the professional growth of employees. Some of these are listed below.

• The **Counseling Referral Service** (C/RS) helps employees to define short- and long-range career goals, to improve their job-seeking skills, and to deal with issues affecting job productivity. The C/RS provides individual counseling, career development, and training workshops on such topics as stress management, relaxation techniques, substance abuse, and weight control. Additionally, the C/RS is available to help employees with any kind of personal problems that may be interfering with job performance. (Contact Dr. Valerie Hampson, Code 9012, (202) 767-6857.)

Dr. Chai-Mei Tang Hui lectures on free-electron lasers at a recent WISE seminar

• A chartered chapter of **Women in Science and Engineering** (WISE) was established at NRL in 1983. Informal monthly luncheons and seminars are scheduled to inform scientists and engineers of women's research at NRL and to provide an informal environment for members to practice their presentations. WISE also sponsors a colloquium series to feature outstanding women scientists. Guest speakers for the 1987-1988 WISE colloquia were Dr. Virginia Trimble of the Astronomy Program, University of Maryland and the Department of Physics, University of California, Irvine and Dr. Susan Soloman of the National Oceanic and Atmospheric Administration (a joint colloquia with Sigma Xi). (Contact Dr. Wendy Fuller at (202) 767-2793, Dr. Debra Rolison at (202) 767- 3617, or Dr. Cha-mei Tang Hui at (202) 767-4148.)

• **Sigma Xi**, the Scientific Research Society, encourages original investigation in pure and applied science. As an honor society for research scientists, individuals who have demonstrated ability to perform original research are elected to membership. Membership is a continuing responsibility and a mechanism for contact among scientists by conducting an active program in support of original research. The NRL chapter, comprised of approximately 450 members, encourages original research by presenting awards annually in pure and applied science to outstanding NRL staff members. The chapter also sponsors lectures at NRL on a wide range of scientific topics. Each spring the chapter sponsors an Edison Day Memorial Lecture in honor of the founder of the Laboratory. A distinguished scientist, usually a Nobel laureate, is invited to speak for the occasion. (Contact Dr. Benjamin Lepson at (202) 767-3438.)

• Employees interested in developing effective self expression, listening, thinking, and leadership potential are invited to join either of two NRL chapters of **Toastmasters International**. Members of these clubs, who possess diverse career backgrounds and talents, meet three times a month in an effort to learn to communicate not by rules but by practice in an atmosphere of understanding and helpful fellowship. NRL's commanding officer endorses Toastmasters (NRLINST 12410.11), and the Employee

Development Branch pays for membership and educational materials for those employees whose supervisors see a need for their active training in public speaking or organizational communication skills. (Contact Mrs. Kathleen Parrish at (202) 767-2782.)

EQUAL EMPLOYMENT OPPORTUNITY (EEO) PROGRAMS

Equal employment opportunity is a fundamental NRL policy for all persons, regardless of race, color, sex, religion, national origin, age, or physical/mental handicap. The EEO Office's major functions include affirmative action in employment; discrimination complaint process; community outreach program; EEO training of supervisors, managers, and EEO collateral duty personnel; advice and guidance to management on EEO policy; and the following special emphasis programs.

- The **Federal Women's Program (FWP)** improves employment and advancement opportunities for women and addresses issues that affect women in the workplace, such as child care and sexual harassment. It provides counseling and referral services and sponsors a chapter of Women in Science and Engineering to recognize outstanding female scientists and engineers. Distinguished women scientists are guest lecturers at quarterly presentations.

- The **Hispanic Employment Program (HEP)** focuses on eliminating employment barriers and advancing the hiring of Hispanics. The program is involved with Hispanic community organizations and local schools and provides activities specifically designed to offer employment opportunities to Hispanics. "El Ingeniero" (The Engineer), which encourages Hispanic youth to pursue a career in engineering, is one such program.

- The **Individuals with Handicaps Program (IHP)** assists managment to improve employment and advancement opportunities for qualified handicapped and disabled-veteran employees. It also advises on accommodations necessary for handicapped persons. It recruits handicapped summer students from colleges and universities for technical positions in engineering and science and paraprofessional positions in accounting and administration; it also seeks Cooperative Education Program (Co-op) candidates who are pursuing degrees in engineering, computer sciences, or the physical sciences.

- The **Community Outreach Program** traditionally has used its extensive resources to foster programs that provide benefits to students and other community citizens. Volunteer employees assist with and judge science fairs, give lectures, tutor, mentor, coach, and serve as classroom resource teachers. The Program also sponsors Black History Month art and essay contests for local schools, a student Toastmasters Youth Leadership Program, and an annual Christmas party for neighborhood children.

Special programs are held during the year to promote an awareness of the contributions and capabilities of women and minorities. (Contact the EEO Office at (202) 767-2486 for all EEO programs.)

OTHER ACTIVITIES

- Other programs that enhance the development of NRL employees include computer clubs (Edison Atari, Edison Commodore, and the NRL-IBM PC) and the Amateur Radio Club. The Recreation Club accommodates the varied interests of NRL's employees with its numerous facilities, such as a 25-yard, 6-lane indoor swimming pool; a gymnasium with basketball, volleyball, and badminton courts; a weight room and exercise area; ping pong; meeting rooms; softball and basketball leagues; jacuzzi whirlpool; sauna; classes in karate, aerobics exercise, swimming, and swimnastics; and specialized sports clubs

(running, skiing, biking, golfing). The Showboaters, a nonprofit drama group that presents live theater for the enjoyment of NRL and the community, performs in two major productions each year, in addition to occasional performances at Laboratory functions and benefits for local charities. The most recent musical productions include "The Foreigner." Though based at NRL, membership in Showboaters is not limited to NRL employees.

Some of the students from area schools who received awards in the Black History Month Art and Essay contests pose with NRL employees

Students from Herschel V. Jenkins High School, Savannah, Georgia perform for the Black History Month Program

Dr. Valerie F. Hampton is the employee assistance counselor for the NRL Counseling and Referral Service

PROGRAMS FOR NON-NRL PEOPLE

Several programs have been established for non-NRL professionals. These programs encourage and support the participation of visiting scientists and engineers in research of interest to the Laboratory. Some of the programs may serve as stepping-stones to federal careers in science and technology. Their objective is to enhance the quality of the Laboratory's research activities through working associations and interchanges with highly capable scientists and engineers and to provide opportunities for outside scientists and engineers to work in the Navy laboratory environment. Along with enhancing the Laboratory's research, these programs acquaint participants with Navy capabilities and concerns.

RECENT Ph.D., FACULTY MEMBER, AND COLLEGE GRADUATE PROGRAMS

• The **National Research Council (NRC)/ NRL Cooperative Research Associateship Program** selects associates who conduct research at NRL in their chosen fields in collaboration with NRL scientists and engineers. The tenure period is 2 years. Following their tenure, the Office of Naval Research offers the associate posttenure research grants tenable at an academic institution. In 1988, 29 associates chose appointments at NRL.

• The American Society for Engineering Education (ASEE) administers the **Office of Naval Technology (ONT) Postdoctoral Fellowship Program** that aims to increase the involvement of highly trained scientists and engineers in disciplines necessary to meet the evolving needs of naval technology. Appointments are for 1 year (renewable for a second and sometimes a third year). These competitive appointments are made jointly by ONT and ASEE.

• The American Society for Engineering Education also administers the Navy/ASEE **Summer Faculty Research Program** for university faculty members to work for 10 weeks with professional peers in participating Navy laboratories on research of mutual interest. NRL hosted 35 of these faculty participants in 1988.

• The **NRL/United States Naval Academy (USNA) Cooperative Program for Scientific Interchange** allows faculty members of the U.S. Naval Academy to participate in NRL research. This collaboration benefits the Academy by providing the opportunity for USNA faculty members to work on research of a more practical or applied nature. In turn, NRL's research program is strengthened by the available scientific and engineering expertise of the USNA faculty.

• The **Office of Naval Research Graduate Fellowship Program** helps U.S. citizens obtain advanced training in disciplines of science and engineering critical to the U.S. Navy. The 3-year program awards fellowships to recent outstanding graduates to support their study and research leading to doctoral degrees in specified disciplines such as electrical engineering, computer sciences, material sciences, applied physics, and ocean engineering. Award recipients are encouraged to continue their study and research in a Navy laboratory during the summer. Nine ONR Graduate Fellows chose NRL for their summer work in 1988.

For further information about the above five programs, please contact Mrs. Jessica Hileman at (202) 767-3865.

• The **United States Naval Academy Ensign Program** assigns Naval Academy graduates to NRL to work in areas of their own choosing commensurate with their academic qualifications. These graduates provide a fruitful summer of research assistance, while gaining valuable experience in the Navy's R&D program. (Contact CDR Tom Nadeau at (202) 767-2103.)

PROFESSIONAL APPOINTMENTS

• **Faculty Member Appointments** use the special skills and abilities of faculty members for short periods to fill positions of a scientific, engineering, professional, or analytical nature.

• **Consultants and experts** are employed because they are outstanding in their fields of specialization, or because they possess ability of a rare nature and could not normally be employed as regular civil servants.

• **Intergovernmental Personnel Act Appointments** temporarily assign personnel from the state or local government or educational institution to the Federal Government (or vice versa) to improve public services rendered by all levels of government.

UNDERGRADUATE COLLEGE STUDENT PROGRAMS

Several programs are tailored to the undergraduate that provide employment and work experience in naval research. These are designed to attract applicants for student and full professional employment in the Laboratory's shortage category positions, such as engineers, physicists, mathematicians, and computer scientists. The student employment programs build an understanding of NRL job opportunities among students and educational personnel so that educators can provide students who will meet NRL's occupational needs. The employment programs for college students include the following:

• The **Cooperative Education Program** alternates periods of work and study for students pursuing bachelor degrees in engineering, computer science, or the physical sciences. Several universities participate in this program.

Dr. Wendy Fuller demonstrates superconducting materials to students from the Thomas Jefferson High School for Science and Technology during National Science and Technology Week

• The **Federal Junior Fellowship Program** hires students entering college to be assistants to scientific, professional, or technical employees.

• The **Summer Employment Program** employs students for the summer in paraprofessional and technician positions in engineering, physical sciences, and computer sciences.

• The **Student Volunteer Program** helps students gain valuable experience by allowing them to voluntarily perform educationally related work at NRL.

• The **1040-Hour Appointment** employs students on a half-time basis to assist in scientific work related to their academic program.

• The **Gifted and Talented Internship Program** provides a meaningful part-time employment experience for high school graduates who plan to pursue a bachelor's degree in engineering, computer science, or the physical sciences.

For additional information, contact Mrs. Cathy Downing at (202) 767-3030.

HIGH SCHOOL PROGRAMS

• The **DoD Science & Engineering Apprentice Program** employs high school juniors and seniors to serve for 8 weeks as junior research associates. Under the direction of a mentor, students gain a better understanding of research, its challenges, and its opportunities through participation in scientific programs. Criteria for eligibility are based on science and mathematics courses completed and grades achieved; scientific motivation, curiosity, and capacity for sustained hard work; a desire for a technical career; teacher recommendations; and achievement test scores. The Naval Research Laboratory Program is the lead program and the largest in the Department of Defense.

For additional information on these programs, please contact the Employee Development Branch, Code 1840, at (202) 767-2956.

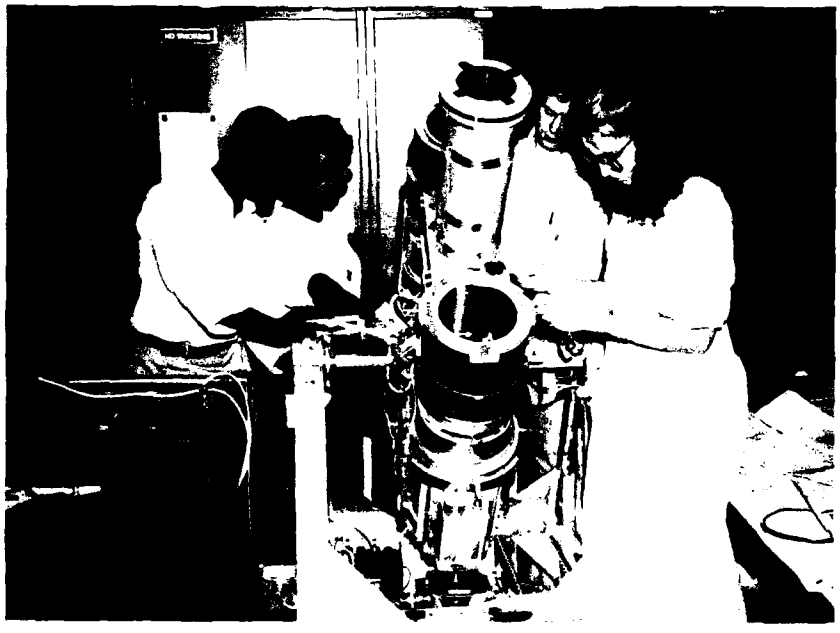

Donovan Kirkland, Rachel Clark, Steven McAllister, and Jennifer Evans run tests on the far UV cameras that will fly on a future space shuttle mission

Paul Slebodnick with Amanda Beaumont (left) and Stephanie Partridge operates the scanning electron microscope (S.E.M.), to determine the mode of failure for a helicopter part that had failed in service

GENERAL INFORMATION

"I think it's important to note that the stability of this Laboratory derives from an organization that is not given to doing precipitous sorts of things. The Navy comprises a very deliberate, very conservative, very professional, and consistently effective group of men and women with a serious, challenging mission. NRL reflects that tradition. There's a lot of pride and professionalism at NRL and no wonder—its part of an organization based on pride, professionalism, and performance."

Captain James O'Donovan
Commanding Officer at NRL,
October 1984 to October 1986

TECHNICAL OUTPUT

In several respects, NRL is like a factory—the input ingredients are the talents and ideas of the people and research funds, and the output product is information. This product is packaged in the form of reports, articles in scientific journals and books, papers presented to scientific societies and topical conferences, and patents.

This section lists a portion of NRL's output for 1988. The omitted parts are oral presentations (about 1500), reports that carry a military security classification, and letter reports to sponsors.

Type of Contribution	Unclass.	Class.	Total
Papers in periodicals, books, and proceedings of meetings	1017	0	1017
NRL Reports	48	22	70
NRL Memorandum Reports	168	27	195
Books			3
Patents granted			21
SIRs			8

A complete listing of the publications by NRL authors, including reports, articles in scientific journals and books, patents, etc. will appear in the *Bibliography of NRL Publications* to be published later this year.

KEY PERSONNEL

Code	Office		Extension*
	EXECUTIVE DIRECTORATE		
1000	Commanding Officer	CAPT J.J. Donegan, USN	73403
1001	Director of Research	Dr. T. Coffey	73301
1002	Chief Staff Officer/Inspector General	CAPT R.W. Michaux, USN	73621
1003	Associate Director of Research for Strategic Planning	Dr. W.M. Tolles	73584
1004	Scientific Consultant to Director of Research	Dr. P. Mange	73724
1005	Head, Office of Management and Admin.	Ms. M. Oliver	73086
1006	Head, Exploratory Development Program Office	Dr. S. Sacks	73666
1200	Head, Command Support Division	CAPT M.A. Howard, USN	73621
1220	Head, Security Branch	Mr. M.B. Ferguson	73048
1240	Safety Officer	Mr. J.N. Stone	72249
1280	Officer in Charge, Flight Support Detachment	LCDR G.R. Viggiano, USN	301-863-3751
1500	Head, Program Coordination Office	Dr. R.T. Swim	73314
2003	Deputy, Small Business	CDR L.E. Bounds, USN	71983
2610	Public Affairs Officer	Mr. J.W. Gately, Jr.†	72541
2700	Officer in Charge, Chesapeake Bay Detachment	CDR S.I. Kummer	301-257-4002
3008	Legal Counsel	Mr. R.H. Swennes	72244
3803	Deputy EEO Officer	Mr. J. Richardson††	72486
6100.2	Officer in Charge, Aberdeen, MD Detachment	CAPT Warren Schultz, USN	71092
	TECHNICAL SERVICES DIRECTORATE		
2000	Associate Director of Research	Mr. J.D. Brown	72879
2020	Head, Administrative Services Officer	Ms. L.V. Dabney	73585
2300	Engineering Services Officer	Mr. L.A. Sentiger	72300
2500	Public Works Officer	CDR C.R. Allshouse, USN	73371
2600	Head, Technical Information Division	Mr. P.H. Imhof	73388
2700	Chesapeake Bay Detachment Officer	CDR S. Kummer, USN	301-257-4002
2800	Head, Research Computation Division	Mr. R.F. Saenger	72751
	BUSINESS OPERATIONS DIRECTORATE		
3000	Associate Director of Research	Mr. R.E. Doak	72879
3200	Head, Contracting Division	Mr. J.H. Ablard	75227
3300	Comptroller	Mr. D.T. Green	73048
3400	Supply Officer	CDR W.E. Ralls, Jr., USN	73446
3800	Head, Civilian Personnel Division	Mrs. B.A. Duffield	73421
	GENERAL SCIENCE AND TECHNOLOGY DIRECTORATE		
4000	Associate Director of Research	Dr. W.R. Ellis	73324
4070	Health Physics Group	Mr. J.N. Stone	72232
4100	Supt., Space Science Division	Dr. H. Gursky	76343
4400	Dir., Lab. for Computational Physics and Fluid Dynamics	Dr. J.P. Boris	73055
4600	Supt., Condensed Matter & Radiation Sciences Division	Dr. D.J. Nagel	72931
4700	Supt., Plasma Physics Division	Dr. S. Ossakow	72723
	WARFARE SYSTEMS AND SENSORS RESEARCH DIRECTORATE		
5000	Associate Director of Research	Mr. R.R. Rojas	73294
5100	Supt., Acoustics Division	Dr. D.L. Bradley	73482
5300	Supt., Radar Division	Dr. M.I. Skolnik	72936
5500	Supt., Information Technology Division	Dr. R.P. Shumaker††	72903
5700	Supt., Tactical Elec. Warfare Division	Dr. J.A. Montgomery	76278
5900	Supt., Underwater Sound Reference Detachment	Dr. J.E. Blue	407-857-5230
	MATERIALS SCIENCE AND COMPONENT TECHNOLOGY DIRECTORATE		
6000	Associate Director of Research	Dr. B.B. Rath	73566
6030	Head, Lab. for Structure of Matter	Dr. J. Karle	72665
6100	Supt., Chemistry Division	Dr. J.S. Murday	73026
6300	Supt., Material Science & Technology Division	Dr. D.U. Gubser	72926
6500	Supt., Optical Sciences Division	Dr. T.G. Giallorenzi	73171
6800	Supt., Electronics Science and Technology Division	Dr. G.M. Borsuk	73525
	NAVAL CENTER FOR SPACE TECHNOLOGY		
8000	Director	Mr. P.G. Wilhelm	76547
8100	Supt., Space Systems Development Department	Mr. R.E. Eisenhauer	72611
8200	Supt., Spacecraft Engineering Department	Mr. R.T. Beal	76407
8300	Supt., Space Systems Technology Department	Mr. L.M. Hammarstrom	73920

*Direct-in-Dialing (202)76; Autovon 29-

†Additional duty

††Acting

ORGANIZATIONAL CHART
RESEARCH ADVISORY COMMITTEE
APRIL 1988

COMMANDING OFFICER
Code 1000
CAPT W.G. Clautice, USN

DIRECTOR OF RESEARCH
Code 1001
Dr. T. Coffey

ASSOCIATE DIRECTORS OF RESEARCH

OFFICE OF STRATEGIC PLANNING
Code 1003
Dr. W.M. Tolles

TECHNICAL SERVICES DIRECTORATE
Code 2000
J.D. Brown

BUSINESS OPERATIONS DIRECTORATE
Code 3000
R.E. Doak

GENERAL SCIENCE AND TECHNOLOGY DIRECTORATE
Code 4000
Dr. W.R. Ellis

WARFARE SYSTEMS AND SENSORS RESEARCH DIRECTORATE
Code 5000
R.R. Rojas

MATERIALS SCIENCE AND COMPONENT TECHNOLOGY DIRECTORATE
Code 6000
Dr. B.B. Rath

NAVAL CENTER FOR SPACE TECHNOLOGY
Code 8000
P.G. Wilhelm

ORGANIZATIONAL CHART (Continued)
EXECUTIVE DIRECTORATE

EXECUTIVE COUNCIL (DIVISION DIRECTORS)

COMMANDING OFFICER
Code 1000
CAPT W.G. Clautice, USN

RESEARCH ADVISORY COMMITTEE

CHIEF STAFF OFFICER
INSPECTOR GENERAL
INTERNAL REVIEW
Code 1002
CAPT M.A. Howard, USN

DIRECTOR OF RESEARCH
Code 1001
Dr. T. Coffey

OFFICE OF STRATEGIC PLANNING
Code 1003
Dr. W.M. Tolles

LEGAL COUNSEL
Code 3008
R.H. Swennes

FLIGHT DETACHMENT SUPPORT
Code 1280
LCDR G.R. Viggiano, USN

SAFETY OFFICER
Code 1240
J. Stone

SCIENTIFIC CONSULTANT TO THE DIRECTOR OF RESEARCH
Code 1004
Dr. P. Mange

DEPUTY EQUAL EMPLOYMENT OPPORTUNITY OFFICER
Code 3803
J. Richardson*

CHESAPEAKE BAY DETACHMENT
Code 2700
CDR S. Kummer, USN

OFFICE OF MANAGEMENT AND ADMINISTRATION
Code 1005
M. Oliver

PUBLIC AFFAIRS OFFICER
Code 2610
J.W. Gately, Jr.

ABERDEEN DETACHMENT
Code 6100.2
CAPT W. Schultz, USN

DEPUTY SMALL BUSINESS
Code 2003
CDR L.E. Bounds, USN

EXPLORATORY DEVELOPMENT MANAGER
Code 1006
Dr. S. Sacks

DIVISION DIRECTORS

COMMAND SUPPORT DIVISION
Code 1200
CAPT M.A. Howard, USN

- Security
- Military Operations
- Military Administration and Personnel
- Flight Support
- Flight Support Detachment
- Safety

PROGRAM COORDINATION OFFICE
Code 1500
Dr. R.T. Swim

ORGA

TECHNICAL SERVICES DIRECTORATE Code 2000

ENGINEERING SERVICES DIVISION Code 2300

L.A. Sentiger

- Mechanical Engineering and Manufacturing
- Electronic Engineering and Fabrication
- Industrial Engineering Services

PUBLIC WORKS DIVISION Code 2500

CDR C.R. Allshouse, USN

- Engineering
- Maintenance and Utilities
- *Contract Administration*
- Maintenance Control
- Administrative
- Planning
- Project Management
- Selective/Facilities Support Contracts

TECHNICAL INFORMATION DIVISION Code 2600

P. Imhof

- Information Services
- Technical Library
- Publications
- Graphic Design Services
- Systems/Photographic
- Historian

CHESAPEAKE BAY DETACHMENT Code 2700

CDR S. Kummer, USN

- *Operations/Security*
- Maintenance & Support

RESEARCH COMPUTATION DIVISION Code 2800

R.F. Saenger

- Software
- User Services
- Computer Operations and Communications
- Information Resources *Management*

BUSINESS OPERATIONS DIRECTORATE Code 3000

CONTRACTING DIVISION Code 3200

J.H. Ablard

FINANCIAL MANAGEMENT DIVISION Code 3300

D. Green

- Budget
- Accounting
- Disbursing
- Equipment Resource Management and Control
- Systems Operations

SUPPLY DIVISION Code 3400

CDR W.E. Ralls, Jr., USN

- Purchasing/Requisition Control
- Receipt Control
- Material
- Automated Inventory *Management*
- Technical
- Material Issue

CIVILIAN PERSONNEL DIVISION Code 3800

B. Duffield

- Staffing and Classification
- Employee Development
- Employee Relations
- Special Recruitment Programs

GENERAL SCIENCE AND TECHNOLOGY DIRECTORATE Code 4000

SPACE SCIENCE DIVISION Code 4100

Dr. H. Gursky

- Atmospheric Physics
- X-Ray Astronomy
- Radio & IR Astronomy
- Upper Atmospheric Physics
- Gamma & Cosmic Ray Astrophysics
- Solar Physics
- Solar Terrestrial *Relationships*
- Ionospheric Effects
- E.O. Hulburt Center for Space Research
- Engineering Management
- Ultraviolet Measurement
- Solar Spectroscopy

LABORATORY FOR COMPUTATIONAL PHYSICS AND FLUID DYNAMICS Code 4400

Dr. J.P. Boris

- Reactive Flow and Dynamical Systems
- Fluid/Structure Interactions
- Fluid Dynamics Developments
- Computational Physics Developments
- *Mathematical Physics*

CONDENSED MATTER AND RADIATION SCIENCES DIVISION Code 4600

Dr. D.J. Nagel

- Radiation Effects
- Directed Energy Effects
- Surface Modification
- Dynamics of Solids
- Complex Systems Theory

PLASMA PHYSICS DIVISION Code 4700

Dr. S. Ossakow

- Plasma Radiation
- Laser Plasma
- High-Power Electromag Radiation
- Experimental Plasma Physics
- Plasma Technology
- Geophysical & Plasma Dynamics
- Plasma Theory
- Advanced Beam *Technologies*
- Charged Particle Physics
- *Joint Programs for* Plasma Physics

WARFARE SYSTEMS AND SENSORS RESEARCH DIRECTORATE Code 5000

ACOUST Code 5

Dr. D.

- Acoustic *Chara*
- Applied
- Physical
- Ocean
- Manne
- Signal
- Acoustic

RADAR Code 5

Dr. M.I.

- Radar A
- Radar T
- Search
- Target
- Identific
- Airborne
- System Resea

INFORM TECHN DIVISIO Code 5

Dr. R.P.

- Navy C Appli Artific
- Comm
- Transm
- Integra
- Human
- Secure Techn

TACTIC WARFA Code 5

Dr. J.A.

- Offboa
- EW Su
- Airborn
- Ships E
- Advanc

UNDER REFER DETAC Code 5

Dr. J.E.

- Acoust
- Techni
- Electro
- Transd
- Measu
- Compu

192

ORGANIZATIONAL CHART (Continued)

WARFARE SYSTEMS AND SENSORS RESEARCH DIRECTORATE Code 5000

ACOUSTICS DIVISION Code 5100

Dr. D. Bradley

- Acoustics Media Characterization
- Applied Ocean Acoustics
- Physical Acoustics
- Ocean Dynamics
- Marine Systems
- Signal Processing
- Acoustic Systems

RADAR DIVISION Code 5300

Dr. M.I. Skolnik

- Radar Analysis
- Radar Techniques
- Search Radar
- Target Characteristics
- Identification Systems
- Airborne Radar
- Systems Control and Research

INFORMATION TECHNOLOGY DIVISION Code 5500

Dr. R.P. Shumaker*

- Navy Center for Applied Research in Artificial Intelligence
- Communication Systems
- Transmission Technology
- Integrated Warfare Technology
- Human-Computer Interaction
- Secure Information Technology

TACTICAL ELECTRONIC WARFARE DIVISION Code 5700

Dr. J.A. Montgomery

- Offboard Countermeasures
- EW Support Measures
- Airborne EW Systems
- Ships EW Systems
- Advanced Techniques

UNDERWATER SOUND REFERENCE DETACHMENT Code 5900

Dr. J.E. Blue

- Acoustic Materials
- Technical Services
- Electronics
- Transducer
- Measurements
- Computer

MATERIALS SCIENCE AND COMPONENT TECHNOLOGY DIRECTORATE Code 6000

LABORATORY FOR STRUCTURE OF MATTER Code 6030

Dr. J. Karle

CHEMISTRY DIVISION Code 6100

Dr. J.S. Murday

- Chemical Dynamics and Diagnostics
- Polymeric Materials
- Surface Chemistry
- Navy Technology Center for Safety and Survivability
- Biomolecular Engineering

MATERIALS SCIENCE AND TECHNOLOGY DIVISION Code 6300

Dr. D. Gubser

- Physical Metallurgy
- Composites and Ceramics
- Mechanics of Materials
- Structural Integrity
- Material Physics

OPTICAL SCIENCES DIVISION Code 6500

Dr. T.G. Giallorenzi

- Advanced Concepts
- Applied Optics
- Laser Physics
- Electro-optical Technology
- Optical Techniques
- Fiber Optics Technology

ELECTRONICS SCIENCE TECHNOLOGY DIVISION Code 6800

Dr. G.M. Borsuk

- Solid State Devices
- Electronic Materials
- Surface Physics
- Microwave Technology
- Semiconductors
- Vacuum Electronics

NAVAL CENTER FOR SPACE TECHNOLOGY Code 8000

SPACE SYSTEMS DEVELOPMENT DEPARTMENT Code 8100

R.E. Eisenhauer

- Spacecraft Engineering
- Advanced Systems Development
- Communication Systems Technology
- Terrestrial Systems
- SDI Office

SPACECRAFT ENGINEERING DEPARTMENT Code 8200

R.T. Beal

- Design, Manufacturing and Processing
- Systems Analysis and Test
- Control Systems
- Concept Development

SPACE SYSTEMS TECHNOLOGY DEPARTMENT Code 8300

L.M. Hammarstrom

- Space Sensing
- Space Applications
- Systems Engineering and Analysis
- Advanced Concepts and Processing

272

*ACTING

— — — ADDITIONAL DUTY

CONTRIBUTIONS BY DIVISIONS AND LABORATORIES

Space Science Division (4100)

NRL Predicts the Great Snow Storm of 1983
by Simon W. Chang and Rangarao V. Madala
Michelson Interferometry - Fifty Years Later
by Kenneth J. Johnston, David Mozurkewich, and Richard S. Simon
Theory of Origin of the Elements Confirmed
by Mark D. Leising and Gerald H. Share
QPOs: A New Astronomical Mystery
by Jay P. Norris and Paul L. Hertz
Understanding the Evolution of the Sun's Large-Scale Magnetic Field
by Neil R. Sheeley, Jr., Ana G. Nash, Yi-Ming Wang, and C. Richard Devore

Laboratory for Computational Physics and Fluid Dynamics (4400)

Very Late Time Mixing from the Rayleigh-Taylor Instability
by Jay P. Boris
The Ablative Rayleigh-Taylor Instability in Three Dimensions
by Jill P. Dahlburg and John H. Gardner

Condensed Matter and Radiation Sciences Division (4600)

Reducing Wiring Fires in Naval Aircraft
by Francis J. Campbell
Theory of High-Temperature Oxide Superconductors
by Warren E. Pickett, Dimitri A. Papaconstantopoulos, and Ronald E. Cohen
Radiation Effects in Space Systems
by James C. Ritter

Plasma Physics Division (4700)

New Horizons in Pulsed-Power Research
by Gerald Cooperstein
Laboratory Laser-Plasma Space Experiments
by Barrett H. Ripin, Charles K. Manka, and Joseph D. Huba
An Efficient Pulsed-Power Source for Photopumping an X-ray Laser
by Frank C. Young and John P. Apruzese
3D Dynamics of Ionospheric Plasma Clouds
by Steven T. Zalesak, Joseph D. Huba, and Margaret J. Mulbrandon

Acoustics Division (5100)

High-Speed, Long-Range, Unmanned Underwater Vehicle Communications Link
by James G. Eskinzes and John R. Bashista
Efficacious Methods of Characterizing Active Systems Performance
by Roger C. Gauss
The Processing Graph Method
by David J. Kaplan
Prediction of Acoustic Scattering and Radiation from Elastic Structures
by Luise S. Schuetz, Joseph Shirron, and Joseph A. Bucaro

Radar Division (5300)

Physical Optics and Plane-Stratified Anisotropic Media
by Henry J. Bilow
High Resolution X-Band Clutter Radar
by James P. Hansen
Data Compression for Spaceborne SAR Imagery—the SARCOM System
by Stephen A. Mango
HF Radar Calibration Through Land-Sea Boundaries
by Benjamin T. Root

Information Technology Division (5500)

Managing Uncertainty in Target Classification Problems
by Lashon B. Booker
Applications of Simulation Languages to Communications System Design
by Jungho Choi
New Interaction Techniques for Human-Computer Communication
by Robert J.K. Jacob

Tactical Electronic Warfare Division (5700)

Visualizing Electronic Warfare Simulations
by Michael R. Bracco and Michael J. Davis
Visualization Enhanced EW Simulations
by Alfred A Di Mattesa
Development of the Low Altitude/Airspeed Unmanned Research Aircraft (LAURA)
by Richard J. Foch and Peggy L. Toot

Underwater Sound Reference Detachment (5900)

Symbolic Integration of Special Functions
by Jean C. Piquette
Investigation of Structure-Property Relationships in Polyurethane Based on Tetramethyl Xylene Diisocyanate
by Gary M. Stack and Rodger N. Capps
An Evanescent Wave Generating Array
by David H. Trivett, Little D. Luker, Sheridan Petrie, Arnie L. Van Buren and Joseph E. Blue

Laboratory for the Structure of Matter (6030)

Automated Preparation of Protein Single Crystals by Using Laboratory Robotics
by William M. Zuk, Keith B. Ward, and Mary Ann Perozzo

Chemistry Division (6100)

Biologically Based Self-Assembly: Bio/Molecular Engineering
by the Bio/Molecular Engineering Branch

New Chemicals from Cluster Science
by Brett I. Dunlap, Andrew P. Baronavski, Mark M. Ross, and Stephen W. McElvany
High-Temperature Corrosion-Resistant Ceramics
by Robert L. Jones

Materials Science and Technology Division (6300)

Prediction of Ripple-Load Effect on Stress-Corrosion Cracking
by Robert A. Bayles, Peter S. Pao, and George R. Yoder
Fiber-Interphase-Matrix Interactions in Ceramic Matrix Composites
by Barry A. Bender and David Lewis III
Growth of Superconducting Y-Ba-Cu-0 Thin Films
by Phillip R. Broussard and Michael S. Osofsky
Research in Ceramic Composites at NRL
by David Lewis III

Optical Sciences Division (6500)

Diamond Synthesis in Flames
by Leonard M. Hanssen, Keith A. Snail, and James E. Butler
Dimensional Stability of Materials for Space Optics
by Paige L. Higby, Charles G. Askins, and E. Joseph Friebele
Time-Division Multiplexing for Fiber Optics Sensors
by Alan D. Kersey and Anthony Dandridge

Electronics Science and Technology Division (6800)

Microfabrication for Nanoelectronics
by Elizabeth A. Dobisz and Christie R. K. Marrian
Growth of Superconductor Materials by Spray Pyrolysis
by Richard L. Henry, Edward J. Cukauskas, and Arnold H. Singer
Light Detection with Granular Superconducting Films
by Ulrich Strom, James C. Culbertson, and Stuart A. Wolf

Space Systems Development Department (8100)

Modal Transients in Pulsed Laser-Diode Arrays
by Wendy L. Lippincott, Anne E. Clement, and William C. Collins

Spacecraft Engineering Department (8200)

Spacecraft Vibroacoustic Response Prediction
by Aaron A. Salzberg

Space Systems Technology Department (8300)

Space-based Tethered Array Antenna
by Michael S. Kaplan and Cynthia A. King

EMPLOYMENT OPPORTUNITIES FOR ENTRY-LEVEL AND EXPERIENCED PERSONNEL

This *Review* illustrates some of the exciting science and engineering carried out at NRL as well as the potential for new personnel.

The Naval Research Laboratory offers a wide variety of challenging positions that involve the full range of work from basic and applied research to equipment development. The nature of the research and development conducted at NRL requires professionals with experience. Typically, there is a continuing need for electronics, mechanical aerospace, ceramic, and materials engineers; metallurgists with bachelor's and/or advanced degrees; and physical and computer scientists with Ph.D. degrees. Opportunities exist in the areas described below.

Ceramic and Materials Scientists/Engineers. These employees work on the mechanical properties, coating and materials processing, and materials research.

Electronics Engineers. These engineers work in the following areas: communications satellite design, analog and digital signal processing, information processing, strategic and tactical communication systems design, instrumentation, microcomputer design, satellite attitude-control systems, image processing, IR sensors, focal plane arrays, radar, inverse scattering phenomena, statistical communication theory, electro-optics, hardware/software interfacing, artificial intelligence, electromagnetic (EM) scattering, digital electronics, fiber optics, optical information processing, semiconductor device processing, microwave tubes, threat systems analysis, electroacoustic optics, RF measurement design, EM propagation, EM theory, HF radar propagation analysis, electronic warfare simulation, pulsed power technology, vacuum electronics, microwave technologies, networking techniques, speech processing, Navy C^3I, electronic countermeasure systems design, spacecraft attitude controls, and orbitology.

Mechanical and Aerospace Engineers. These employees may be assigned to satellite thermal design, structural design, propulsion, experimental fluid mechanics, experimental structural mechanics, solid mechanics, elastic/plastic fracture mechanics, materials characterization of composites, finite element methods, nondestructive elevation, characterization of fracture resistance of structural alloys, and combustion.

Computer Science Graduates. Employees in this field are involved with artificial intelligence, software engineering, software systems specifications, computer design/architecture, systems analysis, and command information systems.

Chemists. Chemists are recruited to work in the areas of inorganic and organometallic synthesis, solution kinetics and mechanisms, surface analysis, organic chemistry, combustion, colloid/surface chemistry, fire suppression, and nuclear decay.

Physicists. Physics graduates may concentrate on such fields as electromagnetics, image processing,

inverse scattering phenomena, acoustics, inversion theory, mathematical modeling of scattering processors, radar system development, electro-optics, focal plane arrays, signal processing, plasma physics, astrophysics, semiconductor technology, relativistic electronics, beam/wave interactions, low-temperature physics, superconductivity, physical/chemical vapor disposition of thin and thick coatings, wave propagation, ionospheric physics, computational hydrodynamics, computational atomic physics, and supersonic, gas-dynamic numerical modeling.

FOR FOREIGN NATIONALS

U.S. citizenship is required for employment at NRL.

APPLICATION AND INFORMATION

Interested applicants should submit a resume or a Federal Employment Application Form (OPM 1282), which can be obtained from local offices of the Office of Personnel Management and Personnel Offices of Federal agencies, to the address below.

Direct inquiries to:

Naval Research Laboratory
Civilian Personnel Division, Code 3830 RV 88
Washington, DC 20375-5000
202-767-3030

NRL REVIEW STAFF

The *NRL Review* is a result of the collaboration of the scientific, engineering, and support staff with the Technical Information Division (TID). In addition to the scientists and engineers who provided material for the *Review*, the following have also contributed to its publication.

Senior Science Editor: Dr. John D. Bultman
Senior TID Editor: Lauraine Key
Associate TID Editor: Patricia Staffieri
TID Consultant: Kathleen Parrish

Head, Technical Information Division: Peter H. Imhof

Graphic design: J. Morrow and B. Zevgolis

Mission page photography by: M. Savell

Photographic production: G. Bennett, D. Boyd, R. Bussey, G. Fullerton, H. Hill, B. Horton, A. McDonald, J. Marshall, C. Morrow, M. C. Petit-Frere, M. Savell, and W. Wiggins

Computerized composition production: D. Gloystein and J. Kogok

Computerized composition assistance: P. Baker, M. Bray, C. Cain, J. Craze, J. Hays, C. Johnson, D. Mitchell, C. Sims, D. Stewart, and D. Wilbanks

Editorial assistance: I. Barron, M. Long, and D. Nelson

Production coordination: T. Calderwood

Distribution: J. Harris

INDEX

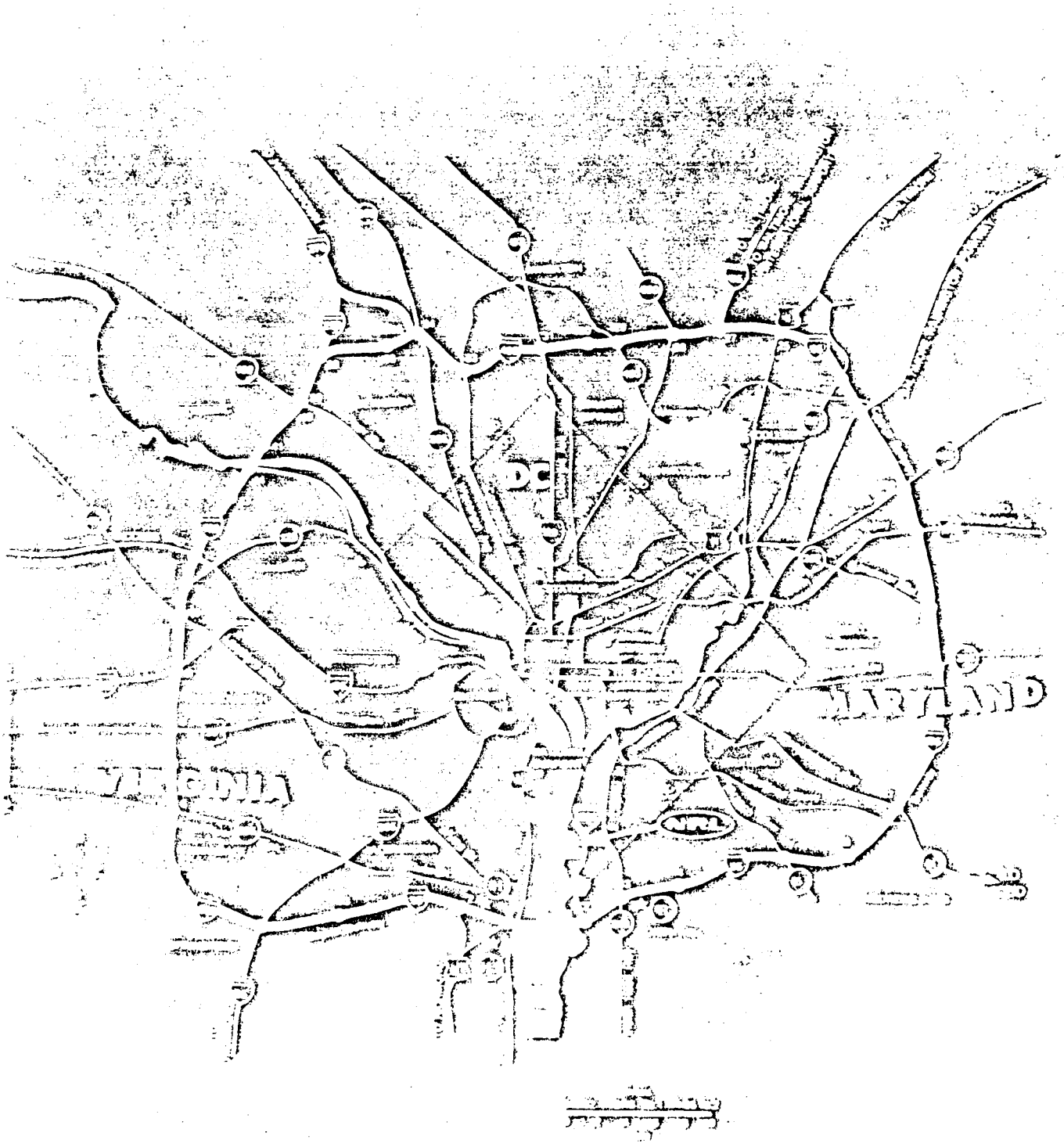
MARYLAND